Individualized Physiologically Based Pharmacokinetic Modeling of Rate Data (iPBPK-R): A Novel Approach to Estimate the Effect of Kidney Disease on Nonrenal Elimination Pathways

by

Yoko Franchetti

BSc, Pharmaceutical Sciences, Kyoto University, 1997

PhD, Biostatistics, University of Pittsburgh Graduate School of Public Health, 2010

Submitted to the Graduate Faculty of
the School of Pharmacy in partial fulfillment
of the requirements for the degree of

Doctor of Philosophy

University of Pittsburgh

2020

UNIVERSITY OF PITTSBURGH

SCHOOL OF PHARMACY

This dissertation was presented

by

Yoko Franchetti

It was defended on

August 21, 2020

and approved by

Thomas D. Nolin, PharmD, PhD, Associate Professor, School of Pharmacy

Raman Venkataramanan, PhD, Professor, School of Pharmacy

Jan H. Beumer, PharmD, PhD, Professor, School of Pharmacy

Philip E. Empey, PharmD, PhD, Associate Professor, School of Pharmacy

Manisha Jhamb, MD, MPH, Associate Professor, School of Medicine

Dissertation Director: Thomas D. Nolin, PharmD, PhD, Associate Professor, School of Pharmacy

Individualized Physiologically Based Pharmacokinetic Modeling of Rate Data (iPBPK-R): A Novel Approach to Estimate the Effect of Kidney Disease on Nonrenal Elimination Pathways

Yoko Franchetti, PhD

University of Pittsburgh, 2020

The impact of chronic kidney disease (CKD) on drug disposition is essential to optimize drug dosing in CKD. Clarifying the role of drug transporters and metabolic enzymes for nonrenally cleared drugs has been an emerging clinical interest for dose optimization. Physiologically-based pharmacokinetic (PBPK) modeling can provide valuable insight in this research area. The primary aim of this dissertation was to develop a novel PBPK approach and measurement procedure, called *individualized PBPK modeling of rate data* (iPBPK-R) to simultaneously estimate parameters for nonrenal elimination pathways in individuals and evaluate the effect of CKD on these pathways. We first described iPBPK-R which is a signal processing based indirect measurement method for measuring enzyme and transporter activities for individuals. In two subsequent studies, iPBPK-R was applied to $^{14}CO_2$ production rate data of erythromycin breath test (EBT) in healthy subjects and patients with end-stage renal disease (ESRD) receiving hemodialysis, respectively. Rate data for $^{14}CO_2$ production, as the approximate first derivative of $^{14}CO_2$ concentration data, allows iPBPK-R to successfully estimate parameters for nonrenal elimination pathways using the single phenotypic probe ^{14}C-erythromycin regardless of rate-limiting steps. iPBPK-R analysis indicated that CYP3A4 activity is much lower than the baseline IVIVE input in healthy subjects, and females had a higher CYP3A4 activity than males. In ESRD patients, estimated adjustment factors indicated that hemodialysis increased CYP3A4 activity minimally while OATPs activity varied among patients without improvement across hemodialysis. BUN was not correlated with any of the nonrenal elimination pathways suggesting that BUN is not a good candidate biomarker. Lastly, iPBPK-R was extended to its application to multiple concentration datasets of temsirolimus and its metabolite sirolimus in healthy subjects. Both temsirolimus and sirolimus are substrates of CYP3A4 and P-gp, and the effect

of concomitantly administered rifampin on these elimination pathways was evaluated. The findings showed that rifampin did not affect CYP3A4 activity on temsirolimus but increased it for sirolimus by 73%. Rifampin did not affect P-gp activity. Collectively, iPBPK-R may facilitate drug dosing based on personalized parameter estimates of nonrenal elimination pathways. iPBPK-R may enable uremic toxin-based biomarker research towards precision dosing in CKD as sketched with hierarchical cluster analysis.

Keywords: PBPK, CYP3A4, drug transporters, kidney disease, hemodialysis, uremic toxins, physiologically based pharmacokinetics, erythromycin, temsirolimus, sirolimus, indirect measurement, non-linear parameter estimation, breath test, precision medicine.

Table of Contents

Preface . . . xix

Abbreviations . . . xxi

1.0 Introduction . . . 1

1.1 Introduction . . . 2

1.2 Dose Optimization in Kidney Disease . . . 3

1.2.1 Evaluation of kidney function and the impact of kidney disease on drug disposition . . . 3

1.2.2 Factors that may affect drug exposure in kidney disease . . . 5

1.2.3 Disease- and population-specific heterogeneity should be accounted for in dose adjustment in kidney disease . . . 6

1.2.4 FDA guidance on PK studies in kidney disease . . . 7

1.2.5 Quantitative approaches for dosing evaluation . . . 8

1.3 PBPK Modeling and Simulations . . . 8

1.4 Examples of PBPK Modeling in Kidney Disease . . . 10

1.4.1 PBPK modeling for renally cleared drugs in CKD . . . 10

1.4.2 PBPK modeling for nonrenally cleared drugs in CKD . . . 13

1.4.3 Top-down PBPK approaches to evaluate altered drug exposure and its causes in kidney disease . . . 15

1.4.4 A middle-out PBPK approach to simultaneously evaluate hepatic transport and metabolism pathways . . . 16

1.4.5 Predictability and interpretation of PBPK modeling and simulation in kidney disease . . . 17

1.5 Opportunities for PBPK Modeling in Kidney Disease . . . 23

1.6 Hypothesis . . . 30

2.0 Indirect Measurement of Hepatic Drug Clearance by Fitting Dynamical Models . . . 31

2.1 Abstract . . . 31
2.2 Introduction . . . 32
2.2.1 Related Work . . . 33
2.2.2 Contribution . . . 35
2.3 Background for Method Development . . . 36
2.3.1 Mathematical Background . . . 36
2.3.2 Pharmaceutical Science Background . . . 36
2.3.3 Erythromycin Breath Test (EBT) . . . 44
2.4 Mathematical Framework of iPBPK-R . . . 44
2.4.1 Problem Description and Approach . . . 45
2.4.2 Clinical data: EBT . . . 47
2.4.3 Reduced Model . . . 47
2.4.4 Reduced Model as a System of Non-linear ODEs . . . 51
2.4.5 Modeling the Measurements . . . 54
2.4.6 Parameter Estimation via Optimization . . . 56
2.4.7 Analysis of iPBPK-R Estimation . . . 58
2.5 The Reduced Order iPBPK-R Model . . . 65
2.5.1 Developing the Reduced Model . . . 65
2.5.2 Matrix Representation of the EBT PBPK Model . . . 75
2.6 Estimation Procedure for iPBPK-R Parameters . . . 78
2.6.1 General Setup and Distance Measure . . . 79
2.6.2 Penalty Terms . . . 81
2.6.3 Objective Function and Optimization Problem . . . 83
2.6.4 Handling Combined Pre/Post Treatment Estimates . . . 84
2.6.5 Numerical optimization methods and implementation . . . 86
2.7 Examples and Results . . . 87
2.7.1 Estimating Parameters in Healthy People . . . 87
2.7.2 Co-Estimation Pre- and Post Dialysis . . . 88
2.8 Discussion . . . 92
2.8.1 iPBPK-R Characteristics . . . 92

2.8.2 Comparison to Other Procedures 95
2.9 Conclusions 98
3.0 Simultaneous Assessment of Hepatic Transport and Metabolism Pathways with a Single Probe Using Individualized PBPK Modeling of $^{14}CO_2$ Production Rate Data (iPBPK-R) 100
3.1 Abstract 101
3.2 Introduction 101
3.3 Materials and Methods 106
3.3.1 Clinical Data Sources 106
3.3.2 PBPK Model Structure 106
3.3.3 Ordinary Differential Equations, Kinetic Parameters, and Data Input 108
3.3.4 Rate Data and Reduced Order Model 110
3.3.5 Model Assumptions 111
3.3.6 Simulations, Optimizations, and Sensitivity Analysis 112
3.3.7 Statistical Analysis 116
3.4 Results 116
3.5 Discussion 133
3.6 Conclusions 139
4.0 Application of iPBPK-R to Evaluate the Effect of Hemodialysis on Nonrenal Clearance Pathways 141
4.1 Abstract 141
4.2 Introduction 142
4.3 Methods 143
4.3.1 Clinical Data Sources 143
4.3.2 PBPK Model Structure 144
4.3.3 Ordinary Differential Equations, Kinetic Parameters, and Data Input 146
4.3.4 Rate Data and Reduced Order Model 150
4.3.5 Model Assumptions 150
4.3.6 Simulations and Optimizations 151
4.3.7 Statistical Analysis 155

4.4 Results . . . 155
4.5 Discussion . . . 177
4.6 Conclusions . . . 181
5.0 Simultaneous Assessment of the Effect of Rifampin on Hepatic Transport and Metabolism Pathways using iPBPK-R Modeling of Temsirolimus and its Metabolite Sirolimus . . . 183
5.1 Abstract . . . 183
5.2 Introduction . . . 184
5.3 Method . . . 186
5.3.1 Clinical Data Sources . . . 186
5.3.2 PBPK Model Structure . . . 187
5.3.3 Ordinary Differential Equations, Kinetic Parameters, and Data Input 189
5.3.4 Coupled Concentration Data and Reduced Order Model . . . 189
5.3.5 Model Assumptions . . . 190
5.3.6 Simulations and Optimizations . . . 190
5.3.7 Statistical Analysis . . . 193
5.4 Results . . . 193
5.5 Discussion . . . 208
5.6 Conclusions . . . 214
6.0 Conclusions and Future Directions . . . 216
6.1 Summary and Key Findings . . . 216
6.2 Clinical Implications and Limitations . . . 221
6.2.1 Clinical implications . . . 221
6.2.2 Limitations . . . 223
6.3 Future Directions . . . 225
Appendix A. Mass Balance Theorem and Quality Analysis . . . 229
A.1 Proof of Theorem 1 . . . 229
A.2 EBT Analysis . . . 230
Appendix B. Detailed ODEs and Proof of Mass Balance for Healthy Subjects 232
B.1 ODEs for Concentration Change . . . 232

B.2 Mass Balance 234
B.3 Equations Depicting Mass Flow as Shown in Figure 38 235
B.4 ODEs for Mass Change 236
Appendix C. Nonlinear Systems of ODEs for Temsirolimus and Sirolimus in Healthy Subjects 240
C.1 ODEs for Concentration Change 240
C.1.1 Parent drug: Temsirolimus 240
C.1.2 Active metabolite: Sirolimus 242
Appendix D. Derivation of IVIVE Values based on MDR1-MDCK Data for sirolimus 245
D.1 In vivo intrinsic clearance of P-gp for sirolimus $CL_{OUT1(m)}$ 245
D.2 In vivo total passive diffusion between extracellular space and hepatocyte for sirolimus $Q_{ES-LC(m)}$ 246
D.3 Calculation of in vitro values for sirolimus from literature 247
Appendix E. A Procedure to Conduct Deep Learning Simulations for Evaluating iPBPK-R 251
Bibliography 252

List of Tables

1 Examples of PBPK modeling including parameters related to kidney function 19

1 Examples of PBPK modeling including parameters related to kidney function (continued) 20

1 Examples of PBPK modeling including parameters related to kidney function (continued) 21

1 Examples of PBPK modeling including parameters related to kidney function (continued) 22

2 Potential factors for evaluation in PBPK modeling in kidney disease 25

3 Key challenges and opportunities in PBPK modeling for dose optimization in kidney disease 26

3 Key challenges and opportunities in PBPK modeling for dose optimization in kidney disease (continued) 27

3 Key challenges and opportunities in PBPK modeling for dose optimization in kidney disease (continued) 28

3 Key challenges and opportunities in PBPK modeling for dose optimization in kidney disease (continued) 29

4 Properties used in PBPK modeling 40

5 Property input parameters for the drug flows and ODEs of ^{14}C-erythromycin 68

6 Mass flows of ^{14}C-erythromycin shown in fig. 7 (left panel) 69

7 ODEs for concentration change of ^{14}C-erythromycin in the organ compartments 70

8 ODEs for mass change of ^{14}C-erythromycin in the input and waste compartments 71

9 ODE for concentration change of $H^{14}CO_3^-$ and ODE for mass change of $^{14}CO_2$ 71

10 List of adjustment factors in iPBPK-R of EBT in healthy subjects 74

11 Entries of matrix $\mathbf{X}$ 79

12 Parameters used for the erythromycin breath test simulations 108

12 Parameters used for the erythromycin breath test simulations 109

12 Parameters used for the erythromycin breath test simulations 110
13 Parameter estimates through the nested optimization and normalized residuals in the iPBPK-R modeling of the EBT study in 12 healthy subjects 128
14 Parameter estimates through the nested optimization and normalized residuals in the iPBPK-R modeling of the EBT study by gender 129
14 Parameter estimates through the nested optimization and normalized residuals in the iPBPK-R modeling of the EBT study by gender 130
15 Spearman correlation coefficients among the estimated PBPK parameters, demographic and physiological data, and uremic solute concentrations in 12 healthy subjects. 131
16 Spearman correlation coefficients among the estimated PBPK parameters, demographic and physiological data, and uremic solute concentrations by gender 132
17 List of assumptions used in iPBPK-R of EBT data from patients with ESRD 147
17 List of assumptions used in iPBPK-R of EBT data from patients with ESRD 148
18 Parameters used for the erythromycin breath test simulations for patients with ESRD 149
19 Parameter estimates via the nested co-optimization in the iPBPK-R modeling of the EBT study in 12 patients with ESRD 157
19 Parameter estimates via the nested co-optimization in the iPBPK-R modeling of the EBT study in 12 patients with ESRD (continued) 158
20 Parameter estimates via nested co-optimization in the iPBPK-R modeling of the EBT study in 12 patients with ESRD by sex 166
20 Parameter estimates via nested co-optimization in the iPBPK-R modeling of the EBT study in 12 patients with ESRD by sex (continued) 167
20 Parameter estimates via nested co-optimization in the iPBPK-R modeling of the EBT study in 12 patients with ESRD by sex (continued) 168
21 Correlation coefficients among estimated PBPK parameters, demographic data, and uremic solute concentrations in 12 patients with ESRD 172
21 Correlation coefficients among estimated PBPK parameters, demographic data, and uremic solute concentrations in 12 patients with ESRD (continued) . . . 173

21 Correlation coefficients among estimated PBPK parameters, demographic data, and uremic solute concentrations in 12 patients with ESRD (continued) . . . 174
22 List of assumptions used in iPBPK-R of temsirolimus and sirolimus for healthy subjects 191
23 Pharmacokinetic parameters of the observed and iPBPK-R-based simulated data of the hypothetical healthy individual 202
24 Co-optimized parameter estimates via the nested co-optimization in the iPBPK-R modeling of temsirolimus and sirolimus in 15 healthy subjects across two study periods 203
25 Independent parameter estimates via the nested co-optimization in the iPBPK-R modeling of temsirolimus and sirolimus in 15 healthy subjects in Period 1 (without rifampin) and Period 2 (without rifampin), respectively 204
26 Parameters used for iPBPK-R simulations of temsirolimus for healthy subjects 205
26 Parameters used for iPBPK-R simulations of temsirolimus for healthy subjects 206
27 Parameters used for iPBPK-R simulations of sirolimus for healthy subjects . 207
27 Parameters used for iPBPK-R simulations of sirolimus for healthy subjects . 208

List of Figures

1 A 1-compartment model. 37

2 A 2-compartment model. 38

3 A simple PBPK model. 40

4 $^{14}CO_2$ production rate at 20 minutes (left) and for 2 hours (right). 45

5 Erythromycin breath test (EBT). 48

6 Example graph for a 3-compartment model. 48

7 The ODE system of ^{14}C-erythromycin (left) and metabolic by-product model (right) in iPBPK-R. 66

8 2D L_2 norm and 2D distance measure 80

9 Box plot of estimated adjustment factors of the Liver in 12 healthy subjects. . 89

10 3D plot of $^{14}CO_2$ production rate-time curve during the optimization in one subject. 89

11 iPBPK-R application to the $^{14}CO_2$ production rate data in patients with kidney disease who underwent dialysis. 90

12 Examples of impact of PBPK parameters on the shape of the $^{14}CO_2$ production rate – time curves compared to the shape of the $^{14}CO_2$ concentration – time curves in the hepatocyte. 104

13 Schematic representation of a PBPK model for describing the time profiles of ^{14}C-erythromycin after intravenous ^{14}C-erythromycin administration in a healthy subject. 107

14 Framework of the application of iPBPK-R to the EBT study in 12 healthy subjects. 113

15 iPBPK-R model fit to the individual EBT data from the 12 healthy subjects. 117

16 Goodness-of-fit plots for the 12 healthy subjects. 118

17 Box plots of estimated IVIVE adjustment factors for PBPK parameters in the liver compartments (ES and LC sub-compartments). 121

18 Estimated IVIVE adjustment values for PBPK parameters in the combined other organs (OT) compartment. 123
19 EBT data interpretation as a result of the application of iPBPK-R. 124
20 Example of sensitivity analysis. Simulated 3D $^{14}CO_2$ production rate – time curves. 126
21 A schematic representation of a seven-compartmental PBPK model (①-⑦) for describing the time profiles of ^{14}C-erythromycin after intravenous ^{14}C-erythromycin administration in a patient with ESRD. 145
22 Framework of the application of iPBPK-R to the EBT study in 12 patients with ESRD. 153
23 iPBPK-R per-individual simultaneous model fit to the EBT data pre- and post-hemodialysis (HD) from the 12 patients with ESRD. 159
24 Goodness-of-fit plots pre- and post-hemodialysis (HD) for the 12 patients with ESRD. 160
25 An example of 3D $^{14}CO_2$ production rate-time curve simulations in one patient. 161
26 Box plots of estimated scaling factors (co-estimated adjustment factors, inhibition coefficients, and total or independently optimized adjustment factors) in the liver. 163
27 Box plots of co-optimized adjustment factors associated with the combined other organs (OT). 164
28 Box plots of selected total adjustment factors associated with nonrenal elimination pathways (OATPs, P-gp, and MRP2 and CYP3A4) pre- and post-hemodialysis are compared by sex. 170
29 Dendrogram of hierarchical cluster analysis when change in adjustment factor for CYP3A4 clearance and change in inhibition coefficient for OATPs were used as features. 175
30 Box plots of change in scaling factors are compared by between a sub-group of ID = 3 and 16 versus others based on the hierarchical clustering analysis (Figure 29)). 176
31 PBPK model structures of temsirolimus and sirolimus in iPBPK-R. 188

32 Framework of the application of iPBPK-R to the four time series of blood concentration data of a drug-drug interaction study of temsirolimus with rifampin in 15 healthy individuals. 196
33 iPBPK-R simultaneous model fitting to the individual concentration data of temsirolimus and sirolimus in the absence and presence of rifampin from the 15 healthy subjects. 197
34 An example of 3D blood concentration-time curve simulations for temsirolimus and sirolimus in one healthy individual. 199
35 Box plots of estimated scaling factors. 200
36 Box plots of estimated induction/inhibition coefficients for CYP3A4 activity on temsirolimus, CYP3A4 activity on sirolimus, and non-CYP3A4 activity on sirolimus in the presence of rifampin (Period 2) compared to the baseline without rifampin (Period 1) in the liver. 201
37 Comparison between general bottom-up PBPK approaches and the middle-out iPBPK-R approach. 218
38 Mass balance in iPBPK-R 239
39 MDR1-MDCK monolayer models for calculating *in vitro* values for sirolimus. 250

List of Equations

1 Change in drug mass A in 1-compartment model . . . 37
2 Concentration-time curve in 1-compartment model . . . 37
3 Change in drug concentration C_1 in 2-compartment model . . . 38
4 Change in drug concentration C_2 in 2-compartment model . . . 38
5 Concentration-time curve for compartment 1 in 2-compartment model . . . 38
6 Change in drug concentration C_{BL} in blood compartment of PBPK model . . . 39
7 Change in drug concentration C_{LV} in liver compartment of PBPK model . . . 39
8 IVIVE equation for metabolic clearance activity of CYP3A4 . . . 40
9 Graph for a system of nonlinear ordinary differential equations (ODEs) . . . 49
10 System invariant for mass balance . . . 49
11 System invariant for mass flow . . . 50
12 Change in drug mass as a function of mass flows . . . 50
13 Convention for direct sum of two vectors . . . 51
14 Definition of indicator function for $\Omega \subset \mathbb{R}$ . . . 52
15 Michaelis-Menten function parameterized by three constants . . . 52
16 Michaelis-Menten function with a parameter transformation . . . 52
17 Definition of operator $\bar{\mathbf{A}}(.)$ . . . 52
18 Entries $b_{ij}(.)$ of matrix $\mathbf{B}$ as scalar functions . . . 53
19 Nonlinear operator $\mathbf{B}(.)$ . . . 53
20 Operator addition $\mathbf{U}(.) + \mathbf{V}(.)$ . . . 53
21 System of nonlinear ODEs using operators . . . 54
22 System of nonlinear ODEs with weighted graph matrix $\mathbf{M}(.)$ . . . 54
23 Operator $\mathcal{F}(.)$ to map the solution of the ODE to breath $^{14}CO_2$ rate . . . 55
24 $^{14}CO_2$ production rate in the breath $B(t)$ using $\mathcal{F}(.)$ . . . 55
25 L_2 norm distance between breath function $B(t)$ and observed data $\vec{S}$ . . . 56
26 Basic parameter estimation as optimization problem . . . 57

27 Basic objective function $\Psi^{\vec{u}}(\vec{r})$ 57
28 Specialized objective function $\Psi^{\vec{u}}(\vec{r})$ with penalty term in iPBPK-R 57
29 Penalty term $\pi(\vec{r},\vec{u})$ 57
30 System of nonlinear ODEs bounded by linearized ODEs 58
31 Homogeneous system of n linear ODEs with a real system matrix $\mathbf{A}$ 59
32 All solution vector functions for homogeneous system of n linear ODEs 59
33 $2n$ nonlinear equations in β_i and θ_i as a solution of jth compartment 60
34 Parameter solution (adjustment factors) as optimization problem of linearized ODEs 61
35 Vector containing adjustment factors for nonrenal elimination pathways 67
36 Flow term $q_{ji}(t)$ as a function of mass flow types Q_1, Q_2, and Q_3 67
37 $\mathbf{X}$ containing the linear part of the system of nonlinear ODEs 76
38 $\tilde{\mathbf{Y}}$ containing the nonlinear part of the system of nonlinear ODEs 76
39 System of nonlinear ODEs used for EBT in iPBPK-R 77
40 $^{14}CO_2$ production rate $B(t)$ returned by $\mathcal{F}(.)$ in iPBPK-R 80
41 Configuration vector in iPBPK-R 80
42 2D distance between B(t) and observed data $\vec{S}$ in iPBPK-R 81
43 Parameter vector $\vec{r}$ in iPBPK-R 82
44 Bias constraint term $\nu(\vec{r},\vec{h}')$ 82
45 Lower bound penalty term $\rho(\vec{r},\vec{h}'')$ 82
46 Drift penalty term $\epsilon(\vec{r})$ 82
47 X-shift penalty term $\psi(\vec{r})$ 83
48 Objective function $\Psi_{\text{2D}}^{\vec{r},\vec{u}}(.,.)$ in iPBPK-R 83
49 Optimization problem in iPBPK-R 84
50 Co-optimized parameter vector $\vec{r}_{\text{c}}$ in iPBPK-R 85
51 Independent parameter vectors $\vec{r}_{\text{i},1}$ and $\vec{r}_{\text{i},2}$ in iPBPK-R 85
52 Combined optimization problem for multiple data series in iPBPK-R 86

Preface

This dissertation is dedicated to my husband, Franz, and our daughter, Hana, whose love, encouragement, and extraordinary support made this accomplishment possible.

I also dedicate this dissertation to my parents, Masamichi and Fumiko Tanaka. My parents have encouraged me by showing their diligence, positive perspectives, and continued support throughout my life.

Six years ago I returned to visit the University of Pittsburgh. My destination was the School of Pharmacy but not the Graduate School of Public Health where I earned my PhD in Biostatistics in 2010. I have been always passionate about deepening my knowledge in drug development, and I wanted to pursue the highest academic degree in Pharmaceutical Sciences. I contacted my current advisor, Dr. Thomas D. Nolin, and met the Associate Dean for Graduate and Postdoctoral Programs Dr. Samuel Poloyac and Director of the Graduate Program in Pharmaceutical Science Dr. Maggie Folan to learn about the Clinical Pharmaceutical Scientist track of the PhD program, which I was very interested in. In 2015 fall, I was admitted to the PhD program at the School of Pharmacy. Upon my enrollment in the program Dr. Nolin and Dr. Poloyac encouraged me and wished me success in this program. Their encouragement has driven me to work towards my dream, earning my PhD in Pharmaceutical Sciences.

Dr. Nolin is a great advisor and communicator. I will always be grateful for his invaluable guidance. Thank you for encouraging me, challenging me to clarify concepts and think critically and proving me the opportunity to learn and grow personally and professionally. I am grateful and would like to thank my thesis committee members, Dr. Raman Venkataramanan, Dr. Jan H. Beumer, Dr. Philip E. Empey, and Dr. Manisha Jhamb for their guidance, time, and critical review of this work from a diverse collection of perspectives.

I am grateful to my current and former lab mates in Nolin's lab: Alexander J. Prokopienko, Melanie Weltman, Morgan A Casal, Linda R. Prebehalla, and Raymond West III. In particular, Alex continuously helped and motivated me in this program. I also appreciate

Melanie and Morgan's intellectual input and discussion during the past years.

In addition to my advisor, committee members and lab mates there were numerous people, the faculty, staff and students at PittPharmacy, who have been a constant source of support throughout my PhD training over the past 5 years. Specifically, I would like to thank Dr. Samuel Poloyac, Dr. Maggie Folan, and Lori Altenbaugh for providing guidance and administrative support in completing my PhD. I would also like to thank the former Associate Dean Dr. Richard Bertz for providing his career mentorship. I would like to thank Chenxiao Tang, Lingjue Li, Junyi Li, Karryn Crisamore, Hongfei Zhang, Ruichao (Richard) Xu, Solomon M. Adams, Xinran Cai, Kunal Jhunjhunwala, Yang Xie, Changrui Xing, Xin Tong, Anne Barbosa, and Joshua Niznik. All of your support and friendship has helped me to gain scientific knowledge and encouraged me to complete this dissertation.

I would like to acknowledge the fellowship support by the U.S. Food and Drug Administration and Oak Ridge Institute for Science and Education (FDA ORISE fellowship) and the grant support by the Extreme Science and Engineering Discovery Environment (XSEDE) Pittsburgh Supercomputing Center Bridges Startup Grant for the past two years. I would like to thank Acting Director of Office of Clinical Pharmacology, OTS, CDER, FDA, Dr. Shiew-Mei Huang and Senior Science Advisor Dr. Qi Liu for their continuous support and mentorship. I would like to thank Quantitative Clinical Pharmacology Reviewer Dr. Jieon Lee for her discussion on PBPK parameters for the work using the FDA database.

I would like to thank again my husband Franz who is Professor at ECE, Carnegie Mellon University for his continuous and profound discussions on programming and mathematical analysis so that I could develop the methodological framework, iPBPK-R. I also would like to thank his student Prerna Singh for investigating the application of a machine learning method as a future direction.

Finally, I would like to thank my late grandparents, in particular my late grandfather, Minoru Tanaka, for being an example of a lifelong scholar. I would like to thank my parents-in-law, Franz and Traude Franchetti, and my brother's family and my extended Austrian family. Back in 2004 when I came to Pittsburgh I was just myself in the US. Now my family circle grew and I appreciate all my family members for their love, support and patience until I come to the stage to finish my PhD in Pharmaceutical Sciences. Thank you so much.

Abbreviations

AUC	Area under the curve
BDDCS	Biopharmaceutics Drug Disposition Classification System
BUN	Blood urea nitrogen
β2-M	β2-microglobulin
CKD	Chronic kidney disease
CL	Clearance
CL_R	Renal clearance
CL_{NR}	Nonrenal clearance
$CL_{H,u}$	Unbound intrinsic clearance in the liver
CL_{PD}	Passive diffusion clearance
C_{max}	Maximum concentration
CYP	Cytochrome P450
CV	Coefficient of variation
DDI	Drug-drug interaction
EBT	Erythromycin breath test
eGFR	Estimated glomerular filtration rate
ES	Extracellular space
ESRD	End-stage renal disease
FDA	U.S. Food and Drug Administration
f_e	Fraction excreted unchanged in urine
f_p	Unbound fraction in plasma
f_u	Fraction unbound
GFR	Glomerular filtration rate
HCA	Hierarchical cluster analysis
IC50	Half maximal inhibitory concentration
IVIVE	In vitro-in vivo extrapolation

iPBPK-R Individualized physiologically based pharmacokinetic modeling of rate production data

iPTH Intact parathyroid hormone

IS Indoxyl sulfate

ISEF Scaling factor per unit of enzyme from recombinant systems to hepatic enzymes

IUPAC International Union of Pure and Applied Chemistry

J_{max} Maximum velocity

K_m Michaelis-Menten constant

KI Kidney impairment

K_i Apparent inhibition constant

LC Liver cell

MATE1 Multidrug and toxin extrusion 1

MATE2 Multidrug and toxin extrusion 2

MDCK cells Madin-Darby canine kidney cells

MDR1 multidrug resistance protein 1 gene (encoding P-gp)

MDR1-MDCK MDCK cells transfected with MDR1

MRP2 Multidrug resistance-associated protein 2

OATP Organic anion transporting peptide

OCT1 Organic cation transporter 1

OCT2 Organic cation transporter 2

ODE Ordinary differential equation

ORISE Oak Ridge Institute for Science and Education

PBPK Physiologically based pharmacokinetic

PK pharmacokinetic

P_{APP} Permeability in an *in vitro* transwell experiment

PCS p-cresyl sulfate

P-gp P-glycoprotein

PSC Pittsburgh Supercomputing Center

PTCPGK Proximal tubular cells per gram kidney

RAF	Relative activity factor
REF	Relative expression factor
RP	Relative percentage
SF	Scaling factor
SCr	Serum creatinine
$t_{1/2}$	Terminal elimination half-life
t_{max}	Time to $t_{1/2}$
TNF-α	Tumor necrosis factor-α
VOC	Volatile organic compound
V_{SS}	Apparent volume of distribution at a steady state

1.0 Introduction

This chapter was published as Franchetti, Y. and Nolin, T.D. Dose Optimization in Kidney Disease: Opportunities for PBPK Modeling and Simulation. *J Clin Pharmacol*, 60: S36-S51, 2020. https://doi-org.pitt.idm.oclc.org/10.1002/jcph.1741. The entire chapter was adapted from the publication.

1.1 Introduction

In the United States approximately 37 million adults, representing more than 10% of the population, are estimated to have chronic kidney disease (CKD) [1], [2]. CKD patients frequently exhibit altered pharmacokinetics (PK) and pharmacodynamics (PD), and thus require special attention to the dosing of their medications in order to optimize safety and efficacy. Hospitalized patients with impaired kidney function often receive medications that are known to be nephrotoxic or require dose adjustment [3]. Unfortunately, CKD patients are commonly prescribed numerous drugs concurrently and are also at high risk for medication related problems in the outpatient setting. Hence, medication selection and dose optimization are critically important for protecting a large segment of the U.S. population and has direct implications to public health.

Drug studies in patients with kidney disease are complex, requiring effort from a multidisciplinary team of stakeholders, typically including pharmaceutical scientists, pharmacologists, regulatory scientists, and clinicians among others [4]. Yet, *pharmacokinetics (PK)*, the quantitative study of drug movement over time in terms of absorption, distribution, metabolism, and excretion (ADME), provides all stakeholders with core principles for refining drug dosing [5] [6]. Kidney function generally declines as kidney disease progresses. Similarly, many factors related to ADME also change as the disease progresses, all of which should be evaluated using PK principles to determine whether systemic exposure is altered, requiring corresponding dose optimization. In addition to the glomerular filtration rate (GFR), factors to be considered include hepatic metabolism, transport, plasma protein binding, and fraction unbound in plasma. These factors may affect not only renal clearance but also nonrenal clearance pathways [7].

In the application of PK modeling it is common to use empirical equations to model ADME and simulate drug concentration–time curve profiles to fit clinically observed concentration–time curve profiles. Parameter estimates obtained via this "top-down" population PK approach are used to adjust drug dosing by comparing subjects with normal kidney function and impaired kidney function [6]. However, physiologically-based pharmacokinetic (PBPK) modeling as a "bottom-up" approach is an alternative option to model

drug concentration-time curves. Since the physiological and drug-specific parameters are included in the model structure, PBPK modeling is at least partially mechanistic. This is advantageous because the factors that are potentially altered in kidney disease can be evaluated via modeling and simulation of drug exposure. A recent Food and Drug Administration (FDA) guidance for industry acknowledges the strengths of PBPK modeling and encourages its use during drug development [8].

We present an overview of PBPK modeling based dose optimization in kidney disease. Several examples of PBPK models incorporating kidney function are provided, and applications and broad opportunities of PBPK modeling for dose optimization in patients with kidney disease are discussed.

1.2 Dose Optimization in Kidney Disease

1.2.1 Evaluation of kidney function and the impact of kidney disease on drug disposition

Optimal drug dosing in kidney disease requires both an accurate evaluation of the kidney function and a mechanistic understanding of the impact of altered kidney function on drug disposition. The current clinical practices of evaluation of kidney function are based on research findings in 1960s to 1970s [9]. By 1970s it became known that patients with kidney disease are more likely to experience adverse drug reactions compared to patients with normal kidney function. It was also recognized that a decline in kidney function will decrease clearance of renally cleared drugs and increase drug exposures [9]. Dettli et al. used creatinine clearance (CLcr) to not only measure kidney function but also estimate nonrenal elimination fraction and presented a dose calculation method [10]. Using serum creatinine concentration Cockcroft and Gault developed a simplified equation (called the CG equation) to estimate CLcr for dose individualization [11].

Accurate evaluation of GFR is one of the essential steps for dose optimization in kidney disease. GFR can be approximately estimated with CLcr using the aforementioned CG

equation. This surrogate measurement is commonly used in clinical practice. CLcr can be alternatively calculated using urinary creatinine concentration but collection of required urine samples is challenging in terms of accuracy and completeness. More recently, several equations to estimate GFR were developed based on large epidemiological studies such as the Modification of Diet in Renal Disease (MDRD) study [12] and the Chronic Kidney Disease Epidemiology Collaboration (CKD-EPI) study [13]. Evaluation of kidney function for dose adjustment may need to be further improved since clinical data in subpopulations such as pediatrics and on new molecular entities are not sufficiently available or analyzed [14] [15] [16] [17].

In terms of the impact of kidney disease on drug disposition, Reidenberg et al. recognized that nonrenal metabolism of sulfisoxazole slowed in kidney disease as early as 1969 [18] and later organized a list of drugs based on metabolic pathways [19]. By 1970s drug distribution (e.g., digoxin), drug-protein binding (e.g., phenytoin), and drug sensitivity (e.g., atropine) were also found to be affected in kidney disease [20] [21] [22] [23]. These early findings were used to inform dose optimization of many drugs in kidney disease.

Glomerular filtration, tubular secretion and reabsorption in the nephron collectively determine an individual's kidney funcion. It is known that tubular secretion is a more efficient mechanism of drug elimination and its dysfunction is associated with a great risk of death independent of estimated GFR [24]. Given these complex clearance processes in the kidney, deeper investigations of the underlying mechanism of altered kidney function and the extent of impact of kidney disease on drug disposition are also warranted [24] [25] [26]. However, accurate and non-invasive evaluation of the impact of kidney disease is not an easy task. Modeling and simulations may be used to investigate the underlying mechanism of altered kidney function and for predicting the impact of kidney disease on drug exposures in relatively inexpensive and non-invasive fashion. The cost-effectiveness of modeling should be validated at some point, for example, in terms of the time spent for collecting preclinical data and modeling and simulation, predictability of the modeling, and the cost to hire scientists versus the time spent for designing and conducting all necessary clinical studies, and recruiting patients with kidney disease, analyzing the clinical data, and the cost to recruit patients and hire operational staff and clinical scientists.

1.2.2 Factors that may affect drug exposure in kidney disease

Multiple patient characteristics (i.e., demographic covariates) can be used for dose optimization in kidney disease. For example, evaluation of kidney function using MDRD and CKD-EPI equations require age, serum creatinine clearance, sex, and race as intrinsic patient information [13] [27] [28]. In recent years, other factors also have been shown to affect drug exposure in kidney disease. First, certain metabolism-mediated and transporter-mediated pathways are known to be altered in kidney disease and this contributes to changes in drug exposure of nonrenally cleared drugs as well as renally cleared drugs [29]. Zhang et al. reported that between 2003 and 2007 [23], NDA submissions for nonrenally cleared drugs included PK data in patients with impaired kidney function, and a quarter of these showed about 2-fold increase in AUC [16]. In addition, the extent of altered nonrenal elimination may vary based on the etiology of CKD (e.g., glomerulonephritis versus non-glomerulonephritis) [30] [31]. Second, accumulated uremic toxins in the systemic circulation may impact enzymatic metabolism and drug transporter function [7]. Uremic toxins are nitrogenous and other waste products accumulated in the blood in chronic kidney disease [7], and they are classified into three groups based on physicochemical properties: (i) small, water soluble compounds with a molecular mass less than 500 Da (ii) middle size compounds with a molecular mass greater than 500 Da, and (iii) protein bound compounds [32]. Identifying a particular uremic toxin out of more than 100 known uremic toxins as a cause of altered drug disposition is difficult [33] [34]. A high concentration of uremic toxin does not necessarily elicit a strong biologic effect [32]. However, some uremic toxins (e.g., hippuric acid, indoxyl sulfate, incole-3-acetic acid, p-cresol, and CMPF) inhibit in vitro CYP3A4-mediated metabolism [35]. Hsueh et al. identified that 12 and 13 out of 72 uremic solutes were inhibitors of renal OAT1 and OAT3 transporters in in vitro studies using a fluorescent probe substrate, 6-carboxylfluorescein[1], respectively [36]. Other uremic toxins have been reported to directly or indirectly affect enzymatic metabolism and drug transport in experimental models of end-stage renal disease (ESRD) [7]. PBPK modeling could facilitate research on the effect of uremic toxins on metabolizing enzyme- and transporter-mediated pathways of

[1]For both OAT1 and OAT3 transporters 6-carboxylfluorescein was commonly used as a substrate.

drug clearance in kidney disease. For example, evaluation of correlations between the plasma concentrations of uremic toxins and the impact of altered enzyme or transporter activities on drug exposure can provide clinical insights and serve as a hypothesis-generating analysis for subsequent targeted biomarker research (i.e., facilitation of research).

1.2.3 Disease- and population-specific heterogeneity should be accounted for in dose adjustment in kidney disease

Patients with kidney disease tend to have multiple comorbidities [2]. The leading cause of death in ESRD is cardiovascular disease, though many other causes are also reported including malignancy [2]. Accordingly, it is important to consider dose optimization for kidney disease in a cross-disciplinary manner. For example, inclusion of patients with impaired kidney function in oncology clinical trials requires special attention due to the potential for increased risk of toxicity [37] [38]. In PK and dose escalation studies in oncology, safety and clinical data are collected from cancer patients to determine maximum tolerated dose (MTD). These patients may or may not have kidney impairment, and evaluation of the impact of the kidney disease on drug disposition can be more complex compared to evaluation of the impact of the kidney disease on disposition of drugs for treating other diseases. For example clinical trials for anticancer drugs often employ unique study designs (e.g., adaptive designs, sequential designs, etc.) and sample sizes for evaluating the impact of kidney disease may not be sufficient when such a study objective is not accounted for in the study design and inclusion/exclusion criteria. In addition, the choice of method to evaluate kidney function requires clinical judgement and affects eligibility to enroll patients [38]. This choice may in particular introduce a bias in dose optimization of narrow therapeutic index drugs, many of which are taken by cancer patients [39].

Evaluation of kidney function and dose adjustment in kidney disease need to be carefully conducted in accordance with the target disease, sex, and age group to treat, not only in oncology but also in geriatrics, pediatrics, hepatic impairment, among others [15] [40] [41] [42] [43]. Target drug classes may include antibiotics and small biologics (< 60 kDa) [44] [45]. If drugs are orally administered, the effect of gut absorption needs to be accounted for in

the evaluation of the effect of kidney function. Crosstalk between the liver and kidneys and particularly the gut-liver-kidney-axis is an emerging research area [46]. Gut-derived uremic toxins are reported to lead to not only kidney disease but also liver disease. The relationship between uremic toxins and these diseases may not be simple. Lin et al. showed a relationship between liver disease and serum concentrations of the uremic toxins indoxyl sulfate and p-cresyl sulfate independent of CKD severity [47]. Accordingly, drug disposition may need to be evaluated by severity of liver disease and/or a choice of uremic toxins (as a candidate biomarker) in the same CKD cohort. It is imperative to account for disease- and population-specific heterogeneity in drug dosing as part of precision medicine, which can be achieved via modeling and simulation [48] [49].

1.2.4 FDA guidance on PK studies in kidney disease

In its 1998 guidance and 2010 revision, the FDA recommends evaluating the effect of kidney disease on PK/PD of investigational drugs to inform dosing recommendations. This guidance provides a decision algorithm for conducting PK studies in kidney disease and describes appropriate study designs where PK/PD data and other clinical factors should be collected. In addition, the revised FDA guidance notably recommends: (1) using the 4-variable MDRD equation in addition to the CG equation to evaluate kidney function, (2) conducting PK studies in kidney disease regardless of route of elimination of drugs (i.e., both renally and nonrenally cleared drugs), and (3) conducting PK studies in hemodialysis (HD) patients [50] [51]. Since the original guidance was issued, a substantial number of approved drugs include dose recommendations for kidney disease in the label [52] [53] [54]. It is anticipated that future revisions to the guidance will further streamline PK research in drug development programs and enable more informed drug regimens for CKD patients [55]. PBPK modeling is a powerful tool to investigate the differential PK/PD of drugs in kidney disease, as it also facilitates evaluation of multiple effects of extrinsic and intrinsic factors on drug exposures and effects in kidney disease in an integral manner.

1.2.5 Quantitative approaches for dosing evaluation

The effect of kidney disease on PK/PD and its variability by physiological, intrinsic, and extrinsic factors are quantitatively evaluated using PK modeling [17]. With noncompartmental approaches, typical PK parameters such as the area under the plasma concentration-time curve (AUC), Cmax, apparent clearance (CL/F), volume of distribution at a steady state (Vss), and half-life ($t_{1/2}$) are estimated. However, compartmental population approaches are more useful to evaluate the effects of multiple factors that may be altered in kidney disease [50]. A model-based dosing strategy is typically proposed based on population PK modeling [56], and prediction of drug exposures by population PK modeling can be enhanced by advanced techniques such as machine learning algorithms [57]. Population PK modeling is usually considered a "top-down" approach as it is constructed on observed data [58]. In contrast, PBPK models generally employ a "bottom-up" approach whereby a set of mathematical equations describe physiological and anatomical structures and drug flows in the system using system-specific and drug properties as parameters [59]. Thus, PBPK modeling is mechanistic in nature and therefore valuable for evaluating unique physiological factors in a special population, such as kidney disease. This mechanistic approach may translate to good precision dosing in the special population, and for this reason PBPK modeling has garnered much attention in clinical pharmacology and drug dosing research [15] [60] [61] [62].

1.3 PBPK Modeling and Simulations

The concept of PBPK modeling is not new, but over the past two decades it has emerged as an essential tool in drug development and regulation [59]. Two main reasons for this trend are (1) development of specialized PBPK software in conjunction with increased computing power, and (2) in vitro – in vivo extrapolation (IVIVE) techniques, by which some parameter inputs necessary for simulation are taken from in vitro data [59], have become an integral part of PBPK modeling. PBPK modeling can be used to predict variability in ADME for different populations prior to conducting clinical trials [63].

The power of PBPK modeling comes from its use of biological variables that facilitate simulation and prediction of drug behaviors over time in virtual populations [58] [59]. This in silico approach consists of three main parts. First, a structural model describing the anatomical arrangement of organs and tissues connected by blood vessels is built for a human body system. Second, parameters for system-specific properties are collected and used as model inputs. Third, parameters for drug properties are collected and used as model inputs. Examples of drug-specific properties are tissue affinity, plasma-protein binding affinity, enzymatic stability, and transporter activity.

IVIVE techniques can further improve PBPK modeling by enabling calculation of a necessary parameter value like intrinsic metabolic clearance, for a large population based on in vitro data, such as that from human liver microsome experiments. Resulting PBPK-IVIVE linked models increase the impact of preclinical data and aid in prediction of clinical variability by utilizing both preclinical and mechanistic information [64].

Traditionally, human PK predictions have been based on an allometric approach, which assumes that the only difference between human and other mammals is size; however, such predictions have been shown to be imprecise [65]. Compared to the allometric approach, the IVIVE approach improves the predictability of plasma concentrations for several drugs [59]. The improved predictability is likely due to PBPK-IVIVE linked models that account for underlying biological variability between species as well as in a population. However, overall predictability of PBPK models needs to be further improved by accounting for intervariability of intrinsic and extrinsic factors of in vitro samples since in vitro experimental data are used to calculate IVIVE values [66]. Intrinsic factors may be genetic polymorphism, smoking, or alcohol drinking of humans from whom hepatocyte samples are obtained. Extrinsic factors may be preparation process and/or storage condition of human liver samples.

PBPK-IVIVE linked models have been particularly useful to investigate variability in hepatic clearance caused by differential drug metabolism and/or transporter activity in a special population [64], which may facilitate PBPK model-based dose optimization. Several equations have been proposed to calculate IVIVE values depending on the type of preclinical experiments [67] [68] [69]. For example, calculating intrinsic metabolic clearance for the whole liver using data from recombinantly expressed CYP enzymes incorporates not only

the maximum velocity (J_{max}) and Michaelis-Menten constant (K_m) of each CYP enzyme in the drug's metabolic pathways, but also the amount of microsomal protein per gram of liver (MPPGL), the liver weight, and a scaling factor per unit of enzyme from recombinant systems to hepatic enzymes (ISEF) for each enzymatic activity and pathway.

A summary querying PBPK publications on PubMed between January 2008 and May 2015 [70] reported the most common uses of published PBPK models to be prediction of DDI, followed by predictions of interindividual variability and dose exposure. Population PBPK modeling has also been utilized for complex analyses of enzyme-transporter interplay [71]. PBPK modeling has been considered to be a key innovation in personalized medicine and dose optimization as it alleviates some of the ethical and methodological hurdles of conducting clinical trials by simulating clinical scenarios and elucidating mechanistic insights in special populations [72] [73].

Applications of PBPK modeling in kidney disease can be aligned with drug development [74]. The FDA issued guidance for PBPK analyses discussed that "throughout a drug's life cycle, PBPK model predictions can be used to support decisions on whether, when, or how to conduct certain clinical pharmacology studies, and to support dosing recommendations in product labeling" [8]. In light of the FDA guidances related to PBPK documentation and conduction of PK studies in kidney impairment [8] [75], it is well envisioned that PBPK modeling will increasingly be used to evaluate dose-exposure relationships and support dose recommendation decision-making in the kidney disease population. PBPK-based findings that are informative for dose optimization in kidney disease have been presented in the past decade both within and beyond drug development [60].

1.4 Examples of PBPK Modeling in Kidney Disease

1.4.1 PBPK modeling for renally cleared drugs in CKD

Accurate evaluation of renal clearance is important for predicting drug exposure of renally cleared drugs. Renal clearance is a net result of glomerular filtration, reabsorption, and

secretion.

A 35-compartment PBPK model verified with 46 test compounds [76] described detailed mechanisms underlying passive reabsorption processes (e.g., tubular water reabsorption, dynamic tubular flow, tubular pH, and microvilli) contributing to renal clearance. The predicted renal clearance was within 2-fold of the observed renal clearance in 87% of drugs tested, showcasing the value of mechanistic PBPK studies in assessing tubular reabsorption and its contribution to renal elimination of xenobiotics.

Renal secretion has been evaluated in multiple PBPK modeling studies. Renal transporters are major contributors to renal secretion, and as such it is essential to understand the mechanism of transporter-mediated activities. Hsu et al. evaluated the utility of a PBPK model incorporating both renal uptake and efflux transporters for three renally cleared drugs: oseltamivir carboxylate, cidofovir, and cefuroxime [77]. Incorporating manual sensitivity searches, they explored the association between drug exposure in kidney disease and both renal transport activity and a system-specific parameter (proximal tubular cells per gram kidney or PTCPGK). Transporter-mediated activity was investigated by ranging the apparent inhibition constant K_i of probenecid in DDI simulations. When the transporter-mediated secretion was modeled, the simulated mean AUC ratio (AUCR) between renally impaired patients and healthy controls improved model predictability for all three drugs. One should note that in this study, no common threshold of PTCPGK across the drugs (i.e., to differentiate drug exposure in kidney impairment from healthy subjects) was determined. This suggests that inhibition of drug transporters is not solely based on the reduction of PTCPGK, but may depend on the relative magnitude of intrinsic transporter clearance of each drug. When simulations for each drug were conducted with probenecid (i.e., DDI simulations), approximate ranges of in vivo K_i were identified for oseltamivir carboxylate and cefuroxime. However, the range of K_i could not be identified for cidofovir since in DDI simulations K_i was not sensitive to the AUC ratio of cidofovir with probenecid versus cidofovir without probenecid. While the authors evaluated a range of 1-100μM for K_i in the sensitivity analysis based on *in vitro* data, the clinical concentration of probenecid can increase up to 520μM in healthy subjects. [78] In this sense, a well-designed follow-up sensitivity analysis may provide further insights on K_i for cidofovir. Hsu et al. also simulated renal cell

concentrations of cidofovir by inhibiting uptake and/or efflux transporters and elucidated a plausible mechanism of the DDI for cidofovir. This in turn contributed to understanding nephrotoxicity, which is believed to be caused by increased renal exposure of cidofovir. This assumed mechanism can be investigated only through modeling and simulation.

Posoda et al. conducted similar PBPK modeling of DDI studies for baricitinib in healthy subjects [79]. In this PBPK application, an IC50 value extrapolated from in vitro data was used to simulate inhibition of nonlinear renal transporter OAT3. The study cohort was composed of healthy subjects. However, this PBPK modeling approach may inform subsequent drug development work for determining dose recommendation in kidney diseases as it evaluated the alteration of renal OAT3 activity. At the same time, one limitation in the PBPK modeling is that extrapolated in vivo parameter inputs may not be sensitive or accurate because of simple assumptions used to derive parameter equations [77] [80] [81] [82].

Scotcher et al. discussed renal drug transport and uncertainty in system- and drug-specific parameters that are used for developing PBPK models for renal drug disposition [83]. In PBPK kidney models of digoxin in healthy subjects, geriatrics, and kidney disease patients, the predicted renal clearance relative to observed renal clearance was improved after renal transporters OATP4C1 and P-gp were added to the model [84]. Furthermore, using sensitivity analyses in PBPK modeling and simulations, it was concluded that either reduced PTCPGK or abundance of OATP4C1 (but not P-gp) is a potential cause of decreased renal secretion of digoxin. Based on this PBPK work, it is anticipated that improving the search algorithm and optimization method for system- and drug-specific parameters will facilitate the utility of PBPK modeling of renal cleared drugs.

In addition to assessing the contribution of renal clearance on exposure of renally cleared drugs, PBPK modeling and simulation may be used to evaluate whether renally cleared drugs affect exposure of concomitant drugs in kidney disease via metabolic inhibition or induction.

Lu et al. applied PBPK modeling to evaluate a potential drug-drug interaction (DDI) of the renally cleared drug orteronel, a weak in vitro inhibitor of CYP1A2, 2C8, 2C9, and 2C19, using data from human liver microsomal studies [85]. PBPK modeling demonstrated that the AUC of four CYP substrates did not significantly differ (AUCR < 1.25) in the presence

and absence of orteronel. This indicated that orteronel is a 'non-inhibitor' as per FDA DDI guidance [86], avoiding the cost for conducting clinical DDI studies before the drug approval.

1.4.2 PBPK modeling for nonrenally cleared drugs in CKD

About 75% of currently approved drugs undergo CYP-mediated metabolism [87] [88] [89] and more than half of nonrenally cleared drugs present altered PK profiles in kidney impaired patients [16]. In CKD patients when metabolic enzymes and drug transporters are involved in drug disposition, the magnitude of altered nonrenal clearance may not be easily determined [73]. PBPK modeling allows us to account for a potential interplay between enzymatic and drug transporter activity in nonrenal clearance, and to evaluate the impact of kidney disease on disposition of nonrenally cleared drugs.

In a simulation study, the impact of kidney disease on repaglinide exposure was evaluated by varying kidney function (down to GFR < 30 mL/min/1.73 m^2) and comparing it to the mean exposure in healthy subjects [60]. Incorporating intrinsic metabolism by CYP3A4 and CYP2C8 and transporter clearance (OATP1B1 uptake) into the PBPK model, the predicted results were relatively consistent with the observed exposure in each population. However, more validation of the model was considered to be necessary.

Zhao et al. evaluated the utility of PBPK modeling for three nonrenally cleared drugs: sildenafil, repaglinide, and telithromycin [90]. Physiological parameters known to be differentially expressed in kidney impaired patients versus healthy subjects, including abundance of CYP3A4 (metabolizing sildenafil, telithromycin, and repaglinide), CYP2C8 (metabolizing repaglinide), and CYP2C9 (metabolizing sildenafil), were incorporated into the model. Predicted and observed AUCR of kidney impaired patients to healthy subjects correlated reasonably well for sildenafil and telithromycin. The predicted AUCR for repaglinide was lower than the observed value (1.2 vs 3.0), but this difference improved after OATP1B1 activity in the model was decreased for the kidney impaired patients. This study emphasizes the importance of incorporating patient-specific system-dependent parameters (such as relative abundance of CYP enzymes) in special population PBPK models. The knowledge gap regarding the effect of kidney disease on hepatic transporter OATP1B1 was also improved

via the PBPK modeling work.

PBPK modeling also demonstrates that the effect of kidney disease on physiological processes, including hepatic clearance, may not be linear to the disease severity [90]. A series of studies investigated the effect of CKD on nonrenal elimination pathways to elucidate whether changes are enzyme and/or transporter specific [91] [92] [93]. Yoshida et al. conducted a systematic evaluation of the effect of CKD on CYP2D6- and CYP3A4/5-mediated clearance of 13 and 18 substrates, respectively, in increasing disease severity: mild, moderate, and severe CKD, and dialysis-independent ESRD [91]. The study concluded that CYP2D6-mediated clearance decreased in parallel with the severity of CKD while there was no apparent relationship between CYP3A-mediated clearance and the severity of CKD. Similarly, Tan et al. conducted a systematic evaluation of CYP1A2-, CYP2C8-, CYP2C9-, CYP2C19-, and OATP-mediated clearances in CKD [92]. The results suggested that CYP2C8- and OATP-mediated clearance decline according to disease severity, but the effect of CKD on the activities of CYP1A2, CYP2C9, and CYP2C19 was variable and minimal.

Subsequent work by Tan et al. utilized PBPK modeling to delineate CYP2C8 and OATP1B activities in CKD using substrates of CYP2C8 (rosiglitazone and pioglitazone), OATP1B (pitavastatin), or both (repaglinide) [93]. PK profiles for severe CKD patients were simulated with altered GFR, plasma protein binding, and activity of CYP2C8 and/or OATP1B in a stepwise fashion. The PBPK analysis suggested that OATP1B activity could be reduced in severe CKD but CYP2C8 activity is not affected by CKD. PBPK modeling was shown to be useful for interrogating elimination pathways of nonrenally cleared drugs.

The reported decreases in pathway-specific nonrenal clearance are informative for clinical pharmacologists and drug developers, as the information may be used to anticipate the need for dose optimization of corresponding drug substrates in patients with kidney disease. One limitation of the systematic evaluations evaluations by Yoshida et al. and Tan et al. (2017) may be a lack of generalizability due to small numbers of model drugs and sample sizes of the studies included (i.e., small sample sizes without pre-planned power calculation) [29]. In addition, statistical analysis did not account for data dependency across disease stages for each drug. Data was not uniformly available across all disease stages and drugs. Although these systematic evaluations require confirmatory studies, it is clear that the subsequent

PBPK modeling and simulation work by Tan et al. (2018) is an advantageous tool for evaluating the complex interplay of multiple nonrenal elimination pathways in kidney disease.

1.4.3 Top-down PBPK approaches to evaluate altered drug exposure and its causes in kidney disease

Uremic toxins accumulate in kidney disease and are suggested to be causes of altered transcription, expression, and activity of CYPs and transporters [73] [94] [95] [96]. To understand the effect of the toxic waste product creatinine on the MATE1 efflux transporter, Almukainzi et al. performed PBPK modeling of the renally-cleared drug metformin in healthy and kidney impaired subjects along with cell culture inhibition studies [97]. The model included OCT2 uptake, and MATE1 and MATE2 efflux transporters in the kidney, OCT1 and MATE1 transporters in the liver, and literature-based differences in system-specific properties (hematocrit, renal blood flow, gastric pH, and GFR value). The study concluded that increased metformin exposure in kidney disease patients could be explained by down-regulation of MATE1 in the kidney and liver in the PBPK analysis. This increased exposure may be mediated by creatinine but creatinine concentration was not statistically associated with the change of metformin uptake in the cell culture studies. The authors discussed that high capacity of MATE1 towards creatinine may be a possible reason that accumulated creatinine did not affect the PK profile of metformin in kidney disease. This finding based on PBPK modeling added to the previous work showing that metformin exposure is altered by decreased OCT2 activity [98]. To further understand the role of uremic toxins on drug disposition, a novel middle-out PBPK approach may be effective.

The above PBPK modeling was a semi top-down approach where levels of transporter (OCT2 and MATE1) expression was varied to find the best values to fit the model to the observed PK profile in kidney disease. Generally, bottom-up PBPK modeling is common. However, a top-down PBPK approach is also possible for the purpose of parameter estimation rather than prediction of PK profiles. Top-down PBPK approaches typically use reduced order models. In reduced order models the number of organ/tissue compartments is limited [59] so that a set of parameters can be estimable with a limited number of observed

samples [99]. Sayama et al. used a variant top-down approach where some PK parameter inputs for CKD patients were statistically obtained from their compiled clinical datasets of 151 compounds (i.e., interquartile ranges were obtained) [100]. The collected PK parameters were: unbound fraction in plasma (f_p, fraction excreted unchanged in urine (f_e), apparent volume of distribution at steady-state, clearance (CL), AUC after oral dosing, and elimination $t_{1/2}$. Relative percentages (RPs) of these PK parameters and scaling factors (SFs) of unbound intrinsic clearance in the liver ($CL_{H,u}$), and renal clearance (CL_R) were calculated to scale PK parameters of healthy subjects to those of patients with kidney disease for any compounds in the same category (basic, acidic, and neutral drugs). SFs calculated with the dataset were derived in a top-down approach. Using SFs as inputs for moderate and severe CKD patients, PBPK modeling of 12 compounds were performed and PK profiles were simulated. The 12 compounds were selected from the 151 compounds. As a result of PBPK modeling, the predicted range of CL contained the observed CL in 83% and 58% of the 12 compounds in moderate and severe CKD conditions, respectively. Although the prediction in moderate CKD seems to be reasonable, the predicted ranges were broad. Furthermore, synthesizing SFs of all different types of drugs and extrapolating them in mechanistic modeling of a particular drug is likely to lead to statistical biases, especially when individual drugs' in vivo parameters are available without extrapolation. In the model structures, detailed renal and nonrenal elimination pathways were not included. Thus, this PBPK top-down method may require some improvement.

1.4.4 A middle-out PBPK approach to simultaneously evaluate hepatic transport and metabolism pathways

In this dissertation research, we develop a top-down + bottom-up or 'middle out' PBPK approach, namely, individualized PBPK modeling of rate data (iPBPK-R) using a reduced order model and apply it to $^{14}CO_2$ production rate data. We also apply iPBPK-R to multiple coupled drug concentration data of parent drug temsirolimus and its metabolite sirolimus to evaluate the feasibility of the method. iPBPK-R enable simultaneous evaluation of hepatic transport and metabolism pathways and exploration of uremic toxin-mediated alterations of

drug disposition in individuals. We describe the details of the development and applications of iPBPK-R in Chapter 2 to Chapter 5.

1.4.5 Predictability and interpretation of PBPK modeling and simulation in kidney disease

During PBPK modeling and simulation it is important to inspect the model for predictability and to conduct careful interpretation. Generally, the decision criterion for acceptable model predictability is simulated PK profiles (AUC, C_{max}, etc,) within 2-fold of the observed PK profiles [76, 90, 93, 101, 102]. Among the PBPK applications discussed above, poor predictability during model development was observed when either essential parameters for intrinsic clearance were not incorporated in the model or uncertainty of the parameter input (e.g., IVIVE value) was likely to be high. For example, Hsu et al. described that when only altered GFR is considered in DDI simulations for severe renal impairment, predicted AUCR between kidney impairment and normal kidney function were between 3- to 5.5-fold [77]. This low predictability was resolved by incorporating the transporter-mediated secretion with reduced PTCPGK in the model. As another example, Scotcher et al. reported that varying IVIVE values of OATP4C1-mediated clearance based on different in vitro data led to 8-fold difference in simulated renal clearance. As illustrated in these examples, to improve the model predictability it is essential to identify impactful system-specific and/or drug-specific property parameters. This can be conducted through sensitivity analysis varying parameters of interest within a clinically relevant range. Also, collecting quality in vitro experimental data for IVIVE is often challenging. In the case of kidney disease, using in vivo parameters which are pre-estimated using a CKD patient database may be one alternative approach as in top-down PBPK modeling. Regardless, good predictability is not guaranteed and PBPK modeling and simulation needs to be carefully designed, improved, and validated. Knowledge may also be gained on system- and drug-specific properties by estimating individual *in vivo* parameters using a middle-out approach to supplement model prediction.

When interpreting the predicted results from PBPK modeling and simulation, it is essential to pay close attention to parameter dependency. PBPK modeling incorporates various

system-specific and drug-specific properties and they should be dependent with each other within the system. Consequently, the effects of these properties may not be obvious and may be mathematically indistinguishable in simulations. This was observed as unidentified properties of PTCPGK and intrinsic transporter clearance in DDI studies and the unidentifiable range of K_i for cidofovir in the study by Hsu et al [77]. At times, it may be necessary to treat multiple transporter phenotypes as a global- or meta-transporter. Understanding mathematical relationships among property parameters and conducting sensitivity analysis on them is essential to have confidence in interpretation.

While kidney function (i.e., GFR) has been included as a covariate in many PBPK applications, the effect of kidney disease itself on physiological parameters (e.g., renal transporters, renal filtration/secretion processes) that impact PK have not been extensively explored using PBPK to date. Another unique aspect of exploring kidney disease in PBPK applications is the ability to evaluate its effect on nonrenal elimination pathways, mainly metabolism-mediated pathways and transporter-mediated pathways in the liver. In addition, the top-down PBPK example used *in vivo* parameter estimates collected from CKD patients, and one middle-out PBPK approach evaluate the effect of hemodialysis in Chapter 4. A variety of applications of PBPK modeling of renally and nonrenally cleared drugs in kidney disease and unique PBPK approaches for evaluating PK parameters mechanistically are presented in Table 1. Table 2 lists potential factors for evaluation based on these applications. In the next section we summarize challenges and opportunities of PBPK modeling for dose optimization in kidney disease.

Table 1: Examples of PBPK modeling including parameters related to kidney function

Application[a]	Substrates	Inhibitors	Model features	Observations[c]	Software or platform	Ref.
Renal clearance	46 compounds[b]	NA	A 35-compartment kidney model; Modeled a mechanism underlying passive reabsorption (e.g., tubular water reabsorption, dynamic tubular flow, tubular pH, and microvilli).	Renal clearance in 87% of drugs was predicted within a threshold (2-fold of observed renal clearance).	Matlab and Simulink	[76]
Renal clearance/ DDI	Oseltamivir carboxylate, cidofovir, cefuroxime	Probenecid	Renal uptake and efflux transporters were modeled; The role of transporters was explored with PTCPGK and K_i.	The simulated mean AUC ratio between renally impaired patients and healthy controls improved model predictability for all three drugs. Approximate ranges of *in vivo* K_i of probenecid were identified for oseltamivir carboxylate and cefuroxime.	Simcyp	[77]
Renal clearance/ DDI	Baricitinib	Probenecid	Nonlinear renal transporter OAT3 was modeled; IC50 was used to evaluate the transporter inhibition.	The role of OAT3 and its potential DDI were predicted.	Simcyp	[79]
Renal clearance	Digoxin	NA	Kidney models for healthy subjects, an elderly cohort, and patients with kidney impairment; Modeled renal uptake and efflux transporters with varying PTCPGK or abundance of transporters.	Parameters causing a decrease in renal clearance were found (PTCPGK or OATP4C1).	Simcyp	[84]

Table 1: Examples of PBPK modeling including parameters related to kidney function (continued)

Application[a]	Substrates	Inhibitors	Model features	Observations[c]	Software or platform	Ref.
Renal clearance/ DDI	Orteronel	Theophylline, repaglinide, (S)-warfarin, omeprazole	CYP1A2, 2C8, 2C9, and 2C19 were modeled; Inhibition of CYPs was evaluated with K_i of each inhibitor.	Orteronel was identified as a non-inhibitor for CYPs evaluated. Simulated AUC for kidney impairment informed subsequent trials. *Dose-related.*	Simcyp	[85]
Nonrenal clearance in CKD	Paroxetine, diltiazem, and repaglinide	NA	CYP2D6 for paroxetine, CYP3A4 for diltiazem, and OATP1B1 for repaglinide were included in models; Drug exposures were simulated for moderate and/or severe CKD (30-59 and $<$ 30ml/min/1.73m^2, respectively) vs. healthy subjects.	Incorporating enzyme- and transporter-mediated clearance into the PBPK model, the predicted results were relatively consistent with the observed exposure in each population. For repaglinide, in vitro data OATP1B1 was limited to use in PBPK modeling, and simulated PK parameters for CKD were underestimated compared to observed data. *Dose-related.*	Simcyp	[60, 103, 104]
Nonrenal clearance in KI	Sildenafil, repaglinide, and telithromycin	NA	CYP3A4, 2C8, 2C9, and OATP1B1 were modeled depending on the substrate specificity; effect of decreased abundance of CYPs with KI was evaluated.	PK profiles were well predicted against observed data in healthy and KI cohorts except for repaglinide. This was improved by altering transporter activity. *Dose-related.*	Simcyp, Phoenix	[90]

Table 1: Examples of PBPK modeling including parameters related to kidney function (continued)

Application[a]	Substrates	Inhibitors	Model features	Observations[c]	Software or platform	Ref.
Nonrenal clearance in CKD	Rosiglitazone, pioglitazone, pitavastatin, and repaglinide	NA	CYP2C8 and/or OATP1B1 were modeled in a stepwise fashion with altered GFR and plasma protein binding for CKD patients	OATP1B1 activity but not CYP2C8 was found to decrease in severe CKD.	Simcyp	[93]
Renal clearance with uremic toxin in KI	Metformin		Renal transporters OCT2, MATE1, and MATE2 were modeled. Hepatic OCT1 and MATE1 were also included; Hematocrit, renal blood flow, Gatric pH, and GFR were altered in KI. The results were evaluated with in vitro inhibition experiments with creatinine.	Down-regulation of MATE1 in kidney and liver was found to explain the altered PK profile of metformin in KI. Creatinine did not affect the PK profile.	GastroPlus	[97]
Use of database-based in vivo clearance in PBPK modeling in CKD	12 compounds[b]		RPs of f_p, f_e, V_{ss}, CL, $t_{1/2}$, and AUC between healthy subjects and CKD patients were statistically obtained from 151 compounds in clinical database. SFs of $CL_{H,u}$ and CL_R were calculated to use in PBPK models. Model predictability was assessed for moderate and severe CKD conditions.	Hepatic and renal clearance were well predicted in half to 2/3 of the model compounds using SFs estimated in a top-down approach.	WinNonlin	[100]

Table 1: Examples of PBPK modeling including parameters related to kidney function (continued)

Application[a]	Substrates	Inhibitors	Model features	Observations[c]	Software or platform	Ref.
Nonrenal clearance/ multiple parameter estimation, role of uremic toxin	^{14}C-erythromycin	NA	A reduced order model with CYP3A4 and hepatic transporters was fit to $^{14}CO_2$ production rate data in healthy individuals; impactful PBPK parameters were estimated. Parameters related to nonrenal elimination pathways were correlated with uremic toxins.	CYP3A4 and hepatic transporter activities were estimated in healthy individuals. Correlations of parameter estimates with uremic toxins were explored.	R with Bridges	[105]
Nonrenal clearance/ hemodialysis effect via parameter co-estimation, role of uremic toxin	^{14}C-erythromycin	NA	A reduced order model with CYP3A4 and hepatic transporters was fit to $^{14}CO_2$ production rate data in individual patients across hemodialysis; impactful PBPK parameters were nested co-estimated. The effect of hemodialysis on CYP3A4 and OATPs activities was evaluated. These parameters were correlated with uremic toxins	The effect of hemodialysis on multiple nonrenal clearance pathways was individually estimated. Correlations of parameter estimates with uremic toxins were explored.	R with Bridges	[106]

NA, not applicable. [a.] Renal clearance denotes that renal clearance was evaluated for renally cleared substrate(s) while nonrenal clearance denotes that nonrenal clearance was evaluated for nonrenally cleared substrate(s) unless it is further indicated. [b.] Model compounds included both renally cleared and nonrenally cleared substrates. [c.] The column includes dose-related if the research problem is related to dose-optimization for kidney disease.

1.5 Opportunities for PBPK Modeling in Kidney Disease

While many PBPK applications have included kidney function as a parameter, kidney disease per se has not been extensively explored by PBPK modeling. Several opportunities in PBPK modeling for dose optimization in kidney disease are presented in Table table 3.

First, accurate evaluation of kidney function is a challenge because renal clearance is an elimination process consisting of GFR, active secretion, and reabsorption in the complex structure of the kidney. Each renal elimination pathway cannot be easily measured separately in a clinical setting. In this situation, PBPK modeling can provide mechanistic insights regarding renal elimination of xenobiotics. Several PBPK studies have shown reasonable predictability of drug exposures when the renal clearance was modeled in detail, such as by incorporating relevant renal transporter and metabolic enzyme intrinsic clearance in PBPK model equations. Detailed kidney models can be developed to simulate and predict drug exposures. Alternatively, reduced order models may be considered to employ top-down and middle-out PBPK approaches and to elucidate a dominant elimination pathway for a particular drug.

Second, there has been great interest regarding the effect of CKD on drug exposure, especially for nonrenally cleared drugs. Evaluating intrinsic clearance by hepatic transporters and metabolic enzymes using PBPK modeling is likely to fill knowledge gaps in drug disposition at different stages of kidney disease. PBPK modeling has also proven to be useful in identifying impactful changes in systemic- and drug-dependent parameters and their association with CKD progression. At the same time, there is still room to improve overall predictability of PBPK-IVIVE linked models, and thus advancing in vitro experimental techniques may partly eliminate biases in parameter inputs.

Third, PBPK modeling and simulation can be applied to prevent DDI-related toxicity in kidney disease. Both perpetrator drugs and victim drugs can be evaluated by PBPK modeling to assess whether a DDI is mediated by renal transporters, hepatic enzymes, or any interplay of transporters and enzymes under the varying condition of kidney impairment. PBPK modeling has proven to be advantageous relative to simple in vitro experiments for DDI studies since it can evaluate various DDI scenarios by ranging parameter values.

Fourth, causes of interindividual variability in kidney disease are important to investigate prior to considering precision dosing. Focusing on a sub-cohort of CKD patients in PBPK modeling may facilitate discovery of factors that contribute to inter-individuality. Sub-cohorts may be CKD-specific (i.e. hemodialysis-independent ESRD patients, administration of drugs pre- and post-hemodialysis, patients with glomerulonephritis versus CKD of non-glomerular etiology) or extrarenal (i.e. various comorbidities, different stages of the human life cycle, and specific classes of drugs).

Fifth, *in vivo* parameter inputs can be explored in combination with top-down and middle-out PBPK approaches to supplement IVIVE techniques. Related examples were reviewed above: a large clinical database study where PBPK parameter inputs in kidney disease were collected and extrapolated into PBPK modeling [100]. As another study, individualized PBPK model fitting can be conducted to indirectly estimate multiple parameters on nonrenal elimination pathways utilizing reduced order models like this dissertation research.

Sixth, PBPK modeling is a dynamic mechanistic approach that enables exploration of the association of uremic toxins as potential causes of altered drug disposition and parameter estimates related to drug elimination pathways. Uremic toxins can be treated as perpetrator drugs in PBPK DDI modeling. Furthermore, PBPK modeling can be co-implemented with in vitro cell culture experiments with an increasing concentration of uremic toxins as reviewed above [97]. Correlation analysis combined with a middle-out PBPK approach is another method to explore the impact of uremic toxins on transporter- and metabolism-mediated pathways. We present such correlation analysis in Chapters 3 and 4.

Lastly, to maximally benefit from PBPK modeling, clinical trial designs may need to be designed and coordinated with subsequent PBPK analyses in mind in order to optimize the clinical information available for subsequent modeling (i.e., optimal sampling times to enhance PBPK modeling) [107].

In summary, PBPK modeling and simulation provides exciting opportunities to support quantitative studies in pharmacology, pharmacokinetics, and drug dosing in the setting of kidney disease. PBPK modeling and simulation enables the integration of data from both in vitro and clinical work pertaining to drug-specific parameters, system-specific parameters

and model structure to make mechanistic inferences on drug exposure. PBPK modeling may be used to accurately evaluate kidney function and to mechanistically understand the impact of kidney disease on drug disposition. FDA guidance related to PBPK and conduction of PK studies in kidney impairment will further incentivize model-based dose finding research in kidney disease.

Table 2: Potential factors for evaluation in PBPK modeling in kidney disease

Type of factors	Factors for evaluation in kidney disease PBPK modeling[ab]
Kidney function/renal clearance[c]	GFR, passive reabsorption processes (e.g., tubular water reabsorption, dynamic tubular flow, tubular pH, and microvilli), secretion processes (e.g., renal transporter intrinsic clearance such as OAT1, OAT3, OCT2, OATP4C1, MATE1, MATE2, and P-gp), PTCPGK
Nonrenal elimination pathways[c]	Intrinsic clearance of hepatic enzymes (e.g., CL_{int}, or J_{max} and K_m of CYP3A4 and CYP2C8) and transporters (e.g., OATP1B, P-gp, OCT1, and MATE1), SF of intrinsic clearance, ISEF
System-specific properties	Organ mass or volume (e.g., hepatocyte volume), blood flow, and tissue composition
Drug-specific properties	Tissue affinity, plasma-protein binding affinity, enzymatic stability and transporter activity (e.g., J_{max} and K_m)
Properties of inhibitors and perpetrators in DDI	IC50, K_i (e.g., CYP2C8, CYP2C9, CYP3A4 inhibitors), uremic toxin concentrations (e.g., creatinine, IS, and PCS)

[a.] The list is not comprehensive but it summarizes factors discussed in the examples of PBPK modeling in kidney disease. [b.] The factors which cannot be parameterized in non-compartmental analysis and population PK modeling may be captured by PBPK modeling. [c.] These are of particular of interest in kidney disease modeling and part of either systemic- or drug-specific properties.

Table 3: Key challenges and opportunities in PBPK modeling for dose optimization in kidney disease

Challenges	Opportunities	Examples and considerations
Accurate evaluation of kidney function	• To model detailed components of kidney function [76, 83]	• Reabsorption [108], active secretion, renal tubule, renal enzyme- and/or renal transporter-mediated pathways such as OAT1 and OAT3 may be considered.
Evaluation of the effect of CKD on renally and nonrenally cleared drugs [91] [92]	• To model relevant drug transporters, metabolic enzymes, and/or interplay of transporters and enzymes in CKD and compare it to normal kidney function [93, 97] • To advance *in vitro* experimental techniques [109] • To evaluate influential system- and drug-dependent parameters in sensitivity analysis	• Interplay between CYP3A4 and P-glycoprotein is well-known for many substrates [110] and whether such interplay affects drug exposure in CKD may be considered. • Experiments with Caco-2 cells modified to express CYP3A4 may be designed and corresponding IVIVE equations may be developed.
Evaluation of enzyme- and transporter-mediated DDI in kidney disease	• To incorporate intrinsic clearance (metabolic enzyme and/or transporter activities) and model a perpetrator drug and/or victim drug in kidney disease [79] [82] [81]	• DDI PBPK modeling in new drug development may be routinely conducted in kidney disease to develop dose recommendations in light of DDI FDA guidance [111].
Evaluation of interindividual variability in kidney disease, model-based dose selection for a sub-population of CKD	• To model ADME in a subpopulation of kidney disease • To conduct parameter estimation via PBPK model fitting in kidney disease and correlation analysis of parameter estimates and disease stage/type	• Altered drug disposition in ESRD (off-dialysis), hemodialysis [49, 106], kidney transplant, glomerulonephritis [31] may be modeled and evaluated. • Individualized PBPK modeling of rate data (iPBPK-R) in CKD may be adopted [106].

Table 3: Key challenges and opportunities in PBPK modeling for dose optimization in kidney disease (continued)

Challenges	Opportunities	Examples and considerations
Evaluation of the effect of renal function on drug disposition, accounting for patient characteristics (other comorbidities and different life stages) [112]	• To model ADME in a relevant special population [62] and/or for a particular class of drugs with and without kidney impairment	• Examples of special populations are: CKD patients in oncology [38,42], pediatrics, [15] pregnancy, [113] and geriatrics [41]; CKD patients with hepatic impairment [46, 47, 114], antibiotics, and small biologics (< 60kDa) [45]. • Ontogeny information may be incorporated into a PBPK model in kidney impairment [43, 115].
Development of a mechanistic rationale for dose optimization in kidney disease	• To conduct top-down PBPK modeling and sensitivity analysis to define impactful parameters (system- and drug-dependent parameters) in CKD patients • To use a synthetic modeling approach in *in vitro* experiments [116] [59] and obtain input parameters for PBPK modeling in kidney disease • To incorporate machine learning/AI into PBPK modeling in kidney disease • To collaborate with engineers and computer scientists to conduct efficient modeling and simulations	• Partition coefficients [117], plasma protein binding [93], PTCPGK [77,84], among others may be investigated as potentially influential parameters. • Alternatively, consider collecting in vivo parameter estimates from a large drug database to conduct top-down PBPK modeling in kidney disease [100].

Table 3: Key challenges and opportunities in PBPK modeling for dose optimization in kidney disease (continued)

Challenges	Opportunities	Examples and considerations
Estimation of PBPK parameters towards personalized dosing in kidney disease	• To conduct middle-out PBPK model fitting with a reduced order models • To individualized PBPK model development [105] [99] • To use of more sensitive data than concentration data	• Production rate data in breath samples using volatile organic compounds (e.g., isoprene and trimethylamine) may be investigated with iPBPK-R modeling [118]; *in vivo* parameters for nonrenally elimination pathways may be individually estimated to inform future personalized dosing in CKD.

Table 3: Key challenges and opportunities in PBPK modeling for dose optimization in kidney disease (continued)

Challenges	Opportunities	Examples and considerations
Evaluation of the effect of uremic toxins [119] as potential mechanism of altered drug disposition in kidney disease	• To conduct PBPK modeling to select candidate uremic toxins for designing *in vitro* inhibition experiments • To estimate personalized parameters via individualized PBPK model fitting (iPBPK-R) and conduct correlation analysis of parameter estimates with uremic toxins	• Uremic toxins indoxyl sulfate (IS) and p-cresyl (PCS) sulfate have been found to increase with CKD severity while liver disease is an independent factor to determine the levels of IS and PCS [47]. Inhibition experiments with IS and PCS may inform PBPK modeling for CKD patients with varying liver disease severity.
Evaluation of exposure – response in kidney disease for dose optimization	• To incorporate a PD model into PBPK modeling in kidney disease, develop and validate PBPK models for model-informed precision dosing at the bedside [120]	• PBPK/PD models for drugs to treat diabetes and cancers and antibiotics may be practical examples for CKD patients given their comorbidities, narrow therapeutic index, and PK/PD literature [121].
Development of optimal clinical designs for studying drug exposure via PBPK modeling and simulation	• To conduct research on sampling time points to optimize a PK study design in kidney disease using PBPK modeling, which may influence parameter estimates	• Research to optimize sampling time points for designing clinical trials in CKD may be conducted using Simcyp simulation similarly to Durmont et al [107].

1.6 Hypothesis

We aim to develop a novel PBPK model and measurement procedure, called iPBPK-R, to simultaneously estimate parameters for various hepatic drug elimination pathways in individuals and evaluate the effect of kidney impairment on these pathways. We hypothesized that utilizing a multi-compartment PBPK model with a nested co-optimization procedure, which is a middle-out PBPK-R approach, we can differentiate multiple hepatic elimination pathways and estimate the effects of kidney impairment on these elimination pathways through high time resolution measurements. Application of iPBPK-R method could be further extended to drug concentration data when the data are observed in multiple compartments. To evaluate these hypotheses the following specific aims have been proposed by chapter.

Specific Aim 1. To describe a novel PBPK methodology, iPBPK-R, for indirectly measuring enzyme and transporter properties that are not directly measurable for individuals

Specific Aim 2. To apply iPBPK-R to $^{14}CO_2$ production rate in the erythromycin breath test (EBT) in individual healthy subjects and simultaneously estimate multiple non-renal elimination pathways

Specific Aim 3. To apply iPBPK-R to $^{14}CO_2$ production rate in the EBT in individual patients with CKD and simultaneously estimate multiple non-renal elimination pathways and evaluate the effect of hemodialysis

Specific Aim 4. To evaluate the ability of iPBPK by extending its application to multiple coupled concentration data of temsirolimus and sirolimus in healthy individuals and estimate multiple non-renal elimination pathways and the effect of rifampin on these pathways

2.0 Indirect Measurement of Hepatic Drug Clearance by Fitting Dynamical Models

2.1 Abstract

We present an indirect signal processing-based measurement method for biological quantities in humans that cannot be directly measured. We develop the method by focusing on estimating hepatic enzyme and drug transporter activity through breath-biopsy samples clinically obtained via the erythromycin breath test (EBT): a small dose of radio-labeled drug is intravenously administered and the subsequent content of radio-labeled CO_2 is measured repeatedly in exhaled breath; the resulting time series is analyzed. To model EBT we developed a 14-variable non-linear reduced order dynamical model that describes the behavior of the drug and its metabolites in the human body well enough to capture all biological phenomena of interest. Based on this system of coupled non-linear ordinary differential equations (ODEs) we treat the measurement problem as inverse problem: we estimate the ODE parameters of individual patients from the measured EBT time series. These estimates then provide a measurement of the liver activity of interest. The parameters are hard to estimate as the ODEs are stiff and the problem needs to be regularized to ensure stable convergence. A formal operator framework was developed to capture and treat the specific non-linearities present, and perturbation analysis was performed to establish properties of the estimation procedure and its solution. Development of the method required 150,000 CPU hours at a supercomputing center, and a single production run takes CPU 24 hours. We introduce and analyze the method in the context of future precision dosing of drugs for vulnerable patients (e.g., nephrology, oncology, or pediatrics) to eventually ensure efficacy and avoid toxicity.

2.2 Introduction

Personalized medicine and precision medicine depend on timely and accurate measurement of biological quantities in patients. In particular, measurement of enzyme and drug transporter activity is a key requirement to carefully adjust dosing of potent drugs for at-risk populations. However, it is impossible to directly measure these activities in live humans. In addition, multiple biological pathways such as metabolic enzyme Cytochrome P450 3A4 (CYP3A4) and drug transport (OATPs) are often interacting and their contributions are hard to separate. They require multi-drug cocktail approaches for population-wide (but not individual) activity estimates [122] [123]. A cocktail approach using multiple activity-specific drugs is one way to statistically evaluate multiple biological activities, however, the cocktail approach may be subject to statistical biases. Alternatively, it is possible to indirectly measure biological activities via modeling. Breath biopsy biomarker samples [124, 125] obtained with use of a probe drug is good candidate data for such modeling since it can be sampled at reasonably high frequency and captures the rate of drug metabolism. Such metabolic rate data approximates the first derivative of the concentration of the generated biomarker of interest as function of time in a target organ where researchers are interested in evaluating biological activities/phenotypes in individuals.

In this chapter, we introduce a signal processing based indirect measurement method for drug clearance activities of the liver in individuals, i.e., the elimination behavior of therapeutic drugs of interest. We provide the theoretical underpinning to estimate certain biological quantities that cannot be directly measured in live humans. An additional complexity we address arises from multiple biological processes that may dependently overlap and thus cannot be easily separated. Our work is set in the context of future personalized medicine and precision medicine applications, and thus focusses on establishing the necessary methodological and mathematical foundations for attempting such future applications.

More specifically, we present a signal processing-based indirect measurement method for enzyme and drug transporter activity in the liver of individual patients, called *individualized physiologically based pharmacokinetic modeling of rate data (iPBPK-R)*. We set up a reduced order physiologically based pharmacokinetic (PBPK) model of the human body, i.e., a system

of 14 coupled non-linear ordinary differential equations (ODEs) where drug concentration in tissues of interest are modeled as state variables. The model is accurate enough to capture all biological effects of interest while keeping the number of model parameters low for stable parameter estimation. A graph representation and an operator formalism are introduced to concisely capture and analyze the particular non-linearities involved, and to perform perturbation analysis to assess the quality of the estimation procedure.

iPBPK-R solves an inverse problem to jointly estimate a set of ODE parameters that best fit a given measurement time series. These parameters provide indirect measurements for enzyme and transporter activity of interest. This is a hard optimization problem that needs to be carefully regularized via penalty terms and requires substantial computing resources, due the stiffness and non-linearity of the coupled ODEs and constraints imposed on the parameters by human biology. The method is implemented using R, and its development required 150,000 CPU hours on the *Bridges* supercomputer at Pittsburgh Supercomputing Center (PSC) [126].

For the development of the iPBPK-R method we leveraged data obtained in previous clinical research [127, 128], which was utilizing the erythromycin breath test (EBT): a small dose of the radio-labeled drug erythromycin is intravenously administered, and then the release rate of radio-labeled CO_2 in the patient's breath is measured at eleven time points over two hours. This resolves the initial transient, the saturated maximum, and the terminal slope of drug behavior in the human body. Further, release *rate* of radioactive CO_2 carries higher information content than conventional concentration data. As an aside, the original EBT analysis procedure was simple and inconclusive, preventing clinical use of the EBT [129] [130]. We see potential future opportunities in utilizing a more advanced analysis method like iPBPK-R for not only EBT but other breath biomarker and probe development in this context since non-invasive breath biopsy research is emerging [124, 131].

2.2.1 Related Work

Biological activity in general cannot be directly measured in human. There are many indirect measurement methods such as MRI or PET scans where the response is captured

with the use of magnetic fields or a radioactive tracers, and computationally processed to estimate activities and construct the respective images. Likewise, we propose a method to indirectly measure activities of the metabolic enzyme Cytochrome P450 3A4 (CYP3A4) and drug transporters in the human liver by modeling breath sample data with use of a test probe in individual subjects, and then computing an activity estimate.

In current clinical practice the interpretation of breath samples obtained with the use of a probe drug is simple. This simplicity leads to lower-than-expected accuracy and makes the application of probe drugs less useful despite ease of data acquisition. A key reason is that the assumptions underlying standard criteria do not account for multiple biological or physiological processes as parameters [132] [133]. We propose to remedy this problem via PBPK modeling that can take these multiple parameters into account when estimating enzyme activity from clinical samples.

This contrasts with the standard clinical research method to indirectly estimate different biological activities in human with the use a cocktail approach. There, a subject takes multiple activity-specific probe drugs and all drug concentrations over time are measured. These measurements are analyzed separately to statistically estimate different biological activities associated with respective probe drugs. While a cocktail approach is commonly used, it uses summary statistics not accounting for inter-individual variability or missing micro-interaction among drugs [122] [123]. This is another drawback of current practice that our iPBPK-R approach addresses.

Population PBPK modeling has been intensively used to predict time-course drug concentration in the pharmaceutical industry [59]. While population PBPK may use some estimation features, high-dimensional parameter estimation in individuals using PBPK modeling has not been done. In contrast, we are interested in back-estimating multiple physiological parameters via PBPK model fitting for individuals. In particular, we are interested in using concentration data of *metabolites* (substances the drugs are converted into by its metabolism) or by-products of metabolism. In this context metabolite production rate data measured in breath can be used to approximate the first derivative of metabolite concentration data in compartments of interest in the PBPK model. As the probe dose is low, detailed sampling of the initial phase of drug concentration as function of time can reveal the characteristics of

the system, similar to how impulse responses are used to characterize systems of interest in signal processing theory [134]. In this sense, breath samples provide a more sensitive data set to estimate parameters via the initial behavior after drug infusion, and thus allows us to estimate the multiple parameters compared to less sensitive drug concentration measurements that are usually evaluated in PK research.

2.2.2 Contribution

This chapter introduces and analyzes the mathematical and computational engineering framework behind iPBPK-R, our method to *estimate* un-observable parameters related to drug clearance activity of the liver in *individuals*. iPBPK-R integrates (1) a reduced order PBPK model that contains our parameters of interest, (2) uses IVIVE parameters as reference values in optimization, (3) fits the model to estimate the parameters of interest via nested optimization via a specialized objective functions, (4) utilizes rate data from EBT that resolves the early transient in the drug behavior for indirect measurement, (5) provides per subject modeling to account for inter-individuality, and (6) is implemented in the programming language and free software environment R 3.4.4 that enables features not available in standard PK software. The iPBPK-R method applies a classical signal processing approach in a biological setting. The purpose of this chapter is to establish the mathematical and computational soundness of the method to enable future clinical research.

We specifically make the following contributions:

- To present both iPBPK-R's general mathematical framework and the particular instance parameterized for the EBT as used in a previous clinical study [127, 128].
- iPBPK-R estimates *in vivo* biological quantities by solving a constrained optimization problem that fits a system of non-linear ODEs to clinical rate measurement data.
- To introduce a graph representation of the coupled system of non-linear ODEs and an operator formalism to model and linearize its state-dependent adjacency matrix.
- To utilize this formalism to provide a detailed mathematical analysis of the method, with focus on its constraints and the quality of its parameter estimates.

Our method differs from the prevailing approach in the PBPK community since we do not

predict drug behavior for a population, but *estimate* parameters for *individuals* given clinical measurement (breath) data.

2.3 Background for Method Development

2.3.1 Mathematical Background

We briefly point to the mathematical concepts and methods used in this chapter. The overall approach is following standard signal processing methodology [134]. We use graphs [135] and non-linear ODEs [136] to model the problem and non-linear operators [137–140] to concisely describe the ODEs. We linearize these ODEs and use the theory of linear ODEs with constant coefficients to characterize the solutions via eigen decomposition of the system matrix [141]. We use perturbation analysis [142] to derive bounds and constraints.

We are estimating parameters of the ODEs to fit measurement data, as discussed in [143–147], and view the indirect measurement as inverse problem [148]. The approach leads to non-linear optimization problems [149, 150] that need to be regularized [151] and to be solved numerically [152, 153]. We implement the optimization in R [154].

2.3.2 Pharmaceutical Science Background

In the pharmaceutical industry PBPK modeling is typically used to predict drug concentration behavior over time. A system of ODEs is solved where each ODE is associated with a specific organ/tissue *compartment* and describes the flows of drug concentrations for that compartment [59]. In *population PBPK*, physiologically meaningful parameters related to drug metabolism and transport, for instance in the liver compartment, can be incorporated in the ODEs. Then they are used to predict drug concentrations of the respective compartments for a population [73] [60] [101]. The prediction by PBPK modeling is informative for designing a clinical trial and for deciding drug dosage since potential safety and efficacy margins of drug concentrations can be statistically derived via simulations. However, all predictive models are concerned about their *out-of-samples* setting, the setting where pre-

dictions and conclusions are made outside of the data range and thus likely to be susceptible to statistical uncertainty [155]. The physiological parameter inputs for these predictions are out-of-samples since equations to calculate the properties are typically developed based on multiple unrelated drug properties and thus extrapolate. The *IVIVE* technique described later is one such common calculation technique [64] [156] [157].

Pharmacokinetics (PK). Pharmacokinetics (PK) is the quantitative study of drug and its metabolites over time in the body [5]. Compartmental models are developed with some parameters related to absorption, distribution, metabolism, and excretion (ADME) to describe the time dependency of drug concentration in the body. The simplest model is the *one compartment model* depicted in fig. 1 to describe an intravenously dosed drug concentration $C(t)$ at time t. For example, let k_e be an elimination rate constant for the central body compartment. Then the equation eq. (2.1) is an ordinary differential equation (ODE) describing the change in drug mass A in the central body compartment with respect to time t as follows:

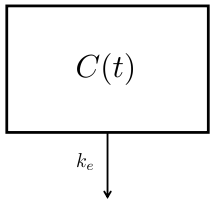

Figure 1: A 1-compartment model.

Equation 1 (Change in drug mass $\boldsymbol{A}$ in 1-compartment model)

$$\dot{A} = -k_e A \tag{2.1}$$

where $\dot{A} = \frac{dA}{dt}$. The result of integration of the ODE eq. (2.1) with the initial condition $C(0) = C_0$ and application of a scaling factor (to convert from mass to concentration) is given by

Equation 2 (Concentration-time curve in 1-compartment model)

$$C(t) = C_0 e^{-k_e t}, \tag{2.2}$$

which describes the actual concentration-time behavior $C(t)$.

Depending on the route of drug dosing and ADME conditions, multiple compartments and parameters can be used in the PK model. In the case of a two-compartment PK model for an intravenously dosed drug (see fig. 2), the general form to describe the change in drug concentration is given in eq. (2.3) and eq. (2.4):

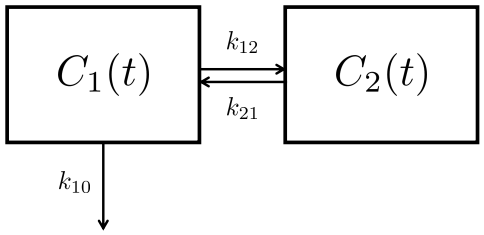

Figure 2: A 2-compartment model.

Equation 3 (Change in drug concentration $\boldsymbol{C_1}$ in 2-compartment model)

$$\dot{C}_1 = -(k_{10} + k_{12})C_1 + k_{21}C_2, \quad \text{and} \tag{2.3}$$

Equation 4 (Change in drug concentration $\boldsymbol{C_2}$ in 2-compartment model)

$$\dot{C}_2 = k_{12}C_1 - k_{21}C_2. \tag{2.4}$$

The concentration in Compartment 1 as a function of time t and can be obtained by solving eq. (2.3) and eq. (2.4) and is given by

Equation 5 (Concentration-time curve for compartment 1 in 2-compartment model)

$$C_1(t) = Pe^{-\alpha t} + Qe^{-\beta t} \tag{2.5}$$

where

$$P = \frac{A_0(\alpha - k_{21})}{\mathrm{V}_1(\alpha - \beta)}, \quad \text{and} \quad Q = \frac{A_0(k_{21} - \beta)}{\mathrm{V}_1(\alpha - \beta)}.$$

Here A_0, α, β, and V_1 are administered drug mass, distribution rate constant, disposition rate constant, and volume of distribution of Compartment 1, respectively.

Physiologically-based pharmacokinetics (PBPK). The concept of PBPK modeling was developed in the 1930's [158] [59]. The entire body is viewed as a system and each organ/tissue is viewed as a compartment. The change in drug mass or concentration in each

organ/tissue is described with an ODE. Then the system of ODEs for the entire body can be solved to evaluate the drug concentrations over time for each compartment. The unique feature of this modeling approach is that physiological parameters are included so that the impact of particular physiological behavior on drug kinetics in the body can be evaluated. As discussed in chapter 1, PBPK models require three components: (1) system-specific properties (e.g., blood flows between compartments), (2) drug properties (e.g., fraction of unbound drug, enzymatic and transporter activities), and (3) the assumed structure of the system compatible with the particular research question at hand (examples are listed in table 4). For more details, see Rowland et al. 2011 [59]. PBPK models can become quite complex depending on the number of compartments. They are typically classified as either full PBPK models or minimum PBPK models. According to Sager et al. [70] a PBPK model with 7 or more compartments is defined as a full model.

fig. 3 shows an example of a simple PBPK model that consists of blood (BL) and liver (LV) compartments with drug elimination from the liver. The changes in drug concentration in the BL compartment and in LV compartment, $\dot{C}_{\mathrm{BL}}$ and $\dot{C}_{\mathrm{LV}}$, are described with the ODEs

Equation 6 (Change in drug concentration $\boldsymbol{C_{\mathrm{BL}}}$ in blood compartment of PBPK model)

$$\dot{C}_{\mathrm{BL}} = \mathrm{Q}_{\mathrm{LV}} \left(\frac{C_{\mathrm{LV}}}{\mathrm{P}_{\mathrm{LV}}} - C_{\mathrm{BL}} \right), \quad \text{and} \tag{2.6}$$

Equation 7 (Change in drug concentration $\boldsymbol{C_{\mathrm{LV}}}$ in liver compartment of PBPK model)

$$\dot{C}_{\mathrm{LV}} = \mathrm{Q}_{\mathrm{LV}} \left(C_{\mathrm{BL}} - \frac{C_{\mathrm{LV}}}{\mathrm{P}_{\mathrm{LV}}} \right) - \mathrm{CL}_{\mathrm{NR}} C_{\mathrm{LV}}, \tag{2.7}$$

where Q_{LV} is the blood flow into the liver, P_{LV} is the partition coefficient of the liver to the blood (a property of tissue affinity), and $\mathrm{CL}_{\mathrm{NR}}$ is the clearance of drug from the liver (non-renal clearance).

In-vitro in-vivo extrapolation (IVIVE). IVIVE extrapolates the mean value of an *in vivo* (clinically relevant) physiological parameter as a function of a corresponding *in vitro* (experimentally/via bench work) obtained value [67] [64]. For example, metabolic clearance activity of CYP3A4 in human (*in vivo* clearance) for a particular drug can be calculated using eq. (2.8) [159] [66].

Table 4: Properties used in PBPK modeling

System-specific properties	organ mass or volume, blood flow, and tissue composition
Drug-specific properties	tissue affinity, plasma-protein binding affinity, membrane permeability, enzymatic stability, and transporter activities
The structural model	a compartmental structure with relationships among compartments for answering research questions (see [59])

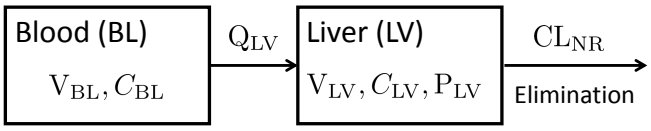

Figure 3: A simple PBPK model.

Equation 8 (IVIVE equation for metabolic clearance activity of CYP3A4)

$$\mathrm{CL_{H,int,CYP3A4}} = \mathrm{CL_{int,rhCYP3A4}}\,\mathrm{abundance_{CYP3A4}}\,\mathrm{ISEF_{CYP3A4}}\,\mathrm{MPPGL}\,\mathrm{LW}. \tag{2.8}$$

Here, $\mathrm{CL_{int,rhCYP3A4}}$ is the intrinsic clearance in recombinant CYP3A4 (*in vitro* clearance) calculated from experimentally obtained enzyme kinetic parameters [μL/min pmol of CYP3A4], $\mathrm{abundance_{CYP3A4}}$ is the amount of CYP3A4 enzyme per unit microsomal protein [pmol of CYP3A4/mg of protein], $\mathrm{ISEF_{CYP3A4}}$ is intersystem extrapolation factor for CYP3A4. MPPGL is the amount of microsomal protein per unit liver [mg of protein/g of Liver], and LW is the human liver weight(g).

Generally, a value calculated via an IVIVE method is subject to substantial variability

on the log scale. For example, experimentally determined ISEF for CYP3A4 clearance has a large 95% confidence interval: according to Proctor et al. 2004 [156] its upper bound is 5.2×10^3 times as high as its lower bound. Furthermore, the calculated metabolic in vivo clearance shown in Figure 1 of Chiba et al. 2009 [66] does not have a strong correlation with experimentally determined in vitro metabolic clearance since the correlation graph is shown in a log-log plot that implies a non-existent (linear) correlation. (Note that a linear regression with unit variance in a log-log plot implies a polynomial correlation with an order of magnitude variance.) Accordingly, the relationship between IVIVE-predicted value and the respective observed *in vivo* value is a unique feature of a particular drug substrate. This indicates that the generalization of such a relationship to other drugs produces bias in IVIVE-based predictions as this is extrapolation in an *out-of-samples* setting.

A scaling factor derived from regression in a log-log plot usually does not predict in vivo metabolic clearance consistently. Therefore, it is not possible to estimate *a particular subject's* in vivo parameters using an IVIVE derived scaling factor given the low predictive power and great variability of this scaling factor. In contrast, we are estimating an *adjustment factor* via PBPK modeling that measures the size of deviation from the baseline IVIVE-based activity in the given subject to estimate the individual's activity of a biological process.

Prediction. As we discussed at the beginning of this section, PBPK modeling is typically used to predict drug concentration-time behavior and evaluate its PK characteristics for particular populations. It is extensively used in the pharmaceutical industry to support decision-making in drug development. To predict drug concentration behavior PBPK modeling requires various parameter inputs of system-specific properties and drug-specific properties (see table 4). Furthermore, researchers can assume some distributions on those parameters and generate distributional parameter inputs for PBPK modeling using Monte Carlo approaches or similar methods. As a result the simulated drug concentration-time curves will vary broadly and have to be statistically summarized. For instance, simulations provide the mean, 95 % confidence interval (95 % CI), median, minimum, maximum, etc. Due to the broader range of simulation curve outputs and the large number of input parameters, PBPK modeling is usually used to construct the statistical bounds of drug safety. In the literature the allowed cutoff for good performance of prediction varies. Typically, mean

ratios of predicted and observed maximum concentration, time to peak, and areas under the concentration-time curves are often considered to be comparable in PK literature if they are within 2 times of observed data [101] [90] [102] [93].

Standard software. A number of software tools are available to conduct PBPK simulations, including the Simcyp Simulator and NONMEM [59]. The Simcyp Simulator was originally developed by Simcyp Ltd. and later acquired by Certara USA, Inc. [160]. This software includes demographic, physiologic and genomic databases so that it provides PBPK modeling for a virtual population that researchers are interested in studying. Various virtual populations can be generated with the Simcyp simulator. This feature allows researchers to evaluate relationships between modeled drug behavior and variability in demographic, physiologic and/or genomic parameters of the interested virtual population prior to conducting a clinical trial. For instance, using a statistical distribution of liver weight for a virtual population, IVIVE calculation of drug property parameters can be implemented. These distributions are subsequently used to simulate drug behavior in the virtual population. Since the Simcyp simulator allows researchers to design clinical PK studies for simulations in a virtual population, the software is frequently used to support decision making in drug development by pharmaceutical companies and regulatory agencies. The Simcyp simulator has some parameter estimation features as well. However, accuracy for high-dimensional parameter estimation is not guaranteed given the large number of parameters used in the simulator.

NONMEM is FORTRAN-based biomathematical modeling software that allows users to explicitly specify mathematical models [59]. It is commercialized by ICON [161]. NONMEM is frequently used for population PK and PK-pharmacodynamic (PD) modeling and also can be used for PBPK modeling. Various parameter estimation methods are available in NONMEM. NONMEM also offers many options for graphically checking model predictions. There are limitations in the allowed number of compartments for user-defined systems of ODEs and types of parameters supported for estimation. Furthermore, there is no flexibility in specifying objective functions and conducting nested co-optimization. The speed of computation is also limited since the software license makes it hard (expensive) to use NONMEM in a high performance computing and batch/cloud computing environment.

ADAPT 5 is another FORTRAN-based biomathematical modeling software. It was developed at the University of Southern California [162] [163]. It offers great flexibility in model specifications, study design options, and parameter estimation algorithms, which enables custom PK/PD modeling. Its flexibility is limited in terms of specification of objective functions, implementation of nested optimization and co-optimization, and the type of observed data.

Custom approaches. All the software discussed so far requires researchers to learn the syntax of legacy programming languages like FORTRAN in combination with system-specific commands and features. This hampers more customized PBPK modeling and for method research as in our case with individualized breath sample modeling. Thus, fully custom approaches are sometimes needed.

R is a free statistics-centered programming languages with a large library of mathematical modules [164]. While R is intensively used for data analysis, PBPK modeling can be implemented with R. For example, ODEs for PBPK modeling need to be explicitly defined in a R script but the set of the ODEs can be easily solved with standard solvers. General and powerful optimization methods are available for model fitting and parameter estimation. This in turn allows for any type of observed data to be modeled, including breath rate data of interest to us. In addition, parameters can be co-optimized to model, for example, dependent behavior across two distinct phases of an clinical intervention. In our work we use this capability to correlate behavior before and after dialysis within patients with kidney disease where some parameters are estimated independently and some are estimated consistently across the two phases.

Therefore, iPBPK-R was developed in the R environment so that nested co-optimization and advanced objective functions can be implemented, and to fine tune the configuration of optimization and ODE integration routines. In particular, we use the *deSolve* package that implements a suite of ODE solvers, including explicit and implicit solvers, adaptive solvers, and Runge Kutta solvers [165] [166] and the R function *optim* that implements Nelder-Mead, quasi-Newton, and conjugate-gradient algorithms [167]. iPBPK-R cannot be implemented with standard PBPK software such as Simcyp and NONMEM since their degree of freedom supported in scripts is far more limited.

2.3.3 Erythromycin Breath Test (EBT)

EBT was originally developed to measure one type of enzyme activity that metabolizes the radio-labeled drug ^{14}C-erythromycin in the liver [168]. EBT is based on the premise that as the drug undergoes the CYP3A4-mediated metabolic pathway, radio-labeled carbon dioxide ($^{14}CO_2$) is released as a final by-product. A noninvasive low dose of ^{14}C-erythromycin is intravenously administered to a subject and breath samples containing $^{14}CO_2$ are collected over 2 hours.

In the clinical setting breath samples were collected before and after a certain change in the subject's state. Then, the EBT's $^{14}CO_2$ production rate data (measured as a percentage of dose exhaled per minute) was originally interpreted via one of the following criteria as shown in fig. 4: the CYP3A4 enzyme activity in the liver increased *if* (1) the time to peak of the breath rate within 2 hours shortened, *or* (2) the area under the curve increased, *or* (3) or the measured $^{14}CO_2$ production rate at 20 minutes increased post the state change. However, other physiological activities (not just one enzyme activity) also seemed to play in eliminating the drug from the liver (e.g., activities in drug transporters) [169] [170] [171], and these original criteria were inconclusively estimating did not necessarily lead to a successful association with the drug's overall clearance from the body [129] [130]. This led to the consensus that (at least with the classical interpretation) the EBT was not accurate enough for clinical measurement of CYP3A4 activity. iPBPK-R is revisiting this conclusion and shows that with more detailed modeling and a more careful interpretation EBT data can provide conclusive information regarding CYP3A4 activity and other physiological factors.

2.4 Mathematical Framework of iPBPK-R

In this section we describe the overall structure of the iPBPK-R approach. We discuss the problem setup, modeling of the clinical use case, the general structure of the non-linear reduced order model, and the parameter estimation approach. Finally, we discuss the limits of parameter estimation in our setup. In section 2.5 and section 2.6 we will then discuss the

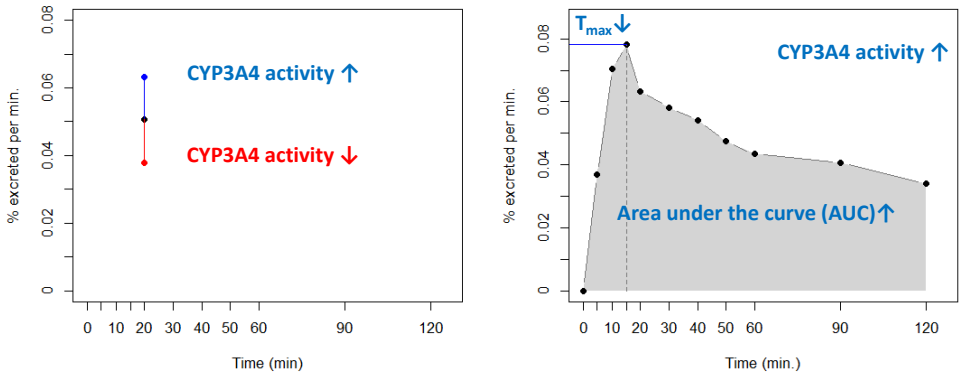

Figure 4: $^{14}CO_2$ production rate at 20 minutes (left) and for 2 hours (right).

instantiation of the general method described in this section for the EBT and the enzyme CYP3A4 activity as used in the results discussed in section 2.7.

2.4.1 Problem Description and Approach

The key idea of iPBPK-R is to develop an *indirect measurement method* to measure (or estimate) values in a particular patient for physiological parameters that cannot be measured directly. The indirectly measured values are *maximally compatible* with the underlying model and samples, i.e., they are model parameters that minimize the mismatch between (noisy) data and a model that is rich enough to capture the measured behavior but simple enough so the estimation is a well-posed inverse problem. Statistically speaking, we are interested in estimating parameters in a *within sampling* setting as opposed to *out-of-samples* setting: given clinically observed breath rate data due to a single probe drug (i.e., EBT), PBPK model fitting (but not prediction) will be used to inversely solve for physiologically meaningful parameters.

Approach. iPBPK-R integrates several methods for conducting multiple-parameter estimation. It is based on a reduced order PBPK model, which is parameterized by our

physiological parameters of interest. IVIVE parameters are utilized as initial guesses that are adjusted for individual subjects based on their measurement data. These IVIVE parameters are also used as constraints in the estimation procedure to ensure biological plausibility. The actual parameter estimation is implemented via optimization to fit the measurements to the reduced model by varying the physiological parameters of interest to minimize the discrepancy between noisy measurement data and the model. Estimation is done via nested optimization or nested co-optimization and utilizes a specialized metric and bias terms. Estimating parameters via the specialized nested optimization approach based on measured breath rate data allows us to resolve the early transient in the drug behavior at both rate-limiting and non-rate limiting steps of the multiple elimination pathways.

Software system. Standard optimization software packages are too general to adapt to a particular pharmacokinetics optimization problem, and there is no guarantee that the parameter estimates are physiologically meaningful solutions even when they are ever obtained by fitting a system of ODEs to measured data using standard metrics. Further, iPBPK-R cannot be implemented in standard PK or PBPK software since multiple-parameter optimization must be carefully tailored to the estimation problem by developing a specialized objective function and constraint terms. Thus, we implemented the iPBPK-R in the R system. However, any high-level computer language can be used to implement iPBPK-R and its modeling and optimization components.

Highly sensitive indirect measurement. PBPK modeling is rarely used for parameter estimation of individual subjects, partly since clinically obtained drug concentration data is too noisy to capture sensitive changes in the physiological parameters needed to estimate the physiological parameters of interest. We overcome this issue by borrowing the idea of parameter estimation by fitting data to a reduced order model from signal processing and indirect physics measurements as we developed iPBPK-R for high-dimensional parameter estimation in our use case. We utilize observed concentration *change* data (*rate* data), which at the same sampling rate and accuracy has higher information contents compared to drug concentration data. iPBPK-R enables us to estimate per-person physiological parameters which are otherwise difficult to capture. The enabling idea is model fitting to measured rate data of individual subject that was collected with a single probe. We anticipate that

iPBPK-R is useful for estimating parameters related to in vivo drug elimination pathway activities simultaneously, and that these estimates are useful for determining individualized drug dosage. This is a step towards personalized medicine that utilizes current biological activity in individuals as decision criterium.

2.4.2 Clinical data: EBT

General background of EBT was provided in section 2.3.3. We now discuss how EBT is modeled in our reduced order model. Recall that a subject receives a single 0.074 mmol short-time intravenous (IV) bolus dose of ^{14}C-erythromycin. This is modeled as a constant-rate influx of drug into the patient. Breath samples are collected at 11 time points within two hours of IV dosing, including the baseline time point prior to dosing [128] [127] (see fig. 5). The sampling time points are unequally spaced: breath is measured more often at early on and then at a lower sampling rate towards the end of the 2 hours. The contents of $^{14}CO_2$ in the breath samples is measured and $^{14}CO_2$ production rates are calculated at each time point from the exhaled volume and $^{14}CO_2$ content.

$^{14}CO_2$ production rate data in an individual's breath is approximately proportional to the first derivative of drug concentration data, i.e. drug concentration change. In clinical settings, breath can be sampled faster over a prolonged period of time compared to drug concentration in the blood, and this higher sampling frequency leads to more accurate estimates when utilized in iPBPK-R. Potential sources of inaccuracies in measuring $^{14}CO_2$ production rate via breath samples: 1) actual breath sampling times may deviate from the designed sampling time points, 2) inconsistent analysis procedure or inaccuracies when measuring $^{14}CO_2$ in breath samples, and 3) inconsistent breathing output by the individual during the EBT. These inaccuracies need to be addressed but in experiments so far did not lead to inaccurate indirect measurements via iPBPK-R.

2.4.3 Reduced Model

We now describe the general shape of our reduced model. This model is underlying the modeling approach and is instantiated for EBT in section 2.5. fig. 6 shows a simple three

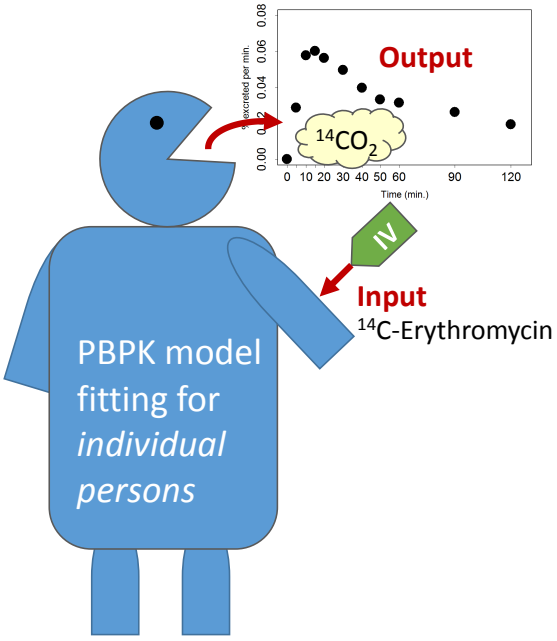

Figure 5: Erythromycin breath test (EBT).

compartment model and all associated quantities used in the discussion below.

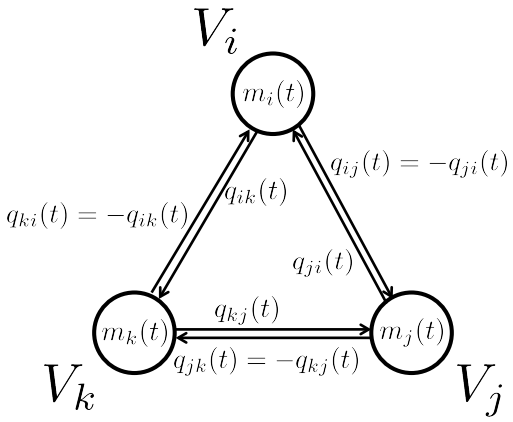

Figure 6: Example graph for a 3-compartment model.

Compartments. The reduced model underlying iPBPK-R is given by a system of nonlinear ordinary differential equations (ODEs) for time $t \geq 0$, that is described as a graph

Equation 9 (Graph for a system of nonlinear ordinary differential equations (ODEs))

$$\mathrm{G} = (\mathrm{V}, \mathrm{E}, \mathrm{W}). \tag{2.9}$$

The set of n vertices $\mathrm{V} = \{V_1, \ldots, V_n\}$ abstracts the compartments. Each compartment V_i has a state variable

$$m_i(t),\ t \geq 0 \quad \text{with} \quad m_i(0) = M_i$$

that is a function of time and expresses the amount of drug mass in compartment V_i at time t. Our model is a closed system: No mass ever enters or leaves the system. This is expressed through the system invariant

Equation 10 (System invariant for mass balance)

$$\sum_{i=1}^{n} m_i(t) = M_0 \quad \textit{for all} \quad t \geq 0, \tag{2.10}$$

where M_0 is the constant drug mass in the system.

Mass flows. The set of edges $\mathrm{E} \subseteq \mathrm{V} \times \mathrm{V}$ captures the channels between compartments. The graph G is a directed graph. Edges $e_{ij} = (V_i, V_j)$ and $e_{ji} = (V_j, V_i)$ are together representing the channel between compartments V_i and V_j for $1 \leq i, j \leq n$. We require that if edge e_{ij} is present then the e_{ji} is present as well, i.e., channels can be viewed from the perspective of either compartment V_i or V_j.

The graph G is a weighted graph. The weight $w_{ij} \in \mathrm{W}$ on edge e_{ij} is given by the mass flow function

$$w_{ij} = q_{ij}(t) \quad \text{for} \quad e_{ij} \in \mathrm{V} \times \mathrm{V},$$

which expresses the flow of drug mass from compartment V_i into V_j over the edge e_{ij} as function of time t. We define

$$q_{k\ell}(t) \equiv 0 \quad \text{if} \quad e_{k\ell} \notin \mathrm{V} \times \mathrm{V},$$

i.e., for edges that do not exist. As an aside, we use the common notation m for mass, and $q = \dot{m} = \frac{dm}{dt}$ for mass flow, i.e., mass flow is the first derivative of mass. Note that $q_{ij}(t)$ and $q_{ji}(t)$ denote the same physical flow, but represented from the perspective of compartment V_i and V_j as flow source, respectively. There are no self flows, i.e., $q_{ii}(t) \equiv 0$ for all $1 \leq i \leq n$. This provides another key invariant of our model,

Equation 11 (System invariant for mass flow)

$$q_{ij}(t) = -q_{ji}(t) \quad \textit{for all} \quad t \geq 0. \tag{2.11}$$

The graph G has a time-dependent anti-symmetric adjacency matrix

$$A(t) = [q_{ij}(t)]_{1 \leq i,j \leq n} \in \mathbb{R}^{n \times n}$$

that concisely captures the system of ODEs. The initial conditions of the system of ODEs are given by

$$m_i(0) = M_i.$$

State equations and invariants. Note that in our model some compartments V_i are *sources* for which all flow $q_{ij} \geq 0$ are non-negative (thus, they are out-flows), and some compartments V_i are *sinks* for which all flow $q_{ji} \geq 0$ are non-negative (thus, they are in-flows). The non-linearity of the model arises through non-linearities of certain flow terms $q_{ij}(t)$ that are induced, for instance, through a Michaelis-Menten style saturation. This is a special kind of monotonically increasing and differentiable non-linearity that does not pose a fundamental issue.

The closed system assumption of eq. (2.10) provides that for each compartment V_i the change of drug mass contents is the sum of all flows $q_{ji}(t)$ from all other compartments $V_j, j \neq i$ to the compartment V_i, and since $q_{ii}(t) \equiv 0$ we obtain

Equation 12 (Change in drug mass as a function of mass flows)

$$\dot{m}_i(t) = \sum_{j=1}^{n} q_{ji}(t), \tag{2.12}$$

as mass can only enter or leave a compartment V_i through a mass flow q_{ij}.

We now show that the anti-symmetry of the mass flows defined by eq. (2.11) and the definition of compartment mass change as sum of mass flows given by eq. (2.12) are sufficient for the ODE system invariant eq. (2.10) to hold. The proof is shown in appendix A.1.

Theorem 1 (Mass balance invariant) *For a model* $\mathrm{G} = (\mathrm{V}, \mathrm{E}, \mathrm{W})$ *as defined above, and* $t \geq 0$ *it holds that*

$$q_{ij}(t) = -q_{ji}(t) \quad \textit{and} \quad \dot{m}_i(t) = \sum_{j=1}^{n} q_{ji}(t) \quad \Rightarrow \quad \sum_{i=1}^{n} m_i(t) = M_0.$$

Finally, note that the change of drug mass contents in compartment V_i expressed in eq. (2.12) is a sum of mass flow $q_{ji}(t)$. Drug mass $m_i(t)$ in V_i at time t can be converted to

drug concentration $C_i(t)$ at time t when $m_i(t)$ is divided by the volume of compartment V_i.

Concentration based model. In Clinical Pharmacology, it is common to express models via drug concentration and its time-dependent change,

$$C_i(t) = \frac{m_i(t)}{V_i} \quad \text{and} \quad \dot{C}_i(t) = \frac{\dot{m}_i(t)}{V_i},$$

respectively (here V_i denotes the volume of the ith compartment), while mass-based equations allow for clearer mathematical treatment of the ODEs. Thus, in pharmacological discussions we will use $C(t)$ and $\dot{C}(t)$ while mathematical discussions will use $m(t)$ and $\dot{m}(t)$, respectively.

2.4.4 Reduced Model as a System of Non-linear ODEs

In this subsection, we define a framework that allows us to describe the system of non-linear ODEs eq. (2.12) via the time-dependent adjacency matrix eq. (2.12) similar to how a system of linear first order ODEs with constant coefficients is described through its constant system matrix. Thus, we express the system of non-linear ODEs eq. (2.12) that underlies iPBPK-R's reduced model as a small deviation of a classical system of in-homogeneous linear ODEs. We specifically show that the particular non-linearity of the reduced model can be expressed with a matrix of scalar differentiable monotonically growing functions of the current state. The formalization naturally generalizes the system matrix of linear ODEs and the matrix-vector product capturing systems of ODEs. The formalization is derived for mass change in molecular weight.

Definitions and conventions. Vectors $x \in \mathbb{R}^n$ are always *column vectors* to allow for matrix-vector products. When necessary to understand equations, we annotate vectors as $\vec{x}$. Transposition of the vector x is denoted by x^T. When the entries of the vector are needed, we denote them as $x_i,\ 1 \leq i \leq n$ and the vector x can be written as $x = (x_i)_{1 \leq i \leq n}$. Real $m \times n$ matrices are denoted as $\mathbf{A} = [a_{ij}]_{1 \leq i \leq m, 1 \leq j \leq n} \in \mathbb{R}^{m \times n}$. Further, the direct sum of two vectors $\oplus$ is defined as

Equation 13 (Convention for direct sum of two vectors)

$$(x_1, \ldots, x_m)^\mathsf{T} \oplus (y_1, \ldots, y_n)^\mathsf{T} = (x_1, \ldots, x_m, y_1, \ldots, y_n)^\mathsf{T}. \tag{2.13}$$

We define the *indicator function of the set* $\Omega \subset \mathbb{R}$,

Equation 14 (Definition of indicator function for $\mathbf{\Omega} \subset \mathbb{R}$)

$$\mathrm{I}_{\Omega}(.) : \mathbb{R} \to \mathbb{R};\, x \mapsto \begin{cases} 1, & x \in \Omega \\ 0 & \text{else,} \end{cases} \tag{2.14}$$

that is called *gating function* in the context of iPBPK-R as it is used to model the IV infusion of the drug. The *Michaelis-Menten* function $\mathrm{MM}_{\mathrm{a,b,c}}$ is a hyperbolic function that is parameterized by three constants a,b, and c,

Equation 15 (Michaelis-Menten function parameterized by three constants)

$$\mathrm{MM}_{\mathrm{a,b,c}}(.) : \mathbb{R} \to \mathbb{R};\, x \mapsto \frac{ax}{b + cx}. \tag{2.15}$$

It is the main non-linearity used in the reduced model, and it is a monotonically increasing differentiable function. The parameters capture the initial slope and the asymptotic value of the function. Note that two parameters would be sufficient to uniquely define a Michaelis-Menten function, but in our application the three-parameter formulation is more convenient. Finally, scaling the input of a Michaelis-Menten function $\mathrm{MM}_{a,b,c}$ with a real constant α results in a new Michaelis-Menten function

Equation 16 (Michaelis-Menten function with a parameter transformation)

$$\mathrm{MM}_{a,b,c}(\alpha x) = \mathrm{MM}_{\alpha a,b,\alpha c}(x), \tag{2.16}$$

i.e., rescaling of the input is a parameter transformation.

We denote a function $f(.)$ that depends on a parameter vector p as $f^p(.)$. In our case the parameters p_i that constitute the vector p (i.e., $\vec{p} = (p_i)_{1 \leq i \leq \ell}$) are to be optimized during estimation.

Notation for non-linear operators. We unify the notation for linear and non-linear vector-valued functions of vectors. This will allow us to analyze the system of non-linear ODEs with its very particular type of non-linearity via its linearization, and to obtain a good characterization of the original non-linear system with respect to parameter estimation. We follow the notation and ideas developed in [139] [138]. Recall that all linear mappings are given by a matrix and the respective matrix-vector product. We define the operator $\bar{\mathbf{A}}(.)$ that is induced by the matrix $\mathbf{A}$,

Equation 17 (Definition of operator $\bar{\mathbf{A}}(.)$)

$$\bar{\mathbf{A}} : \mathbb{R}^n \to \mathbb{R}^m;\, x \mapsto \mathbf{A}x \quad \textit{with} \quad \mathbf{A} \in \mathbb{R}^{m \times n}. \tag{2.17}$$

With this notation we can write $\bar{\mathbf{A}}(x)$ for the matrix-vector product $\mathbf{A}x$ and thus do not have to distinguish linear and non-linear operators. When clear from the context, we may drop the $\bar{(.)}$ and write $\bar{\mathbf{A}}(.) = \mathbf{A}(.) = \mathbf{A}$, i.e., in this case we do not distinguish the matrix and its induced operator as they are essentially the same.

We next generalize the matrix-vector product to matrices where the entries are scalar functions. Assume that entries at location (i, j) of a $m \times n$ matrix $\mathbf{B}$ are scalar functions

Equation 18 (Entries $\boldsymbol{b_{ij}(.)}$ of matrix $\mathbf{B}$ as scalar functions)

$$b_{ij}(.) : \mathbb{R} \to \mathbb{R};\ x \mapsto b_{ij}(x). \tag{2.18}$$

We use $\mathbf{B}$ to define the *non-linear operator* $\mathbf{B}(.)$ as

Equation 19 (Nonlinear operator $\mathbf{B(.)}$)

$$\mathbf{B}(.) : \mathbb{R}^n \to \mathbb{R}^m;\ \mathbf{B}(x_1, \ldots, x_n) = (y_1, \ldots, y_m) \quad \textit{with} \quad y_i = \sum_{j=1}^{n} b_{ij}(x_j). \tag{2.19}$$

The definition of $\mathbf{B}(.)$ is compatible with and generalizes the standard matrix-vector product. Finally, we define operator addition $\mathbf{U}(.) + \mathbf{V}(.)$ as

Equation 20 (Operator addition $\mathbf{U(.) + V(.)}$)

$$\big(\mathbf{U}(.) + \mathbf{V}(.)\big)(x) = \mathbf{U}(x) + \mathbf{V}(x), \tag{2.20}$$

compatible with the usual addition of matrices.

Reduced model ODE as non-linear operator. With the notation introduced above we now describe the system of non-linear ODEs concisely as a sum of operators. Our state vector is the vector of mass in all compartments of the n-compartment model, $\vec{m} = (m_i)_{1 \le i \le n}$. The forcing function

$$z(t) = (0, \ldots, 0)^{\mathsf{T}} \oplus \tau \mathrm{I}_{[0,t_0]}(t) \oplus (0, \ldots, 0)^{\mathsf{T}} \tag{2.21}$$

models the IV injection of the drug as constant-rate for the time interval $\Omega = [0, t_0]$. The linear part of the system of ODEs is given by a real $n \times n$ matrix $\mathbf{X}$. All non-linearities are collected in the $n \times n$ matrix of scalar functions $\mathbf{Y} = \big[y_{ij}(.)\big]_{i,j}$ where all entries $y_{ij}(.)$ are either the *zero function* $\bar{0}(.)$, a Michelis-Menten function, or a sum of two Michelis-Menten

functions,

$$y_{ij}(.) = \begin{cases} \bar{0}(.) \\ \mathrm{MM}_{a,b,c}(.) \\ \big(\mathrm{MM}_{a,b,c}(.) + \mathrm{MM}_{d,e,f}(.)\big)(.) \end{cases} . \tag{2.22}$$

The matrix of functions $\mathbf{Y}$ is used as operator $\mathbf{Y}(.)$ as defined in (2.19).

With these definitions, the full system of non-linear ODEs is given by

Equation 21 (System of nonlinear ODEs using operators)

$$\frac{d\vec{m}}{dt} = \mathbf{X}\vec{m} + \mathbf{Y}(\vec{m}) + z(t). \tag{2.23}$$

Using the promotion of matrix $\mathbf{X}$ to the linear operator $\bar{\mathbf{X}}(.)$, we can define the non-linear operator

$$\mathbf{M}(.) = \big(\bar{\mathbf{X}}(.) + \mathbf{Y}(.)\big). \tag{2.24}$$

Dropping the $\vec{(.)}$ annotation from $\vec{m}$ we can now write the full system of non-linear ODEs concisely as

Equation 22 (System of nonlinear ODEs with weighted graph matrix $\mathbf{M(.)}$)

$$\dot{m} = \mathbf{M}(m) + z(t). \tag{2.25}$$

Note that $\mathbf{M}(.)$ is the state-dependent adjacency matrix of the weighted graph abstraction of the n-compartment model introduced in section 2.4.3 and captures the state-dependent mass flows q_{ij} (depending on m_i and m_j). Thus, analysis of the solution of (2.25) and convergence and uniqueness of parameter estimation via optimization is reduced to analyzing $\mathbf{M}$.

By construction, the non-linear behavior of $\mathbf{M}$ is limited to Michaelis-Menten saturation. Given the well-understood behavior of systems of linear ODEs and the particular type of non-linearity, we are able to analyze solution properties of (2.25) via perturbation analysis of the entries of $\mathbf{M}$ and by analyzing the linearized bounds of $\mathbf{M}$. This is done in section 2.4.6.

2.4.5 Modeling the Measurements

So far, we have defined a system of ODEs with eq. (2.12) and eq. (2.25), which describes the change in drug concentration and the change in drug mass over time for all compartments. Next we model the pathway of the drug by-product $^{14}CO_2$ from the liver to the breath and

its ultimate concentration measurement in the breath. This is described as a measurement operator $\mathcal{F}(.)$ that maps the solution vector $\vec{C}(t)$ of (2.25) (in drug concentration form) to a scalar function $B(t)$.

Measurement function. We describe the relationship between the solution of the n compartment model $\vec{C}(t) = \big(C_i(t)\big)_{1\leq i\leq n}$ and the breath-time function $B(t)$ to be measured abstractly as given by an operator

$$\mathcal{F}(.) : (\mathbb{R} \to \mathbb{R}^n) \to (\mathbb{R} \to \mathbb{R}). \tag{2.26}$$

The operator $\mathcal{F}(.)$ maps a vector-valued time-dependent function (the solution of the ODE) to a scalar time dependent function (the $^{14}CO_2$ content in the breath). In the case of the EBT this models the part of the drug which enters the metabolism pathway in the liver and subsequently produces $^{14}CO_2$ traveling to the lung to get released in the breath. We call the operator $\mathcal{F}(.)$ the *measurement function* as it models how the final measurement is derived from the solution of the ODE. The measurement function is not part of the dynamical system as it does not feed back into the ODE.

Note that the clinical measurement in EBT is $^{14}CO_2$ production rate in the breath of the subject, $B(t)$. Under the assumption of instantaneous metabolism of the drug in the liver and instantaneous transfer of $^{14}CO_2$ from the liver (denoted as compartment j) to the lung we define

Equation 23 (Operator $\boldsymbol{\mathcal{F}(.)}$ to map the solution of the ODE to breath $\mathbf{^{14}CO_2}$ rate)

$$\mathcal{F}(.) : (\mathbb{R} \to \mathbb{R}^n) \to (\mathbb{R} \to \mathbb{R});\ (f_i(t))_{1\leq i\leq n} \mapsto \frac{df_j(t)}{dt}. \tag{2.27}$$

Via an application of (2.27) to the solution of the system of ODEs, $\vec{C}(t)$, the operator $\mathcal{F}(.)$ returns the breath function or the first derivative of the concentration of the liver compartment (denoted as jth compartment), i.e.,

Equation 24 ($\mathbf{^{14}CO_2}$ production rate in the breath $\boldsymbol{B(t)}$ using $\boldsymbol{\mathcal{F}(.)}$)

$$B(t) = \mathcal{F}(\vec{C}(t)) = \dot{C}_j(t). \tag{2.28}$$

More realistic variants of $\mathcal{F}(.)$ could be defined to model the transfer of $^{14}CO_2$ from the liver to the lung more accurately. The exact equation used in this work and its underlying model assumptions will be provided in section 2.6.

Comparing model and measurement. Next we define how to compare the modeled

breath function $B(t)$ as defined in (2.28) to clinical breath rate measurements. We assume that a set of measurements consist of T samples $m_\ell = (t_\ell, w_\ell)$ measuring $^{14}CO_2$ production rate taken at time points t_ℓ for $\ell = 1, \ldots, T$. We collect the samples in a vector of 2D points, $\vec{S} = \big((t_\ell, w_\ell)\big)_{1 \le \ell \le T} \in \mathbb{R}^{T \times 2}$. Our goal is to compare the simulated measurement $B(t)$ with the sampled clinical measurement vector $\vec{S}$. We define a distance function $d(.,.)$ to denote the distance (or disagreement) between the simulated function and the sampled data,

$$d(.,.) : (\mathbb{R} \to \mathbb{R}) \times \mathbb{R}^{T \times 2} \to \mathbb{R}. \tag{2.29}$$

A straight-forward example for a distance function $d(.,.)$ would be the L_2 norm of the breath function $B(t)$ evaluated at the sample time points t_ℓ minus the measured data at the same time points,

Equation 25 ($\mathbf{L_2}$ norm distance between breath function $\boldsymbol{B(t)}$ and observed data $\boldsymbol{\vec{S}}$)

$$d_2(\mathcal{F}(\vec{C}(t)), \vec{S}) = d_2(B(.), \vec{S}) = \|(B(t_\ell))_\ell - (w_\ell)_\ell\|_2, \quad \ell = 1, \ldots, T. \tag{2.30}$$

The definition of (2.30) is provided as an example to make the discussion in section 2.4.6 more understandable. We will use the generic function $d(.,.)$ in the remainder of this section as we will use a variety of such functions to handle systematic measurement problems, misalignment, and penalty terms used to steer the parameter estimation via optimization. We present the full definition and detailed discussion of the actually used distance functions in section 2.6 when the detailed model and estimation procedure is presented.

2.4.6 Parameter Estimation via Optimization

The estimation of biological parameters is cast as an optimization problem that fits a dynamical model (system of ODEs) to measurement data. The biological parameters of interest are derived from the estimated ODE parameters that produce the best fit. Formally, we aim to find a vector $\vec{r}$ that parameterizes the system of ODEs (2.25) (in concentration form) so that the distance $d(.,.)$ in (2.29) for a given measurement vector $\vec{S}$ is minimized. Further, constant parameters are captured by a parameter vector $\vec{u}$. Therefore the flow terms $q_{ij}(t)$ in (2.12) are parameterized by $\vec{r}$ and $\vec{u}$ and need to be written as

$$q_{ij}^{\vec{r},\vec{u}}(t).$$

This leads to a system of ODEs that is parameterized by $\vec{r}$ and $\vec{u}$. We denote the solution of this system of ODEs, parameterized by a vector $\vec{u}$ of constant parameters and a vector $\vec{r}$ of parameters to be optimized, by

$$\vec{C}^{\vec{r},\vec{u}}(t).$$

The basic parameter estimation is set up as optimization problem

Equation 26 (Basic parameter estimation as optimization problem)

$$\vec{r} = \arg\min_{\vec{r}'} \Psi^{\vec{u}}(\vec{r}') \quad \textit{for configuration } \vec{u}. \tag{2.31}$$

In (2.31), a parameter vector $\vec{r}$ is found that minimizes the objective function $\Psi^{\vec{u}}(.)$ for a constant parameter vector $\vec{u}$. A simple choice for the objective function $\Psi^{\vec{u}}(\vec{r}')$ is given by

Equation 27 (Basic objective function $\boldsymbol{\Psi^{\vec{u}}(\vec{r}')}$)

$$\Psi^{\vec{u}}(\vec{r}') = d(\mathcal{F}(\vec{C}^{\vec{r},\vec{u}}(.,.)), \vec{S}). \tag{2.32}$$

In this case the optimization finds the parameter vector $\vec{r}$ that minimizes the distance between the simulated measurement for the solution of the system of ODEs, $B(t) = \mathcal{F}(\vec{C}^{\vec{r},\vec{u}}(t))$, and the clinical measurement $\vec{S}$. Note that in this formulation both $d(.,.)$ and $\mathcal{F}(.)$ are unspecified functions that allow us to state the problem in general terms.

In iPBPK-R we estimate multiple parameters called scaling factors or *adjustment factors* (see section 2.3.2) via a specialized objective function,

Equation 28 (Specialized objective function $\boldsymbol{\Psi^{\vec{u}}(\vec{r}')}$ with penalty term in iPBPK-R)

$$\Psi^{\vec{u}}(\vec{r}') = d(\mathcal{F}(\vec{C}^{\vec{r},\vec{u}}(.)), \vec{S}) + \pi(\vec{r}, \vec{u}), \tag{2.33}$$

which consists of appropriately chosen distance $d(.,.)$ and penalty term $\pi(\vec{r}, \vec{u})$. In addition to minimizing $d(.,.)$, this ensures that the estimation returns biologically plausible values and adjustment factors related to non-renal elimination pathways in the liver as close to 1 as possible when a PBPK model is fit to individuals' EBT data. Accordingly, the penalty function $\pi(.,.)$ needs to be chosen carefully. The penalty term is defined as

Equation 29 (Penalty term $\boldsymbol{\pi(\vec{r}, \vec{u})}$)

$$\pi(\vec{r}, \vec{u}) = u_{\mathrm{b}}\nu(\vec{r}) + u_{\mathrm{c}}\rho(\vec{r}) + u_{\mathrm{d}}\epsilon(\vec{r}) + u_{\mathrm{x}}\psi(\vec{r}). \tag{2.34}$$

In (2.34), the terms $\nu(\vec{r})$, $\rho(\vec{r})$, $\epsilon(\vec{r})$, and $\psi(\vec{r})$ are constraint or penalty terms that depend on the parameter vector $\vec{r}$, and the constants u_{b}, u_{c}, u_{d}, and u_{x} are weighting factors that

are collected in the configuration vector $\vec{u}$.

These constraint and penalty terms and weighting factors need to be carefully chosen to drive parameter estimation towards *biologically plausible* parameter values, i.e. values that clinically makes sense or are accepted in the clinical pharmacology community. IVIVE values are biologically plausible, but care needs to be taken not to distort the optimization problem to a degree that the parameter estimation produces bad results due to strong constraints and penalties of the objective function. The exact forms of the penalty terms will be discussed in in section 2.6.1.

2.4.7 Analysis of iPBPK-R Estimation

In the previous subsections we have described the general form of the objective function and optimization procedure in iPBPK-R. In this subsection, we establish the characteristics of convergence in the optimization procedure by analyzing the ODE system and parameter optimization. We also discuss how many parameters can be generally estimated in iPBPK-R.

We first linearize the system of non-linear ODEs and discuss the properties of the solution to the system. We establish that in our problem setup the linear bounds are sufficient for statements regarding parameter optimization. We then analyze perturbing the linear system to establish convergence properties of the parameter optimization procedure. This approach allows us to conclude that parameter estimation as it is set up in iPBPK-R is converging as long as good starting values (in our case IVIVE estimates) are known and the number of estimated parameters is properly bounded.

Linearization of the system of ODEs. First, we analyze linearized upper and lower bounds for the system of nonlinear ODEs. The nonlinear ODE system eq. (2.25) can be bounded as

Equation 30 (System of nonlinear ODEs bounded by linearized ODEs)

$$(\mathbf{X} + \mathbf{Y}^{-})\vec{m}(t) + \vec{z}(t) \preceq \frac{d\vec{m}(t)}{dt} \preceq (\mathbf{X} + \mathbf{Y}^{+})\vec{m}(t) + \vec{z}(t) \tag{2.35}$$

($\preceq$ denotes *element-wise* comparison) where

$$\mathbf{Y}^{-} = \left[y_{ij}^{-}\right]_{i,j=1,\ldots,n} \quad \text{with} \quad y_{ij}^{-} = \min_{t \geq 0} \dot{y}_{ij}\big(m_j(t)\big) \tag{2.36}$$

and

$$\mathbf{Y}^{+} = \left[y_{ij}^{-}\right]_{i,j=1,\ldots,n} \quad \text{with} \quad y_{ij}^{+} = \max_{t\geq 0} \dot{y}_{ij}\big(m_j(t)\big). \tag{2.37}$$

$\mathbf{Y}^{-}$ and $\mathbf{Y}^{+}$ are matrices representing elementwise upper and lower bounds on the matrix elements of $\mathbf{Y}$. Therefore, the bounds

$$y_{ij}^{-} m_j(t) \;\leq\; y_{ij}\big(m_j(t)\big) \;\leq\; y_{ij}^{+} m_j(t) \tag{2.38}$$

holds for all matrix elements of $\mathbf{Y}$ for all $t \geq 0$. For iPBPK-R to produce stable parameter estimates, the distance between the boundaries $|y_{ij}^{+} - y_{ij}^{-}|$ needs to be small enough. In this case arguments for the linearized upper and lower bounds also hold for the system of non-linear ODEs since all non-linearities are small and monotonically growing. The exact bounds are problem dependent and can be checked post-hoc. In practice, this is ensured by the low probe dose given when using the EBT clinically.

Solution of linearized ODE. Next we discuss the solution to a homogeneous system of n linear ODEs with a real system matrix $\mathbf{A}$,

Equation 31 (Homogeneous system of $\boldsymbol{n}$ linear ODEs with a real system matrix $\mathbf{A}$)

$$\frac{d\vec{x}(t)}{dt} = \mathbf{A}\vec{x}(t), \quad \vec{x}(t) \in \mathbb{R}^n, \quad \mathbf{A} \in \mathbb{R}^{n\times n}, \quad t \geq 0. \tag{2.39}$$

We can set $\mathbf{A}^{-} = (\mathbf{X} + \mathbf{Y}^{-})$ and $\mathbf{A}^{+} = (\mathbf{X} + \mathbf{Y}^{+})$, and ignore the forcing function $\vec{z}(t)$ since $\vec{z}(t) \equiv 0$ for $t > t_0$. Let θ_i and $\vec{c}_i$ denote eigenvalues and eigenvectors of the system matrix $\mathbf{A}$, respectively. Assume that $\mathbf{A}$ is a *simple* matrix, i.e., that it has n linearly independent eigenvectors and thus an eigenvalue decomposition. Further, all eigenvalues and all eigenvectors are real. For iPBPK-R this holds in practical applications due to the characteristics of the flow terms and mass conservation. Further, the only eigenvalue with multiplicity greater than 1 is $\theta_0 = 0$. All solution vector functions for the ODEs eq. (2.39) are then given by

Equation 32 (All solution vector functions for homogeneous system of $\boldsymbol{n}$ linear ODEs)

$$\vec{x}(t) = \sum_{i=1}^{n} \beta_i \vec{c}_i e^{\theta_i t} \quad \textit{with} \quad \vec{x}(t) = \left(x_j(t)\right)_{j=1,\ldots,n} \tag{2.40}$$

where β_i are real constants. The jth element of $\vec{x}(t)$ is the scalar solution for the jth

compartment,

$$x_j(t) = \sum_{i=1}^{n} \beta_i c_{j,i} e^{\theta_i t} \quad \text{with} \quad \mathbf{C} = [\vec{c}_i]_{i=1,\ldots,n} = [c_{j,i}]_{i,j=1,\ldots,n}. \tag{2.41}$$

The function $x_j(t)$ is the projection of $\vec{x}(t)$ into the jth dimension (i.e., jth compartment). The matrix $\mathbf{C}$ is an invertible matrix collecting the eigenvectors $\vec{c}_i$. Further, θ_i, $i = 1, \ldots, n$ are the roots of the characteristic polynomial of the system of ODEs, and the eigendecomposition of $\mathbf{A}$ is given by

$$\mathbf{A} = \mathbf{C}\text{diag}(\theta_i)\mathbf{C}^{-1}. \tag{2.42}$$

We will analyze the general solution of the linearized ODE regarding stability of parameter estimates and map the results back to the system of non-linear ODEs of interest in iPBPK-R.

Construction of ODE solution from projection. We now consider the projection of the solution into one compartment (i.e., dimension j) and observed data in this compartment. We derive the conditions under which *the entire solution* $\vec{x}(t)$ of eq. (2.39) can be reconstructed from the jth dimension.

A measurement consists of T samples $(t_\ell,\, x_j(t_\ell))_{\ell=1,\ldots,\mathrm{T}}$ of the function $x_j(t)$. Under our assumptions all eigenspaces of $\mathbf{A}$ are one-dimensional and thus the (normalized) eigenvectors $\vec{c}_i$ are functions of the eigenvalues θ_i. This allows us to set up a system of $2n$ non-linear equations in β_i and θ_i,

Equation 33 ($2n$ nonlinear equations in $\boldsymbol{\beta_i}$ and $\boldsymbol{\theta_i}$ as a solution of jth compartment)

$$x_j(t_\ell) = \sum_{i=1}^{n} \beta_i c_{j,i}(\theta_i) e^{\theta_i t_\ell} \quad \textit{for} \quad \ell = 1, \ldots, T. \tag{2.43}$$

The system of non-linear equations (2.43) has $2n$ independent variables to solve for. This leads to the requirement that at least $2n$ observed samples are necessary to estimate the $2n$ unknown values β_i and θ_i. If more than $2n$ samples are available, (2.43) can be solved as non-linear least squares problem.

A slight complication stems from the fact that the eigenvalue $\theta_0 = 0$ can have higher multiplicity. Careful analysis reveals that this does not pose a problem as the nullspace of $\mathbf{A}$ captures the source and sink of the dynamical system. In our model it is not necessary to uniquely determine the solution in the sources and sinks, given their particular model

characteristics. This establishes that under practical conditions the solution of the linearized ODEs can be sufficiently reconstructed from observed data in one compartment.

Perturbation of ODE for the linearized system. Next we show that both the constants β_i and the eignevalues θ_i (and thus the eignevectors $\vec{c}_i(\theta_i)$) continuously and differentiably depend on the entries a_{ij} of the system matrix $\mathbf{A}$ as long as eigenvalue multiplicities and the eigenspace structure of the matrix do not change. We define a small perturbation $\alpha \approx 1$ for a matrix entry a_{ij}, i.e., replace a_{ij} with αa_{ij} and view the resulting matrix $\tilde{\mathbf{A}}$ as a function of α, i.e., $\tilde{\mathbf{A}}(\alpha)$. For small enough α the eigenvalues of $\tilde{\mathbf{A}}$ depend continuously and differentiably on α. This can be shown by using Laplace's formula for the determinant and the fact that the zeroes of a polynomial depend continuously and locally differentiably on the coefficients of the polynomial. Carmer's formula then implies that unit eigenvectors for eigenvalues with multiplicity 1 also continuously and differentiably depend on α. Thus, for a small enough α the partial derivatives

$$\frac{\partial \theta_i}{\partial \alpha} \quad \text{and} \quad \frac{\partial \beta_i}{\partial \alpha}$$

exist at least locally. Therefore, the solution eq. (2.40) of the perturbed linear ODE changes continuously and differentiably with α under weak assumptions that are met in practice by iPBPK-R. The above discussion generalizes to multiple perturbations α_i.

Parameter estimation for the linearized system. So far, we have shown that the solution of the perturbed linear ODE depends continuously and differentiably on α for small enough α. Further, we have shown that we can estimate the entire solution $\vec{x}(t)$ of the ODE from enough data points in one compartment. Our goal is to estimate a set of M adjustment factors α_i for the linearized system of ODEs (2.36) and (2.37), respectively, that minimize the difference between the measured data $x_j(t_\ell)$ and the values for the corresponding $x_j(t_\ell)$ predicted by (2.39). Further, we aim to establish the number M of maximally estimable adjustment factors α_i and the minimum number of samples T required to do so.

The set of T non-linear equations (2.43) can be recast as non-linear least squares problem for $\vec{\alpha} = (\alpha_1, \ldots, \alpha_M)$,

Equation 34 (Parameter solution (adjustment factors) as optimization problem of linearized ODEs)

$$(\alpha_1, \ldots, \alpha_M) = \underset{\tilde{\alpha} \in \mathbb{R}^M}{\arg\min} \sum_{\ell=1}^{T} \left(x_j(t_\ell) - \sum_{i=1}^{n} \beta_i(\tilde{\alpha}) c_{j,i}(\tilde{\alpha}) e^{\theta_i(\tilde{\alpha}) t_\ell} \right)^2 \tag{2.44}$$

that has at least one solution that can be found for initial values close to the optimum. Thus, the adjusted system matrix $\tilde{\mathbf{A}}(\vec{\alpha})$ needs to be close to the matrix $\mathbf{A}$, which is derived from IVIVE parameters. The local minimum $\vec{\alpha}$ closest to $\mathbf{1}_M = (1, \ldots, 1)$ is the most *biologically plausible* estimate.

We now analyze how many perturbations (i.e., adjustment factors) can be estimated in the linear case. As we described, the system matrix $\mathbf{A}$ of eq. (2.39) has eigendecomposition eq. (2.42). Since θ_i are the roots of the characteristic polynomial of eq. (2.39), which has degree n, at maximum n independent perturbations α_i can be estimated, i.e., $M \leq n$. The number of estimable perturbations could be less than n, depending on the exact locations of α_i in the matrix $\mathbf{A}$. For the estimation of all M adjustment factors α_i to be successful, at least $2n$ data points $x_j(t_\ell)$ are needed.

Parameter estimation for nonlinearity. As last step we discuss the limits on parameter estimation for the non-linear components of (2.25). Recall that all non-linearities are of Michaelis-Menten form and have two true parameters (initial slope at 0 and maximum value at infinity). The nonlinear Michaelis-Menten saturation suppresses the peaks of the exponential terms in the solution $\vec{x}(t)$ and thus the shapes of the solution-time curves deviate from those of the corresponding pure exponential terms, in particular for high values of $\|\vec{x}(t)\|$. This happen in the initial transient of the solution. To estimate such nonlinearities, observed samples around the peaks of the exponentials are required. At least 2 samples per nonlinear Michaelis-Menten term in a adjustment factor α_i are needed to estimate its two parameters.

Note that this discussion generalizes to the non-homogeneous system of ODEs used in iPBPK-R as the forcing function $\vec{z}(t)$ is non-zero only for a short initial time period t_0. In addition, We assumed that $x_j(t_\ell)$ are data points in a compartment while in the full iPBPK-R setup the measurement operator $\mathcal{F}(.)$ will be applied. Finally, we assumed a quadratic optimization problem. In the full iPBPK-R setup a more complex objective function $\Psi^{\vec{r},\vec{u}}(.)$ based on a general distance $d(.,.)$ is used and lead extra penalty terms in the objective

function. These generalizations need to be carefully managed but do not pose fundamentally new issues.

Relationship to statistical model fitting. In pharmacology, *statistical* model fitting is an ubiquitous tool. Our model fitting procedure is distinctly different from statistical model fitting, e.g., with nonlinear mixed models. This is despite the fact that both methods may lead to similar non-linear least squares problems. The key difference is that in our case *model selection* cannot be performed as dropping a variable would require dropping a compartment and thus formal model reduction would have to be applied. This is in contrast to statistical data fitting where a likelihood criterium would be used to select the correct model, i.e., pick the right number of variables. Model selection in our case would be inherently a reduction transformation on the differential equation, not a statistical transformation on the model, and thus not considered a statistical method.

Summary and discussion on iPBPK-R estimation. In this subsection we evaluated the characteristics of the convergence in the optimization procedure for the system of non-linear ODEs used in iPBPK-R by analyzing a perturbed linearized ODE system. The system of non-linear ODEs can be bounded by its linearized ODEs. Therefore, we considered how small changes in adjustment factors of interest affect the solution of the linearized ODEs and thus the solution of the non-linear ODEs with Michaelis-Menten saturation. Our analysis shows that the iPBPK-R approach allows us to obtain reasonably accurate parameter estimates via optimization. However, one needs to keep in mind the following characteristics for the system of non-linear ODEs with n compartments:

1. The distance between the linearized boundaries of the nonlinear term, $|y_{ij}^{+} - y_{ij}^{-}|$, needs to be small enough to produce stable parameter estimates.
2. All nonlinear terms are assumed to be described with a Michaelis-Menten function eq. (2.15).
3. At maximum n adjustment factors α_i in the linearized matrix can be estimated.
4. At maximum n nonlinearities (2 parameters per nonlinear term) can be estimated.
5. Parameter estimation can be cast as an optimization problem which behaves well locally around the solution for small perturbations α_i and requires the solution of nonlinear least squares optimization.

6. The size of the attractor of the estimated minimum depends on the nonlinearity of the original system of ODEs, the numerical values of eigenvalues θ_i, the eigenbasis, and parameters.

7. A solution is guaranteed and can be investigated to assess its stability and plausibility.

8. Since iPBPK-R solves a nonlinear high-dimensional optimization problem, there is no guarantees that the global optimum is found.

9. The objective function $\Psi^{\vec{r},\vec{u}}(.)$ introduces penalty terms to push the optimization towards the biologically most plausible parameter solution.

In the above list, 5. and 6. together indicate that good starting values (e.g., values chosen based on IVIVE or biological plausibility) are absolutely essential. iPBPK-R utilizes such values as references and constraints in a specialized objective function in the optimization procedure.

The discussion in this section provides a worst-case estimate and bounds on how many samples are needed and how many parameters can be estimated from data in a single compartment. In practice, the particular form of the system matrix/operator $\mathbf{M}(.)$ and objective function $\Psi^{\vec{r},\vec{u}}(.)$ has substantial impact of what can be soundly estimated. As we will see in section 2.5, a smaller number of modes θ_i may be relevant and observable in the measurement compartment j, and all scaling factors α_i may be acting only on these modes. The other modes may not have to be estimated uniquely as they may be unobservable or part of the null space of the operator. If so, a smaller number T of samples is sufficient to resolve the visible modes of the system in compartment j. In this case the scaling factors parameterize a lower-dimensional manifold in the M-dimensional parameter space spanned by the α_i that captures the non-linear functional dependency that the parameters may exhibit. The particular form of the objective function $\Psi^{\vec{r},\vec{u}}(.)$ serves to disambiguate parameters that have a functional dependency as it normalizes the parameter estimates so that they are closest to the IVIVE estimate, i.e., $\vec{r} \approx \mathbf{1}_M$. This allows us to set up problems with more than n scaling factors α_i and let the optimization problem resolve the resulting ambiguity. The appeal of this possibility is to cast a wider net and investigate a larger number of potential biologically induced adjustments that have functional co-dependencies.

2.5 The Reduced Order iPBPK-R Model

In the previous section we gave an overview of the mathematical underpinning of iPBPK-R using EBT data. We expressed the system of non-linear ODEs matrix function representation, and introduced the general forms of the optimization method and its objective function. In this section we provide the detailed model description of iPBPK-R as an instance of the general framework laid out in section 2.4.

2.5.1 Developing the Reduced Model

The core of our system is a seven-compartmental PBPK model of ^{14}C-erythromycin as shown in eq. (2.45)–eq. (2.51). This model is an instance of the non-linear ODE system eq. (2.12). See the corresponding fig. 7 (left panel; adapted from [105] with permission of American Society for Pharmacology and Experimental Therapeutics (ASPET)) depicting the ODE system of ^{14}C-erythromycin. The model contains compartments for artery, vein, lung, kidney, extracellular space, liver cells, and combined other organs. Further, there are supporting source and sink compartments used for mass balance that capture IV dosing, exponential decay in other organs, urine, bile, and metabolic by-product $^{14}CO_2$.

Our ODE system is a minimum full model according to Sager et al [70]. On the other hand, this ODE system can be also viewed as a reduced order model since the number of compartments are limited so that parameters in the model are estimable. The seven-compartmental PBPK model was built using the drug flow and mass balance following section 2.4.3.

Method description. Building an iPBPK-R model (in our case of $^{14}CO_2$ production rate in healthy subjects) entails defining compartments and flow terms between the compartments. The compartments were listed in fig. 7. Next, the flow terms need to be specified. They are summarized in table 5 to table 8. In table 5, property input parameters for each compartment, as an instance of table 4, are listed. Using the parameters in table 5, mass flow equations of ^{14}C-erythromycin for all compartments were set up in table 6. Then, the set of ODE equations of ^{14}C-erythromycin in healthy subjects were constructed as in table 7

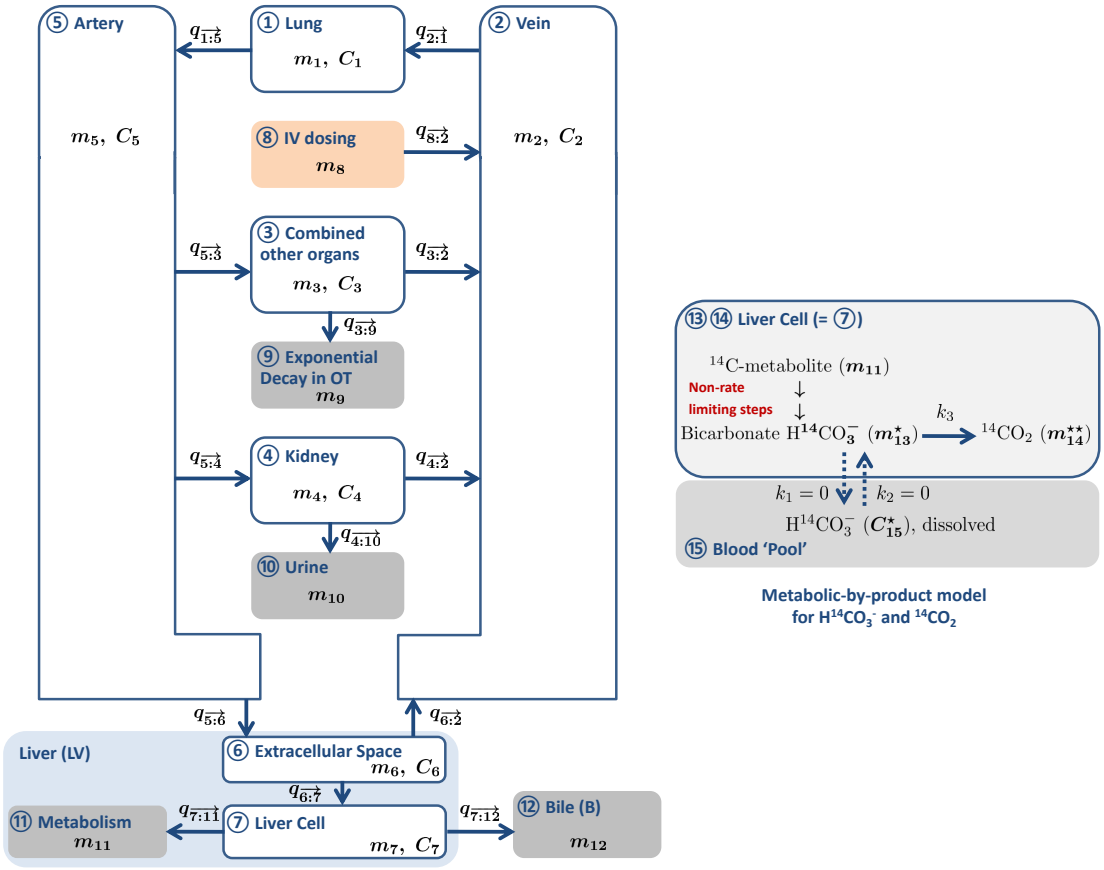

Figure 7: The ODE system of ^{14}C-erythromycin (left) and metabolic by-product model (right) in iPBPK-R.

and table 8 using these mass flows.

The Greek letters with a subscript (i.e., $\alpha_k, \beta_k, \gamma_k, \gamma_i, \gamma_j, \lambda_k, \kappa_{ij}$) are adjustment factors that will be collected in a parameter vector $\vec{r}$. They are explained in the paragraphs titled *Shape of flow terms* and *Conventional model description* in this section and in section 2.6. Note that all Michaelis-Menten kinetic terms in these tables are described with $\mathrm{MM}_{\mathrm{a,b}} = \mathrm{MM}_{\mathrm{a,b,1}}$ using eq. (2.15). As noted above, beyond the seven organ compartments comprising the seven-compartmental PBPK model, five other compartments (input and waste compartments) for ^{14}C-erythromycin that are included in fig. 7 and table 8 in order to retain the mass balance in the entire system. This mass balance is a instance of theorem 1

(see section 2.4.3 and appendix A.1).

Shape of flow terms. Next we discuss the flow mass terms in our PBPK model. The mass flows $q_{ji}(t)$ of ODEs eq. (2.12) are expressed as a function of drug concentration C_i and C_j in the compartments V_i and compartment V_j, respectively. First, let $\vec{r}$ be a parameter vector containing adjustment factors,

Equation 35 (Vector containing adjustment factors for nonrenal elimination pathways)

$$\vec{r} = (\alpha_k, \beta_k, \gamma_k, \gamma_i, \gamma_j, \lambda_k, \kappa_{ij}), \tag{2.59}$$

which can affect the shape of drug mass flows eq. (2.60). Using the *Kronecker delta* function

$$\delta_{mn} = \begin{cases} 1 & \text{if } m = n \\ 0 & \text{else} \end{cases}$$

the mass flow between two compartments V_i and V_j is given by three types of mass flow explained below in (2.61), (2.62), and (2.64). The flow term $q_{ji}(t)$ is either one of the mass flow types Q_1, Q_2, and Q_3, or a combination of two or three types of mass flows Q_1, Q_2, and Q_3 given by

Equation 36 (Flow term $\boldsymbol{q_{ji}(t)}$ as a function of mass flow types $\boldsymbol{Q_1}$, $\boldsymbol{Q_2}$, and $\boldsymbol{Q_3}$)

$$q_{ji}^{\vec{r},\vec{u}}(t) = \begin{cases} (-1)^{\delta_{ki}}\, \mathcal{Q}_1^{\vec{r}_1} \;\; or \;\; (-1)^{\delta_{ki}}\, \mathcal{Q}_2^{\vec{r}_2} \;\; or \;\; \mathcal{Q}_3^{\vec{r}_3} \\ (-1)^{\delta_{ki}}\, (\mathcal{Q}_1^{\vec{r}_1} + \mathcal{Q}_2^{\vec{r}_2}) \\ (-1)^{\delta_{ki}}\, (\mathcal{Q}_1^{\vec{r}_1} + \mathcal{Q}_2^{\vec{r}_2}) + \mathcal{Q}_3^{\vec{r}_3}. \end{cases} \tag{2.60}$$

In (2.60) $\vec{r}_1 = (\alpha_k, \gamma_k)$, $\vec{r}_2 = (\alpha_k, \gamma_k, \beta_k, \lambda_k, h)$, and $\vec{r}_3 = (\kappa_{ij}, \gamma_i, \gamma_j)$, $\vec{u}$ is a configuration vector, h, $k \in \vec{u}$ are configuration constants, where $h = 0/1$ implies competitive/non-competitive mass flow inhibition and $k = i$ or j. The details of the mass flows Q_1, Q_2, and Q_3 are as follows.

- *Q_1 is linearly proportional to the drug concentration C_k* of a single compartment,

$$Q_1^{(\alpha_k,\gamma_k)} = \alpha_k \mathrm{K}_{k,1} \frac{\mathrm{L}_k}{\gamma_k \mathrm{P}_k} C_k, \;\; k = i \text{ or } j, \tag{2.61}$$

  with IVIVE constants $\mathrm{K}_{k,1}$ (clearance). In particular, this IVIVE value expresses a theoretical volume of drug moved from the compartment V_k per time, which is called clearance. α_k is an adjustment factor, which is a parameter to be optimized to scale $\mathrm{K}_{k,1}$. L_k is a biological constant consisting of one or more factors (such as fraction

Table 5: Property input parameters for the drug flows and ODEs of ^{14}C-erythromycin

Parameter	definition
M_0	total mass of ^{14}C-erythromycin in the system in fig. 7
t_0	time of duration of the IV dosing
Q_1	total blood flow
Q_2	blood flow from Compartment 6 to Compartment 2
Q_3	blood flow in and out of Compartment 3
Q_4	blood flow in and out of Compartment 4
Q_5	blood flow from Compartment 5 to Compartment 6
Q_{67}	passive diffusion between Compartment 6 and Compartment 7
P_i	partition coefficient of Compartment i to blood
P_{ip}	partition coefficient of Compartment i to plasma
f_i	fraction unbound in Compartment i
f_{ib}	fraction unbound in blood
δG_{fr}	estimated glomerular filtration rate (GFR), G_{fr}, scaled with the fraction of the drug filtered via GFR (δ)
J_a, J_b, J_c	maximum velocity of transporter a, b, and c, respectively (IVIVE)
K_a, K_b, K_c	Michaelis-Menten constant of transporter a, b, and c, respectively (IVIVE)
η	distribution ratio of drug transporter b in Compartment 4 to 7
μ	exponential decay parameter of the parent drug (initial value)
Q_{cyp}	clearance of CYP3A4 calculated via IVIVE
k_1	distribution rate constant of $H^{14}CO_3^-$ from liver cell to the pool compartment; assumed to be 0 based on [172]
k_2	distribution rate constant of $H^{14}CO_3^-$ from the pool to liver cell; assumed to be 0 based on [172]
k_3	excretion rate constant of $^{14}CO_2$ in the liver cell
ϕ	conversion factor of $^{14}CO_2$ from its molecular weight to Ci (a unit of radioactivity) ($\phi = 1$ in our simulations as done in molar base).

Table 6: Mass flows of ^{14}C-erythromycin shown in fig. 7 (left panel)

Drug mass flows
$q_{\overrightarrow{8:2}} = \begin{cases} M/t_0 \quad \text{for} \quad 0 \leq t \leq t_0, \\ 0 \quad \text{else} \end{cases}$
$q_{\overrightarrow{2:1}} = \mathrm{Q}_1 \left(C_2 - \frac{C_1}{\mathrm{P}_1} \right)$
$q_{\overrightarrow{1:5}} = \mathrm{Q}_1 \left(\frac{C_1}{\mathrm{P}_1} - C_5 \right)$
$q_{\overrightarrow{4:2}} = \mathrm{Q}_4 \left(\frac{C_4}{\mathrm{P}_4} - C_2 \right)$
$q_{\overrightarrow{4:10}} = \delta \mathrm{G}_{\mathrm{fr}} \frac{\mathrm{f_b}}{\mathrm{P}_4} C_4 + \mathrm{MM}_{\eta \mathrm{J_b}, \mathrm{K_b}} \left(\frac{\mathrm{f_b}}{\mathrm{P}_4} C_4 \right)$
$q_{\overrightarrow{5:4}} = \mathrm{Q}_4 \left(C_5 - \frac{C_4}{\mathrm{P}_4} \right)$
$q_{\overrightarrow{3:2}} = \mathrm{Q}_3 \left(\frac{C_3}{\mathrm{P}_3} - C_2 \right)$
$q_{\overrightarrow{5:3}} = \mathrm{Q}_3 \left(C_5 - \frac{C_3}{\mathrm{P}_3} \right)$
$q_{\overrightarrow{3:9}} = \mu_3 C_3$
$q_{\overrightarrow{5:6}} = \mathrm{Q}_5 C_5$
$q_{\overrightarrow{6:2}} = \mathrm{Q}_2 C_{2\|6}$
$q_{\overrightarrow{6:7}} = \mathrm{MM}_{\mathrm{J_a}, \mathrm{K_a}} \left(\frac{\mathrm{f_6}}{\mathrm{P_{6p}}} C_6 \right) + \mathrm{Q}_{67} \left(\frac{\mathrm{f_6}}{\mathrm{P_{6p}}} C_6 - \frac{\mathrm{f_7}}{\mathrm{P_{7p}}} C_7 \right)$
$q_{\overrightarrow{7:12}} = \mathrm{MM}_{\mathrm{J_b}, \mathrm{K_b}} \left(\frac{\mathrm{f_7}}{\mathrm{P_{7p}}} C_7 \right) + \mathrm{MM}_{\mathrm{J_c}, \mathrm{K_c}} \left(\frac{\mathrm{f_7}}{\mathrm{P_{7p}}} C_7 \right)$
$q_{\overrightarrow{7:11}} = \mathrm{Q}_{\mathrm{cyp}} \frac{\mathrm{f_7}}{\mathrm{P_{7p}}} C_7$

Table 7: ODEs for concentration change of ^{14}C-erythromycin in the organ compartments

	Compartment	ODE for concentration change	
1	Lung	$\frac{dC_1}{dt} = \frac{1}{\mathrm{V}_1}\left[\mathrm{Q}_1\left(C_2 - \frac{C_1}{\mathrm{P}_1}\right) - \mathrm{Q}_1\left(\frac{C_1}{\mathrm{P}_1} - C_5\right)\right]$	(2.45)
2	Venous blood	$\frac{dC_2}{dt} = \frac{1}{\mathrm{V}_2}\left[\mathrm{Q}_4\left(\frac{C_4}{\mathrm{P}_4} - C_2\right) + \mathrm{Q}_2 C_{2\|6} + \mathrm{Q}_3\left(\frac{C_3}{\gamma_3 \mathrm{P}_3} - C_2\right) - \mathrm{Q}_1\left(C_2 - \frac{C_1}{\mathrm{P}_1}\right)\right]$	(2.46)
3	Other organs	$\frac{dC_3}{dt} = \frac{1}{\mathrm{V}_3}\left[\kappa_{35}\mathrm{Q}_3\left(C_5 - \frac{C_3}{\gamma_3 \mathrm{P}_3}\right) - \mathrm{Q}_3\left(\frac{C_3}{\gamma_3 \mathrm{P}_3} - C_2\right) - \alpha_3\mu_3 C_3\right]$	(2.47)
4	Kidney	$\frac{dC_4}{dt} = \frac{1}{\mathrm{V}_4}\left[\mathrm{Q}_4\left(C_5 - \frac{C_4}{\mathrm{P}_4}\right) - \mathrm{Q}_4\left(\frac{C_4}{\mathrm{P}_4} - C_2\right) - \left(\delta \mathrm{G}_{\mathrm{fr}}\frac{\mathrm{f}_\mathrm{b}}{\mathrm{P}_4}C_4 + \mathrm{MM}^{\beta_{7,1}}_{\eta \mathrm{J_b},\mathrm{K_b}}\left(\frac{\mathrm{f}_\mathrm{b}}{\mathrm{P}_4}C_4\right)\right)\right]$	(2.48)
5	Arterial blood	$\frac{dC_5}{dt} = \frac{1}{\mathrm{V}_5}\left[\mathrm{Q}_1\left(\frac{C_1}{\mathrm{P}_1} - C_5\right) - \mathrm{Q}_4\left(C_5 - \frac{C_4}{\mathrm{P}_4}\right) - \mathrm{Q}_5 C_{5\|6} - \kappa_{35}\mathrm{Q}_3\left(C_5 - \frac{C_3}{\gamma_3 \mathrm{P}_3}\right)\right]$	(2.49)
6	Extracellular space	$\frac{dC_6}{dt} = \frac{1}{\mathrm{V}'_6}\left[\mathrm{Q}_5 C_5 - \mathrm{Q}_2\frac{C_6}{\mathrm{P}_6} - \mathrm{MM}^{\beta_6}_{\mathrm{J_a},\mathrm{K_a}}\left(\frac{\mathrm{f}_6}{\mathrm{P}_{6\mathrm{p}}}C_6\right) - \kappa_{67}\mathrm{Q}_{67}\left(\frac{\mathrm{f}_6}{\mathrm{P}_{6\mathrm{p}}}C_6 - \frac{\mathrm{f}_7}{\mathrm{P}_{7\mathrm{p}}}C_7\right)\right]$	(2.50)
7	Liver cell	$\frac{dC_7}{dt} = \frac{1}{\zeta_7 \mathrm{V}_7}\left[\mathrm{MM}^{\beta_6}_{\mathrm{J_a},\mathrm{K_a}}\left(\frac{\mathrm{f}_6}{\mathrm{P}_{6\mathrm{p}}}C_6\right) + \kappa_{67}\mathrm{Q}_{67}\left(\frac{\mathrm{f}_6}{\mathrm{P}_{6\mathrm{p}}}C_6 - \frac{\mathrm{f}_7}{\mathrm{P}_{7\mathrm{p}}}C_7\right) - \mathrm{MM}^{\beta_{7,1}}_{\mathrm{J_b},\mathrm{K_b}}\left(\frac{\mathrm{f}_7}{\mathrm{P}_{7\mathrm{p}}}C_7\right) - \mathrm{MM}^{\beta_{7,2}}_{\mathrm{J_c},\mathrm{K_c}}\left(\frac{\mathrm{f}_7}{\mathrm{P}_{7\mathrm{p}}}C_7\right) - \alpha_7 \mathrm{Q}_{\mathrm{cyp}}\frac{\mathrm{f}_7}{\mathrm{P}_{7\mathrm{p}}}C_7\right]$	(2.51)

Table 8: ODEs for mass change of ^{14}C-erythromycin in the input and waste compartments

	Compartment	ODE for mass change	
8	IV dosing	$\frac{dm_8}{dt} = -\begin{cases} M/t_0 & \text{for} \quad 0 \le t \le t_0, \\ 0 & \text{else} \end{cases}$	(2.52)
9	Exponential decay in other organs	$\frac{dm_9}{dt} = \alpha_3 \mu_3 C_3$	(2.53)
10	Urine	$\frac{dm_{10}}{dt} = \delta \mathrm{G_{fr}} \frac{\mathrm{f_b}}{\mathrm{P}_4} C_4 + \mathrm{MM}^{\beta_{7,1}}_{\eta \mathrm{J_b}, \mathrm{K_b}} \left(\frac{\mathrm{f_b}}{\mathrm{P}_4} C_4 \right)$	(2.54)
11	Metabolism	$\frac{dm_{11}}{dt} = \alpha_7 \mathrm{Q_{cyp}} \frac{\mathrm{f}_7}{\mathrm{P_{7p}}} C_7$	(2.55)
12	Bile	$\frac{dm_{12}}{dt} = \mathrm{MM}^{\beta_{7,1}}_{\mathrm{J_b}, \mathrm{K_b}} \left(\frac{\mathrm{f}_7}{\mathrm{P_{7p}}} C_7 \right) + \mathrm{MM}^{\beta_{7,2}}_{\mathrm{J_c}, \mathrm{K_c}} \left(\frac{\mathrm{f}_7}{\mathrm{P_{7p}}} C_7 \right)$	(2.56)

Table 9: ODE for concentration change of $\mathrm{H}^{14}\mathrm{CO}_3^-$ and ODE for mass change of $^{14}\mathrm{CO}_2$

	Compartment	ODE	
13	Liver cell ($\mathrm{H}^{14}\mathrm{CO}_3^-$)	$\frac{dm^\star_{13}}{dt} = \alpha_7 \mathrm{Q_{cyp}} \frac{\mathrm{f}_7}{\mathrm{P_{7p}}} C_7 - \zeta_7 \mathrm{V}_7 (\mathrm{k}_1 + \mathrm{k}_3) C^\star_{13} + \zeta_7 \mathrm{V}_7 \mathrm{k}_2 C^\star_{15}$	(2.57)
14	Liver cell ($^{14}\mathrm{CO}_2$)	$\frac{dm^{\star\star}_{14}}{dt} = \phi \zeta_7 \mathrm{V}_7 \mathrm{k}_3 C^\star_{13}$	(2.58)

unbound). P_k is a biological constant called partition coefficient that is optimized via a corresponding adjustment factor γ_k.

- *Q_2 is nonlinearly proportional to the drug concentration C_k* of a single compartment,

$$Q_2^{(\alpha_k,\gamma_k,\beta_k,\lambda_k,h)} = \frac{\beta_k^{\delta_{0h}} \mathrm{K}_{k,21} \frac{\mathrm{L}_k}{\gamma_k \mathrm{P}_k} C_k}{\lambda_k^{\delta_{1h}} \mathrm{K}_{k,22} + \frac{\mathrm{L}_k}{\gamma_k \mathrm{P}_k} C_k}, \; k = i \text{ or } j, \tag{2.62}$$

with IVIVE constants $\mathrm{K}_{k,21}$ (maximum drug mass flow), and $\mathrm{K}_{k,22}$ (drug concentration where 50% of $\mathrm{K}_{k,21}$ is achieved). β_k and λ_k are adjustment factors to scale $\mathrm{K}_{k,21}$ and $\mathrm{K}_{k,22}$, respectively, and

$$h = \begin{cases} 0 & \text{if the type of reduced activity of mass flow is non} - \text{competitive,} \\ 1 & \text{if the type of reduced activity of mass flow is competitive.} \end{cases} \tag{2.63}$$

- *Q_3 is proportional to the difference in drug concentration* between compartments C_i and C_j,

$$Q_3^{(\kappa_{ij},\gamma_i,\gamma_j)} = \kappa_{ij} \left(\mathrm{K}_{j,3} \frac{\mathrm{L}_j}{\gamma_j \mathrm{P}_j} C_j - \mathrm{K}_{i,3} \frac{\mathrm{L}_i}{\gamma_i \mathrm{P}_i} C_i \right), \tag{2.64}$$

where $\mathrm{K}_{i,3}$ and $\mathrm{K}_{j,3}$ are biological constants consisting of one or more factors including IVIVE value of clearance. κ_{ij} is an adjustment factor to optimize the whole term eq. (2.64) as a diffusion-based flow.

Adjustment factors appeared in Q_1, Q_2, and Q_3 (i.e., $\alpha_k, \beta_k, \gamma_k, \gamma_i, \gamma_j, \lambda_k, \kappa_{ij} \in \vec{r}$) are candidate scaling parameters for optimization either to evaluate biological activities in non-renal drug elimination pathways or to improve the iPBPK-R model fit to the observed $^{14}CO_2$ production rate data individually. Thus, these parameters may control the mass flows Q_1, Q_2, and Q_3 and thus, $q_{ji}(t)$.

Conventional model description. The types of candidate parameters for optimization in the liver were described as part of mass flows Q_1, Q_2, and Q_3 in the paragraph *Shape of flow terms* above. They are proportional to either (1) concentration, (2) a nonlinear (Michaelis-Menten style saturation) function of concentration, or (3) the difference in concentrations between two compartments. The reference values for the optimization of these parameters are IVIVE values that were calculated based on literature in pharmacology. Therefore, these parameters, i.e., adjustment factors, were included as the parameters of interest in the ODEs in table 7 to table 9. The definition of all adjustment factors is summarized in table 10.

Remember that ultimately in iPBPK-R these adjustment factors are optimized to explain how much the reference IVIVE values needed to change in the model fit optimization. While our main goal was to estimate parameters in the liver consisting of the extracellular space and liver cell sub-compartments, some parameters in non-liver compartments were also optimized to improve the model fit to $^{14}CO_2$ production rate data based on sensitivity analysis. The production rate of the metabolic-by-product $^{14}CO_2$ as a function of drug concentration in the liver is given by the *measurement function* $\mathcal{F}(.)$ that was introduced in eq. (2.26).

Modeling Blood with Vein and Artery compartments. In iPBPK-R, Vein and Artery compartments were separately modeled as eq. (2.46) and eq. (2.49) in table 7. This is different from classical PBPK models where blood tissue is viewed as one compartment in clinical pharmacology. In the connection from Artery, Extracellular Space, through to Vein compartment, we assumed the two algebraic relationships (see fig. 7). First, the mass flow from Artery to Extracellular Space $q_{\overrightarrow{5:6}}$ is fast and thus modeled instantaneous as

$$C_{5|6} = C_6. \tag{2.65}$$

Second, we assumed the 2-blood compartment model (i.e., a model with Vein and Artery compartments) for the blood tissue to be well-stirred, which necessitated a second algebraic relationship

$$C_{2|6} = \frac{C_6}{\mathrm{P}_6}. \tag{2.66}$$

Thus, eq. (2.65) and eq. (2.66) are necessary assumptions in iPBPK-R to approximate the drug flows between the blood tissue and liver organ when the blood is modeled with two separate compartments, Artery and Vein, while retaining the well-stirred model assumption for the blood tissue.

Modeling $^{14}CO_2$ dynamics. Beyond the drug and its metabolite, $^{14}CO_2$ production rate in the EBT needs to be modeled. Therefore we added a one-compartment metabolic-by-product to the system which describes the non-rate limited CYP3A4-enzyme pathway within the liver cell sub-compartment (right panel of fig. 7). This metabolic-by-product model was originally proposed by Sugiyama et al. 2011 [172]. The one-compartment metabolic-by-product model starts with the catalytic conversion from the parent drug, ^{14}C-erythromycin, to its metabolite ^{14}C-metabolite by CYP3A4. Sugiyama et al. assumed a slow $H^{14}CO_3^-$ turnover between organ and blood 'pool' compartments with two rate constants, k_1 and k_2

Table 10: List of adjustment factors in iPBPK-R of EBT in healthy subjects

Adjustment factor	Definition: *adjustment factor of*
α_3	exponential decay in Other Organs compartment
α_7	CYP3A4 activity in Liver Cell compartment
β_6	drug transporter a in the liver
$\beta_{7,1}$	drug transporter b in the liver
$\beta_{7,2}$	drug transporter c in the liver
γ_3	partition coefficient of Other Organs compartment to blood
ζ_7	volume of Liver Cell compartment
κ_{35}	arterial blood flow into Other Organs compartment
κ_{67}	passive diffusion between Extracellular Space compartment and Liver Cell compartment

($H^{14}CO_3^-$ is dissolved in the blood). In this dissertation, we referred to their in vivo rat PBPK study and set both parameters to be 0. Accordingly, we simply assumed that the final-by-product $^{14}CO_2$ gets released from $H^{14}CO_3^-$ in the liver cell with an excretion rate constant, k_3. Let $C_{13}^\star$ and $C_{15}^\star$ denote the concentration of $H^{14}CO_3^-$ in the liver cell and in the blood pool, respectively. We assume that the respired amount of $H^{14}CO_3^-$ and exhaled $^{14}CO_2$ have a one-to-one molar relationship (no rate-limiting step). Furthermore, let $m_{14}^{\star\star}$ be the exhaled amount of $^{14}CO_2$ in breath, which is assumed to instantaneously travel from the liver cell to the lung. Then, ODEs of mass change of $H^{14}CO_3^-$ and $^{14}CO_2$ are shown in table 9, respectively. Property parameters of these ODEs are listed in table 5. $dm_{14}^{\star\star}/dt$ in eq. (2.58) is the amount of $^{14}CO_2$ sampled in the breath at time t.

2.5.2 Matrix Representation of the EBT PBPK Model

In this section we present the reduced model used in iPBPK-R in the formalism described in section 2.4.4. We here provide the full specification of all matrix elements of both the linear and the non-linear part of the system of ODEs that constitute eq. (2.25) in section 2.4.4.

Remember that eq. (2.25) is a nonlinear set of n ODEs consisting of the linear term $\mathbf{X}\vec{m}(t)$ and nonlinear Michaelis-Menten function term $\mathbf{Y}(\vec{m}(t))$ with a short-time intravenous drug dosing term $\vec{z}(t)$ as forcing function. Setting the dosing rate $\tau = M/t_0$ and the short dosing interval $\Omega = [0,\, t_0]$, the 14 ODEs in table 7–table 9 can be described with the real matrix

Equation 37 (**X** containing the linear part of the system of nonlinear ODEs)

$$\mathbf{X} = \begin{bmatrix} x_{1,1} & x_{1,2} & . & . & x_{1,5} & . & . & . & . & . & . & . & . & . \\ x_{2,1} & x_{2,2} & x_{2,3} & x_{2,4} & . & x_{2,6} & . & . & . & . & . & . & . & . \\ . & x_{3,2} & x_{3,3} & . & x_{3,5} & . & . & . & . & . & . & . & . & . \\ . & x_{4,2} & . & x_{4,4} & x_{4,5} & . & . & . & . & . & . & . & . & . \\ x_{5,1} & . & x_{5,3} & x_{5,4} & x_{5,5} & x_{5,6} & . & . & . & . & . & . & . & . \\ . & . & . & . & x_{6,5} & x_{6,6} & x_{6,7} & . & . & . & . & . & . & . \\ . & . & . & . & . & x_{7,6} & x_{7,7} & . & . & . & . & . & . & . \\ . & . & . & . & . & . & . & . & . & . & . & . & . & . \\ . & . & x_{9,3} & . & . & . & . & . & . & . & . & . & . & . \\ . & . & . & x_{10,4} & . & . & . & . & . & . & . & . & . & . \\ . & . & . & . & . & . & x_{11,7} & . & . & . & . & . & . & . \\ . & . & . & . & . & . & . & . & . & . & . & . & . & . \\ . & . & . & . & . & . & x_{13,7} & . & . & . & . & . & x_{13,13} & . \\ . & . & . & . & . & . & . & . & . & . & . & . & x_{14,13} & . \end{bmatrix}, \tag{2.67}$$

that captures the linear part of the model, and the matrix of functions

Equation 38 ($\tilde{\mathbf{Y}}$ containing the nonlinear part of the system of nonlinear ODEs)

$$\tilde{\mathbf{Y}} = \begin{bmatrix} . & . & . & . & . & . & . & . & . & . & . & . & . & . \\ . & . & . & . & . & . & . & . & . & . & . & . & . & . \\ . & . & . & . & . & . & . & . & . & . & . & . & . & . \\ . & -\mathrm{MM}_{\beta_{7,1}\eta \mathrm{J_b},\mathrm{K_b}} & . & . & . & . & . & . & . & . & . & . & . & . \\ . & . & . & . & . & . & . & . & . & . & . & . & . & . \\ . & . & . & -\mathrm{MM}_{\beta_6 \mathrm{J_a},\mathrm{K_a}} & . & . & . & . & . & . & . & . & . & . \\ . & . & . & \mathrm{MM}_{\beta_6 \mathrm{J_a},\mathrm{K_a}} & -(\mathrm{MM}_{\beta_{7,1}\mathrm{J_b},\mathrm{K_b}} + \mathrm{MM}_{\beta_{7,2}\mathrm{J_c},\mathrm{K_c}}) & . & . & . & . & . & . & . & . & . \\ . & . & . & . & . & . & . & . & . & . & . & . & . & . \\ . & . & . & . & . & . & . & . & . & . & . & . & . & . \\ . & \mathrm{MM}_{\beta_{7,1}\eta \mathrm{J_b},\mathrm{K_b}} & . & . & . & . & . & . & . & . & . & . & . & . \\ . & . & . & . & . & . & . & . & . & . & . & . & . & . \\ . & . & . & . & \mathrm{MM}_{\beta_{7,1}\mathrm{J_b},\mathrm{K_b}} + \mathrm{MM}_{\beta_{7,2}\mathrm{J_c},\mathrm{K_c}} & . & . & . & . & . & . & . & . & . \\ . & . & . & . & . & . & . & . & . & . & . & . & . & . \\ . & . & . & . & . & . & . & . & . & . & . & . & . & . \end{bmatrix} \tag{2.68}$$

that captures the non-linear Michaelis-Menten style saturation. Dots . in $\mathbf{X}$ *and* $\tilde{\mathbf{Y}}$ *stand for 0 and that the entries of* $\mathbf{X}$ *is provided in table 11. Given a scaling matrix*

$$\mathbf{D} = \mathrm{diag}\left(0,0,0,\frac{\mathrm{f_b}}{\mathrm{V_4 P_4}},0,\frac{\mathrm{f_6}}{\mathrm{V_6' P_{6p}}},\frac{\mathrm{f_7}}{\zeta_7 \mathrm{V_7 P_{7p}}},0,0,0,0,0,0,0\right) \tag{2.69}$$

we can write the full system of non-linear ODEs used for EBT in iPBPK-R as

Equation 39 (System of nonlinear ODEs used for EBT in iPBPK-R)

$$\frac{d\vec{m}(t)}{dt} = \mathbf{X}\vec{m}(t) + \tilde{\mathbf{Y}}(\mathbf{D}\vec{m}(t)) + z(t). \tag{2.70}$$

The diagonal elements of $\mathbf{D}$ pre-scale the vector elements $m_i(t)$ before $\tilde{\mathbf{Y}}(.)$ is applied and can be propagated into the parameters of $y_{i,j}(.)$ using the identity (2.16). This allows us to convert (2.70) into the normal form given by (2.25) with system operator matrix

$$\mathbf{A}(.) = \mathbf{X}(.) + \mathbf{Y}(.) \quad \text{with} \quad \mathbf{Y}(.) = \tilde{\mathbf{Y}}(.) \circ \mathbf{D}(.).$$

In eq. (2.70) and the entries of the matrices eq. (2.67) and eq. (2.68), we omit the bicarbonate concentration in the pool compartment, $C^{\star}_{15}$, since $k_1 = k_2 = 0$ was assumed (table 5). As a result, the total number of ODEs in iPBPK-R of EBT for healthy subjects is $n = 14$.

Analysis. Having expressed iPBPK-R's reduced PBPK model and all its dependencies on parameters and adjustment factors as instance of (2.25) enables us to analyze iPBPK-R's estimation capabilities and stability. We want to emphasize that iPBPK-R uses standard numerical solvers for ODE integration and optimization. The theoretical framework developed in section 2.4.7 is *not* used to compute the solutions but to analyze the solution quality and soundness of the approach.

We base the discussion below on analyzing the eigendecompositions of the upper and lower matrix approximations $\mathbf{A}^+$ and $\mathbf{A}^-$ of the system operator matrix $\mathbf{A}$ of (2.25). The element-wise distance $|a^+_{i,j} - a^-_{i,j}|$ is small as required, and both $\mathbf{A}^+$ and $\mathbf{A}^-$ are indeed simple matrices.

The first observation is that while the EBT iPBPK-R model has 14 compartments for the purpose of modeling mass balance, the underlying dynamical system has only 7 compartments. The 5 source/sink compartments and the 2 further helper compartments lead to a null space of dimension 6 and can be disregarded in the discussion. Inspection of Figure 15 of chapter 3 and the simulated curves in all 7 compartments (shown in [105]) as well as Figure 23 of chapter 4 indicate that at most four distinctive estimable mode θ_i are present in the liver compartment. Thus, the $T = 11$ sampling points and the associated noise is sufficient to estimate the modes to a reasonable accuracy level. The $T = 11$ measurements are clustered at the early transient phase and thus allow for estimating non-linear saturation due to Michaelis-Menten behavior. We provide the eigenanalysis of the EBT example at concentration 0 in appendix A.2 to give a flavor of the necessary analysis. The analysis

shows that the spectrum of the 7 compartment model has indeed three to five dominant and distinguishable modes (32.1, 23.7; −2119.7; −434.0; −290.5, −221.4; −12.7).

Secondly, The number of adjustment parameters that can be distinguished is limited to $M = 7$ functionally independent α_i at max. iPBPK-R has K = 9 adjustment parameters, and thus they must have a functional (non-linear) dependence. The dependence is actually shown in [105] as the four main levers that shape the $^{14}CO_2$ production rate curve. The condition that the adjustment factor vector $\vec{r}$ needs to be as close to $\mathbf{1}_M$ as possible disambiguates the functional dependency. This regularizes the estimates and pushes them towards the global optimum analogous to the arguments presented in [151], and thus makes the estimates stable. Further adding to stability is the nested optimization procedure employed by iPBPK-R.

In this section we described the detail of the ODE system and adjustment factor parameters used in iPBPK-R of the EBT data. Part of these parameters are to be optimized and estimated using the objective function introduced in the previous section. In the next section we formally define the objective function and describe the details of the optimization procedure in iPBPK-R, presented in the next section.

2.6 Estimation Procedure for iPBPK-R Parameters

In section 2.4.6, we have discussed that the biologically plausible multiple-parameter estimation via iPBPK-R is treated as an optimization problem for a subset of parameters in the system of ODEs eq. (2.12). This optimization problem is to optimize a subset of adjustment factors of all drug flow terms (2.60) by minimizing the distance $d(.,.)$ between observed and simulated data as shown in eq. (2.29). In the previous section $\vec{r}$ in (2.59) denotes a parameter vector containing adjustment factors. Some of the optimized adjustment factors will provide parameter estimates for activities of metabolic enzyme and drug transporters in individuals, in non-renal drug clearance. For example, optimized adjustment factor α_7 (see table 7 and table 10) will explain how much the IVIVE input value of the CYP3A4 activity needs to be scaled for the particular individual in the individualized model fitting. We developed an EBT specific objective function (an instance of eq. (2.33)) consisting of a

Table 11: Entries of matrix $\mathbf{X}$

$x_{1,1} = -2\frac{\mathrm{Q_1}}{\mathrm{V_1P_1}}$, $x_{1,2} = \frac{\mathrm{Q_1}}{\mathrm{V_1}}$, $x_{1,5} = \frac{\mathrm{Q_1}}{\mathrm{V_1}}$,
$x_{2,1} = \frac{\mathrm{Q_1}}{\mathrm{V_2P_1}}$, $x_{2,2} = -\frac{\mathrm{Q_1+Q_3+Q_4}}{\mathrm{V_2}}$, $x_{2,3} = \frac{\mathrm{Q_3}}{\gamma_3\mathrm{V_2P_3}}$, $x_{2,4} = \frac{\mathrm{Q_4}}{\mathrm{V_4P_4}}$, $x_{2,6} = \frac{\mathrm{Q_2}}{\mathrm{V_2P_6}}$,
$x_{3,2} = \frac{\mathrm{Q_3}}{\mathrm{V_3}}$, $x_{3,3} = -\frac{(\kappa_{35}+1)\frac{\mathrm{Q_3}}{\gamma_3\mathrm{P_3}}+\alpha_3\mu_3}{\mathrm{V_3}}$, $x_{3,5} = \frac{\kappa_{35}\mathrm{Q_3}}{\mathrm{V_3}}$,
$x_{4,2} = \frac{\mathrm{Q_4}}{\mathrm{V_4}}$, $x_{4,4} = -\frac{2\mathrm{Q_4}+\delta\mathrm{G_{fr}f_b}}{\mathrm{V_4P_4}}$, $x_{4,5} = \frac{\mathrm{Q_4}}{\mathrm{V_4}}$,
$x_{5,1} = \frac{\mathrm{Q_1}}{\mathrm{V_5P_1}}$, $x_{5,3} = \frac{\kappa_{35}\mathrm{Q_3}}{\gamma_3\mathrm{V_5P_3}}$, $x_{5,4} = \frac{\mathrm{Q_4}}{\mathrm{V_5P_4}}$, $x_{5,5} = -\frac{\mathrm{Q_1}+\kappa_{35}\mathrm{Q_3}+\mathrm{Q_4}}{\mathrm{V_5}}$, $x_{5,6} = -\frac{\mathrm{Q_5}}{\mathrm{V_5}}$,
$x_{6,5} = \frac{\mathrm{Q_5}}{\mathrm{V_6'}}$, $x_{6,6} = -\frac{1}{\mathrm{V_6'}}\left(\frac{\kappa_{67}\mathrm{Q_{67}f_6}}{\mathrm{P_{6p}}} + \frac{\mathrm{Q_2}}{\mathrm{P_6}}\right)$, $x_{6,7} = \frac{\kappa_{67}\mathrm{Q_{67}f_6}}{\mathrm{V_6'P_{7p}}}$,
$x_{7,6} = \frac{\kappa_{67}\mathrm{Q_{67}f_6}}{\zeta_7\mathrm{V_7P_{6p}}}$, $x_{7,7} = -\frac{(\kappa_{67}\mathrm{Q_{67}}+\alpha_7\mathrm{Q_{cyp}})\mathrm{f_7}}{\zeta_7\mathrm{V_7P_{7p}}}$, $x_{9,3} = \frac{\alpha_3\mu_3}{\mathrm{V_3}}$, $x_{10,4} = \frac{\delta\mathrm{G_{fr}f_b}}{\mathrm{V_4P_4}}$,
$x_{11,7} = \frac{\alpha_7\mathrm{Q_{cyp}f_7}}{\zeta_7\mathrm{V_7P_{7p}}}$, $x_{13,7} = \frac{\alpha_7\mathrm{Q_{cyp}f_7}}{\zeta_7\mathrm{V_7P_{7p}}}$, $x_{13,13} = -k_3$, $x_{14,13} = \phi k_3$

distance measure and penalty terms that regularizes the problem. The estimation procedure we describe here can be viewed as an indirect measurement procedure for multiple activities in drug disposition such as enzymatic metabolism and drug transport.

2.6.1 General Setup and Distance Measure

For the high-dimensional parameter optimization procedure of iPBPK-R we developed a tailored objective function consisting of distance measure with bias, lower bound, drift, and x-shift penalty terms, eq. (2.33) with eq. (2.34). We now formally define each component of the objective function. Before defining each component, let us first formally describe the operator $\mathcal{F}(.)$ discussed in eq. (2.26).

Operator to model $^{14}CO_2$ rate data. As in section 2.4.5, we here describe the operator eq. (2.26) in detail as follows. Remember that $B(t)$ denotes a $^{14}CO_2$ production rate at time t and $\vec{C}(t)$ denotes a solution vector of eq. (2.12) that were converted to drug

concentrations. Furthermore, consider differentiating one element of $\vec{C}(t)$ that is associated with the $i^\star$ compartment and denote $\dot{C}_{i^\star}(t)$ the differentiated form of the element $C_{i^\star}(t)$. Then, the operator $\mathcal{F}(.)$ returns $\dot{C}_{i^\star}(t)$, i.e.,

Equation 40 (**$^{14}CO_2$** production rate $\boldsymbol{B(t)}$ returned by $\boldsymbol{\mathcal{F}(.)}$ in iPBPK-R)

$$B(t) = \mathcal{F}(\vec{C}(t)) = \dot{C}_{i^\star}(t). \tag{2.71}$$

This is an instance of eq. (2.28). When the $i^\star$ compartment denotes the Liver compartment for $^{14}CO_2$ in table 9, $\dot{C}_{i^\star}$ is approximately viewed as a modeled $^{14}CO_2$ production rate at time t in the breath sample. Thus, $\mathcal{F}(.)$ provides modeled $^{14}CO_2$ production rate data using the solution vector $\vec{C}$ of the system of ODEs.

Configuration vector. We define the configuration vector

Equation 41 (Configuration vector in iPBPK-R)

$$\vec{u} = \left(h, \vec{h}', \vec{h}'', (u_\ell)_\ell, u_{\mathrm{b}}, u_{\mathrm{c}}, u_{\mathrm{d}}, u_{\mathrm{x}}\right) \tag{2.72}$$

where $h \in \mathbb{R}$, $\vec{h}' \in \mathbb{R}^K$, and $\vec{h}'' \in \mathbb{R}^K$. K is the length of the parameter vector $\vec{r}$. h is the indicator defined in eq. (2.63) and influences the ODE terms. The indicator vectors $\vec{h}'$ and $\vec{h}''$ are used within penalty terms to configure which adjstment factors may be penalized. $(u_\ell)_{\ell=1,\ldots,\mathrm{T}}$, is a vector of weights for each sampling point. u_{b}, u_{c}, u_{d}, and u_{x} are weights for bias, lower boundary, drift, and x-shift terms, respectively.

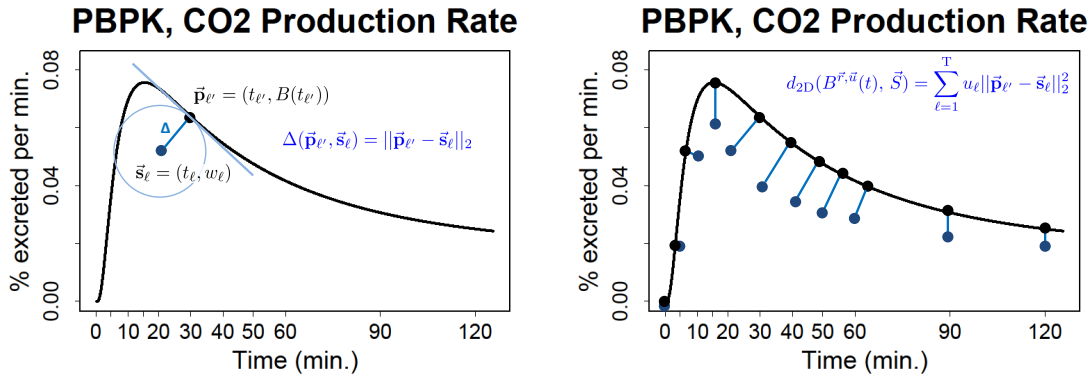

Figure 8: 2D L_2 norm and 2D distance measure

Distance measure. Clinical measurements may be slightly shifted relative to the planned time point. We introduce a 2D distance that was used as a distance measure between simulated and measured $^{14}CO_2$ production rate in iPBPK-R. This distance generalizes the usual L_2 norm distance eq. (2.30) by allowing for some (penalized) misalignment in x direction in addition to value mismatch in y direction. Let us define the ℓth measurement point measured at time t_ℓ as $\vec{s}_\ell = (t_\ell, w_\ell)$. We define the point

$$p_{\ell'} = (t_{\ell'}, B(t_{\ell'})) \quad \text{such that} \quad t_{\ell'} = \underset{t' \in [t_\ell - \delta, t_\ell + \delta]}{\arg\min} \|(t', B(t')) - (t_\ell, w_\ell)\|_2$$

for an appropriately chosen δ. We denote the distance between measurement and simulation at sample point ℓ as $\Delta_\ell = \|\vec{p}_{\ell'} - \vec{s}_\ell\|_2$. See the left panel of fig. 8 for an illustration.

We collect the T measurements $\vec{s}_\ell$ at time points t_ℓ as vector of measurements $\vec{S} = \big((t_\ell, \vec{s}_\ell)\big)_{\ell=1,\ldots,T}$. Then, the 2D distance $d_{2D}(.,.)$ between the simulated function $B(t)$ parameterized by $\vec{r}$ and $\vec{u}$ and the measurement vector $\vec{S}$, is defined as follows. Per time point ℓ and measurement $\vec{s}_\ell$ the minimal Euclidean distance Δ_ℓ between the observed data point $\vec{s}_\ell$ and the modeled $^{14}CO_2$ production rate-time curve $B(t)$ is found. The 2D distance between $B^{\vec{r},\vec{u}}(t)$ and $\vec{S}$ is then given as the weighted sum of all squared Δ_ℓ for $\ell = 1, \ldots, T$. Formally, the 2D distance is defined as

Equation 42 (2D distance between B(t) and observed data $\vec{\boldsymbol{S}}$ in iPBPK-R)

$$d_{2D}(B^{\vec{r},\vec{u}}(t),\, \vec{S}) = \sum_{\ell=1}^{T} u_\ell \Delta_\ell^2 = \sum_{\ell=1}^{T} u_\ell ||\vec{p}_{\ell'} - \vec{s}_\ell||_2^2. \tag{2.73}$$

See the right panel of fig. 8 for an illustration.

2.6.2 Penalty Terms

Next we discuss the specific shapes and rationales for the penalty terms and their parameterizations. These terms are the EBT spcific instances of the general form shown in section 2.4.6.

Bias constraint term. We introduce a bias term to disambiguate potential functional relationships between estimation parameters and ensure that the final estimate is as close to the initial IVIVE values as possible while matching the measurement data within its noise bounds. The parameter vector,

Equation 43 (Parameter vector $\vec{\boldsymbol{r}}$ in iPBPK-R)

$$\vec{r} = (r_i)_{i=1,\ldots,\mathrm{K}}, \tag{2.74}$$

which contains adjustment factors such as $\alpha_k, \beta_k, \gamma_k, \gamma_i, \gamma_j, \lambda_k$, and κ_{ij}, is biased towards the IVIVE scaling estimate $\vec{r}_0$. Not all elements of $\vec{r}$ have to be used in the bias term. This is encoded in an indicator vector $\vec{h}' \in \{0,1\}^{\mathrm{K}}$. Whether or not a particular element of $\vec{r}$ is included is decided based on IVIVE or on biological plausibility. Then the bias term is formally defined as

Equation 44 (Bias constraint term $\boldsymbol{\nu(\vec{r}, \vec{h}')}$)

$$\nu(\vec{r}, \vec{h}') = \|\mathrm{diag}(\vec{h}')(\vec{r} - \vec{r}_0)\|_2^2 \tag{2.75}$$

which is the *masked* squared Euclidean distance between $\vec{r}$ and $\vec{r}_0$.

Lower bound penalty term. To avoid biologically unrealistic parameter estimation, a lower bound penalty term is included in the objective function. The parameter vector

$$\vec{r}_{\mathrm{L}} = (r_i^{\mathrm{L}})_{i=1,\ldots,\mathrm{K}} \tag{2.76}$$

captures the lower bounds for all scaling factors. Below these bounds, a penalty is added to the objective function. Again, not all elements of $\vec{r}$ have to be used in the penalty term. This is encoded in an indicator vector $\vec{h}'' = (h_i'')_{i=1,\ldots,\mathrm{K}} \in \{0,1\}^{\mathrm{K}}$. Whether or not a particular element of $\vec{r}$ is included is decided based on IVIVE or on biological plausibility. The lower bound penalty term is given by

Equation 45 (Lower bound penalty term $\boldsymbol{\rho(\vec{r}, \vec{h}'')}$)

$$\rho(\vec{r}, \vec{h}'') = \sum_{i=1}^{\mathrm{K}} h_i'' \min(r_i - r_i^{\mathrm{L}}, 0)^2. \tag{2.77}$$

Drift penalty term. Ensuring the correct height of the peak of the simulated curve $B(t)$ requires a separate penalty term called *drift* as the simulated function can "shoot up" between samples if not properly constrained. Thus, we progressively penalize $B(t)$ for deviations in peak height from the maximum measured data point w_ℓ. The drift penalty term is defined as the squared distance between the maximum values of modeled and observed $^{14}CO_2$ production rate data,

Equation 46 (Drift penalty term $\boldsymbol{\epsilon(\vec{r})}$)

$$\epsilon(\vec{r}) = \big(\max_{t \in [t_0, t_{\mathrm{T}}]} B^{\vec{r},\vec{u}}(t) - \max_{\ell=1,\ldots,\mathrm{T}} w_\ell\big)^2. \tag{2.78}$$

X-shift penalty term. The 2D distance $d_{2D}(.,.)$ allows for slight x shifts of the measurements relative to their nominal sampling time points t_ℓ. To minimize the per-timepoint shift we penalize differences between t_ℓ and $t_{\ell'}$ linearly. We define the x shift penalty term as

Equation 47 (X-shift penalty term $\boldsymbol{\psi(\vec{r})}$)

$$\psi(\vec{r}) = \sum_{\ell=1}^{\mathrm{T}} |t_{\ell'} - t_\ell|. \tag{2.79}$$

In practice, using a linear penalty term for x shift but bound the maximum shift worked best for our purpose.

2.6.3 Objective Function and Optimization Problem

We now combine the distance function and all penalty terms into the overall objective function $\Psi(.)$ and formally state the exact iPBPK-R EBT parameter estimation problem. The problem is an instance of the general form discussed in section 2.4.6.

Objective function in iPBPK-R. Our tailored objective function is expressed as a weighted combination of the 2D norm distance, and constraint and penalty terms. Using the previously defined weights in the configuration vector eq. (2.72) and 2D distance, constraint and penalty terms in eq. (2.73), eq. (2.75), eq. (2.77), eq. (2.78), and eq. (2.79), the objective function is expressed as

Equation 48 (Objective function $\boldsymbol{\Psi_{2D}^{\vec{r},\vec{u}}(.,.)}$ in iPBPK-R)

$$\Psi_{2D}^{\vec{r},\vec{u}}(.,.) : (B^{\vec{r},\vec{u}}(t),\, \vec{S}) \mapsto d_{2D}(B^{\vec{r},\vec{u}}(t)),\, \vec{S}) + u_{\mathrm{b}}\nu(\vec{r},\vec{h'}) + u_{\mathrm{c}}\rho(\vec{r},\vec{h''}) + u_{\mathrm{d}}\epsilon(\vec{r}) + u_{\mathrm{x}}\psi(\vec{r}). \tag{2.80}$$

Note that different variants of $\Psi_{2D}^{\vec{r},\vec{u}}(.,.)$ can be configured via indicator vectors and weights. Such configurations are collected in the configuration vector $\vec{u}$ defined in eq. (2.72).

Estimation as optimization problem. Recall that the biologically plausible multiple-parameter estimation via iPBPK-R is treated as an optimization problem where a subset of parameters of all drug flow terms are optimized to best fit the system of ODEs to the measured data $\vec{S}$. The result is the parameter/adjustment factor vector $\vec{r}$ defined in (2.74). Given the configuration vector $\vec{u}$ defined in (2.72), optimization of the parameter vector is performed by minimizing the objective function eq. (2.80). Formally, iPBPK-R solves the

optimization problem

Equation 49 (Optimization problem in iPBPK-R)

$$\vec{r} = \arg\min_{\vec{r}'} \Psi_{\text{2D}}^{\vec{r}',\vec{u}}\big(\mathcal{F},\, \vec{S}\big) \quad \textit{for configuration } \vec{u} \tag{2.81}$$

to estimate the most likely configuration $\vec{r}$. The full optimization space allows for 7 independent parameters, but in practice not all of them are strongly influencing the fit. Depending on the goodness-of-fit of modeling, some less influential parameters in $\vec{r}$ can be fixed as constants and not necessarily be optimized. This is achieved through appropriate setting of the indicator vectors $\vec{h}'$ and $\vec{h}''$.

2.6.4 Handling Combined Pre/Post Treatment Estimates

The impact of a treatment on biological parameters is often the focus in clinical pharmacology studies. An intervention is performed on an individuals, and the goal is to evaluate the effect of the intervention by comparing the same type of data obtained before and after the intervention.

Treatment effect on estimates. In our case of chapter 4, the intervention of interest is dialysis. In a kidney disease study where EBT is used before and after the patients receive dialysis, our goal is to apply iPBPK-R to these two data series to estimate the effect of dialysis on biological parameters of individual patients. We assume that *independent parameters* remain unchanged while *co-optimization parameters* change from pre-dialysis to post-dialysis. To estimate both co-optimization parameters and independent parameters, we developed a co-optimization method by introducing additional parameters and extending the optimization discussed in eq. (2.81), discussed next.

Suppose that the same data sampling procedure using configuration $\vec{u}$ is performed pre and post dialysis, leading to data sets $\vec{S}_1$ and $\vec{S}_2$. From the corresponding parameter estimates $\vec{r}_1$ and $\vec{r}_2$ we derive the simulated breath curves $B_1(t)$ and $B_2(t)$. The parameters vectors $\vec{r}_1$ and $\vec{r}_2$ are not independent: we set

$$\vec{r}_1 = \vec{r}_{\text{c}} \oplus \vec{r}_{\text{i},1} \quad \text{and} \quad \vec{r}_2 = \vec{r}_{\text{c}} \oplus \vec{r}_{\text{i},2}$$

where $\oplus$ denotes the vector direct sum,

Equation 50 (Co-optimized parameter vector $\vec{r}_{\mathbf{c}}$ in iPBPK-R)

$$\vec{r}_{\mathrm{c}} = (\beta_k, \gamma_k, \gamma_i, \gamma_j, \lambda_k, \kappa_{ij}), \tag{2.82}$$

denoting the co-optimized parameter vector, and

Equation 51 (Independent parameter vectors $\vec{r}_{\mathbf{i,1}}$ and $\vec{r}_{\mathbf{i,2}}$ in iPBPK-R)

$$\vec{r}_{\mathrm{i},1} = (\xi_1, \alpha_{k,1}), \quad \textit{and} \quad \vec{r}_{\mathrm{i},2} = (\xi_2, \alpha_{k,2}), \tag{2.83}$$

denoting the independent parameter vectors, respectively (the subscript i stands for independent). ξ_1 and ξ_2 are inhibition parameters as elements of $\vec{r}_{\mathrm{i},1}$ and $\vec{r}_{\mathrm{i},2}$, respectively. Further $\alpha_{k,j}$, $j = 1, 2$ are independent adjustment factors in mass flow Q_1 (see eq. (2.61)).

Co-optimization setup. Now we discuss how the three parameter vectors are used to co-optimize pre- and post-dialysis parameters. In the *pre-dialysis modeling* of the EBT data, $\vec{r}_{\mathrm{i},1}$ and $\vec{r}_{\mathrm{c}}$ are optimized while ξ_1 is used to replace β_k and λ_k with $\xi_1\beta_k$ and $\xi_1\lambda_k$ in nonlinear mass flow Q_2 of ODEs (see eq. (2.62)). Similarly, in the *post-dialysis modeling* of the EBT data, $\vec{r}_{\mathrm{i},2}$ and $\vec{r}_{\mathrm{c}}$ are optimized while ξ_2 is used to replace β_k and λ_k with $\xi_2\beta_k$ and $\xi_2\lambda_k$ in Q_2 of ODEs. Thus, ξ_1 and ξ_2 act as additional inhibition (as stated above). The parameter vector $\vec{r}_{\mathrm{i},1}$ and $\vec{r}_{\mathrm{c}}$ are optimized for pre-dialysis while $\vec{r}_{\mathrm{i},2}$ and $\vec{r}_{\mathrm{c}}$ are optimized post-dialysis. Thus, $\vec{r}_{\mathrm{c}}$ encodes the pre/post constraint while $\vec{r}_{\mathrm{i},1}$ and $\vec{r}_{\mathrm{i},2}$ encode the independent adjustment factors.

As example let $Q_{2,1}$ and $Q_{2,2}$ be nonlinear mass flows in pre- and post-dialysis, respectively. These are pre/post dialysis inbstances of eq. (2.62). Compared to the original mass flow Q_2 defined in eq. (2.62) where biological inhibition is not accounted for, $Q_{2,1}$ and $Q_{2,2}$ can be written as

$$Q_{2,1}^{(\xi_1,\alpha_{k,1},\gamma_k,\beta_k,\lambda_k,h)} = \frac{(\xi_1\beta_k)^{\delta_{0h}}\mathrm{K}_{k,21}\frac{\mathrm{L}_k}{\gamma_k\mathrm{P}_k}C_k}{(\xi_1\lambda_k)^{\delta_{1h}}\mathrm{K}_{k,22} + \frac{\mathrm{L}_k}{\gamma_k\mathrm{P}_k}C_k}, \ k = i \text{ or } j, \tag{2.84}$$

and

$$Q_{2,2}^{(\xi_2,\alpha_{k,2},\gamma_k,\beta_k,\lambda_k,h)} = \frac{(\xi_2\beta_k)^{\delta_{0h}}\mathrm{K}_{k,21}\frac{\mathrm{L}_k}{\gamma_k\mathrm{P}_k}C_k}{(\xi_2\lambda_k)^{\delta_{1h}}\mathrm{K}_{k,22} + \frac{\mathrm{L}_k}{\gamma_k\mathrm{P}_k}C_k}, \ k = i \text{ or } j. \tag{2.85}$$

The mass flows $Q_{2,1}$ and $Q_{2,2}$ show that we used inhibition parameters to scale adjustment factors of interest and to indicate altered or reduced biological activity from the adjusted IVIVE values in iPBPK-R (Note: An adjusted IVIVE value means an IVIVE value multiplied by a corresponding adjustment factor). Usually the values of inhibition parameters range from 0 to 1 but they can take a value greater than 1 if the parameters should describe

increased biological activity from the adjusted IVIVE values.

Combined optimization problem. With the above setup we can formally express co-optimization across treatment in an EBT study using patients with kidney disease. Again, we have two data sets $\vec{S}_1$ and $\vec{S}_2$ obtained pre- and post-dialysis, respectively, and two solutions of the respective pre- and post-dialysis systems of ODEs, $B_1(t)$ and $B_2(t)$. The same configuration $\vec{u}$ is used for both pre- and post-dialysis. Estimating parameter vectors $\vec{r}_1$ and $\vec{r}_2$ (or $\vec{r}_{\mathrm{i},1}$, $\vec{r}_{\mathrm{i},2}$, and $\vec{r}_{\mathrm{c}}$) is expressed as a single optimization problem,

Equation 52 (Combined optimization problem for multiple data series in iPBPK-R)

$$(\vec{r}_1, \vec{r}_2) = \underset{\vec{r}'_{\mathrm{c}}, \vec{r}'_{\mathrm{i},1}, \vec{r}'_{\mathrm{i},2}}{\arg\min} \sum_{j=1}^{2} \Psi_{\mathrm{2D}}^{\vec{r}'_{\mathrm{c}} \oplus \vec{r}'_{\mathrm{i},j}, \vec{u}} \big(B_j^{\vec{r}'_{\mathrm{c}} \oplus \vec{r}'_{\mathrm{i},j}, \vec{u}}(t),\, \vec{S}_j \big). \tag{2.86}$$

As a note, inhibition parameters like ξ_1 and ξ_2 can be introduced dependent on the addressed research question. In our application of EBT using patients with kidney disease pre- and post-dialysis in chapter 4, we introduce inhibition parameters to multiply to the adjustment factors related to the non-renal elimination pathways (β_6, $\beta_{7,1}$, and $\beta_{7,2}$ in table 7 – table 8) and to evaluate the effect of dialysis on the non-renal elimination pathways. In a general application of co-optimization in iPBPK-R, parameters beyond $\vec{r}$ defined in (2.59) may need to be included in $\vec{r}_1$ and $\vec{r}_2$, and $\vec{u}$ needs to be chosen carefully to model pre/post dependencies and address particular research.

2.6.5 Numerical optimization methods and implementation

We implemented optimization discussed in section 2.6.3 and section 2.6.4 in the R system. We used the R function `ode` in the `deSolve` package that implements a suite of ODE solvers, including explicit and implicit solvers, adaptive solvers, and Runge Kutta solvers [165] [166]. Optimization was performed using the `L-BFGS-B` and `BFGS` algorithms provided by the R function `optim` that implements quasi-Newton method with or without a limited-memory modification, respectively [167]. The nested optimization used for co-optimizing estimates is implemented via a generalized Hill Climbing approach. Optimization of the independent parameter vectors $\vec{r}_{\mathrm{i},1}$ and $\vec{r}_{\mathrm{i},2}$ were performed first independently in a inner loop. Optimization of the co-optimization parameter vector $\vec{r}_{\mathrm{c}}$ was implemented in an outer loop. This iteration was performed iteratively until sufficient convergence.

2.7 Examples and Results

This section provides a brief summary of two applications of iPBPK-R in terms of method perspectives. The detailed results and pharmacological interpretations of the first application in healthy subjects are described in chapter 3. The second application of iPBPK-R in patients with kidney disease is detailed in chapter 4, of which preliminary results were presented as a poster at the American Society of Nephrology 2019 (Kidney Week 2019) [106].

2.7.1 Estimating Parameters in Healthy People

The first application of iPBPK-R is to model $^{14}CO_2$ production rate data obtained from 12 healthy subjects in an EBT study to estimate biological parameters. The study design of the EBT study is described in section 2.4.2 and chapter 3 [105]. Briefly, 12 healthy subjects received a single IV dose of ^{14}C-erythromycin and breath samples were collected immediately at 11 time points within two hours including the baseline time point of EBT. $^{14}CO_2$ production rates in the collected breath samples were calculated.

The model structure of iPBPK-R and the system of ODEs were shown earlier in fig. 7 and table 7–table 9, respectively. For all nonlinear mass flow terms in the ODEs we assumed the type of reduced activity of mass flow to be non-competitive, and thus set $h = 0$ in eq. (2.63). The initial values of the input parameters in table 5 including IVIVE values can be found in table 12 of chapter 3. Note that fraction of the drug filtered via GFR (δ) and distribution ratio of drug transporter b in Compartment 4 to Compartment 7 (η) in table 5 were not available in the literature. We pre-estimated these two parameters by applying iPBPK-R to the mean value of $^{14}CO_2$ production rate at 20 minutes obtained from a published clinical EBT study [169], and used them as fixed values in the iPBPK-R modeling of EBT data of 12 healthy subjects.

Through an initial manual investigation we first identified that nine parameters were either impacting the shape of the simulated rate-time curve $B(t)$ or biologically relevant. Using the notation in table 7, these nine parameters were

$$J_a,\ J_b,\ J_c,\ Q_{cyp},\ V_7,\ P_3,\ \mu_3,\ Q_3,\ \text{and}\ Q_{67},$$

(see table 10), and their respective adjustment factors

$$\beta_6,\ \beta_{7,1},\ \beta_{7,2},\ \alpha_7,\ \zeta_7,\ \gamma_3,\ \alpha_3,\ \kappa_{35},\ \text{and}\ \kappa_{67}. \tag{2.87}$$

were optimized.

The results are summarized in Figure 15 of Chapter 3. The iPBPK-R model fit well for individual $^{14}CO_2$ production rate-time curves as result of high-dimensional parameter optimization. Among the optimized adjustment factors summarized in eq. (2.87), factors β_6, $\beta_{7,1}$, $\beta_{7,2}$, α_7, ζ_7, and κ_{67} were associated with the Liver compartment, where activities in non-renal elimination pathways are target of the research. The estimated values of these parameters are shown in Figure 9, which is identical with Figure 17 (A) in chapter 3. While adjustment factors $\beta_{7,1}$ and $\beta_{7,2}$ did not have impact on the model fit in the figure, we forced them into the iPBPK-R model to satisfy mechanistic considerations. Among the parameter estimates of interest, α_7 was stratified and evaluated by gender. This led to our finding of *gender difference in enzyme-mediated drug elimination* in the liver as described in Chapter 3 [105]. This finding also aligned with literature where the gender-related difference was seen in the same enzyme expression in human liver bank samples [173]. The 3D plot in fig. 10 is an instance of change in the $^{14}CO_2$ production rate-time curve from one subject during the high-dimensional parameter optimization. Section 2.4.7 provides the theoretical foundation for accuracy of our estimates, given the number of parameters in the optimization and initial IVIVE values. In addition, we run numerical experiments during the development of iPBPK-R that indicated the practical stability of the method.

In this application we were able to estimate parameters on both rate-limiting step and non-rate-limiting steps in the non-renal elimination pathways of erythromycin in individual healthy subjects via iPBPK-R taking advantage of the reduced order model as well as high information contents of the rate data. A production simulation run on average required about 10 CPU hours per subject on the *Bridges* supercomputer at PSC [126].

2.7.2 Co-Estimation Pre- and Post Dialysis

The second example is the application of iPBPK-R to the $^{14}CO_2$ production rate data obtained from 12 patients with kidney disease in an EBT study. The study design of the

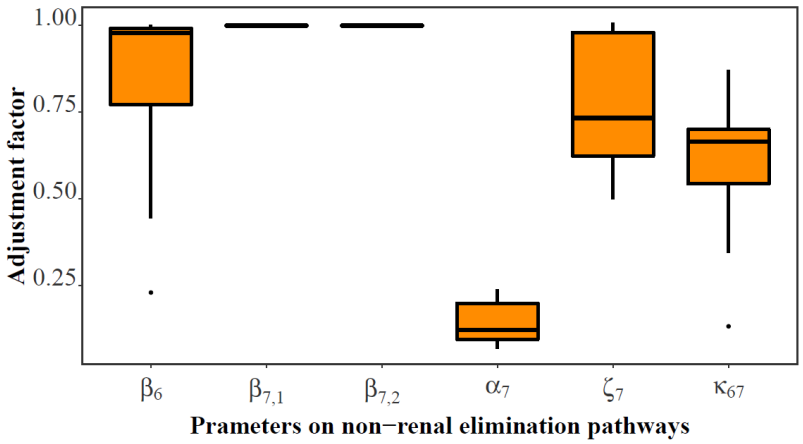

Figure 9: Box plot of estimated adjustment factors of the Liver in 12 healthy subjects.

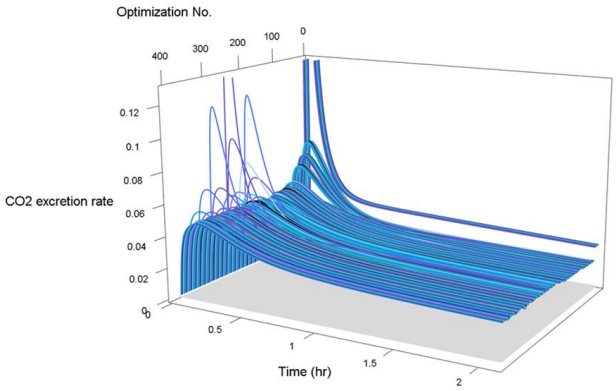

Figure 10: 3D plot of $^{14}CO_2$ production rate-time curve during the optimization in one subject.

EBT study is illustrated in fig. 11 and described in Chapter 4 [128] [106]. Briefly, 12 patients with end-stage renal disease received a single IV dose of ^{14}C-erythromycin before taking a 4-hour dialysis. Two hours post-dialysis these patients received another single IV dose of ^{14}C-erythromycin. In each EBT breath samples were collected immediately at 11 time

points within two hours of IV, including the baseline time point of EBT. Subsequently $^{14}CO_2$ production rates in the collected breath samples were calculated for the pre- and post-dialysis EBTs.

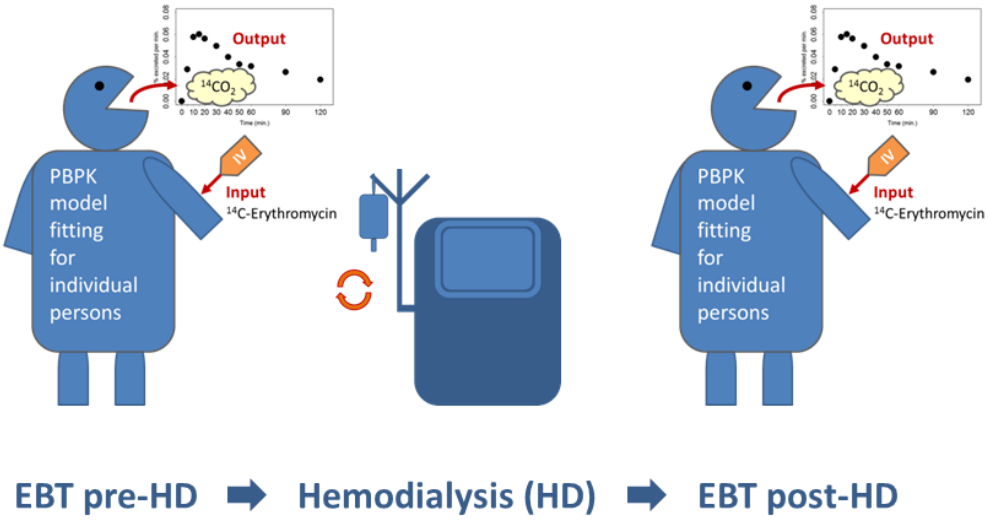

Figure 11: iPBPK-R application to the $^{14}CO_2$ production rate data in patients with kidney disease who underwent dialysis.

The model structure of iPBPK-R and the system of ODEs were similar to those in the first example with healthy subjects, and we assumed that the type of reduced activity of mass flow is non-competitive. The mass flow from the Kidney compartment to the Urine compartment (see fig. 7) was removed assuming no kidney function in the patients and drug removal by dialysis was assumed negligible. Note that it is generally possible to account for the effect of dialysis on the drug clearance of the pre-dialysis dosing and simulate its carryover drug concentrations for the subsequent drug dosing in iPBPK-R. Since we assumed that the percentage of drug removal was 0, we simply simulated the drug concentrations at nine hours of the first EBT without the effect of dialysis and superimposed them on the baseline drug concentrations of the second EBT. Nine hours was assumed to be the time interval between the start of the first EBT and the start of the second EBT. Although the timing of dialysis and time interval between two EBTs were assumed to be the same for all patients in this example, different timings of dialysis can be also incorporated in iPBPK-R.

We selected the same set of parameters for optimization as the in first example with healthy subjects. In the optimization procedure with the two EBT datasets pre- and post-dialysis, we implemented a nested co-optimization for each patient as described in section 2.6.4. One difference from the previous example is that the adjustment factor α_7 in eq. (2.87) was optimized in the inner loop rather than the outer loop of the nested co-optimization so that the linear mass flow associated with CYP3A4 activity can be evaluated pre- and post-dialysis independently. Thus, the adjustment factors pre- and post-dialysis for CYP3A4 activity were independently estimated. Inhibition parameters associated with drug transporters were also estimated independently pre- and post-dialysis in the inner loop so that the change in the activity of each drug transporter could be evaluated by comparing the inhibition parameters pre- and post-dialysis.

We show the resulting iPBPK-R model fit for all patients pre- and post dialysis in Figure 23 of chapter 4. The iPBPK-R model fit the individual $^{14}CO_2$ production rate-time curves pre- and post-dialysis well. Two sets of parameters corresponding to pre- and post-dialysis EBT, respectively,

$$(\xi_6^{\mathrm{pr}}, \xi_{7,1}^{\mathrm{pr}}, \xi_{7,2}^{\mathrm{pr}}, \alpha_7^{\mathrm{pr}}), \quad \text{and} \quad (\xi_6^{\mathrm{ps}}, \xi_{7,1}^{\mathrm{ps}}, \xi_{7,2}^{\mathrm{ps}}, \alpha_7^{\mathrm{ps}}),$$

were independently estimated in the inner loop. Using these estimates, activities of CYP3A4 enzyme and drug transporters could be compared between pre- and post-dialysis in each patient so that the effect of dialysis on the non-renal elimination pathways could be evaluated. iPBPK-R enabled us to individually estimate both rate-limiting and non-rate-limiting steps of non-renal elimination pathways and their changes in drug disposition. The changes in parameter estimates could be also used to evaluate correlations between the activities in the non-renal elimination pathways and candidate biomarkers such as plasma concentrations of uremic toxins across patients. A production simulation run on average required 24 CPU hours per patient on the *Bridges* supercomputer at PSC. The comprehensive results are described in chapter 4.

2.8 Discussion

In this section we discuss the iPBPK-R method and its comparisons with other traditional pharmacokinetics modeling. As briefly reviewed in Section 2.7, we demonstrate that experimental findings in literature are captured by our method in Chapter 3. Our estimated adjustment factor on CYP3A4 activity show gender-related difference similarly to a study where the CYP3A4 in human liver bank samples was analyzed, and we detail this biological significance in Chapter 3. In this chapter, several techniques of iPBPK-R that enabled us to simultaneously estimate multiple physiological parameters in individuals were described.

2.8.1 iPBPK-R Characteristics

Use of rate data. Production rate data as the first derivative of drug concentration data was used in the iPBPK-R model fitting. The simulated $^{14}CO_2$ production rate data was used in nested (co-)optimization to inversely estimate multiple parameters of interest. Through the dynamic changes in the early phase of a $^{14}CO_2$ production rate-time curve, parameters of both rate-limiting and non-rate-limiting steps could be estimated. Even with one dosage, small but detectable variation in the data allowed us to infer parameters governing nonlinearity through the coupled system of ODEs. We also benefited from the frequently sampled $^{14}CO_2$ production rate data within the first 2 hours of the breath test since it provided the sensitive signals of physiological changes that we were interested in. While we used a rate measurement in the examples with EBT, multiple drug concentration datasets per individual can be also used in iPBPK-R if available. Such datasets can be coupled through rate relationships within a system of ODEs. Using multiple drug concentration datasets is explored in chapter 5 as the next step of iPBPK-R development.

Use of reduced order model. We used a reduced order model in iPBPK-R. As explained in section 2.5, the number of compartments was limited so that parameters in the model could be estimable. At the same time the model structure we used in the examples with EBT was a full PBPK model according to Sager et al. [70]. It is essential to use a reduced order model in iPBPK-R since the main purpose of this method is not to predict

drug concentration behaviors but to back estimate multiple physiological parameters of a system of nonlinear ODEs in individuals. In section 2.4.7, we showed that the parameter estimation in iPBPK-R can be cast as an optimization problem and that the optimization behaves well locally around the solution given a carefully designed objective function. Given the number of compartments we provided the theoretical foundation regarding the number of parameters (or adjustment factors) that we can generally estimate with iPBPK-R. iPBPK-R differs from conventional PBPK modeling where a limitless number of parameters is used to capture all foreseen variabilities in various clinical scenarios or populations. iPBPK-R is complemental to the conventional PBPK approaches.

Objective function in iPBPK-R. We developed a specialized objective function for parameter optimization of iPBPK-R. In the objective function a 2D distance measure between simulated and observed rate data was combined with constraint and penalty terms such as bias, lower bound, drift, and x-shift (see section 2.6.1). Furthermore, these terms can be weighted depending on optimization problem characteristics. When the underlying system of ODEs includes instable nonlinear terms a considerable effort is generally required for stable parameter estimation. Our objective function aids convergence without skewing the results of high-dimensional optimization as discussed in section 2.4.7. Optimization with the objective function is implemented using a quasi-Newton method with or without a limited-memory modification as described in section 2.6.5.

Use of biological knowledge as reference. A priori knowledge in related literature, for example, clinically anticipated physiological parameters derived from *in-vitro in-vivo extrapolation (IVIVE)*, were used as reference values in parameter optimization as well as in the aforementioned objective function. This is part of aiding convergence around the solution and it is useful in selecting sensitive parameters as optimization parameters. In the system of nonlinear ODEs we introduced and estimated adjustment factors which measure the size of deviation from reference values such as IVIVE values in individuals. This technique allows us to obtain biologically plausible estimates for parameters of interest. As established in section 2.4.7 parameter estimates via iPBPK-R are close to IVIVE values since the starting values of the optimization are derived from IVIVEs. This is a major strength of iPBPK-R even though the global minimum in parameter optimization is not guaranteed.

Co-optimization for estimating altered physiological parameters. In order to estimate some physiological parameters independently while co-estimating other physiological parameters as unchanged before and after intervention in each individual, we developed a nested co-optimization approach. Independent parameters are optimized in the inner optimization loop while common parameters are optimized in the outer optimization loop. The nested co-optimization is based on a generalized Hill Climbing algorithm as described in section 2.6.4. We provided a brief summary of the application example using EBT data in patients with kidney disease who received EBTs pre- and post-dialysis. The nested co-optimization was conducted to estimate altered parameters by dialysis in section 2.7.2. The results of this example showe consistent and plausible parameter estimates in each patient and across patients in chapter 4. The timing of dialysis were assumed to be the same for all patients but different timings of dialysis across patients can be also modeled in iPBPK-R. The biological details of the parameter estimates and clinical interpretations are described in chapter 4. Co-optimization to estimate altered physiological parameters can be applied to evaluation on the impact of not only intervention but also disease progression or some status change due to co-medication in individuals. iPBPK-R is a powerful tool to identify particular changes in modeled physiological activities in particular individuals and thus differentiate the individuals based on the physiological activities that cannot be measured directly.

Computational cost and time. Lastly, iPBPK-R simulation and parameter optimization was implemented using R, which demanded high computational resources and resulted in long run times. We conducted the large-scale simulations needed for production runs, method development, and design space exploration at the *Bridges* supercomputer at PSC. iPBPK-R model fitting took four hours to eight days per individual. A total of 150,000 CPU hours was approximately spent in the development and applications of iPBPK-R. The execution time depends on the difficulty of the optimization problem. By switching to a more efficient programming language like C++ it would be possible to shorten the simulation time enormously and improve the efficiency of iPBPK-R. This would come at substantial development cost and should only be done when the method development has fully concluded.

2.8.2 Comparison to Other Procedures

As mentioned above, iPBPK-R was developed for estimating multiple physiological parameters. This is distinctly different from classical approaches for estimation and prediction. A *cocktail approach* where a subject takes multiple activity-specific probe drugs is the standard method to indirectly estimate different biological activities [122] [123]. The group-wide activities associated with the respective drugs are statistically estimated, in contrast to individual estimates in iPBPK-R. In conventional *population PBPK modeling*, IVIVE values are generally used as fixed input for simulations and prediction. It is assumed that the extrapolated physiological values from preclinical literature are population means in humans and corresponding assumed variance may be given. Thus, population PBPK modeling is a statistics-based modeling approach. Population PBPK modeling for prediction are generally conducted before observed data from clinical studies are available. Such PBPK models are later validated when observed clinical data become available.

Mechanistically dependent parameters are estimated in iPBPK-R. Unlike population PBPK modeling for prediction, iPBPK-R does not use distributional assumptions for physiological parameters but uses them as reference values. It then numerically fits to individual observed data to perform parameter estimation (i.e., estimation of adjustment factors). The iPBPK-R approach makes sense when we are interested in estimating individual parameters for precision medicine and when these physiological parameters are mechanistically dependent in the system. If we instead use a population PBPK model and inversely solve for multiple parameters of the underlying system of ODEs, it is likely to produce biased estimates since many physiological parameters in the population model are treated as independent in their distributional assumptions. iPBPK-R overcomes this potential bias by utilizing a reduced order model and numerically optimizing multiple parameters simultaneously via individual model fitting.

Adjustment factors explain interindividual variability. IVIVE values which are used in both population PBPK and iPBPK-R modeling, are not guaranteed to be a clinically relevant population mean values. The mathematical equations used to extrapolate *in vitro* experimental values to obtain IVIVE values are based on relatively simple mathematical

models. *In vitro* data may not necessarily represent the average value of response in a particular type of cells when the sample size is small or experimental conditions for cell culture vary. While a log-log plot is commonly used to show a good linear correlation in IVIVE research, it does not mathematically indicate a linear relationship if the plot deviates from the diagonal line. In iPBPK-R, we estimate adjustment factors to measure the exact size of deviation from the IVIVE references individually. iPBPK-R overcomes the limitations of the typical use of IVIVE.

Real-time and parallel validation with observed data. In population PBPK modeling, a model validation step is required to confirm its predictive ability when observed data become available. Sufficient predictive ability of a population PBPK model is essential if, for example, the model is subsequently used to predict lower and upper bounds of the drug concentration-time behavior for another population. On the other hand, iPBPK-R uses a pre-determined model structure and the model fits to individual observed data to inversely estimate parameters given the model structure. In this sense iPBPK-R does not require a separate model validation step with observed data. Instead, visual inspection of a goodness-of-fit plot with every individual dataset serves as independent and parallel validation steps. Successful high-dimensional parameter optimization also serves as model validation.

Use of nonlinear ODE system for estimation but not for covariate selection. The core of the methodological procedure to estimate multiple physiological parameters of iPBPK-R is a high-dimensional parameter optimization procedure. iPBPK-R does not rely on model selection in the same sense as population PK modeling. Unlike PBPK modeling, classical PK modeling is a non-mechanistic modeling approach and it is frequently implemented with specialized PK software such as NONMEM. Population PK modeling is useful to identify important covariates (e.g., ethnicity, gender, age, clinical laboratory data among others) that impact on inter-individual variability in drug exposure. Covariate selection or model selection is an important part of the modeling procedure. While population PK modeling itself is typically based on a nonlinear model structure, covariate selection is done within a linear term of the model structure. Apparently mechanistically-unrelated covariates are selected to explain systematic differences in a clearance term, for example. The selection criteria are based on some statistical method such as a likelihood ratio test. iPBPK-R, on

the other hand, is based on a pre-defined system of nonlinear ODEs as a model structure which needs to sufficiently describe mechanistically dependent relationships in the system of interest. Multiple physiological parameters in both linear and nonlinear terms across ODEs are optimized rather than being dropped or added. These parameters may be functionally dependent unlike in population PK modeling where covariates are assumed to be independent variables.

In iPBPK-R, the dependent parameters comprise a complex optimization problem instead of a model selection problem. Unlike population PK modeling where *two sets of linear covariate combinations* between nested models are compared, *multiple potentially dependent mechanistical parameters* of a system of nonlinear ODEs are simultaneously estimated in iPBPK-R. There is no formal statistical test to compare two sets of multiple dependent parameters with respect to model fitting in iPBPK-R. However, it is generally understood that such two sets of parameters for the same system of nonlinear ODEs result in quite different sets of solutions. Consequently, high-dimensional parameter (co-)optimization of iPBPK-R is expected to produce accurate parameter estimates as we have established via the theoretical foundation in section 2.4.7.

Conditions to avoid overfitting and stability issues. In absence of covariate selection in iPBPK-R, one might be concerned with potential model overfitting and parameter stability issues. In particular, these issues might be raised when two application examples in section 2.7 have shown that iPBPK-R model fitting was consistently good as in Figure 15 of chapter 3 and Figure 23 of chapter 4. As we have established the theoretical foundation in section 2.4.7, the numbers of optimized parameters in these examples were within the maximum number of estimable parameters in the system of nonlinear ODEs for ^{14}C-erythromycin. This supports that the application examples of iPBPK-R were free from overfitting and parameter stability issues. In addition, the computational cost and time for high-dimensional parameter (co-)optimization were substantial on the supercomputer at the PSC, making numerical stability experiments and Monte Carlo style evaluation beyond a few samples impractical. We established good numerical behavior within the practical limits posed by our fully exploited grant of 150,000 CPU hours at PSC.

Novel, indirect measurement approach. In summary, iPBPK-R is a novel *indirect*

measurement approach which is useful to estimate multiple physiological parameters in individuals using clinical observed data. Breath biopsy data [124, 125] is particularly well-suited as it can be modeled as first derivative of drug concentration data. Using a reduced order model and a specialized objective function with IVIVE references, adjustment factors are optimized via nested optimization that can be used for investigating inter-individual variability. By implementing nested co-optimization, altered physiological parameters by an intervention can be also estimated per individual. Unlike population PK modeling and population PBPK modeling, covariate selection or model validation is irrelevant in our approach. The core part of the iPBPK-R procedure is high-dimensional optimization in a system of nonlinear ODEs across all data of an individual. In iPBPK-R other types of clinical datasets including multiple drug concentration datasets per individual can be used, which we address in Chapter 5 and future work.

2.9 Conclusions

In this chapter we presented a novel PBPK approach we call *iPBPK-R* that allows us to estimate multiple parameters on physiological activities that cannot be directly measured in individuals. This *indirect measurement* approach integrates several features: rate data, use of a reduced order model as a PBPK model structure, specialized objective functions utilizing a prior knowledge obtained from *in vitro* experiments (i.e., use of IVIVE), and nested (co-)optimization. Thus, iPBPK-R can be applied to clinical rate data sampled from a breath test. We provide the theoretical foundation of the parameter estimation and provide evidence that multiple parameter estimates in iPBPK-R are stable and accurate.

In an application of iPBPK-R to $^{14}CO_2$ production rate data from an EBT it has been demonstrated that biological findings derived from parameter estimates were compatible with biological experiments. Furthermore, physiological activities pre- and post-dialysis were independently estimated in individual patients via the nested co-optimization. iPBPK-R uses high-dimensional parameter estimation. It is an approach complementary to population PK and PBPK modeling. Based on the success with the applications to EBT, we anticipate

various opportunities to apply iPBPK-R and assist future precision drug dosing and personalized medicine. At this point the iPBPK-R approach is computationally costly but it can be made fast and cheap enough for deployment through proper performance-oriented software engineering. We also anticipate that iPBPK-R can be applied to multiple datasets of drug concentrations per individual. The first application to such data is shown in Chapter 5 and discussed as our next research direction for iPBPK-R in Chapter 6.

3.0 Simultaneous Assessment of Hepatic Transport and Metabolism Pathways with a Single Probe Using Individualized PBPK Modeling of $^{14}CO_2$ Production Rate Data (iPBPK-R)

This chapter has been published in *the Journal of Pharmacology and Experimental Therapeutic* (2019) 371:151–161; DOI: https://doi.org/10.1124/jpet.119.257212.

3.1 Abstract

Erythromycin is a substrate of cytochrome P4503A4 (CYP3A4) and multiple drug transporters. Although clinical evidence suggests that uptake transport is likely to play a dominant role in erythromycin's disposition, the relative contributions of individual pathways are unclear. Phenotypic evaluation of multiple pathways generally requires a probe drug cocktail. This approach can result in ambiguous conclusions due to imprecision stemming from overlapping specificity of multiple drugs. We hypothesized that an individualized physiologically-based pharmacokinetic modeling approach incorporating $^{14}CO_2$ production rates (iPBPK-R) of the erythromycin breath test (EBT) would enable us to differentiate the contribution of metabolic and transporter pathways to erythromycin disposition. A seven-compartmental PBPK model was built for ^{14}C-erythromycin administered intravenously. Transporter and CYP3A4 clearance were embedded in hepatic compartments. $^{14}CO_2$ production rates were simulated taking the first derivative of by-product $^{14}CO_2$ concentrations. Parameters related non-renal elimination pathways were estimated by model fitting the EBT data of 12 healthy subjects individually. Optimized iPBPK-R models fit the individual rate data well. Using one probe, nine PBPK parameters were simultaneously estimated per individual. Maximum velocity of uptake transport, CYP3A4 clearance, total passive diffusion and others were found to collectively control $^{14}CO_2$ production rates. The median CYP3A4 clearance was 12.2% of the input clearance. Females had higher CYP3A4 activity than males by 11.3%. We applied iPBPK-R to EBT data to distinguish and simultaneously estimate the activity of multiple non-renal elimination pathways in healthy subjects. The iPBPK-R framework is a novel tool for delineating rate-limiting and non-rate-limiting elimination pathways using a single probe.

3.2 Introduction

The macrolide antibiotic erythromycin is a nonrenally cleared drug that undergoes hepatic elimination via multiple pathways [110] [174] [171] [175] [87]. In the past, erythromycin

was commonly used as a metabolic probe drug. It was administered intravenously and employed in the erythromycin breath test (EBT) to noninvasively measure in vivo hepatic cytochrome P450 (CYP) 3A4 (CYP3A4) activity [176] [177] [128] [178]. Use of the EBT in this manner relied on the premise that intravenously administered radiolabeled erythromycin undergoes N-demethylation by CYP3A4 in the liver and that $^{14}CO_2$, a final by-product of the CYP3A4-mediated elimination pathway, is rapidly detected in breath [176] [128]. However, it is now known that erythromycin also undergoes hepatic drug transport, i.e., hepatic clearance by organic anion transporting polypeptides (OATPs), P-glycoprotein (P-gp), and multidrug resistance-associated protein 2 (MRP2)-mediated elimination pathways [174] [171] [169] [170] [175] [179] [180].

After hepatic uptake transport by OATPs into the cells, ^{14}C-erythromycin partly undergoes N-demethylation by CYP3A4 and gets converted to N-demethylated metabolites and ^{14}C-formaldehyde. ^{14}C-formaldehyde gets mostly converted to ^{14}C-formate. Subsequently, $^{14}CO_2$ is released and exhaled in breath in this CYP3A4-mediated pathway. Meanwhile, unmetabolized drug and N-demethylated metabolites are excreted by the transporter P-gp [169] [170]. Accordingly, interpretations of EBT data were misleading under the assumption the erythromycin clearance was dependent solely on CYP3A4-mediated metabolism [133] [132]. While some studies with EBT concluded that there was a positive or inverse relationship between an EBT measure and a change in CYP3A4 activity [177] [128] [178], a pilot pediatric study show neither a consistent peak of $^{13}CO_2$ flux across preterm infants nor a potential use of EBT for measuring CYP3A activity in these patients [176]. The EBT has been reported to correlate poorly with the clearance of other drugs [129] [130]. Furthermore, clinical studies with OATP and/or P-gp inhibitors [169] [170] or a MRP2 variant [171] indicated that the effects of uptake and efflux transporters on erythromycin disposition would need to be accounted for in the interpretation of EBT results. Consequently, research using the EBT became less attractive and less common. In fact, it was determined that more research on the EBT itself was necessary in order to establish its reliability [169] [132] [181] [168].

The $^{14}CO_2$ production *rate* measurement of EBT results may provide a unique opportunity to differentiate contributions of metabolic versus transporter-mediated pathways to erythromycin disposition since $^{14}CO_2$ concentration in breath is proportional to the $^{14}CO_2$

production rate in the hepatocyte. Moreover, contributions of specific pathways may be estimated within individuals or *per person* when physiologically-based pharmacokinetic (PBPK) modeling is applied to $^{14}CO_2$ production rate data. By measuring the breath concentration as proxy for $^{14}CO_2$ production rate, a hidden behavioral signal can be captured, which is usually unrecognized and treated as noise in modeling mean drug concentrations [134]. Thus, the advantage of incorporating measured $^{14}CO_2$ production rate into PBPK modeling is that the *concentration change*, or *rate*, contains greater information and is more sensitive to physiological changes compared to concentration itself as described in *Highly sensitive indirect measurement* of Section 2.4.1 (Chapter 2) and also described in the Method Section (Section 3.3.4) along with Figure 12 in this chapter. Therefore, multiple elimination pathways of a single drug can be differentially estimated using the rate data. The mechanism and validity of differentially dissecting the multiple parameter estimates are provided via the detailed analysis of estimation and use of regularization in Chapter 2 (see Sections 2.6 and 2.4.7).

The aim of this work was to estimate the activity and corresponding contribution of mutliple nonrenal clearance pathways to the elimination of a single probe (erythromycin) with our novel individualized PBPK modeling approach using rate data (iPBPK-R). The present study establishes proof of concept that rate data may be used as a method for estimating the activities and differentiating the contribution of multiple clearance pathways to the elimination of a single probe drug that exhibits overlapping substrate specificity. We anticipate that the iPBPK-R framework will be applicable to breath rate data of other compounds such as volatile organic compounds [118] [182] to evaluate drug-drug interactions, disease effects on drug disposition, and the relationship between potential biomarkers and intervention, among others.

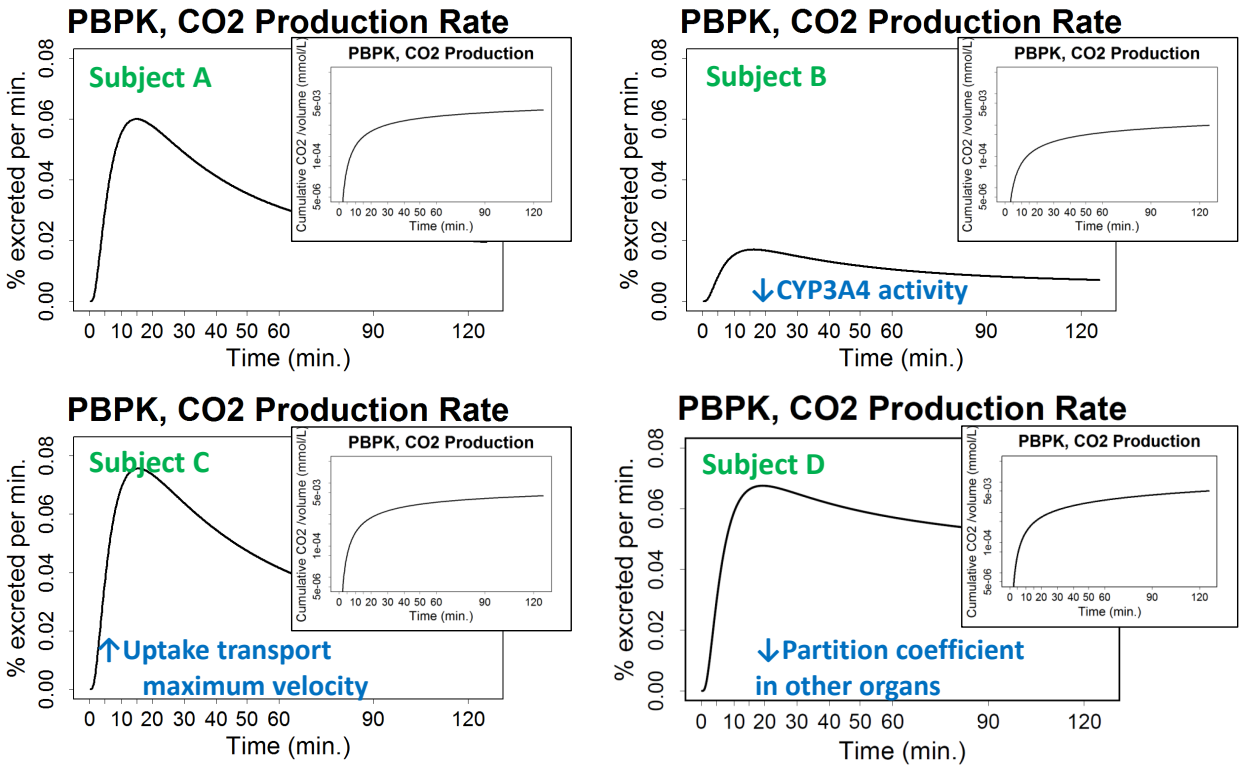

Figure 12: Examples of impact of PBPK parameters on the shape of the $^{14}CO_2$ production rate – time curves compared to the shape of the $^{14}CO_2$ concentration – time curves in the hepatocyte.

When drug concentration-time curves (inset panel figures) and corresponding rate-time curves (larger panel figures) are simulated, the number of parameters for which information can be extracted via modeling differs between the drug concentration data versus rate data. The rationale is provided in *Highly sensitive indirect measurement* in Section 2.4.1 (Chapter 2) and in Section 3.3.4 (Chapter 3). We here illustrate three parameter examples[1] visually affecting the rate-time curves (while the concentration-time curves are generally described with two parameters) using four hypothetical subjects A-D. In each of the four panels (A – D), the main plot shows the $^{14}CO_2$ production rate – time curve and the inset smaller panel shows the corresponding $^{14}CO_2$ concentration – time curve. Both curves were simulated using PBPK modeling. The upper left panel: this panel illustrates $^{14}CO_2$ pro-

[1]As a result of the application of iPBPK-R, we found that more than three parameters affect the rate-time curves as described in the Result Section (Section 3.4).

duction rate – time curve and $^{14}CO_2$ concentration – time curve for a hypothetical healthy subject denoted Subject A. The upper right panel for Subject B: Compared to the $^{14}CO_2$ production rate – time curve of Subject A, Subject B has a lower CYP3A4 clearance and the $^{14}CO_2$ production rate – time curve of Subject B is flatter without presenting a sharp peak accordingly. The lower left panel for Subject C: Compared to Subject A, Subject C has a higher peak of the $^{14}CO_2$ production rate – time curve due to the increased maximum velocity of the uptake drug transport. The lower right panel for Subject D: Compared to Subject A, Subject D shows the greater AUC of the $^{14}CO_2$ production rate – time curve due to the decreased volume of the hepatocyte. Subject D has less steep slopes in the first and second elimination phases of the $^{14}CO_2$ production rate – time curve due to the decreased partition coefficient of the combined other organs compared to those of Subject A. Note that the curves of Subject B – D were simulated by changing particular parameter(s) based on the curves of Subject A, and these subjects are hypothetical examples. Figure 12 was adapted from [105] with a modification to clarify the AUC of the $^{14}CO_2$ production rate – time curve increases with a decreased partition coefficient of the combined other organs.

3.3 Materials and Methods

3.3.1 Clinical Data Sources

The $^{14}CO_2$ production rate data were obtained from a prospective cohort study in which the EBT was administered to 12 healthy Caucasian subjects (7 male) [127]. Briefly, a single 0.074 mmol (0.04 mg, 3 μCi) dose of [14C-N-methyl] erythromycin (Metabolic Solutions Inc., Nashua, NH) was intravenously administered and breath samples were collected immediately before receiving the dose and at 5, 10, 15, 20, 30, 40, 50, 60, 90, and 120 min post dosing as previously described [128]. The study adhered to the Declaration of Helsinki and was approved by the Maine Medical Center Institutional Review Board and the Radiation Safety Committee. Parameters for which no in vitro values were available in the published literature and that could not be calculated using the in vitro–in vivo extrapolation (IVIVE) approach were estimated by applying the PBPK-R model (described in the next subsections) to the previously published $^{14}CO_2$ production rate at 20 minutes [169].

3.3.2 PBPK Model Structure

As shown in Figure 13, a PBPK model comprising six organ compartments was built with pharmacokinetic parameters for ^{14}C-erythromycin. These compartments were artery (Art), Vein, lung (LG), liver (LV), kidney (KD), and combined other organs (OT). The liver compartment consisted of two sub-compartments, extracellular space (ES) and liver cell (LC). A non-linear meta-uptake transporter (OATPs are combined; see 'Model Assumptions') and total passive diffusion modeled the drug transfer between the ES and LC sub-compartments. Non-linear efflux transporters (P-gp and MRP2) and CYP3A4 clearance were modeled in the LC compartment. CYP3A4 clearance was observed to be linear, which is not surprising since a low dose of ^{14}C-erythromycin was administered and it was expected that its concentration was well below the maximum velocity of nonlinear kinetics.

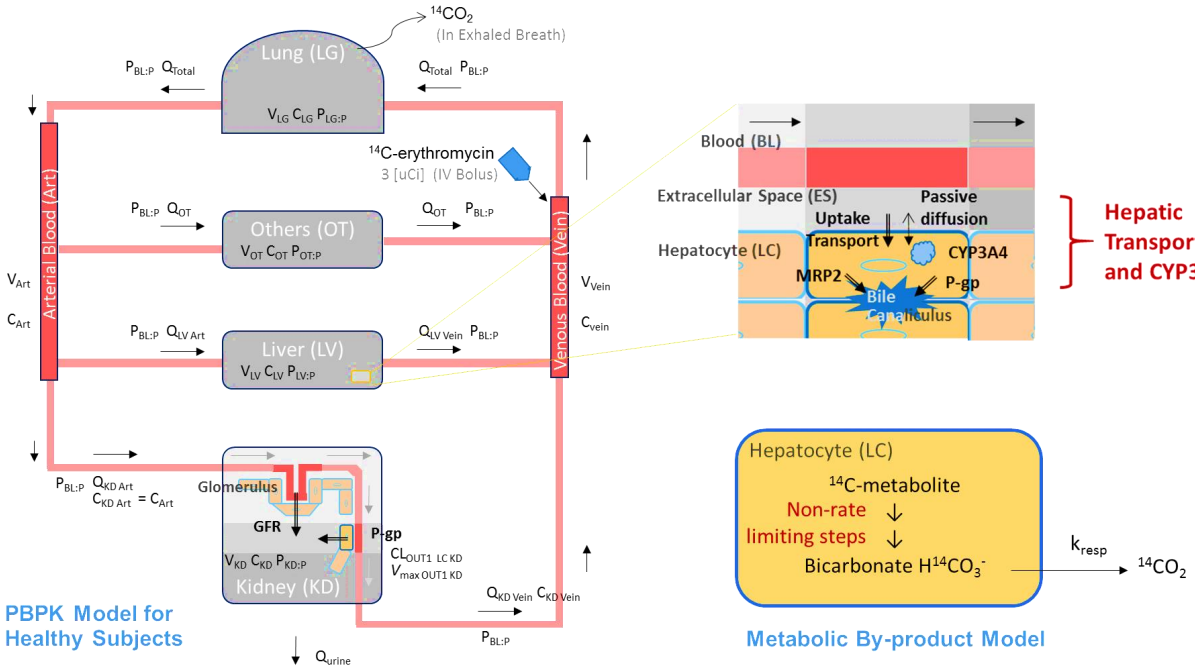

Figure 13: Schematic representation of a PBPK model for describing the time profiles of ^{14}C-erythromycin after intravenous ^{14}C-erythromycin administration in a healthy subject.

The PBPK model consisting of six organ compartments was built with pharmacokinetic parameters for ^{14}C-erythromycin. The upper right shows the liver comprised of two sub-compartments (extracellular space (ES) and liver cell or hepatocyte (LC)) where non-linear uptake and efflux transporters and linear enzymatic clearance were embedded. In the lower right, the metabolic by-product model is illustrated where the metabolite ^{14}C-formate is converted to radiolabeled bicarbonate $H^{14}CO_3^-$ in the CYP3A4-mediated pathway and dissolved in the LC sub-compartment. The series of conversion from 14C-formaldehyde to $H^{14}CO_3^-$ is assumed to be a rapid process and non-rate-limiting. Then, $^{14}CO_2$ is produced and exhaled in breath as a result of the first-order elimination of bicarbonate (with a constant kresp) from the LC sub-compartment.

3.3.3 Ordinary Differential Equations, Kinetic Parameters, and Data Input

Changes in drug concentrations of all compartments and sub-compartments contained within the PBPK model were mathematically described with a set of ordinary differential equations (ODEs) (see B). We used permeability-limited liver models in the ODEs associated with the ES and LC sub-compartments [101]. In addition, we referred to Kanamitsu et al. [183] for the metabolic by-product model in order to describe the series of non-rate-limiting steps from ^{14}C-formaldehyde to bicarbonate and subsequent $^{14}CO_2$ generation within the LC sub-compartment This allowed us to approximate the CO2 concentration in the breath through the first derivative of the cumulative CO2 concentration generated in the LC sub-compartment (CO2 concentration rate of the LC sub-compartment) (see Figure 13 and 'Model Assumptions'). Table 12 provides physiological and kinetic parameters that were calculated based on IVIVE. These parameter values were used as initial input values in the iPBPK-R model fitting.

Table 12: Parameters used for the erythromycin breath test simulations

Description (units)	Notation	Value	Reference/Comments
Dose (mmol)		0.074	
Volume of kidney (L)	V_{KD} (= V_4)	0.270	[184]
Volume of lung (L)	V_{LG} (= V_1)	0.775	[184]
Volume of vein (L)	V_{vein} (= V_2)	2.700	[184]
Volume of the combined other organs (L)	V_{OT} (= V_3)	52.337	Calculated based on [184]
Volume of artery (L)	V_{art} (= V_5)	2.700	[184]
Volume of extracellular space in the liver (L)	V_{ES} (= V_6)	0.340	Calculated based on [184] [101] [185]
Effective volume of Extracellular space in the liver (L)	$V_{ES,eff}$ (= V'_6)	0.543	Based on modification of equation 2 of [101]
Volume of hepatocyte (L)	V_{LC} (= V_7)	1.139	Calculated based on [184] [101] [185]
Blood flow of kidney (L/hr)	Q_{KD} (= Q_4)	66	[5]
Estimated glomerular filtration rate (L/hr)	eGFR (= δG_{fr})	5.964	Average value of this cohort of the 12 healthy subjects
Total body blood flow (L/hr)	Q_{Total} (= Q_1)	300	[5]
Blood flow of the combined other organs (L/hr)	Q_{OT} (= Q_3)	136	Calculated based on [5]

Table 12: Parameters used for the erythromycin breath test simulations

Description (units)	Notation	Value	Reference/Comments
Blood flow of hepatic artery (L/hr)	$Q_{LV,Art}$ (= Q_5)	98	Calculated based on [186]; Portal blood hepatic artery blood flow were combined to simplify the model
Blood flow of hepatic vein (L/hr)	$Q_{LV,Vein}$ (= Q_2)	98	[186]
Total passive diffusion between extracellular space and hepatocyte (L/hr)	Q_{ES-LC} (= Q_{67})	227	[187]
Clearance via hepatic uptake transport (L/hr)	CL_{UP1}	212.29	[187]
Clearance via Pgp (L/hr)	CL_{OUT1}	0.347	Assumed based on an initial simulation using [169]
Clearance via MRP2 (L/hr)	CL_{OUT2}	1.735×10^{-4}	Calculated by J_{max} and K_m
Clearance via CYP3A4 (L/hr)	CL_{CYP} (= Q_{cyp})	176.4	[183]
Fraction unbound in blood	$f_{u,BL}$ (= f_b)	0.27	Assumed based on [188]
Fraction unbound in extracellular space	$f_{u,ES}$ (= f_6)	0.425	Calculated based on [189] [190] [191] [192][2]
Fraction unbound in hepatocyte	$f_{u,LC}$ (= f_7)	0.05	[187]
Partition coefficient of lung to plasma	$P_{LG:P}$	0.33	Assumed based on [194]
Partition coefficient of the combined other organs to plasma	$P_{OT:P}$	0.801	Calculated based on [195] [196] [188]
Partition coefficient of blood to plasma	$P_{BL:P}$ (= P_b)	0.854	[186]
Partition coefficient of kidney to plasma	$P_{KD:P}$	2.23	[186]
Partition coefficient of hepatocyte to plasma	$P_{LC:P}$ (= P_{7p})	2.71	[186]
Partition coefficient of extracellular space to plasma	$P_{ES:P}$ (= P_{6p})	1.10	Assumed based on partition coefficient of epithelial lining fluid to plasma in [194]

[2] $f_{u,ES}$ was calculated applying the assumption proposed for general physiological PK modeling by Khor et al. to our modeling. This assumption was 'the blood protein to which the drug binds is also present in interstitial fluid and that the association binding constant is the same in both blood and interstitial fluid' [189]. Extracellular space matrix (ECM) is known to have many proteins such as fibrillar collagens, proteoglycans, growth factors, cytokines, chemokines, enzymes, among others [193]. We treat these proteins in ECM in the liver as a general protein that can bind to erythromycin in the modeling.

Table 12: Parameters used for the erythromycin breath test simulations

Description (units)	Notation	Value	Reference/Comments
Maximum velocity of hepatic uptake transport (mmol/hr)	$J_{max,UP1}$ (= J_a)	9.6833×10^{-3}	[187] [67] [184] [197]
Michaelis constant of MRP2 (mM)	$K_{m,OUT2}$ (= K_c)	64.4×10^{-3}	[171]
Maximum velocity of transport by MRP2 (mmol/hr)	$J_{max,OUT2}$ (= J_c)	11.17314×10^{-6}	[171]
Elimination constant of bicarbonate (hr^{-1})	k_{resp} (= k_3)	12.72	[172]

3.3.4 Rate Data and Reduced Order Model

Frequently sampled rate data has more information compared to equivalently sampled concentration data[3]. However, it requires more effort to extract the information. Non-linear model fitting of measured first derivative data is often performed to estimate sensitive parameters in established methodologies utilized in digital signal processing and other engineering disciplines [134]. We modeled the $^{14}CO_2$ production rates from the EBT study using the same concept, which is illustrated in Figure 12. Accordingly, the iPBPK-R method was applied to the $^{14}CO_2$ production rate data, and multiple hepatic elimination pathways, i.e., uptake and efflux transport and passive diffusion parameters, were estimated using the single probe drug ^{14}C-erythromycin. In order to achieve high precision in model fitting to the high resolution $^{14}CO_2$ rate data, we used a reduced order model as detailed in Section 2.5 in Chapter 2 [198]. Reduced order models are generally complex enough to capture the behavior of interest but simple enough so that the mathematical models are well-posed providing estimable parameters. Based on this rationale, the seven-compartmental PBPK model was built as described in Subsections 3.3.2 and 3.3.3.

[3]In other words, we here specifically contrast the mathematical properties between drug concentration data and rate data both of which are observed or calculated data at the same sampling points and accuracy as described in *Highly sensitive indirect measurement* of Section 2.4.1. The difference between the data is the measurement unit, and the observed rate data as treated as the first derivative of drug concentration data leads to higher accuracy and thus good separation of estimated model parameters.

3.3.5 Model Assumptions

The number of compartments was limited to seven including sub-compartments to facilitate fitting of PBPK models to EBT data while enabling estimation of the activity and corresponding of effect of CYP3A4 and drug transporters on erythromycin disposition. The modeling was carried out under the following assumptions:

- ^{14}C-erythromycin is intravenously administered for 30 seconds. Except for the liver and kidney compartments, all compartments were assumed to be perfusion-limited where the distribution of a drug rapidly reaches equilibrium via passive diffusion and the unbound concentration in the compartment is the same as those in the diffused space at equilibrium. Perfusion-limited compartments were described with a well-stirred model [183] [199].
- Pathways from the ES compartment to the LC compartment for erythromycin are comprised of total passive diffusion + summation of uptake transporters only. Erythromycin mainly undergoes hepatic uptake transport by OATP isoforms OATP1B1 and OATP1B3. These uptake transport processes were modeled as a single meta-uptake process.
- CO^2 is present in the systemic circulation under steady state conditions. Accordingly, $^{14}CO_2$ is instantaneously released in breath via the lung without being stored in or released from any other compartments after it gets generated in the LC sub-compartment.
- We assume that a metabolite ^{14}C-formate is converted to radiolabeled bicarbonate $H^{14}CO_3^-$ as a by-product in the CYP3A4-mediated pathway and dissolved in the LC sub-compartment. The series of conversion from ^{14}C-formaldehyde, ^{14}C-formate through to $H^{14}CO_3^-$ is rapid and not rate-limiting as assumed by Sugiyama et al. [172]. The final by-product $^{14}CO_2$ in this elimination pathway is produced and exhaled in breath as a result of a first-order elimination of bicarbonate (with a constant kresp) from the LC sub-compartment [172].
- The liver (composed of ES and LC sub-compartments) and the kidneys (KD compartment) are elimination organs. In addition, a parameter μ was included in the

OT compartment to explain the exponential decay that was seen in the observed $^{14}CO_2$ production rate data. We anticipated that this parameter μ would improve the model fitting. Thus, the exponential decay was assumed to explain any loss or decomposition of the drug before the drug reaches the liver in the system.

- The unbound drug, but not the bound drug, is subject to uptake and efflux transport, enzymatic metabolism, and elimination in the liver.
- For the intrinsic clearance of CYP3A, linearity was assumed after investigating the model fitting in comparison to non-linear intrinsic clearance.

3.3.6 Simulations, Optimizations, and Sensitivity Analysis

We developed the iPBPK-R framework shown in Figure 14. Specifically, concentration-time curves of ^{14}C-erythromycin and enzymatic by-products $H^{14}CO_3^-$ and $^{14}CO_2$ were simulated for individual subjects based on the ODEs (Figure 13 and appendix B). $^{14}CO_2$ production rates were simultaneously simulated by taking the first derivative of cumulative $^{14}CO_2$ data generated.

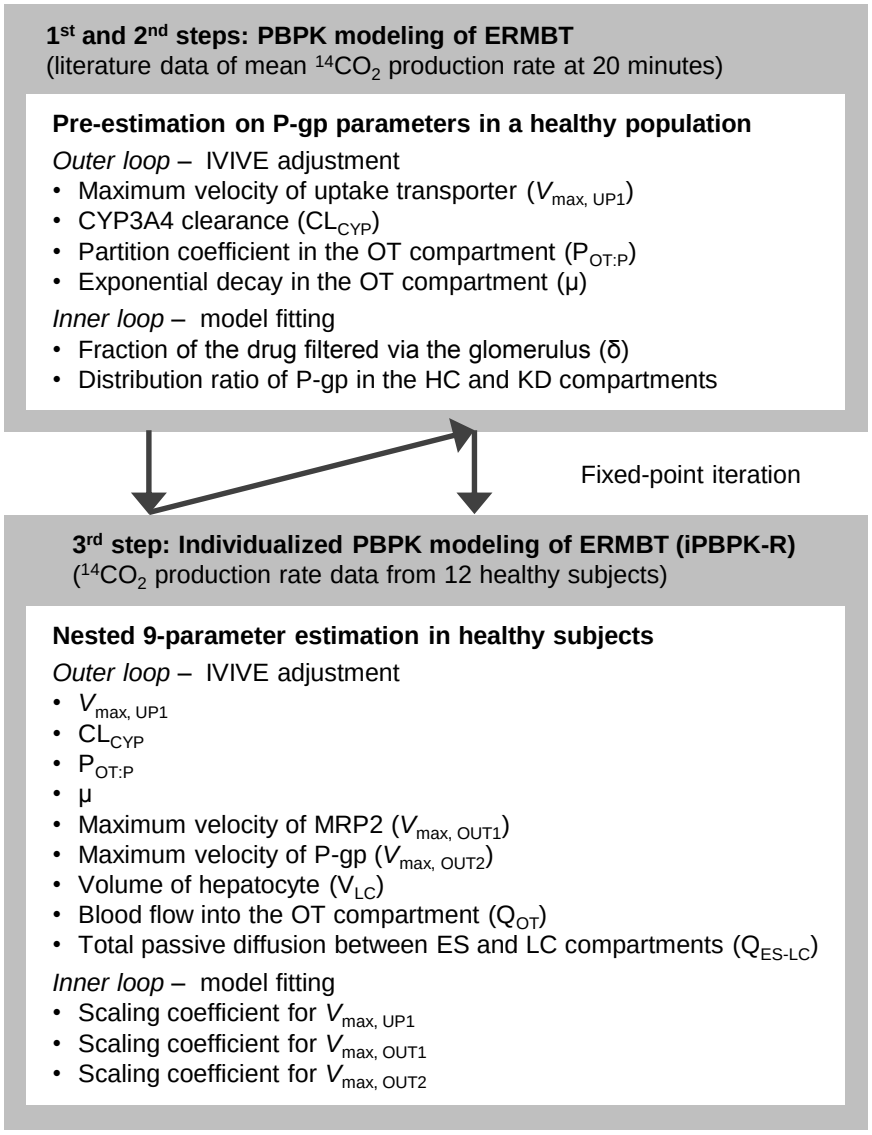

Figure 14: Framework of the application of iPBPK-R to the EBT study in 12 healthy subjects.

The optimization setup in the application of iPBPK-R to the EBT data per subject was mathematically described using objective function with regularization in Section 2.6.3. The bottom box of the framework diagram depicts which parameters are estimated in the co-optimization setting in the actual application to the $^{14}CO_2$ production rate data set of

healthy subjects, and a co-optimization of multiple parameters with outer and inner loops was conducted in each subject accordingly. The top box of the diagram illustrates the parameter estimation using clinical EBT literature that was conducted prior as described in Section 3.3.6.

Parameters were optimized via a 3-step iPBPK-R framework (Figure 14). In each step, a nested optimization was used. In the first and second steps, the fraction of the drug filtered via the glomerulus (δ) and expression ratio of P-gp transporters between liver and kidney compartments were pre-estimated in the inner optimization loop of the iPBPK-R model fitting to the previously published mean $^{14}CO_2$ production rate at 20 minutes post EBT [169]. In the same two steps, four PBPK parameters (maximum velocity of the meta uptake transport process, CYP3A4 clearance, partition coefficient in the combined other organs, and exponential decay parameter μ) were pre-estimated via the outer loop optimization. The pre-estimated parameter values in the first two steps were used as initial input values in the third step. In the third step (main step), the nested optimization process consisting of the inner loop and outer loop was used to optimize and estimated IVIVE adjustment factors for five PBPK parameters (maximum velocity of two efflux transporters: P-gp and MRP2, volume of total hepatocyte, blood flow into the combined other organs, and total passive diffusion between extracellular space and hepatocyte). This was done so that we could implement iPBPK-R model fitting to the observed $^{14}CO_2$ production rates between 0-120 minutes in 12 healthy subjects. In this step, the model fit was evaluated using goodness-of-fit plots, normalized residuals between predicted and observed rates, visual inspection, and plausibility of the resulting parameter estimates. Among the PBPK parameters in Table 12, nine outer loop parameters (see Figure 14, 3rd Step) were selected[4] to optimize and estimate since they were essential parameters for model fitting based on visual investigation and sensitivity analysis. In fact, adjustment factors for maximum velocity of efflux transporters did not have a critical effect of controlling the shape of the $^{14}CO_2$ production rate – time curves. However, these parameters were kept for optimization since they were part of nonrenal elimination pathways. The three scaling parameters in the inner optimization loop in the third step (Figure 14) were used to calculate final adjustment factors for IVIVE values of transporter kinetics. One cycle of fixed-point iteration was conducted and the results of the third step outer loop were used in subsequent simulations to refine the parameter estimates.

[4]The number of observed samples per individual in this simultaneous PBPK model fit is 11 time points. The number of functionally dependent parameters to optimize here (i.e., nine outer loop parameters) is valid as as shown in the analysis of iPBPK-R estimation using regularization in Section 2.4.7. Also see Section 2.5.2 where the analysis of matrix in the iPBPK-R model identified three to five dominant and distinguishable modes (Appendix A.2).

All the simulations and parameter estimations were implemented with the programming language and free software environment R 3.4.4. The R package *deSolve* was utilized for solving the set of ODEs, and large-scale simulations were conducted via the Bridges supercomputer at the Pittsburgh Computing Center [126]. Methodological details of the iPBPK-R approach were described in Chapter 2.

3.3.7 Statistical Analysis

Our primary aim was to simultaneously estimate PK parameters associated with metabolic versus transporter-mediated pathways within individual study subjects using iPBPK-R. Descriptive statistics were presented with mean ± SD and/or median (range). Twenty-fifth and 75th percentiles were also obtained for creating box plots. This study explored feasibility and estimability on model parameters, and no statistical test was powered in advance. Assuming that all measurements were non-normally distributed, one-sided Wilcoxon-Mann-Whitney tests were conducted for comparing two independent groups. Spearman's ρ correlation coefficients were calculated in correlation analysis for studying the relationships between estimated adjustment factors for non-renal elimination parameters and baseline demographic or uremic solute concentrations (BUN, SCr, and TNF-α). An adjustment factor of 1 means that there was no need to adjust the initial parameter input value in the optimization. A P-value < 0.05 was considered statistically significant for all comparisons. All statistical analyses were conducted using SAS 9.4 (SAS Institute Inc., Cary, NC).

3.4 Results

The iPBPK-R model was applied to fit the observed $^{14}CO_2$ production rate data for the 12 healthy subjects (Figure 15). The nested optimization procedure yielded parameter estimates for all subjects, and the excellent model fit was confirmed with the goodness-of-fit plots across subjects, normalized residuals (mean 10^{-4}, standard deviation 10^{-4}) (Figure 16, Table 13, and Table 14).

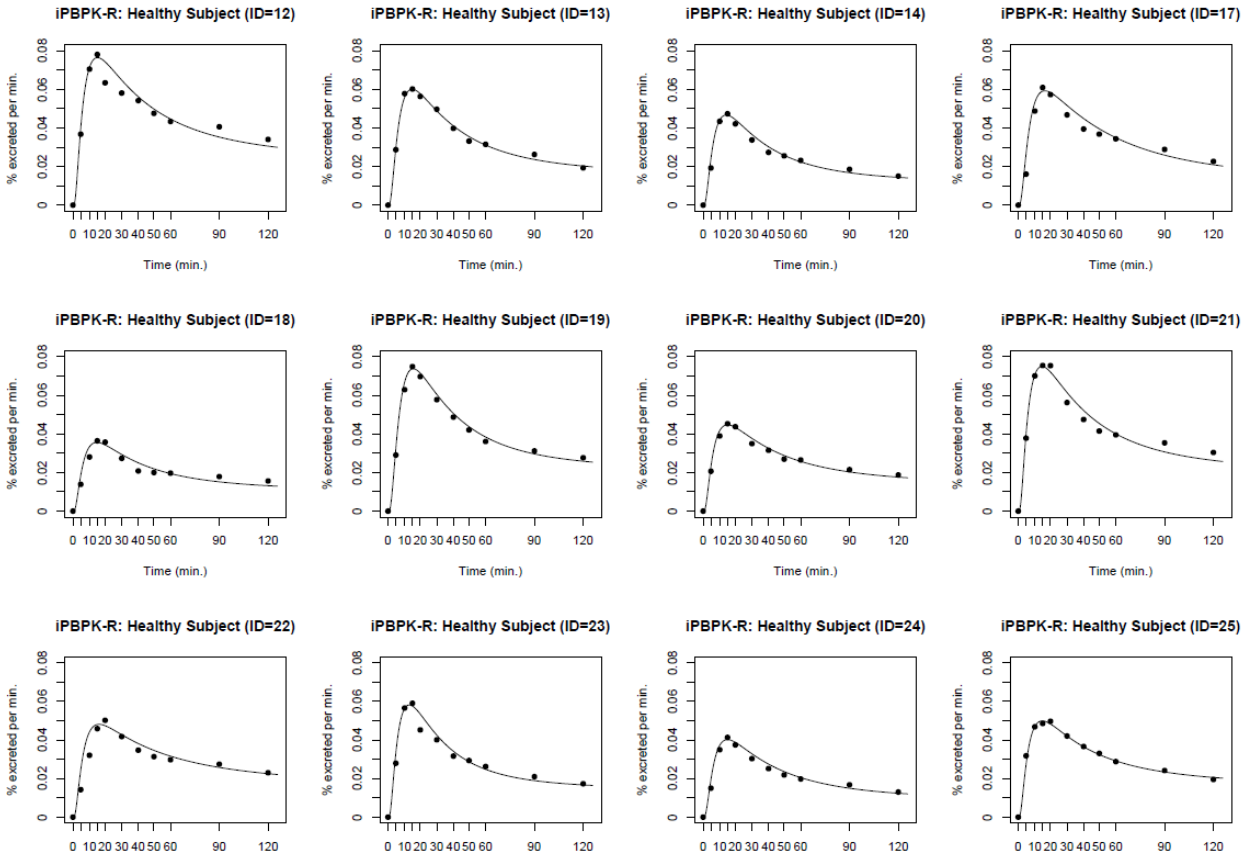

Figure 15: iPBPK-R model fit to the individual EBT data from the 12 healthy subjects.

The black lines are modeled $^{14}CO_2$ production rate-time curves and the black dots indicate the observed $^{14}CO_2$ production rates. The goodness-of-fit of these curves are discussed in Section 3.5 along with Figure 16.

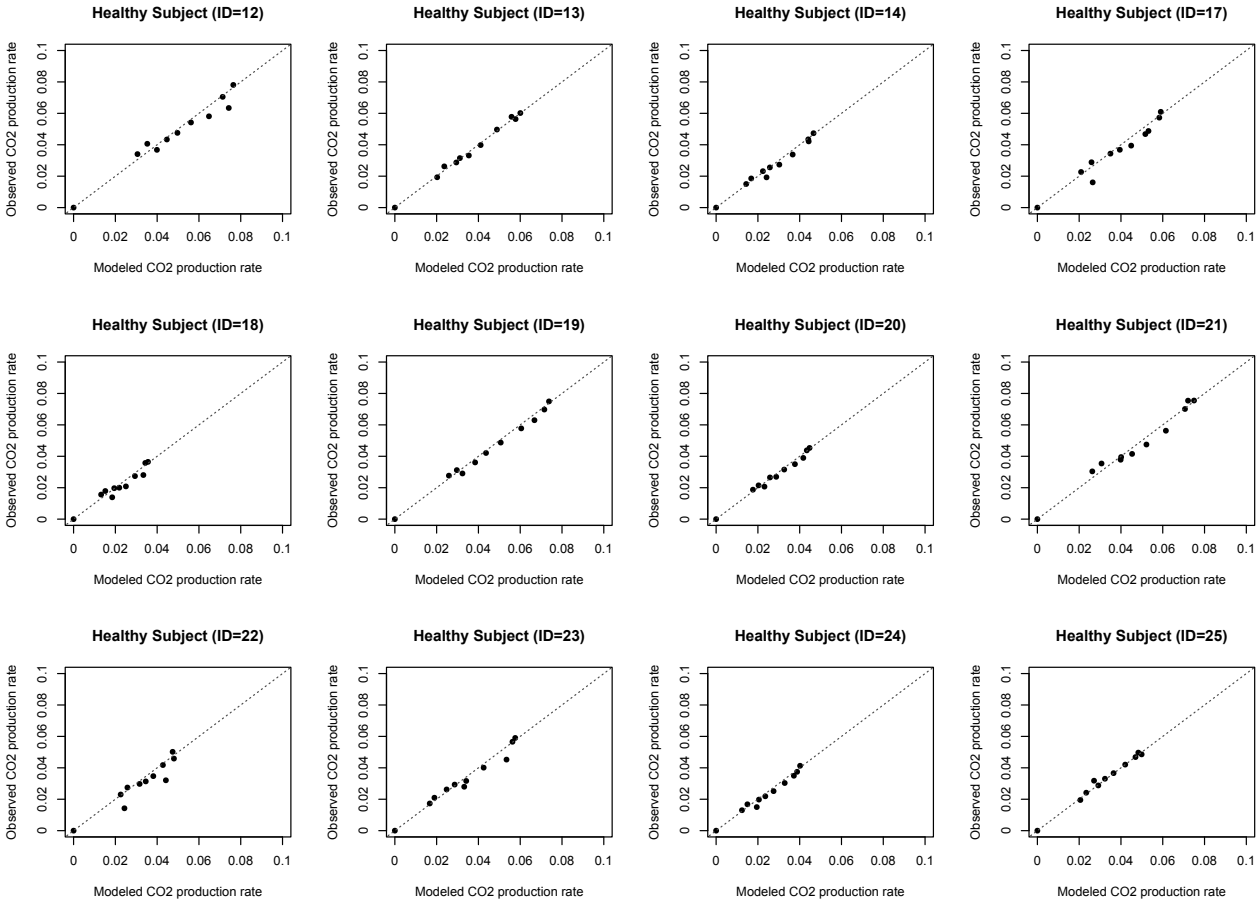

Figure 16: Goodness-of-fit plots for the 12 healthy subjects.

Observed versus modeled (simulated) $^{14}CO_2$ production rates are shown[5], which correspond to the iPBPK-R model fit to the EBT data (See Figure 15). While there are data points slightly off from the diagonal line in the patients of ID = 12, ID = 17, and ID = 22, these may be potentially caused by protocol deviations on sample collection times. These data points do not appear critically off the diagonal line and the iPBPK-R model fitting excelled in the overall performance as discussed in Section 3.5.

[5]Rather than the normalized residual-time plots in our published article [105], goodness-of-fit plots are being presented here. The normalized residuals were calculated as the difference between modeled and simulated $^{14}CO_2$ production rates divided by the observed $^{14}CO_2$ production rate at each sampling time. Such normalized residuals may lead to misinterpretation of the actual model fit at the earlier sampling times since the absolute size of the observed $^{14}CO_2$ production rate is quite small, which makes the normalized residual % quite large even though the simulated data are well performed results and very close to the observed data points.

The estimated adjustment factors for parameters in the liver and combined other organ compartments are shown in Figures 17 (A) and 18, respectively. The estimated median CYP3A4 clearance was 87.8% lower than the original IVIVE value (adjustment factor = 0.122 in Figure 17 (A)) and the median adjustment factor for total passive diffusion was 33.5% lower than the original IVIVE value (adjustment factor = 0.665 in Figure 17 (A)). The adjustment factor for maximum velocity (Vmax) of the meta-uptake transporter varied by individuals (25th quantile adjustment factor 0.74; 75th quantile adjustment factor 0.99). When stratified by gender (Figure 17 (B)), the adjustment factor for J_{max} of the meta-uptake transporter did not differ by gender; a few female healthy subjects had reduced uptake transport activity (the median adjustment factor in male: female = 0.99: 0.67; the one-sided exact p-value P = 0.10). J_{max} of efflux transporters (P-gp and MRP2) did not require an adjustment from the original IVIVE values since the estimated median and mean adjustment factors were 1.00. The median adjustment factors for total hepatocyte volume, CYP3A4 clearance, and total passive diffusion varied among individuals (Figure 17 (A)). In the combined other organs compartment (Figure 18), arterial blood flow barely required IVIVE adjustment (median adjustment factor 0.87 or 13% decrease from the IVIVE value) while IVIVE values of exponential decay μ and partition coefficient needed to be adjusted as high as 4.0 and 18.8 times (by median), respectively. The latter two parameters did not vary by individuals but the adjustment factor for arterial blood flow relatively varied by individuals (25th quantile adjustment factor 0.52; 75th quantile adjustment factor 0.99). Since the meta-uptake transporter, CYP3A4 clearance, volume of total hepatocyte, and total passive diffusion varied in their adjustment factor, we stratified these adjustment factors by gender in the box-and-whisker plots (Figure 17 (B)). When compared by gender using one-sided Wilcoxon-Mann-Whitney tests, the CYP3A4 clearance was significantly lower in male than in female (the median reduction from the IVIVE value in male: female = 89.3%:78.0%; the one-sided exact P = 0.04). The total hepatocyte volume and total passive diffusion did not differ by gender (the one-sided exact p-values = 0.27 and 0.17, respectively).

The observed $^{14}CO_2$ production rate – time curves of 12 healthy subjects had three phases: (i) increasing absorption/distribution phase, (ii) the first elimination phase, and (ii) the second elimination phase (depicted by the black dots in Figure 15). Through the sensitiv-

ity analysis in the iPBPK-R model fitting, we found that multiple physiological parameters interact and control the shape of the $^{14}CO_2$ production rate – time curve (Figure 19). When CYP3A4 clearance increases, the peak height and the area under the curve (AUC) increase with a steeper absorption phase. J_{max} of uptake drug transport and total passive diffusion together control the peak height, the first elimination phase, and the second elimination phase of the curve. As part of the sensitivity analysis, we simulated $^{14}CO_2$ production rate – time curves with one additional varying parameter (see 3-dimensional plots in Figure 20). In Figure 20 (A), CYP3A4 clearance varied from 1% to 100% of the IVIVE value. In Figure 20 (B), J_{max} of the meta-uptake transporter varied from 1% to 200% while keeping the total passive diffusion at 50% of its optimal value. Modeled $^{14}CO_2$ production rates were sensitive to changes in CYP3A4 clearance (see Figure 20 (A)). Changes in total passive diffusion and uptake drug transport together have an effect on the shape of $^{14}CO_2$ production rate – time curves (Figure 20 (B)).

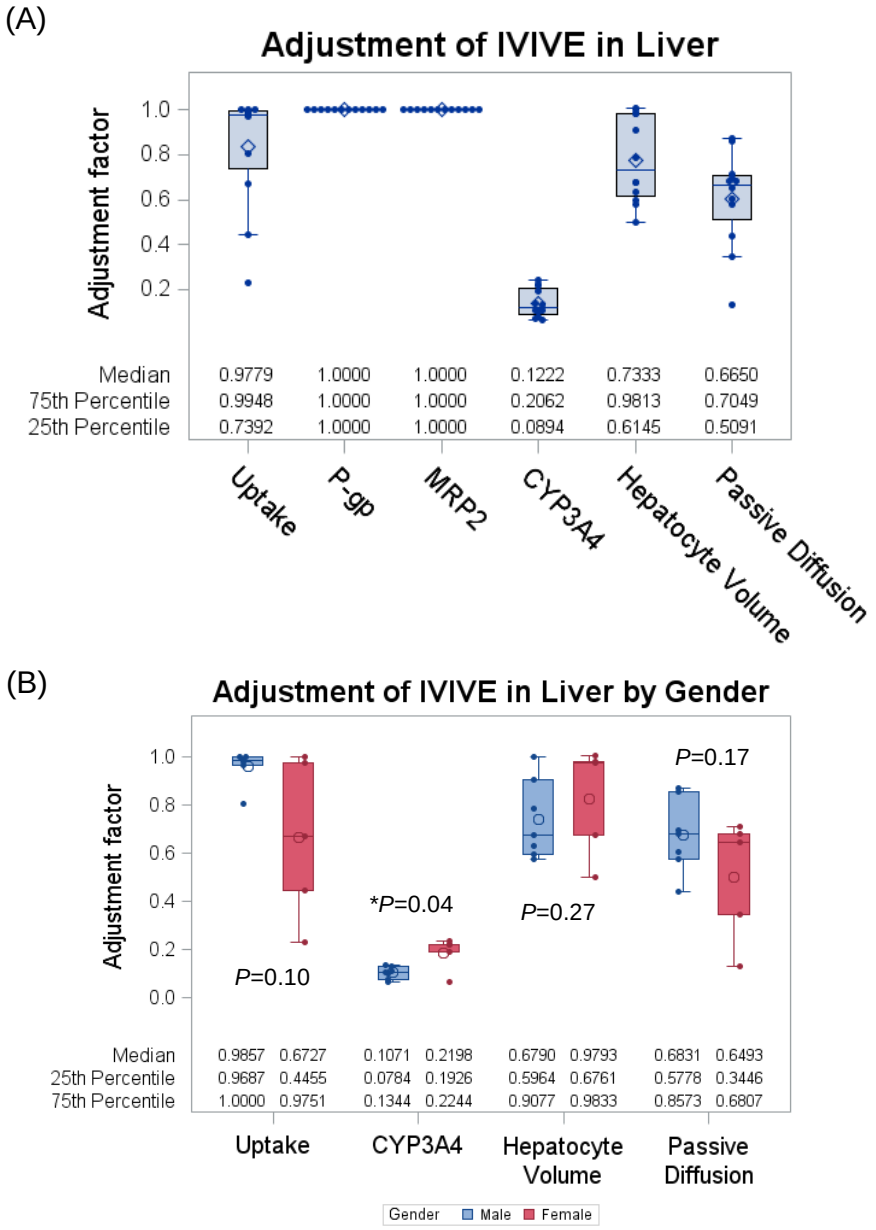

Figure 17: Box plots of estimated IVIVE adjustment factors for PBPK parameters in the liver compartments (ES and LC sub-compartments).

The PBPK parameters are maximum velocity of the meta-uptake transporter, maximum velocity of P-gp, maximum velocity of MRP2, CYP3A4 clearance, the volume of the hepatocyte, and total passive diffusion between ES and LC sub-compartments (from the left to the

right on the x-axis). These PBPK parameters were estimated in the main step (3rd step) of the iPBPK-R framework as shown in Figure 14. N = 12 in all box plots. (B) Estimated IVIVE adjustment factors in the liver compartments stratified by gender. N = 7 for males and N = 5 for females. These selected estimates adjust CYP3A4 clearance, the volume of the hepatocyte, and total passive diffusion between ES and LC sub-compartments. When the IVIVE adjustment factor is estimated to be 1, it is interpreted that the parameter input was not adjusted from the original IVIVE input value through the iPBPK-R model fitting. Exact p-values are shown based on Wilcoxon-Mann-Whitney tests for comparing between male and female (one-sided test). $\star$ indicates a statistically significant difference at a significance level of 0.05.

As described in Statistical Analysis Section (Section 3.3.7) statistical tests to compare two groups are not powered. Thus, these statistical tests are treated as exploratory analyses. Note that a clinical threshold for comparing adjustment factors is not 2-fold and has not been established as this is the first study to simultaneously estimate multiple functionally dependent parameters in an automated fashion as discussed in Section 3.5.

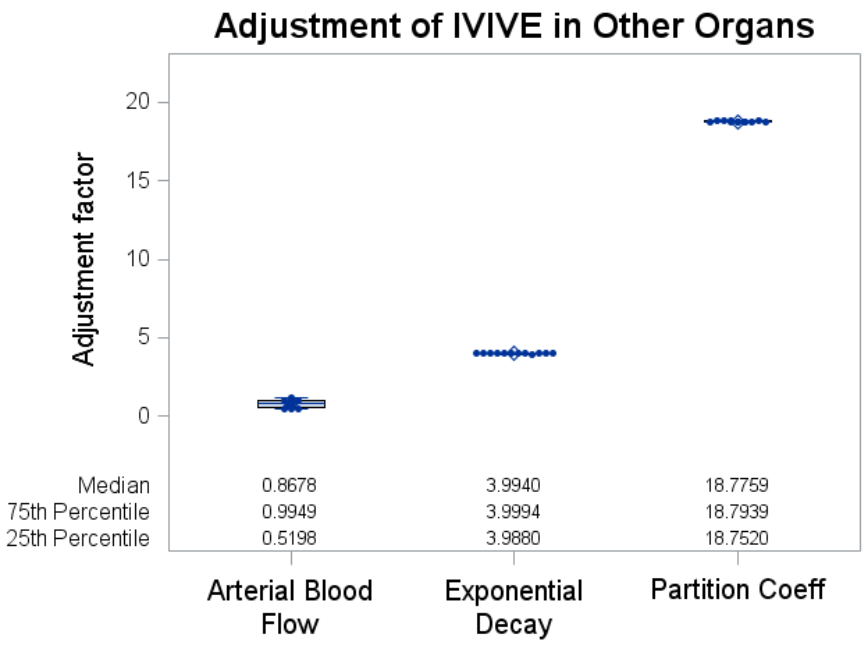

Figure 18: Estimated IVIVE adjustment values for PBPK parameters in the combined other organs (OT) compartment.

The PBPK parameters are arterial blood flow, exponential decay, and partition coefficient between OT and plasma, respectively (from the left to the right on the x-axis). These PBPK parameters were estimated in the main step (3rd step) of the iPBPK-R framework as shown in Figure 14. When the IVIVE adjustment value is estimated to be 1, it is interpreted that the parameter input was not adjusted from the original IVIVE input value through the iPBPK-R model fitting. N = 12 in all box plots.

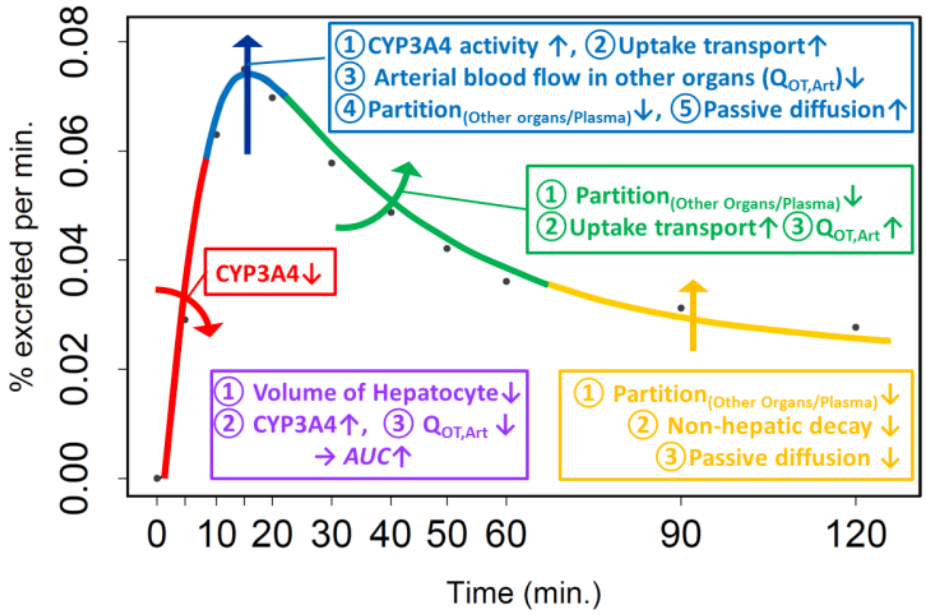

Figure 19: EBT data interpretation as a result of the application of iPBPK-R.

The modeled $^{14}CO_2$ concentration – time curve represents three phases: the increasing absorption phase, the first elimination phase after the peak of the curve, and the second elimination phase. Red line and texts: the increased absorption phase gets less steep as CYP3A4 clearance decreases. Blue line and texts: The peak of the curve increases as (1) CYP3A4 clearance increases, (2) maximum velocity of the meta-uptake transporter increases, (3) arterial blood flow in the combined other organ (OT) compartment ($Q_{OT,Art}$) decreases, (4) the partition coefficient of OT to plasma decreases, and/or (5) total passive diffusion between ES and LC sub-compartments increases. Green line and texts: the first elimination phase of the curve gets less steep as (1) the partition coefficient of OT to plasma decreases, (2) maximum velocity of the meta-uptake transporter increases, and/or (3) $Q_{OT,Art}$ increases. Yellow line and texts: the second elimination phase of the curve gets less steep or shifts upwards as (1) the partition coefficient of OT to plasma decreases, (2) exponential decay in the OT compartment decreases, and/or (3) total passive diffusion between ES and LC sub-compartments decreases. Purple texts: the AUC of the curve increases as (1) the volume of the hepatocyte decreases, (2) CYP3A4 clearance increases, and/or (3) $Q_{OT,Art}$ decreases. It

is not feasible to show all the sensitivity analysis results on multiple functionally dependent parameters, which were conducted along with the model development using more than 50,000 CPU hours (= 5.7 CPU years) on the Bridges supercomputer. As discussed in Section 3.4, two examples of sensitivity analyses are shown in Figures 20(A) and 20(B) of which findings contributed to developing this interpretation figure. It is important to remember that general interpretations for plasma concentration-time curves do not apply to $^{14}CO_2$ concentration – time curves as explained earlier using Figure 12.

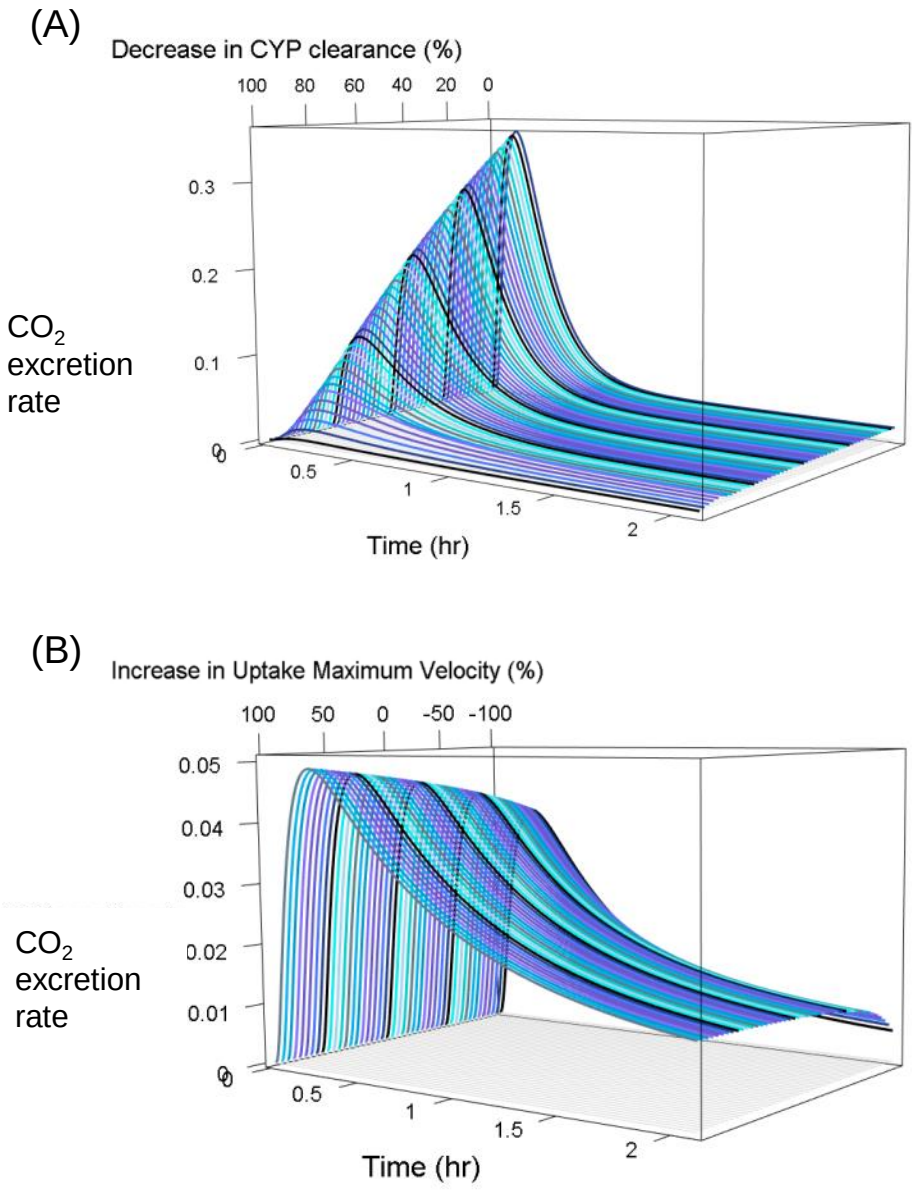

Figure 20: Example of sensitivity analysis. Simulated 3D $^{14}CO_2$ production rate – time curves.

(A) CYP3A4 clearance was varied from 1% to 100% of the IVIVE value and (B) maximum velocity of the meta-uptake transporter was varied from 1% to 200% while keeping the total passive diffusion at 50% of its optimal value.

As an exploratory analysis, Spearman correlation analysis between the estimated adjustment factors for non-renal elimination parameters (J_{max} of meta-uptake transporters, CYP3A4 clearance, and total passive diffusion) and baseline parameters was conducted (see Table 15 and Table 16). These baseline parameters were demographic and physical factors (height, weights, age, and estimated GFR) and uremic solute concentrations including SCr, BUN (a low molecular weight solute), and TNF-α (a middle molecular weight solute). In all 12 subjects, the correlation coefficient between BUN and the adjustment factor for J_{max} of meta-uptake transporters was estimated to be negative and strong, and this correlation was statistically significant (ρ = -0.608; P=0.04) (Table 15). In the male subjects, BUN was negatively correlated with the adjustment factors for J_{max} of meta-uptake transporters, CYP3A4 clearance, and passive diffusion (ρ = -0.857; P=0.01, ρ = -0.857; P=0.01, and ρ = -0.821; P=0.02, respectively), which were very strong according to Evans' correlation criteria [200] (Table 16).

Table 13: Parameter estimates through the nested optimization and normalized residuals in the iPBPK-R modeling of the EBT study in 12 healthy subjects

Estimated parameter	Mean ± SD	Median (Range)
IVIVE adjustment (adjustment factor)		
Meta-uptake transporter	0.84 ± 0.26	0.98 (0.23, 1.00)
P-gp	1.00 ± 0.00	1.00 (1.00,1.00)
MRP2	1.00 ± 0.00	1.00 (1.00, 1.00)
CYP3A4 clearance	0.14 ± 0.06	0.12 (0.07, 0.24)
Hepatocyte volume	0.78 ± 0.19	0.73 (0.50, 1.01)
Partition coefficient in the combined other organs	18.77 ± 0.03	18.78 (18.72, 18.84)
Blood flow in the combined other organs	0.80 ± 0.27	0.87 (0.45, 1.22)
Exponential decay parameter in the combined other organs	3.99 ± 0.01	3.99 (3.97, 4.03)
Total passive diffusion between ES and LC	0.60 ± 0.21	0.67 (0.13, 0.87)
Model fit: normalized residual	$10^{-4} \pm 10^{-4}$	0.0001 (0, 4×10^{-4})

Table 14: Parameter estimates through the nested optimization and normalized residuals in the iPBPK-R modeling of the EBT study by gender

	Male		Female		
N	7		5		
Estimated parameter	Mean ± SD	Median (Range)	Mean ± SD	Median (Range)	p-value[a]
IVIVE adjustment (adjustment factor)					
Meta-uptake transporter	0.96 ± 0.07	0.99 (0.81, 1.00)	0.66 ± 0.33	0.67 (0.23, 1.00)	0.101
P-gp	1.00 ± 0.00	1.00 (1.00, 1.00)	1.00 ± 0.00	1.00 (1.00, 1.00)	0.265
MRP2	1.00 ± 0.00	1.00 (1.00, 1.00)	1.00 ± 0.00	1.00 (1.00, 1.00)	0.254
CYP3A4 clearance	0.10 ± 0.03	0.11 (0.07, 0.14)	0.19 ± 0.07	0.22 (0.07, 0.24)	0.037[b]
Hepatocyte volume	0.74 ± 0.16	0.68 (0.58, 1.00)	0.83 ± 0.23	0.98 (0.50, 1.01)	0.265
Partition coefficient in the combined other organs	18.78 ± 0.03	18.78 (18.74, 18.84)	18.77 ± 0.03	18.78 (18.72, 18.80)	0.319
Blood flow in the combined other organs	0.83 ± 0.28	0.90 (0.45, 1.22)	0.75 ± 0.28	0.83 (0.45, 1.01)	0.378

Table 14: Parameter estimates through the nested optimization and normalized residuals in the iPBPK-R modeling of the EBT study by gender

	Male		Female		
N	7		5		
Estimated parameter	Mean ± SD	Median (Range)	Mean ± SD	Median (Range)	p-value[a]
Exponential decay parameter in the combined other organs	3.99 ± 0.01	3.99 (3.99, 4.00)	3.99 ± 0.01	4.00 (3.98, 4.00)	0.378
Total passive diffusion between ES and LC	0.68 ± 0.15	0.68 (0.44, 0.87)	0.50 ± 0.25	0.65 (0.13, 0.71)	0.172
Model fit: normalized residual	$1\times 10^{-4} \pm 10^{-4}$	1×10^{-4} (0.00, 4×10^{-4})	$2\times10^{-4} \pm 10^{-4}$	1×10^{-4} (10^{-4}, 3×10^{-4})	

[a]Exact p-value of a Wilcoxon-Mann-Whitney test to compare between male and female (one-sided test)

[b]p-value < 0.05 indicating a statistically significant difference between male and female

Table 15: Spearman correlation coefficients among the estimated PBPK parameters, demographic and physiological data, and uremic solute concentrations in 12 healthy subjects.

		HT	WT	BMI	Age	eGFR	SCr	BUN	TNF-α
IVIVE adjustment (adjustment factor)									
Meta-uptake transporter	ρ[a]	0.371	0.147	-0.259	-0.372	0.007	0.351	-0.608	-0.161
	p-value	0.235	0.648	0.417	0.234	0.983	0.263	0.036[b]	0.618
CYP3A4 clearance	ρ[a]	-0.529	-0.378	0.154	0.319	-0.571	0.092	-0.504	-0.399
	p-value	0.077	0.225	0.633	0.312	0.053	0.775	0.095	0.199
Total passive diffusion between ES and LC	ρ[a]	0.476	0.308	-0.175	-0.204	-0.175	0.414	-0.196	0.112
	p-value	0.117	0.330	0.589	0.526	0.586	0.181	0.542	0.729

WT, weight (kg); HT, height (cm); BMI, body mass index (kg/m2); eGFR, estimated Glomerular Filtration Rate (L/hr); SCr, serum creatinine (mg/dL); BUN, blood urea nitrogen (mg/dL); TNF-α, tumor necrosis factor-α (pg/mL)

[a]Spearman correlation coefficient; [b]p-value < 0.05 indicating a statistically significant correlation

Table 16: Spearman correlation coefficients among the estimated PBPK parameters, demographic and physiological data, and uremic solute concentrations by gender

		Male								Female							
	7							5									
		HT	WT	BMI	Age	eGFR	SCr	BUN	TNF-α	HT	WT	BMI	Age	eGFR	SCr	BUN	TNF-α
IVIVE adjustment (adjustment factor)																	
Meta-uptake transporter	ρ[a]	0.321	0.429	0.250	-0.321	-0.286	0.309	-0.857	-0.250	-0.308	-0.300	-0.300	0.300	-0.200	0.289	-0.200	-0.500
	p-value	0.482	0.337	0.589	0.482	0.535	0.500	0.014[b]	0.589	0.614	0.624	0.624	0.624	0.747	0.638	0.747	0.391
CYP3A4 clearance	ρ[a]	-0.071	0.214	0.357	-0.250	-0.250	0.273	-0.857	-0.143	-0.667	-0.400	0.100	0.100	-0.600	0.866	-0.600	-0.500
	p-value	0.879	0.645	0.423	0.589	0.589	0.554	0.014[b]	0.760	0.219	0.505	0.873	0.873	0.285	0.058	0.285	0.391
Total passive diffusion between ES and LC	ρ[a]	0.393	0.571	0.464	-0.286	-0.357	0.309	-0.821	-0.179	0.462	-0.600	-0.900	0.500	-0.600	0.289	0.400	0.300
	p-value	0.383	0.180	0.294	0.535	0.432	0.500	0.023[b]	0.702	0.434	0.285	0.037[b]	0.391	0.285	0.638	0.505	0.624

WT, weight (kg); HT, height (cm); BMI, body mass index (kg/m2); eGFR, estimated Glomerular Filtration Rate (L/hr); SCr, serum creatinine (mg/dL); BUN, blood urea nitrogen (mg/dL); TNF-α, tumor necrosis factor-α (pg/mL)

[a]Spearman correlation coefficient; [b]p-value < 0.05 indicating a statistically significant correlation

3.5 Discussion

This is the first study to show that the activity of multiple non-renal elimination pathways can be estimated within individual study subjects with a single probe drug, erythromycin, via PBPK modeling and optimization-based model fitting of rate data (iPBPK-R). The iPBPK-R method is distinctly different from and advantageous over other approaches that use multiple pathway-specific probes (i.e., the 'cocktail' approach). The cocktail approach may lead to higher imprecision due to (1) uncertainty in parameter estimates pertinent to different probes' characteristics, (2) varying interactions with physiological properties, and (3) inter-cohort variabilities [122] [123]. The iPBPK-R method overcomes these by utilizing the distinct and dynamic information contained in rate data solely obtained with a single probe.

Non-linear model fitting of measured rate data [134] was adopted in our individualized PBPK modeling, which enabled multiple-parameter optimization to achieve high accuracy as shown in the goodness-of-fit plots in Figure 16. In these individual goodness-of-fit plots, the simulated and observed $^{14}CO_2$ production rates are on or close to the diagonal line including the data points in the lower range of $^{14}CO_2$ production rate. There are data points slightly off from the diagonal line in the patients of ID = 12, ID = 17 and ID = 22. These may be caused by the actual sample collection times that deviated from the planned sample collection times as the breath samples were intensively collected within the two hours. Since the general decision criterion for acceptable PBPK model simulation is within 2-fold of the observed C_{max} and AUC[6] [76,90,93,101,102], which suggests that PBPK model fitting is generally considered to be difficult, the iPBPK-R model fitting excelled in the overall performance. Figure 12 illustrates that the $^{14}CO_2$ production rate data contains more information than the cumulative $^{14}CO_2$ concentration data when they are observed. First, as shown in the inset panels for hypothetical subjects A, B, C, and D, the simulated curves of the cumulative amount of $^{14}CO_2$ generated during the study period are not sensitive to any underlying parameter changes since all four subjects' cumulative curves look similar.

[6]This criterion is just for population mean values of C_{max} and AUC but not individually simulated values of C_{max} and AUC since individual PBPK modeling is rarely conducted.

On the other hand, simulated curves of $^{14}CO_2$ production rates show a dynamic change depending on the parameter change since the shape of the rate-time curves visibly differ across the subjects. This illustrates that, for a given measurement accuracy, measuring the first derivative data allows us to estimate parameter differences while these differences cannot be estimated from the original data. The iPBPK-R method utilized here leverages this for the purposes of characterizing multiple non-renal clearance pathways simultaneously.

Historically, erythromycin was commonly used as a metabolic probe drug. It was administered intravenously and employed in the EBT to noninvasively measure in vivo activity of hepatic CYP3A4 [176] [177] [128] [178]. However, it is now known that erythromycin undergoes hepatic clearance by OATPs, P-gp, and MRP2-mediated elimination pathways as well [174] [171] [169] [170] [175] [179] [180]. Accordingly, interpretations of EBT data were misleading under the assumption that erythromycin clearance was dependent solely on CYP3A4-mediated metabolism [133] [132]. We were interested in accounting for the multiple nonrenal elimination pathways of erythromycin and estimating corresponding kinetic parameters within individual healthy subjects through modeling observed rate data. Rate data is commonly utilized in engineering disciplines, typically in digital signal processing. We anticipated that by applying mechanistic iPBPK-R to the EBT data we could simultaneously estimate the activity of multiple non-renal elimination pathways. Although this is a pilot study, we found that CYP3A4 activity was consistently estimated to be lower than the IVIVE-based CYP3A4 activity in all subjects. This lower estimated value of CYP3A4 clearance can be explained by our consideration of the functional dependency among parameters for not only CYP3A4 activity but also for transporter activities and other properties in the modeling. Accordingly, parts of the estimate value, which would have been solely allocated to CYP3A4 activity in a simple population model, were allocated to other dependent parameter effects. Thus the size of CYP3A4 activity may have decreased because iPBPK-R models the detailed physiological processes in an integral manner. In addition to the explanation based on the functional dependency, the lower estimated value of CYP3A4 activity may be also explained by the Biopharmaceutics Drug Disposition Classification System (BDDCS)-based prediction for erythromycin [201]. In BDDCS, erythromycin is classified into class 3, and class 3 drugs are highly soluble and poorly metabolized. Thus, the low estimated

value of CYP3A4 activity aligns with this predicted poor metabolism. Regarding OATP, its estimated activity showed a large interindividual variability. If the abundance of tranporters in hepatocytes is assumed to be correlated with the OATP activities in hepatocytes, the estimated variability of OATP activity aligned with the large variabilities of the abundance in OATP1B1 and OATP1B3 estimated in a meta-analysis of Caucasians abundance data in the literature [68]. These transporters showed the highest coefficient of variation (CV)% values (66 and 70, respectively) in the abundance analysis among the evaluated transporters (OCT1, NTCP, MATE1, P-gp, BSEP, MRP2, MRP3, and BCRP). The 20-minute $^{14}CO_2$ flux of the observed data showed a CV value of 22% [127], which is viewed as a result of projection of a trajectory in a high dimensional space (as a solution of a system of nonlinear ODEs) to one plane in iPBPK-R as detailed in Chapter 2. iPBPK-R allowed us to differentiate the multiple functionally dependent adjustment factors and to estimate them, including the adjustment factor for OATP activity that showed a large variability. This estimated large variability aligns with or is supported by the meta-analysis literature [68] as discussed above, and thus it presents the soundness of the iPBPK-R method.

Simultaneous estimation of the activity of multiple non-renal elimination pathways facilitates studying the interaction between enzymatic metabolism and drug transport or *enzyme-transporter interplay* [110]. As discussed previously, the EBT was actively used to probe in vivo CYP3A catalytic activity in the past. However, across clinical studies using the EBT, there were conflicting results in predicting total body clearance from the $^{14}CO_2$ production rate analysis. Rivory et al. discussed possible causes for the inconsistent results among the EBT studies [132]. The reasons included high inter-individual variability of the $^{14}CO_2$ production rate data, potential overestimation of $^{14}CO_2$ production in females, and use of different type of measurements among studies (i.e., inverse time to the peak, $^{14}CO_2$ production rate at 20 minutes, and AUC from 0 to 2 hours). As erythromycin was found to be a substrate of not only CYP3A but also P-gp, Mrp2, and Oatp2 in in vitro studies [180] [171], studying the effect of enzyme-transporter interplay on non-renal drug elimination became essential [174]. To study the enzyme-transporter interplay, mechanistic PBPK modeling is a useful tool as it allows us to explicitly describe the activity of each elimination pathway in the whole body system. iPBPK-R showed that OATP activity controls the peak of $^{14}CO_2$

production rate-time curve while P-gp did not have a significant role. These findings aligned with the results of a EBT DDI study by Frasseto et al [169]. They compared the 20-min $^{14}CO_2$ fluxes between EBT alone versus EBT with a single dose rifampin (as an OATP inhibitor) as well as between EBT alone versus EBT with a P-gp inhibitor lansoprazole in 16 healthy subjects. The 20-min $^{14}CO_2$ flux increased by the OATP inhibitor but did not significantly increase by the P-gp inhibitor. Paine et al. evaluated the interplay between CYP3A4 activity and P-gp activity using two types of EBT tests [202]. One was to intravenously administer a small amount of ^{14}C-erythromycin (0.07 μmol EBT_{IV}, similar to our EBT data) and the other was to orally administer 500mg of ^{13}C-erythromycin (EBT_{PO}). The 20-min $^{14}CO_2$ fluxes were compared for both EBT_{IV} and EBT_{PO} between EBT alone versus EBT with troleandomycin (CYP3A4 inhibitor) as well as EBT alone versus EBT with repeatedly administered rifampin (CYP3A4 inducer as well as P-gp inducer) in 14 young healthy subjects (21-43 years old). It was found that erythromycin undergoes CYP3A4 metabolism in the liver and in the intestine. In addition, no change was observed in the 20-min $^{14}CO_2$ flux of EBT_{PO} in the presence of rifampin, which led to a conclusion that erythromycin undergoes the P-gp-mediated absorption in the intestine. Thus, these results did not contradict our findings since we evaluated nonrenal elimination pathways of erythromycin. Hepatic P-gp might not have a significant role for erythromycin because more erythromycin undergoes CYP3A4 metabolism first in the liver and has a less likelihood to undergo the P-gp-mediated pathway (i.e., the order of being exposed to these nonrenal pathways may matter). On the other hand, the authors did not exclude the possibility of the significant role of hepatic P-gp activity on erythromycin. However, this study design could not allow the authors to differentially evaluate P-gp activities in the liver and in the intestine. Other limitations of this study to compare to our results were a small sample size, a young cohort, different doses of erythromycin between EBT_{IV} and EBT_{PO}, which may have led to linear and nonlinear CYP3A4 metabolism of erythromycin, respectively. In iPBPK-R, by combining the set of mathematical equations with multi-parameter optimization, one can indirectly estimate the activity of different elimination pathways in the target organ [174]. The iPBPK-R approach overcomes infeasible direct sampling of drug concentrations from the target organ where the in vivo enzyme-transporter interplay may be occurring.

In studies using the EBT, $^{14}CO_2$ production may have been overestimated in females and the difference between genders was around 20-25% [132]. We observed higher CYP3A4 activity in females than in males and the difference between genders was about 11%. In fact, the result for females aligned with the study of human liver bank samples where expression levels of CYP3A4 in female samples were found to be higher than in male samples [173]. No correlation was observed between CYP3A4 activity or drug transport activity and physiological factors, weight, height, or BMI in all subjects or in each gender. Accordingly, our study indicated that there is a sex-related difference in CYP3A4 activity.

It is important to emphasize that the main purpose of the iPBPK-R research is to successfully back-estimate multiple functional dependent parameters, adjustment factors, and interrogate the activities of nonrenal elimination pathways as presented in Figures 17(A) and 17(B). In other words, we do not compare AUC or C_{max} of plasma concentrations[7] as such comparison is not aligned with the purpose. The clinical threshold for an adjustment factor is not a 2-fold difference that is typically used for AUC and C_{max} of plasma concentrations in PBPK modeling. Establishing a clinical threshold for changes in adjustment factors for activity of CYP3A4 (as well as other nonrenal clearance pathways) will require extensive research accounting for pharmacologic and pharmacotherapeutic considerations such as a drug's therapeutic window. However, it is clear that a change in CYP3A4 activity estimated by iPBPK-R is impactful enough to dramatically alter the shape of the $^{14}CO_2$ production rate-time curves in breath samples (and not plasma concentration-time curves) after controlling for other dependent parameters as shown in Figure 20(A) as a part of sensitivity analysis. This is also discussed in the application of iPBPK-R to the EBT data in patients with kidney disease in Section 4.5.

We further conducted correlation analysis on the adjustment factors for non-renal elimination clearance with plasma concentrations of uremic solutes. There was a significant inverse correlation between the uremic solute BUN and the adjustment factor for J_{max} of the meta-uptake transporter (OATPs) in 12 subjects (ρ = -0.608). In males, significant inverse correlations were observed between BUN and maximum velocity of OATPs, CYP3A4 clearance, and passive diffusion, respectively. Despite the small sample size, we showed

[7]Plasma concentrations were not measured in the study [127].

that correlation analysis can be used to explore relationships between the activity of non-renal elimination pathways and potential surrogate biomarkers (such as uremic solutes) after iPBPK-R modeling.

There are several limitations in this study. First, the detailed structures in the kidney compartment were omitted and were not modeled so that multiple parameters could be estimated using a reduced order model. Second, in the reduced order PBPK model it is not possible to distinguish the value of maximum velocity and the number of individual transporters. Third, we did not distinguish in vitro parameter values between ^{14}C-erythromycin and erythromycin for IVIVE calculations. The two compounds are not the same but they are used interchangeably in clinical research. Therefore, the literature values are the best parameters that we could use. Fourth, no genetic variant data of OATPs was available, so we could not conclude whether low CYP3A4 activity was truly caused by the gender difference or the interplay with OATP variants. Fifth, OATP1B1 and OATP1B3 uptake transporters in the liver were modeled as a meta-transporter. The reasons are (1) we used a reduced order model to limit the number of parameters, (2) the literature used for IVIVE calculation did not provide separate intrinsic clearances for the two uptake transporters, and (3) it is unknown whether two transporters having the same role of drug transport in the system of nonlinear ODEs can be separately estimated. It may be possible to differentially estimate parameters for such two transporters but as the feasibility would depend on the initial input values, which leads to requiring further mathematical research like Chapter 2. For the same reason without mathematical investigation, P-gp and MRP2 efflux transporters could not be differentiated in the iPBPK-based estimation. Via sensitivity analysis, we found that P-gp and MRP2 did not have impact on the $^{14}CO_2$ production rate-time curves (because CYP3A4-mediated elimination seems to be dominant when the functional dependencies of multiple parameters are simultaneously accounted in the system of nonlinear ODEs) so we could take them out from the model. However, we forced them into the model to satisfy mechanistic considerations and as such, we prefer to retain them. Sixth, IVIVE values were calculated based on an average 70 kg male data. Although both males and females were enrolled in the clinical study with EBT, the average body weight was close to 70 kg (68 kg). Therefore, use of the average 70 kg male data is not expected to cause a large bias. The

variability in weight is reflected in the estimated adjustment factors for the total hepatic volume. Finally, the CYP3A4 and transporter activity estimates derived from iPBPK-R modeling were not compared to or validated using specific pharmacologic probe substrates as controls. The fitted model cannot be validated against the measurements beyond the breath data. However, the model is a reduced order model, and we could establish that the model was not overfitted. Furthermore, the goodness-of-fit plots, visual inspection, and normalized residuals calculated from predicted and observed curves indicated excellent model fit across all individual subjects. By conducting simultaneous optimizations of parameters and sensitivity analysis, we showed the robustness of parameter estimates and consistency in the estimated CYP3A4 activity across 12 subjects. Similarly, the estimated uptake transporter activity was robust and consistent across males while a wider variability was seen in females.

iPBPK-R can be applied to any rate-derived data beyond EBT. Ideal characteristics of measurements are: (1) rate measurement with long elimination half-life and frequent sampling, (2) in vitro data sufficient for IVIVE, (3) intravenous dosing, and (4) individual data. The underlying idea for (1) is that rate information can be utilized to capture both non-rate-limiting and rate-limiting steps in elimination pathways of interest. As another example, breath rate data of volatile organic compounds can be used to study the role of potential biomarkers on hemodialysis efficiency [118]. Other potential areas of application include drug-drug interaction, pathophysiological effects, and the effect of intervention, polypharmacy, or any other extrinsic factors on drug disposition by estimating adjustment factors and conducting correlation analysis. In the future, we plan to apply the iPBPK-R framework to rate data of other compounds that are known to be cleared by multiple nonrenal elimination pathways.

3.6 Conclusions

The iPBPK-R approach was applied to evaluate $^{14}CO_2$ production rate data of the EBT in healthy subjects. Optimized iPBPK-R models fit the individual data well and it allowed us to distinguish and simultaneously estimate the activity of multiple non-renal elimination

pathways of the single probe ^{14}C-erythromycin. The median in vivo CYP3A4 activity was estimated as low as 12.2% of the IVIVE-based CYP3A4 clearance. $^{14}CO_2$ production rate data has rich information allowing estimation of per-person rate-limiting and non-rate limiting PK parameters. Accordingly, we found that the multiple PK and physiological parameters collectively control the $^{14}CO_2$ production rate – time curve of the EBT. Adjustment factors for the activity of drug transporters were also estimated in all subjects. Lastly, correlation analysis can be used to explore relationships between the activity of non-renal elimination pathways and potential surrogate biomarkers (such as uremic solutes) via iPBPK-R modeling. In summary, we applied iPBPK-R to EBT data to distinguish and simultaneously estimate the activity of multiple non-renal elimination pathways in healthy subjects. This serves as proof of principle that the iPBPK-R framework is a novel tool for delineating rate-limiting and non-rate limiting elimination pathways using a single probe.

4.0 Application of iPBPK-R to Evaluate the Effect of Hemodialysis on Nonrenal Clearance Pathways

4.1 Abstract

The aim of this study was to apply iPBPK-R modeling of $^{14}CO_2$ production rates measured by the EBT to characterize the effect of hemodialysis on the function of nonrenal clearance pathways in patients with end-stage renal disease (ESRD). Twelve patients previously received ^{14}C-erythromycin intravenously pre- and post-hemodialysis. Serial breath samples were collected after each dose over two hours. Eight PBPK parameters were co-estimated across periods, while activity of CYP3A4 was independently estimated for each period. Inhibition coefficients for OATP, P-gp, and MRP2 activities were also estimated. Nonrenal clearance parameter estimates were explored regarding sex differences, correlations with uremic toxins, and used in hierarchical cluster analysis (HCA). Relationships between the function of nonrenal clearance pathways and uremic toxin concentrations were explored. Mean CYP3A4 clearance increased by 2.2% post-hemodialysis. Uptake transporter activity was highly variable between subjects across hemodialysis. Five females had 22.2% and 29.8% higher median CYP3A4 activity than seven males pre- and post-hemodialysis, respectively. Exploratory HCA identified two patients had an increased CYP3A4 activity (measured by the adjustment factors pre and post-hemodialysis which were used as *features* in HCA; median increase 8.6% versus 0.7% in others) with decreased plasma concentration of intact parathyroid hormone post-hemodialysis[1]. This is the first study to utilize the iPBPK-R approach to simultaneously estimate multiple in vivo nonrenal elimination pathways in individual patients with kidney disease and to assess the effect of hemodialysis.

[1]HCA analysis used the iPBPK-R based estimated values of adjustment factors for CYP3A4 activity pre- and post-hemodialysis, and the two patients found in the same cluster as a result of HCA had a decreased concentration of intact parathyroid hormone (iPTH) from pre- to post-hemodialysis. This is an exploratory analysis and does not make a mechanistic inference by itself beyond the temporal relationship between the two types of measurements, adjustment factors and concentrations of iPTH. See the discussion on HCA analysis in Section 4.5.

4.2 Introduction

iPBPK-R is a novel PBPK approach to indirectly and simultaneously measure the activity of multiple nonrenal elimination pathways within individual subjects via parameter estimation [105]. Recently, we used iPBPK-R and $^{14}CO_2$ production rate data generated from the EBT to demonstrate proof of principle that erythromycin may serve as a single phenotypic probe to simultaneously assess and differentiate contributions of nonrenal metabolic and transport pathways to its disposition in healthy subjects [105][2]. This strategy may be leveraged to study the interplay between metabolic enzymes and transporters and to overcome the limitations of using a single probe drug that exhibits overlapping substrate specificity or using a cocktail approach (see the statistical rationale of the limitations described in Section 2.2.1). As such, it has particular appeal for use in assessing the effects of complex disease states, drugs or other interventions on multiple nonrenal elimination pathways.

Chronic kidney disease (CKD) afflicts millions of people worldwide [203,204]. The disease is notorious for impacting the disposition of both renally and nonrenally cleared substances [17], and for complicating the selection and dosing of drugs, particularly as kidney disease progresses. This is further complicated by initiation of renal replacement therapies such as intermittent hemodialysis (HD) because it clears dialyzable substances [87, 205, 206]. In addition, hemodialysis may improve the function of nonrenal clearance pathways, though the precise mechanism and pathways impacted are unclear [17, 87, 205, 206]. For example, hemodialysis was shown to improve hepatic CYP3A4 activity in a population PK analysis of EBT data pre- and post-hemodialysis [128]. It may be possible that this improvement was caused by some uremic toxins (e.g., iPTH [207,208]) removed by hemodialysis. On the other hand, Thomson et al. showed that AUC of midazolam (nonrenally cleared specific probe for CYP3A4) was higher in ten patients who were on hemodialysis than eight patients with CKD who were not dependent on hemodialysis [209]. In another study, patients with ESRD

[2]As described in the previous chapter (Section 3.2), the mechanism and validity of differentially dissecting the multiple parameter estimates are provided via the detailed analysis of estimation and use of regularization in Chapter 2 (see Sections 2.6 and 2.4.7). This principle can be applied to the application of iPBPK-R to the patient data in this chapter as well.

receiving hemodialysis was shown to have reduced nonrenal transporter activity compared to healthy subjects using PO fexofenadine while CYP3A4 activity was not affected in those ESRD patients compared to healthy subjects using PO midazolam [210]. Novel strategies to ascertain the impact of kidney disease and hemodialysis on drug disposition and individual nonrenal clearance pathways are needed. We hypothesized that the iPBPK-R approach may be applied to EBT data in patients with stage 5 CKD [i.e., end-stage renal disease (ESRD)] to evaluate the effect of chronic intermittent HD on nonrenal clearance pathways.

The aims of this chapter were to apply iPBPK-R (1) to differentially estimate contributions of nonrenal clearance pathways to erythromycin in individual patients with ESRD pre- and post-HD, (2) to investigate the effect of hemodialysis on these pathways, and (3) to explore the relationships between parameter estimates and uremic toxin concentrations.

4.3 Methods

4.3.1 Clinical Data Sources

The $^{14}CO_2$ production rate data was collected from a prospective cohort study where 12 ESRD patients (7 male; 11 white, 1 black) receiving chronic intermittent hemodialysis treatment received the EBT. A single 0.074 mmol (0.04 mg, 3 μCi) dose of [^{14}C-N-methyl] erythromycin (Metabolic Solutions Inc., Nashua, NH) was given intravenously. Breath samples were collected directly before receiving the dose and at 5, 10, 15, 20, 30, 40, 50, 60, 90, and 120 min post dosing as previously described [128]. The study was approved by the Maine Medical Center Institutional Review Board and the Radiation Safety Committee and it adhered to the Declaration of Helsinki. Published clinical EBT data [169] was used to pre-estimate parameters that could not be obtained via the *in vitro–in vivo* extrapolation (IVIVE) by applying the PBPK-R model, which follows our previous study [105].

4.3.2 PBPK Model Structure

A PBPK model consisting of seven organ/tissue compartments and sub-compartments (①-⑦ in Figure 21) was built with physiological and kinetic parameters (i.e., PBPK parameters) for ^{14}C-erythromycin. The compartments included were artery (Art), vein, lung (LG), liver (LV), kidney (KD), and combined other organs (OT). The liver compartment consisted of extracellular space (ES) and liver cell (LC) sub-compartments. The model structure is similar to the model for healthy subjects as published previously [105]. A *non-linear meta-uptake transporter* (combining OATPs; see *Model Assumptions* in Section 4.3.5) and *total passive diffusion* were included to model the drug transfer between ES and LC. Non-linear efflux transporters (P-gp and MRP2) were modeled using maximum velocity and Michaelis-Menten constant or intrinsic clearance in LC. CYP3A4 clearance was modeled to be linear since the drug concentration with a low dose of ^{14}C-erythromycin was well below the maximum velocity of nonlinear kinetics [105].

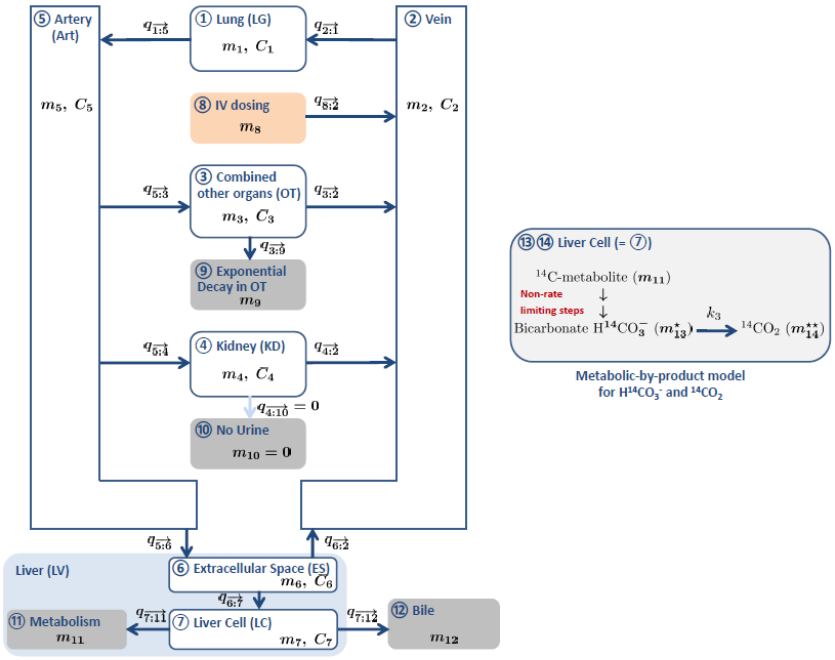

Figure 21: A schematic representation of a seven-compartmental PBPK model (①-⑦) for describing the time profiles of ^{14}C-erythromycin after intravenous ^{14}C-erythromycin administration in a patient with ESRD.

Adapted from [105] with permission. m, q, and C denote drug mass, drug mass flow, and drug concentration. The liver comprised of two sub-compartments (extracellular space (ES) and liver cell or hepatocyte (LC)) where non-linear uptake and efflux transporters and linear enzymatic clearance were included in $q_{\overrightarrow{6:7}}$, $q_{\overrightarrow{7:12}}$, and $q_{\overrightarrow{7:11}}$ as detailed in Table 6 and Supplemental materials of [105]. In the right figure, the metabolic by-product model is illustrated where the metabolite ^{14}C-formate is converted to radiolabeled bicarbonate $H^{14}CO_3^-$ in the CYP3A4-mediated pathway and dissolved in the LC sub-compartment. The series of conversion from H^{14}C-formaldehyde to $H^{14}CO_3^-$ is assumed to be a non-rate-limiting. $^{14}CO_2$ is produced in breath as a result of the first-order elimination of bicarbonate (with a constant k_{resp}) from the LC. Based on this iPBPK-R model, a system of nonlinear ordinary differential equations (ODEs) was set up for simulations to maintain the mass balance of ^{14}C-erythromycin in the body system [105].

4.3.3 Ordinary Differential Equations, Kinetic Parameters, and Data Input

Drug concentration dynamics of all compartments and sub-compartments were mathematically described with a set of ODEs. The ODEs were the same as those for healthy subjects in Chapter 3 [105] except for the ODE modeling the KD compartment, which did not include the clearance terms of P-gp (assuming negligible tubular secretion in the patients [211]) nor glomerular filtration rate for the patients with ESRD. The ODE of the vein compartment was identical to that for healthy subjects since the percentage of drug removal via hemodialysis was set to 0 (See 10. of Table 17 in *Model Assumptions*). Permeability-limited liver models were used in the ODEs associated with ES and LC [101] (See 2. of Table 17 in *Model Assumptions*). We referred to Kanamitsu et al. [183] for the metabolic by-product model to describe the series of non-rate limiting steps from ^{14}C-formaldehyde to bicarbonate $H^{14}CO_3^-$ and subsequent $^{14}CO_2$ generation within the LC sub-compartment. This enabled us to approximate the $^{14}CO_2$ production rate in the breath by the first derivative of the cumulative $^{14}CO_2$ concentration generated in LC (see *Model Assumptions* in Section 4.3.5). Parameters in Table 12 for healthy subjects were also used for ESRD patients except for the parameters listed in Table 18. Thus, Table 18 provides parameters which were uniquely obtained for ESRD patients. These parameters were used as input values in the estimation of scaling factors, which is described later.

Table 17: List of assumptions used in iPBPK-R of EBT data from patients with ESRD

Number	Assumption
1	The duration of intravenous dosing of ^{14}C-erythromycin was 30 seconds.
2[a]	Our model is well-stirred [183] [199]. Thus, the distribution of a drug rapidly reaches equilibrium via passive diffusion and the unbound concentration in the compartment is the same as those in the diffused space at equilibrium. All compartments except for the liver compartment are perfusion-limited[3]. For the liver, permeability-limited model[4] was used as detailed in 3.
3	Pathways from the extracellular space to the liver cells (ES $\rightarrow$ LC sub-compartment) for erythromycin consist of total passive diffusion and summation of uptake transporters. The hepatic uptake transport processes of ^{14}C-erythromycin by OATP isoforms OATP1B1 and OATP1B3 were modeled as a single meta-uptake process.
4	After being generated in the LC sub-compartment, $^{14}CO_2$ is instantaneously released in breath via the lung without being stored in or released from any other compartments. CO_2 in the systemic circulation is at steady state.
5	In the CYP3A4-mediated pathway, the series of conversion from 14C-erythromycin, ^{14}C-formaldehyde, 14C-formate through to a by-product radiolabeled bicarbonate ($H^{14}CO_3^-$) is rapid and not rate-limiting as assumed by Sugiyama et al. [172] $H^{14}CO_3^-$ is dissolved in the LC sub-compartment and the final by-product $^{14}CO_2$ in this pathway is produced and exhaled in breath as a result of a first-order elimination of $H^{14}CO_3^-$ (with a constant k_{resp}) from the LC sub-compartment [172].

[3]A perfusion-limited kinetic model describes the limiting process that is defined by the blood flow to the tissue [212].

[4]A permeability-limited kinetic model describes the limiting process that is defined by the permeability of drug across the cell membrane. Rather than depending on the blood flow, the time to reach equilibrium of the drug concentrations across the membrane is highly dependent on the drug-specific permeability such as active transport processes [212].

Table 17: List of assumptions used in iPBPK-R of EBT data from patients with ESRD

Number	Assumption
6[a]	The liver consisting of ES and LC sub-compartments is an elimination organ. In addition, a parameter μ was incorporated in the OT compartment to explain the exponential decay that was seen in the observed $^{14}CO_2$ production rate data. We expected that this μ would improve the model fitting. Thus, the exponential decay was assumed to account for any loss or decomposition of the drug before the drug reaches the liver within the system.
7	The unbound drug was subject to uptake and efflux transport, enzymatic metabolism, and elimination in the liver.
8	We assumed linearity for the intrinsic clearance of CYP3A after investigating the model fitting in the iPBPK-R development.
9[b]	All patients received the second EBT at nine hours post dosing of the first EBT.
10[b]	Patients underwent a 4-hour hemodialysis after the two-hour sample collection of the first EBT, the drug removal by hemodialysis in the carryover concentration of the first EBT to the second EBT was negligible [213, 214][5].

[a]The assumption was modified for the ESRD patient population from the corresponding assumption used in our previous model application for healthy subjects since the kidney compartment is not an elimination organ in ESRD. [b]The assumption was newly added in this model application because of the study design with 2 study b periods (pre- and post-HD).

[5]Based on the references [213, 214], %dialyzed of erythromycin is low (0-7%) and supplemental dosing is not required for erythromycin during hemodialysis (HD). Accordingly, we assumed that erythromycin does not get removed by HD. The only difference from the case to account for a minor removal of erythromycin is whether we will have a carryover $^{14}CO_2$ production rate from pre-HD EBT at the beginning of EBT post-HD. As seen Figure 23 the assumption of no removal of the drug leads to accounting for the maximum possible carryover $^{14}CO_2$ production rate, which showed great model fit to the observed data at the baseline of the $^{14}CO_2$ production rate-time curves post-HD. Accordingly, this assumption was considered to be appropriate and sufficient, and sensitivity analysis on %dialyzed would not have any impact but rather make the simulated curves fit less to the observed data at the baseline of post-HD EBT.

Table 18: Parameters used for the erythromycin breath test simulations for patients with ESRD

Description (units)[6]	Notation	Value	Reference/Comments
Glomerular filtration rate (L/hr)	eGFR (= δG_{fr})	0	Assumed
Clearance via Pgp (L/hr)	CL_{OUT1}	0.1735	Pre-estimated for the liver based on an initial simulation using [169]
Fraction unbound in blood	$f_{u,BL}$ (= f_b)	0.30	Assumed for ESRD based on [188]
Fraction unbound in extracellular space	$f_{u,ES}$ (= f_6)	0.462	Calculated for ESRD based on [189] [190], [191], and [192][7]
Partition coefficient of the combined other organs to plasma	$P_{OT:P}$	0.775	Calculated based on [195] [196] [188]

[6]This table lists the input parameters which were uniquely obtained for patients with ESRD and different from those for healthy subjects in Table 12 of Chapter 3.

[7]$f_{u,ES}$ was calculated applying the assumption proposed for general physiological PK modeling by Khor et al. to our modeling. This assumption was 'the blood protein to which the drug binds is also present in interstitial fluid and that the association binding constant is the same in both blood and interstitial fluid' [189]. Extracellular space matrix (ECM) is known to have many proteins such as fibrillar collagens, proteoglycans, growth factors, cytokines, chemokines, enzymes, among others [193]. We treat these proteins in ECM in the liver as a general protein that can bind to erythromycin in the modeling.

4.3.4 Rate Data and Reduced Order Model

Frequently sampled production rate data has mathematically higher *information content* (i.e., it enables higher accuracy of estimated model parameters) compared to equivalently sampled concentration data (see the details in *Highly sensitive indirect measurement* of Section 2.4.1 or in Section 3.3.4). However, more effort is required to extract this information [105]. In digital signal processing and other engineering disciplines, non-linear model fitting of observed first derivative data is often conducted to estimate sensitive parameters [134]. We borrowed this concept in our previous application of iPBPK-R [105]. In this chapter, the $^{14}CO_2$ production rate data from the EBT study in patients with ESRD was modeled in a similar fashion. The iPBPK-R model was fit to the $^{14}CO_2$ production rate data via a nested co-optimization procedure. Multiple nonrenal elimination pathways, i.e., uptake and efflux transport and total passive diffusion parameters, were estimated via scaling factors relative to IVIVE using the single probe drug ^{14}C-erythromycin. The types of scaling factors used were: (1) co-optimized adjustment factors, (2) independent adjustment factors, (3) inhibition coefficients, and (4) total adjustment factors (see *Simulations and Optimizations* in Section 4.3.6). In order to obtain high precision in the model fitting, we used a reduced order model [198]. Reduced order models are sufficiently complex to capture the behavior of interest but simple enough to be well-posed, providing estimable parameters. Based on this rationale, the total number of compartments and sub-compartments was limited to seven, as described in the preceding subsections.

4.3.5 Model Assumptions

Adopting the concept of reduced order model enabled us to achieve superior goodness-of-fit in iPBPK-R modeling of EBT data and to implement high-dimensional parameter estimation. We performed the iPBPK-R modeling under similar assumptions that were previously used for healthy subjects [105]. A part of these assumptions were adapted for patients with ESRD due to the disease stage and study design. The list of assumptions for the present study is shown in Table 17.

4.3.6 Simulations and Optimizations

Concentration-time curves of ^{14}C-erythromycin and by-products $H^{14}CO_3^-$ and $^{14}CO_2$ were simulated for individual patients using the system of ODEs as in Chapter 3 [105] with minor modifications described in Section 4.3.3. By taking the first derivative of cumulative $^{14}CO_2$ concentrations in LC, $^{14}CO_2$ production rates were simulated.

Prior to conducting the high-dimensional parameter optimization for patients with ESRD, the following PBPK parameters were pre-estimated as in Chapter 3 using literature data [105] [169]: maximum velocity of the meta uptake transporter, maximum velocity of the hepatic P-gp, CYP3A4 clearance, partition coefficient in the combined other organs, and exponential decay parameter. These pre-estimated parameter values were used in the high-dimensional parameter optimization as starting values for patients with ESRD.

iPBPK-R uses a nested co-optimization procedure, which consists of the inner loop and outer loop to optimize PBPK parameters (Figure 22) (See Section 2.6.4 of Chapter 2). In the *outer loop*, eight scaling factors for the following PBPK parameters were optimized[8]: maximum velocity of OATPs, P-gp, and MRP2 ($J_{max,UP1}$, $J_{max,OUT1}$, and $J_{max,OUT2}$), volume of total hepatocyte (V_{LC}), total passive diffusion between extracellular space and hepatocyte (Q_{ES-LC}), arterial blood flow into the combined other organs (Q_{OT}) , exponential decay parameter (μ), and partition coefficient of the combined other organs to plasma ($P_{OT:P}$). These parameters were assumed to be shared between pre- and post-HD and thus co-optimized within individuals. We called these scaling factors *co-optimized adjustment factors*. In model fitting, the co-optimized adjustment factors result in patient-specific baseline adjustment of population IVIVE (or input values) regardless of the study periods. In the *inner loop*, four scaling factors in each study period (pre- and post-HD, for a total of eight scaling factors) were *independently* optimized[9]: scaling parameters for the nonlinear OATPs, P-

[8]The number of observed samples per individual in this simultaneous PBPK model fit is 11 time points $\times$ 2 datasets (pre- and post-hemodialysis) = 22 data points. The number of functionally dependent parameters to optimize here (i.e., 8 outer loop parameters) is sound as shown in the analysis of iPBPK-R estimation using regularization in Section 2.4.7.

[9]The number of observed samples per individual in this simultaneous PBPK model fit is 11 time points for each EBT test (pre- and post-hemodialysis, respectively). The number of independent parameters to optimize here (i.e., 2 inner loop parameters pre- and post-hemodialysis, respectively) is valid as these inner loop optimization steps are independent of the outer-loop optimization in the nested co-optimization process as described in 2.7.2.

gp, and MRP2 clearance, and an *adjustment factor* for linear CYP3A4 clearance (CL_{CYP}). The scaling parameters for drug transporters are interpreted as non-competitive *inhibition coefficients* in the pathophysiological state (i.e., ESRD). Inhibition coefficients are used to evaluate the reduction in the co-optimized adjustment factor for $J_{max,UP1}$, $J_{max,OUT1}$, and $J_{max,OUT2}$ pre- and post-HD. Scaling factors were estimated via nested co-optimization that minimizes the errors of the fitted model of $^{14}CO_2$ production rates.

The model fit was evaluated using goodness-of-fit plots, normalized residuals between predicted and observed rates, visual inspection, and plausibility of the parameter estimates. Among the PBPK parameters in Table 18, aforementioned outer loop and inner loop parameters were selected for optimization. Using sensitivity analysis in healthy subjects, these selected parameters were found to be essential for fitting the model to the EBT data [105]. Adjustment factors for maximum velocity of efflux transporters were not sensitive enough to contribute to controlling the shape of the $^{14}CO_2$ production rate-time curves. However, these parameters were kept in the optimization since they were part of nonrenal elimination pathways. The inhibition coefficients in the inner optimization loop were used to calculate *total adjustment factors* for IVIVE values of transporter kinetics pre- and post-HD, where total adjustment factor = co-optimized adjustment factor $\times$ inhibition coefficient.

Simulations and parameter co-optimization were implemented with R 3.4.4. The R package *deSolve* was used for solving the set of ODEs, and large-scale simulations were performed via the Bridges supercomputer at PSC [126]. Methodological details of iPBPK-R were described in Chapter 2.

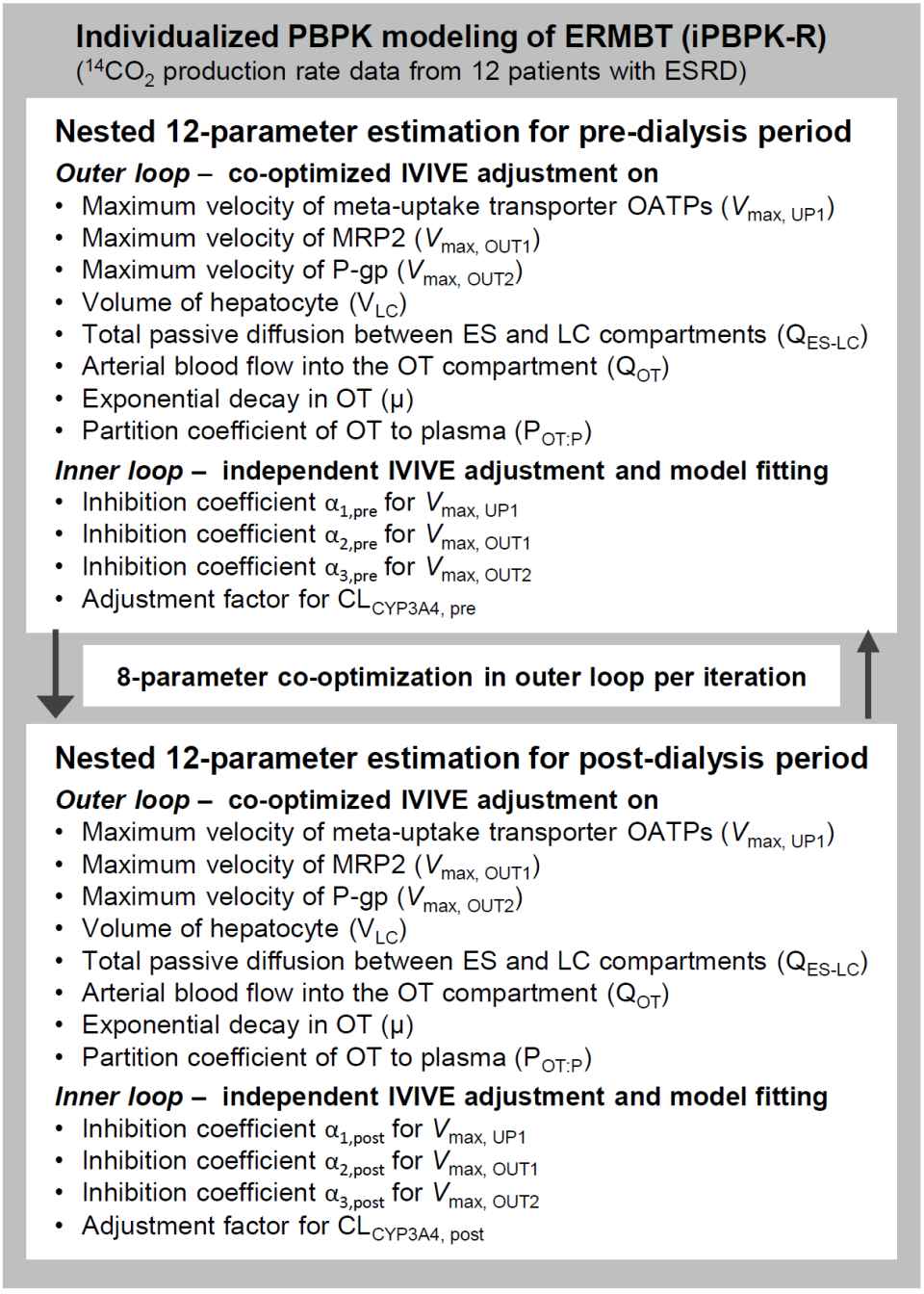

Figure 22: Framework of the application of iPBPK-R to the EBT study in 12 patients with ESRD.

The optimization setup in the application of iPBPK-R to two EBT datasets per patient was mathematically described in Section 2.6.4. The framework diagram illustrates which parameters are estimated in the nested co-optimization setting in the actual application to

the $^{14}CO_2$ production rate data set pre- and post-hemodialysis, and a nested co-optimization of multiple parameters with outer and inner loops was conducted in each patient accordingly.

4.3.7 Statistical Analysis

Mean ± SD and/or median (range) were used as descriptive statistics. Box plots were created for visualization of estimation results. No statistical test was powered in advance since the study explored feasibility and estimability. For comparing parameters pre- and post-HD, paired t-tests were conducted in case of normally distributed measurements. Otherwise, Wilcoxon signed-rank tests were conducted. One-sided tests were used to test an increase in activity of metabolic enzyme and drug transporters by the effect of hemodialysis. Two-sided Wilcoxon-Mann-Whitney tests were conducted for comparing two independent subgroups. One-sided tests were used to evaluate a higher enzyme activity in females than in males that was found in our previous study [105]. Spearman's ρ correlation coefficients were obtained in correlation analysis to explore the relationships between estimated parameters and baseline demographic or uremic solute concentrations pre-HD, post-HD, and in the change from pre- to post-HD. Finally, hierarchical clustering analysis (HCA) [215] was applied to parameter estimates to explore potential cluster sub-groups and interindividual differences. In all comparisons a P-value < 0.05 was considered statistically significant. Scaling factors were interpreted as follows. An adjustment factor 1 indicates that the estimated parameter did not require any adjustment from the initial input parameter value as a result of parameter optimization. Inhibition coefficient of 0 indicates complete non-competitive inhibition while inhibition coefficient of 1 indicates no non-competitive inhibition. All statistical analyses were conducted using SAS 9.4 (SAS Institute Inc., Cary, NC).

4.4 Results

The iPBPK-R model was fit to the observed $^{14}CO_2$ production rate data pre- and post-HD for the 12 patients with ESRD (Figure 23). The nested co-optimization procedure yielded parameter estimates for all patients, and goodness-of-fit plots across subjects showed an excellent model fit for all patients (Figure 24). Figure 25 provides an example of 3D $^{14}CO_2$ production rate-time curve simulations in one patient where the nested co-optimization leads

to the final model fit pre- and post-HD simultaneously. This procedure provides eight outer loop and four inner loop parameters per study period (Figure 22 and Table 19).

Table 19: Parameter estimates via the nested co-optimization in the iPBPK-R modeling of the EBT study in 12 patients with ESRD

Estimated parameter	Pre- and post-hemodialysis periods Mean ± SD	Median (Range)
IVIVE adjustment: co-optimized adjustment factor		
Meta-uptake transporter OATPs (baseline deviation from IVIVE)	1.09 ± 0.18	1.04 (0.98, 1.65)
P-gp (baseline deviation from IVIVE)	1.00 ± 0.01	1.00 (1.00,1.02)
MRP2 (baseline deviation from IVIVE)	1.01 ± 0.03	1.00 (1.00, 1.09)
Hepatocyte volume	1.06 ± 0.19	1.06 (0.81, 1.39)
Total passive diffusion between ES and LC	0.41 ± 0.24	0.37 (0.13, 0.92)
Arterial blood flow in the combined other organs	0.64 ± 0.41	0.46 (0.45, 1.86)
Exponential decay parameter in the combined other organs	4.33 ± 0.86	4.07 (4.03, 7.06)
Partition coefficient in the combined other organs	18.77 ± 0.06	18.79 (18.60, 18.82)

Table 19: Parameter estimates via the nested co-optimization in the iPBPK-R modeling of the EBT study in 12 patients with ESRD (continued)

Estimated parameter	Pre-hemodialysis period Mean ± SD	Median (Range)	Post-hemodialysis period Mean ± SD	Median (Range)	P-value
Scaling factor: inhibition coefficient					
Meta-uptake transporter OATPs[a]	0.66 ± 0.28	0.62 (0.25, 1.00)	0.46 ± 0.26	0.38 (0.09, 0.97)	0.957
P-gp[b]	1.00 ± 0.00	1.00 (1.00, 1.00)	1.00 ± 0.00	1.00 (1.00, 1.00)	0.125
MRP2[b]	1.00 ± 0.00	1.00 (1.00, 1.00)	1.00 ± 0.00	1.00 (1.00, 1.00)	0.125
IVIVE adjustment : total adjustment factor					
CYP3A4 clearance[a]	0.17 ± 0.13	0.13 (0.05, 0.40)	0.20 ± 0.14	0.12 (0.07, 0.44)	0.033*
Meta-uptake transporter OATPs[a]	0.71 ± 0.29	0.72 (0.27, 1.10)	0.49 ± 0.26	0.49 (0.10, 0.99)	0.964
P-gp[b]	1.00 ± 0.01	1.00 (1.00, 1.02)	1.00 ± 0.01	1.00 (1.00, 1.02)	0.125
MRP2[b]	1.01 ± 0.03	1.00 (1.00, 1.09)	1.01 ± 0.03	1.00 (1.00, 1.09)	0.125

ESRD, end-stage renal disease; IVIVE, in-vitro in-vivo extrapolation; OATPs, organic anion transporting polypeptides; P-gp, P-glycoprotein; MRP2, multidrug resistance-associated protein 2; CYP3A4, cytochrome P450 3A4

[a]One-sided paired t-test was conducted.; [b]One-sided paired Wilcoxon signed rank test was conducted. $\star$ indicates a statistically significant increase from pre- to post-hemodialysis at a significance level of 0.05.

Note that a clinical threshold for evaluating adjustment factors has not been established as this is the first study in ESRD patients to simultaneously estimate multiple dependent parameters in an automated fashion as discussed in Section 4.5.

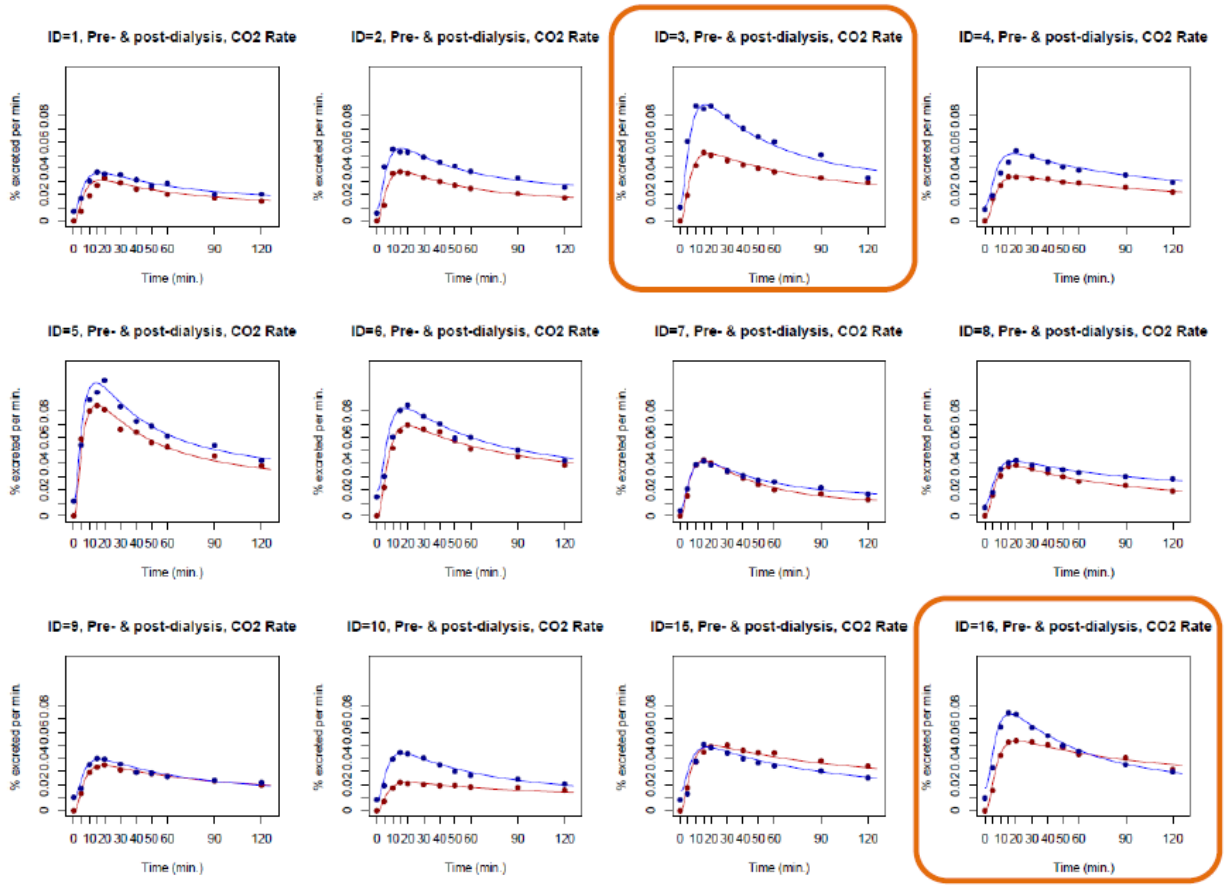

Figure 23: iPBPK-R per-individual simultaneous model fit to the EBT data pre- and post-hemodialysis (HD) from the 12 patients with ESRD.

The red lines and blue lines are modeled $^{14}CO_2$ production rate-time curves pre- and post-HD, respectively. The dark red and dark blue dots indicate the observed $^{14}CO_2$ production rates pre- and post-HD, respectively. The goodness-of-fit of these curves are discussed in Section 4.5 along with Figure 24. The orange lines indicate the subjects (ID = 3, 16) identified as a cluster group in the hierarchical clustering analysis as described in Figure 29.

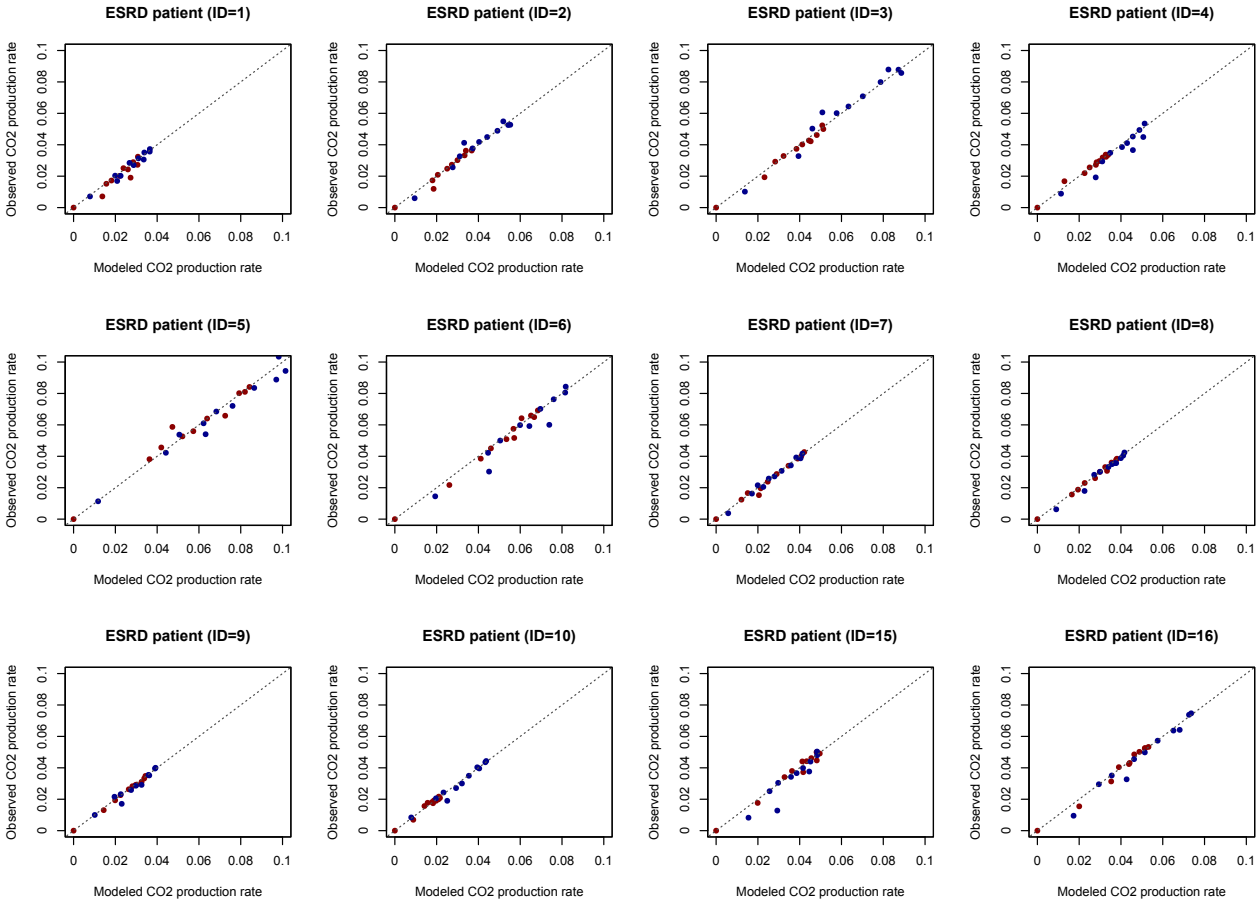

Figure 24: Goodness-of-fit plots pre- and post-hemodialysis (HD) for the 12 patients with ESRD.

Observed versus modeled (simulated) $^{14}CO_2$ production rates are shown[10], which correspond to the iPBPK-R model fit to the EBT data in Figure 23. The dark red and dark blue dots indicate the results pre- and post-HD, respectively. The simulated and observed $^{14}CO_2$ production rates are on or close to the diagonal line across the 12 patients pre- and post-dialysis. There are data points slightly off from the diagonal line in the patients of ID = 5, ID = 6, and ID = 15. These may be caused by the actual sample collection times that deviated from the planned sample collection times as the breath samples in the early phase were intensively collected within the two hours. This is discussed in Section 4.5.

[10]Rather than the normalized residual-time plots, goodness-of-fit plots are being presented here for the same reason described in Figure 16.

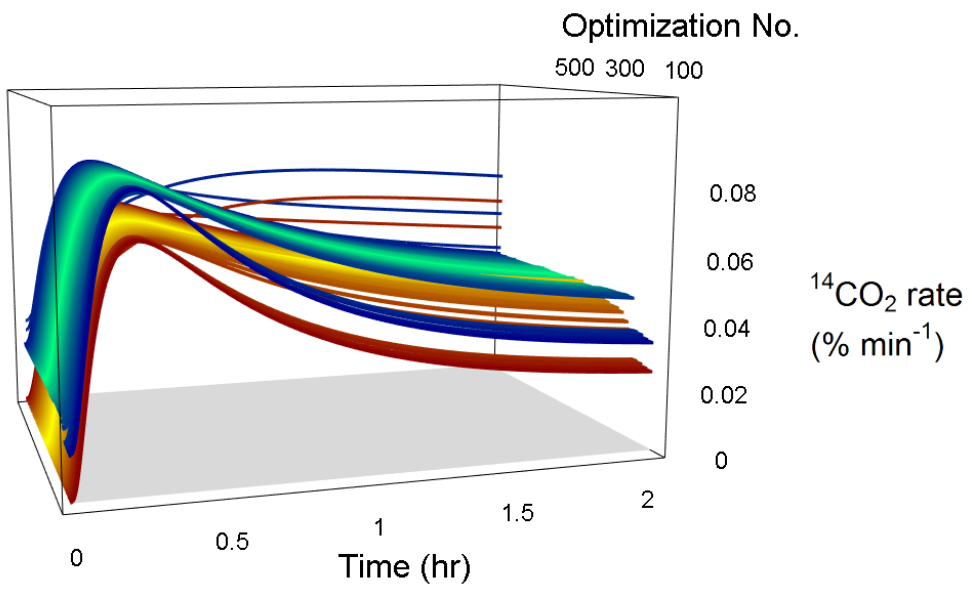

Figure 25: An example of 3D $^{14}CO_2$ production rate-time curve simulations in one patient.

The nested co-optimization simultaneously leads to the final model fit pre- and post-hemodialysis (HD). The curves in the blue – green – blue color transition show the simulated curves pre-HD and the curves in the red – yellow – red color transition show the simulated curves post-HD during the nested parameter co-optimization (high-dimensional parameter estimation). Both curves were simultaneously fit to the patient's observed data pre- and post-HD at the end of the optimization process. In other words, this figure presents one individual's iPBPK-R example that iPBPK-R is searching multiple parameter values simultaneously and consistently, which are visualized via the $^{14}CO_2$ production rate-time curve simulations at earlier optimization numbers (z-axis). This search finds a solution of multiple functionally dependent parameters (adjustment factors) and simulates the final curves pre- and post-HD at the last optimization number due to the successful nested co-optimization with the well-crafted regularization described in Sections 2.4.7, 2.6, and 2.6.4.

Table 19 shows eight co-optimized adjustment factors for $J_{max,UP1}$, $J_{max,OUT1}$, $J_{max,OUT2}$, V_{LC}, Q_{ES-LC}, Q_{OT}, μ, and $P_{OT:P}$ in the outer loop (Figure 22). Most mean co-optimized adjustment factors in the liver were close to 1 (indicating no adjustment of IVIVE or population input value) except for Q_{ES-LC} (0.41 $\pm$ 0.24, mean $\pm$ SD). Co-optimized adjustment factors were relatively variable for Q_{ES-LC} and V_{LC} (1.06 $\pm$ 0.19) (Figure 26(A)). In the OT compartment, all co-optimized adjustment factors differed from 1 (0.64 $\pm$ 0.41 for Q_{OT}, 4.33 $\pm$ 0.86 for μ, and 18.77 $\pm$ 0.06 for $P_{OT:P}$) (Figure 27). Though the co-optimized adjustment factors in the OT compartment do not provide biological implication, they were included in the optimization for the purpose of model fitting, similarly to our previous study [105]. In the inner loop, adjustment factors for CL_{CYP3A4} and inhibition coefficients for OATPs, P-gp, MRP2 were estimated independently pre- and post-HD, respectively (Figure 26(B)). In Figure 26(C), the total adjustment factor (co-optimized adjustment factor $\times$ inhibition coefficient) for $J_{max,UP1}$ had relatively large interindividual variability, which did not improve from pre- to post-HD (0.71 $\pm$ 0.29 pre-HD; 0.49 $\pm$ 0.26 post-HD, p=0.96). The total adjustment factors for $J_{max,OUT1}$ and $J_{max,OUT2}$ were close to 1 and they did not show interindividual variability both pre- and post-HD. The adjustment factor for CL_{CYP3A4} increased slightly from pre- to post-HD (0.17 $\pm$ 0.13 pre-HD; 0.20 $\pm$ 0.14 post-HD, p=0.03); mean CL_{CYP3A4} at the beginning of the study was 17% of the IVIVE value and was increased by 2.2% (mean paired difference, not tabulated) after hemodialysis.

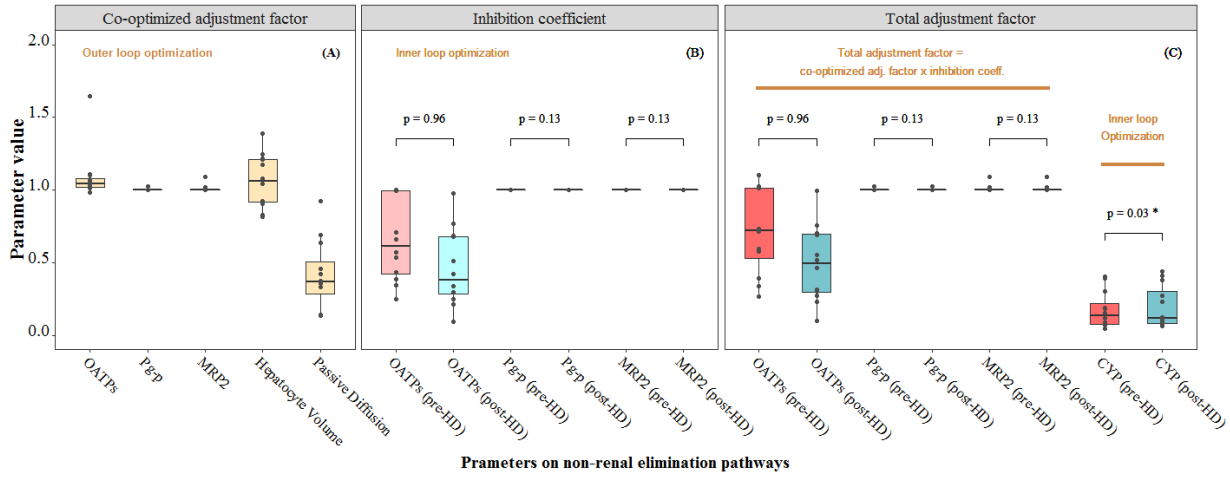

Figure 26: Box plots of estimated scaling factors (co-estimated adjustment factors, inhibition coefficients, and total or independently optimized adjustment factors) in the liver.

(A) Co-optimized adjustment factors for maximum velocity of OATPs, P-gp, and MRP2 ($J_{max,UP1}$, $J_{max,OUT1}$, $J_{max,OUT2}$), hepatocyte volume (V_{LC}), and passive diffusion between extracellular space and liver cell (Q_{ES-LC}) in the outer loop. (B) Inhibition coefficients for OATPs, P-gp, and MRP2 pre- and post-hemodialysis (HD) in the inner loop. (C) Total adjustment factors for OATPs, P-gp, MRP2, and CYP3A4 pre- and post-HD, respectively. The total adjustment factors for CYP3A4 pre- and post-HD were independently estimated in the inner loop. The total adjustment factors for transporters were calculated by co-optimized adjustment factor $\times$ inhibition coefficient. One sided exact or t-test p-values are shown and $\star$ indicates a statistically significant difference at a significance level of 0.05. N = 12 in all box plots.

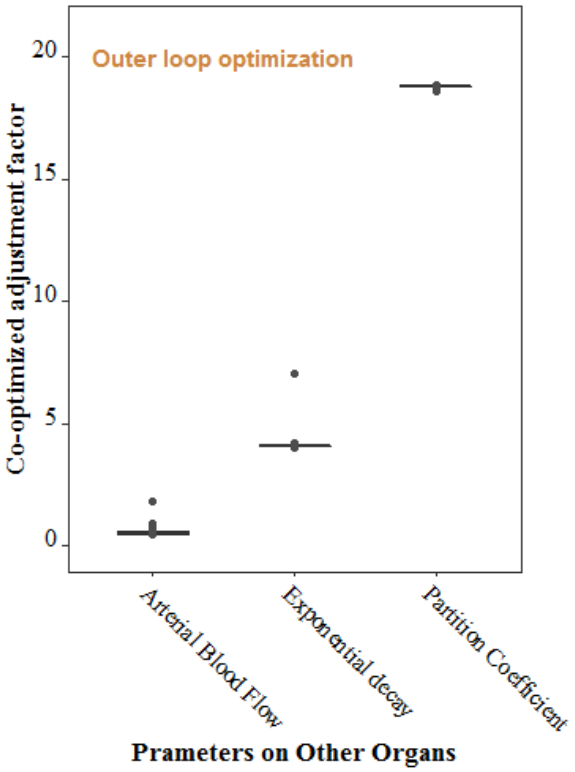

Figure 27: Box plots of co-optimized adjustment factors associated with the combined other organs (OT).

Co-adjustment factors for arterial blood flow, exponential decay, and partition coefficient of OT to plasma are shown. N = 12 in all box plots.

Next, parameters were compared by sex (Table 20(B) and (C)). The total adjustment factor for $J_{max,UP1}$ did not differ by sex pre- and post-HD (p=0.76 and p=0.15, respectively). The adjustment factor for CL_{CYP3A4} was significantly greater in females than in males pre-HD (the median reduction from the IVIVE value in males: females = 92%:70%, p=0.005). The adjustment factor for CL_{CYP3A4} post-HD showed a similar sex difference (the median reduction from the IVIVE value in males: females = 92%:62%, p=0.003) (Figure 28). The co-optimized adjustment factor which indicates patient-specific baseline adjustment differed for OATPs by sex (Table 20(A)). The co-optimized adjustment factor for V_{LC} also differed by sex (p=0.003) but it did not differ for Q_{ES-LC} (p=0.64).

Table 20: Parameter estimates via nested co-optimization in the iPBPK-R modeling of the EBT study in 12 patients with ESRD by sex

	Male		Female		
N	7		5		
Estimated parameter	Mean ± SD	Median (Range)	Mean ± SD	Median (Range)	p-value[a]
(A) IVIVE adjustment: co-adjustment factor					
Meta-uptake transporter	1.02 ± 0.03	1.02 (0.98, 1.07)	1.20 ± 0.25	1.10 (1.05, 1.65)	0.005⋆⋆
P-gp	1.00 ± 0.00	1.00 (1.00, 1.00)	1.00 ± 0.01	1.00 (1.00, 1.02)	0.88
MRP2	1.00 ± 0.01	1.00 (1.00, 1.02)	1.02 ± 0.04	1.00 (1.00, 1.09)	0.27
Hepatocyte volume	0.93 ± 0.10	0.92 (0.81, 1.08)	1.25 ± 0.08	1.22 (1.17, 1.39)	0.003⋆⋆
Total passive diffusion between ES and LC	0.43 ± 0.19	0.37 (0.13, 0.69)	0.39 ± 0.32	0.33 (0.14, 0.92)	0.64
Arterial blood flow in the combined other organs	0.54 ± 0.17	0.47 (0.45, 0.91)	0.78 ± 0.61	0.45 (0.45, 1.86)	0.53
Exponential decay parameter in the combined other organs	4.08 ± 0.05	4.06 (4.03, 4.18)	4.68 ± 1.33	4.10 (4.05, 7.06)	0.20
Partition coefficient in the combined other organs	18.79 ± 0.01	18.79 (18.78, 18.82)	18.75 ± 0.08	18.79 (18.60, 18.79)	0.76

[a] Exact p-value of a Wilcoxon-Mann-Whitney test to compare between male and female (two-sided test).

⋆⋆ indicates a statistically significant difference between male and female at a significance level of 0.01.

Table 20: Parameter estimates via nested co-optimization in the iPBPK-R modeling of the EBT study in 12 patients with ESRD by sex (continued)

	Male		Female		
N	7		5		
Estimated parameter	Mean ± SD	Median (Range)	Mean ± SD	Median (Range)	p-value[a]
(B) Pre-hemodialysis period					
Scaling factor: inhibition coefficient					
Meta-uptake transporter OATPs	0.67 ± 0.34	0.71 (0.25, 1.00)	0.64 ± 0.22	0.57 (0.43, 1.00)	0.44
P-gp	1.00 ± 0.00	1.00 (1.00, 1.00)	1.00 ± 0.00	1.00 (1.00, 1.00)	0.92
MRP2	1.00 ± 0.00	1.00 (1.00, 1.00)	1.00 ± 0.00	1.00 (1.00, 1.00)	0.31
IVIVE adjustment : Total adjustment factor[b]					
CYP3A4 linear clearance[c]	0.10 ± 0.05	0.08 (0.05, 0.19)	0.29 ± 0.12	0.30 (0.15, 0.40)	0.005**
Meta-uptake transporter OATPs	0.68 ± 0.35	0.73 (0.27, 1.03)	0.74 ± 0.21	0.71 (0.57, 1.10)	0.76
P-gp	1.00 ± 0.00	1.00 (1.00, 1.00)	1.00 ± 0.01	1.00 (1.00, 1.02)	0.88
MRP2	1.00 ± 0.01	1.00 (1.00, 1.02)	1.02 ± 0.04	1.00 (1.00, 1.09)	0.27

[a] Exact p-value of a Wilcoxon-Mann-Whitney test to compare between male and female (two-sided test).

[b] Total adjustment factors for nonlinear clearance by drug transporters were calculated by co-adjustment factor times inhibition coefficient.

[c] One-sided tests were applied due to the prior knowledge in literature.

**indicates a statistically greater median value in female compared to male at a significance level of 0.01.

Table 20: Parameter estimates via nested co-optimization in the iPBPK-R modeling of the EBT study in 12 patients with ESRD by sex (continued)

	Male		Female		
N	7		5		
Estimated parameter	Mean ± SD	Median (Range)	Mean ± SD	Median (Range)	p-value[a]
(C) Post-hemodialysis period					
Scaling factor: inhibition coefficient					
Meta-uptake transporter OATPs	0.59 ± 0.27	0.68 (0.22, 0.97)	0.28 ± 0.12	0.30 (0.09, 0.42)	0.11
P-gp	1.00 ± 0.00	1.00 (1.00, 1.00)	1.00 ± 0.00	1.00 (1.00, 1.00)	0.12
MRP2	1.00 ± 0.00	1.00 (1.00, 1.00)	1.00 ± 0.00	1.00 (1.00, 1.00)	0.15
IVIVE adjustment : Total adjustment factor[b]					
CYP3A4 linear clearance[c]	0.10 ± 0.06	0.08 (0.07, 0.23)	0.33 ± 0.13	0.38 (0.13, 0.44)	0.003**
Meta-uptake transporter OATPs	0.60 ± 0.27	0.69 (0.23, 0.99)	0.34 ± 0.18	0.31 (0.10, 0.55)	0.15
P-gp	1.00 ± 0.00	1.00 (1.00, 1.00)	1.00 ± 0.01	1.00 (1.00, 1.02)	0.88
MRP2	1.00 ± 0.01	1.00 (1.00, 1.02)	1.02 ± 0.04	1.00 (1.00, 1.09)	0.27

[a] Exact p-value of a Wilcoxon-Mann-Whitney test to compare between male and female (two-sided test).

[b] Total adjustment factors for nonlinear clearance by drug transporters were calculated by co-adjustment factor times inhibition coefficient. [c] One-sided tests were applied due to the prior knowledge in literature.

**indicates a statistically greater median value in female compared to male at a significance level of 0.01.

As described in Statistical Analysis Section (Section 4.3.7) statistical tests to compare two groups are not powered. Thus, these statistical tests are treated as exploratory analyses. Note that a clinical threshold for comparing adjustment factors has not been established as this is the first research to simultaneously estimate multiple functionally dependent parameters in ESRD patients in an automated fashion as discussed in Section 4.5.

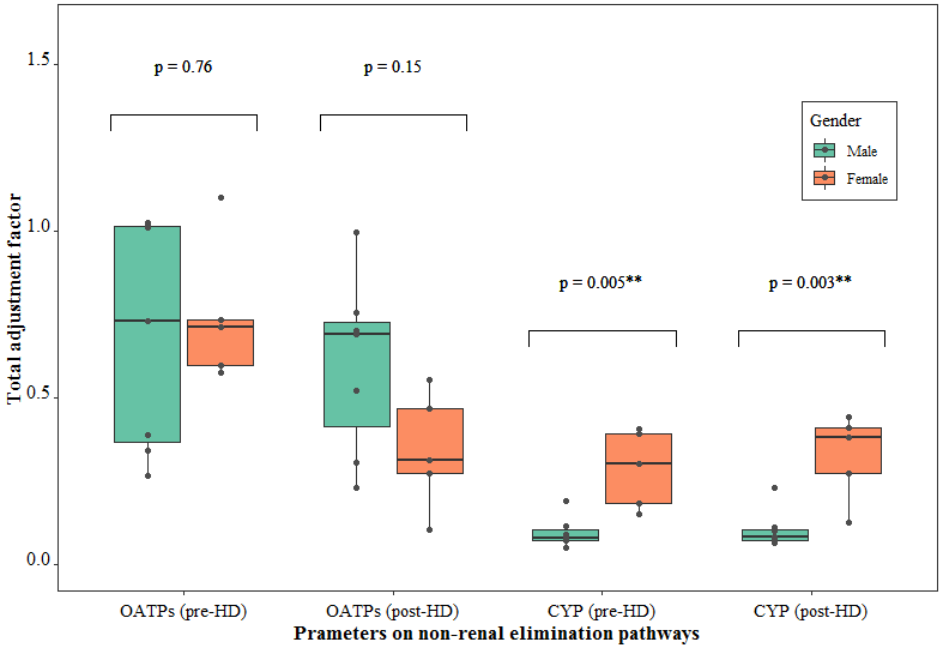

Figure 28: Box plots of selected total adjustment factors associated with nonrenal elimination pathways (OATPs, P-gp, and MRP2 and CYP3A4) pre- and post-hemodialysis are compared by sex.

Exact p-values are shown and $\star\star$ indicates a statistically significant difference at a significance level of 0.01. N = 7 for males and N = 5 for females.

As an exploratory analysis in the 12 patients (see Table 21), Spearman correlations between inhibition coefficients, total adjustment factors, and adjustment factors for non-renal elimination parameters ($J_{max,UP1}$, CL_{CYP3A4}, and Q_{ES-LC}) versus BMI, age, and uremic solute concentrations were estimated. Uremic solutes included SCr, BUN (low molecular weight solutes), and TNF-α, β_2-M, and iPTH (middle molecular weight solutes)[11]. The inhibition coefficient and total adjustment factor for $J_{max,UP1}$ were strongly correlated with β_2-M (ρ=0.692, p=0.01 and ρ=0.643, p=0.02, respectively) pre-HD, based on Evans' correlation criteria [200], but they did not correlate post-HD nor in the change from pre- to post-HD. The adjustment factor for CL_{CYP3A4} was strongly correlated with age both pre- and post-HD (ρ=0.657, p=0.02 and ρ=0.755, p=0.005), but its change between pre-and post-HD was not. The co-optimized adjustment factor for Q_{ES-LC} was negatively and strongly correlated with TNF-α pre-HD, but it was positively correlated with its change from pre- to post-HD. There was no correlation with TNF-α post-HD.

Figure 29 shows the result of the exploratory HCA. Clustering was performed using the estimated changes in inhibition coefficient for $J_{max,UP1}$ and adjustment factor for CL_{CYP3A4} from pre- to post-HD (average silhouette width = 0.45 for three clusters). The HCA identified two patients (ID = 3 and 16 marked in Figure 23) who showed more increased CYP3A4 activity by hemodialysis compared to the other patients (median increase 8.6% versus 0.7%, p=0.03; Figure 30(A)). The average change in the concentration of iPTH in these two patients was numerically much lower (without overlapping ranges) than that for the other patients (Figure 30(C)). However, with just two patients identified in the cluster analysis, it did not provide a statistically significant difference.

[11]This iPBPK-R study used the published clinical data [128] and these uremic toxins were designed to serve as model uremic toxins for different weight classes in the published clinical study.

Table 21: Correlation coefficients among estimated PBPK parameters, demographic data, and uremic solute concentrations in 12 patients with ESRD

Period	Estimated PBPK parameter on		BMI	Age	SCr	BUN	β_2M	TNF-α	iPTH[12]
Pre-hemodialysis	Meta-uptake transporter OATPs (inhibition coefficient)	ρ^a	0.407	-0.077	0.049	-0.088	0.692	0.091	-0.329
		p-value	0.189	0.812	0.880	0.787	0.013*	0.779	0.297
	Meta-uptake transporter OATPs (total adjustment factor)	ρ^a	0.365	-0.028	0.112	0.052	0.643	0.035	-0.441
		p-value	0.244	0.931	0.729	0.871	0.024*	0.914	0.152
	CYP3A4 clearance (IVIVE adjustment factor)	ρ^a	-0.305	0.657	-0.315	-0.518	-0.476	-0.021	0.105
		p-value	0.335	0.020*	0.319	0.084	0.118	0.948	0.746
	Total passive diffusion between ES and LC (IVIVE co-adjustment factor)	ρ^a	-0.119	-0.077	0.504	0.361	0.203	-0.636	0.000
		p-value	0.712	0.812	0.095	0.249	0.527	0.026*	1.000

BMI, body mass index (kg/m^2); SCr, serum creatinine (mg/dL); BUN, blood urea nitrogen (mg/dL); TNF-α, tumor necrosis factor-α (pg/mL); ES, extracellular space; LC, liver cell; IVIVE, in-vitro in-vivo extrapolation; β_2-M , β_2-microglobulin; iPTH, intact parathyroid hormone; NA, not applicable since the PBPK parameter was co-estimated between pre- and post-hemodialysis. [a]Spearman correlation coefficient. $\star$ and $\star\star$ indicate a statistically significant correlation at a significance level of 0.05 and 0.01, respectively.

[12]This iPBPK-R study used the published clinical data [128] and these uremic toxins were designed to serve as model uremic toxins for different weight classes in the published clinical study.

Table 21: Correlation coefficients among estimated PBPK parameters, demographic data, and uremic solute concentrations in 12 patients with ESRD (continued)

Period	Estimated PBPK parameter on		BMI	Age	SCr	BUN	β_2M	TNF-α	iPTH
Post-hemodialysis	Meta-uptake transporter OATPs (inhibition coefficient)	ρ^a	0.291	-0.322	0.322	0.558	-0.196	0.259	0.014
		p-value	0.358	0.308	0.307	0.059	0.542	0.417	0.966
	Meta-uptake transporter OATPs (total adjustment factor)	ρ^a	0.126	-0.280	0.350	0.505	-0.126	0.091	0.084
		p-value	0.696	0.379	0.264	0.094	0.697	0.779	0.795
	CYP3A4 clearance (IVIVE adjustment factor)	ρ^a	-0.225	0.755	-0.392	-0.414	0.007	-0.098	0.371
		p-value	0.483	0.005**	0.207	0.181	0.983	0.762	0.236
	Total passive diffusion between ES and LC (IVIVE co-adjustment factor)	ρ^a	NA	NA	0.333	0.126	-0.119	-0.399	0.070
		p-value	NA	NA	0.291	0.696	0.713	0.199	0.829

BMI, body mass index (kg/m^2); SCr, serum creatinine (mg/dL); BUN, blood urea nitrogen (mg/dL); TNF-α, tumor necrosis factor-α (pg/mL); ES, extracellular space; LC, liver cell; IVIVE, in-vitro in-vivo extrapolation; β_2-M , β_2-microglobulin; iPTH, intact parathyroid hormone; NA, not applicable since the PBPK parameter was co-estimated between pre- and post-hemodialysis. [a]Spearman correlation coefficient. $\star$ and $\star\star$ indicate a statistically significant correlation at a significance level of 0.05 and 0.01, respectively.

Table 21: Correlation coefficients among estimated PBPK parameters, demographic data, and uremic solute concentrations in 12 patients with ESRD (continued)

Period	Estimated PBPK parameter on		BMI	Age	SCr	BUN	β_2M	TNF-α	iPTH
Change from pre- to post-hemodialysis	Meta-uptake transporter OATPs (inhibition coefficient)	ρ^{a}	-0.123	-0.168	0.084	-0.225	0.490	0.098	-0.028
		p-value	0.704	0.602	0.795	0.482	0.106	0.762	0.931
	Meta-uptake transporter OATPs (total adjustment factor)	ρ^{a}	-0.123	-0.168	0.084	-0.225	0.490	0.098	-0.028
		p-value	0.704	0.602	0.795	0.482	0.106	0.762	0.931
	CYP3A4 clearance (IVIVE adjustment factor)	ρ^{a}	-0.421	0.350	-0.196	0.134	0.042	0.301	-0.084
		p-value	0.173	0.265	0.542	0.679	0.897	0.342	0.795
	Total passive diffusion between ES and LC (IVIVE co-adjustment factor)	ρ^{a}	NA	NA	-0.329	-0.548	-0.154	0.797	0.014
		p-value	NA	NA	0.297	0.065	0.633	0.002**	0.966

BMI, body mass index (kg/m^2); SCr, serum creatinine (mg/dL); BUN, blood urea nitrogen (mg/dL); TNF-α, tumor necrosis factor-α (pg/mL); ES, extracellular space; LC, liver cell; IVIVE, in-vitro in-vivo extrapolation; β_2-M , β_2-microglobulin; iPTH, intact parathyroid hormone; NA, not applicable since the PBPK parameter was co-estimated between pre- and post-hemodialysis. [a]Spearman correlation coefficient. $\star$ and $\star\star$ indicate a statistically significant correlation at a significance level of 0.05 and 0.01, respectively.

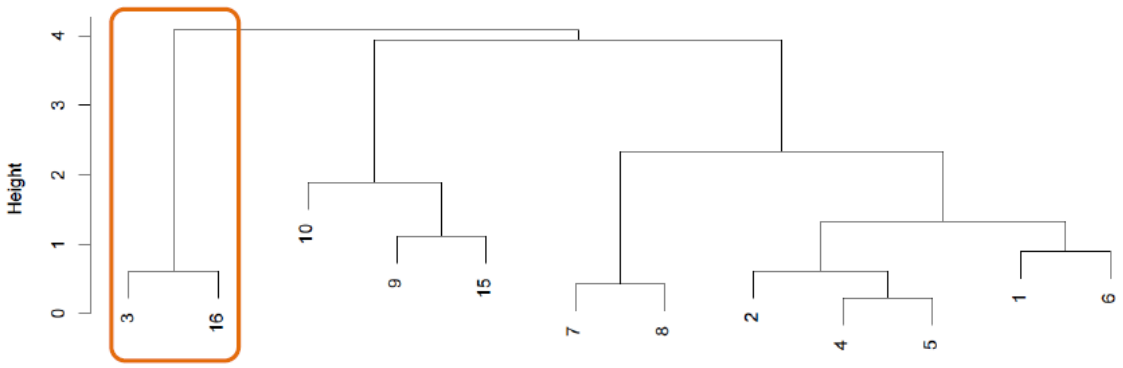

Figure 29: Dendrogram of hierarchical cluster analysis when change in adjustment factor for CYP3A4 clearance and change in inhibition coefficient for OATPs were used as features.

Hierarchical cluster analysis (HCA), a data mining technique in statistics (also one of the techniques used in machine learning), was conducted using the estimated adjustment factors for CYP3A4 activity pre- and post-HD and the estimated adjustment factors for OATP activity pre- and post-HD as features[13] (features are essentially used in HCA). The numbers shown at the bottom of the dendrogram are patient IDs that correspond to the patient IDs in Figure 23. ID = 3 and 16 in the orange square make a distinct cluster group that are marked in Figure 23. As discussed in Section 4.5 the purpose of this HCA analysis is to just suggest a new approach and its feasibility, and this HCA should be treated as exploratory analysis. In Figure 23, it does not look to be feasible to visually identify which patients may differ from the others within the same ESRD cohort. However, this HCA showed the potential to identify unique patients since the above two patients in a cluster showed a greater decrease in adjustment factor for CYP3A4 activity from the rest of patients as shown in Figure 30.

[13]Various combinations of estimated adjustment factors were explored as features in HCA analyses. Figure 29 provided the best average silhouette width value [215], which indicates that using adjustment factors for CYP3A4 activity pre- and post-HD and adjustment factors for OATP activity pre- and post-HD makes best clustering of the samples.

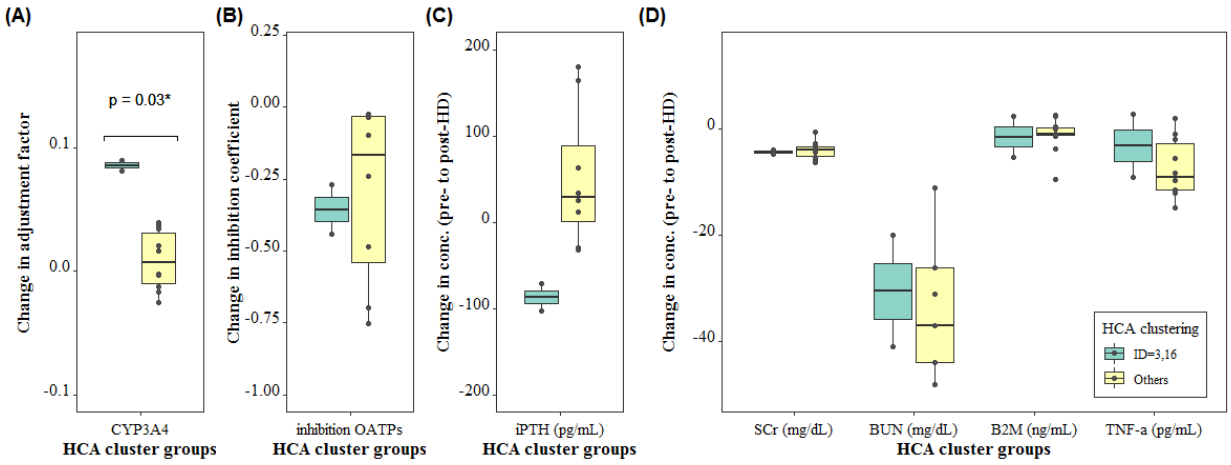

Figure 30: Box plots of change in scaling factors are compared by between a sub-group of ID = 3 and 16 versus others based on the hierarchical clustering analysis (Figure 29)).

The changes scaling factors are for CYP3A4 and OATPs. Exact p-values are shown and $\star$ indicates a statistically significant difference at a significance level of 0.05.

4.5 Discussion

We present an application of iPBPK-R to EBT data in patients with ESRD to evaluate the effect of chronic intermittent hemodialysis on nonrenal clearance pathways. Alterations in erythromycin disposition were mechanistically evaluated within individual patients. Two sets of $^{14}CO_2$ production rate data (pre- and post-HD) were simultaneously modeled and a total of 16 scaling factors (adjustment factors and inhibition coefficients) were estimated per patient via the nested co-optimization.

Similar to the study in healthy subjects, the $^{14}CO_2$ production rate-time curves of 12 patients had three phases. However, the slopes of the curves differed pre- and post-HD and the curves varied among patients (Figure 23). In the goodness-of-fit plots (Figure 24), the simulated and observed $^{14}CO_2$ production rates are on or close to the diagonal line across the 12 patients pre- and post-dialysis. There are data points slightly off from the diagonal line in the patients of ID = 5, ID = 6, and ID = 15. These may be caused by the actual sample collection times that deviated from the planned sample collection times since the breath samples were intensively collected within the two hours. However, considering that the general decision criterion for acceptable PBPK model simulation as high as 2-fold of the observed C_{max} and AUC [76, 90, 93, 101, 102] as discussed in Section 3.5, the iPBPK-R model fitting performed well pre- and post-HD. The parameter estimates of hepatic CYP3A4 and uptake transport activities were consistent with those in healthy subjects [105]. Thus, CYP3A4 activity was estimated to be lower than the IVIVE-based CYP3A4 activity in all patients. An increase in CYP3A4 activity from pre- to post-HD of just 2.2% on average was observed. Although the 2.2% increase in post-HD CYP3A4 activity is numerically small, it represents a change in rate and quite possibly could have enough of an effect to increase the 20-minute $^{14}CO_2$ flux of EBT after hemodialysis because the value affects an exponential term of the solution of the model. Whether or not a 2.2% increase in post-HD CYP3A4 activity is clinically significant is unclear. The effect of hemodialysis on *in vivo* CYP3A4 activity has not been estimated in *individual* patients while accounting for system- and drug-specific parameters and their dependency using the phenotypic probe erythromycin to date. Establishing a threshold for changes in activity of CYP3A4 (as well as other nonrenal clear-

ance pathways) for clinical applications will require extensive research within the context of individual drugs, i.e., accounting for pharmacologic and pharmacotherapeutic considerations such as a drug's therapeutic window. However, it is clear that a small change in CYP3A4 activity estimated by iPBPK-R is impactful enough to alter the shape of the $^{14}CO_2$ production rate-time curves after controlling for other dependent parameters. This was shown in the part of our previous sensitivity analysis in healthy subjects [105], in Figure 20(A) where a small %change in adjustment factor[14] alters the $^{14}CO_2$ production rate-time curve dramatically, and was reproduced in the present study. Note that depending on observed data, it is possible to see a case where a dynamic change in $^{14}CO_2$ production rate-time curve is observed while zero %change is estimated for the adjustment factor for CYP3A4 activity from pre- to post-hemodialysis because the effects of other dependent adjustment factors affect the $^{14}CO_2$ production rate-time curve. To understand the clinical meaning of specific adjustment factors in the system built in iPBPK-R, more observed data is necessary to evaluate their relationships with clinical outcome, biomarkers, ideally in different patient cohorts (e.g., if it's kidney disease, patients in different stages including the end-stage on- and off-hemodialysis). Because of this reason, again, establishing a clinical meaningful threshold for adjustment factors requires formally designed clinical research/program as discussed above, potentially in a collaborative manner.

The results of our iPBPK-R analysis suggest that OATP activity (meta-uptake transporter) did not increase from pre- to post-HD (Figure 26 (C)). Uptake transporter activity pre- and post-HD was variable ranging from 10% to 110% of the IVIVE value. We and others have previously shown that transporter function, likely hepatic OATP uptake, is decreased in patients with kidney disease, including patients with ESRD receiving hemodialysis [30, 92, 93, 209, 210, 216]. While OATP activity recovers after kidney transplantation and restoration of kidney function [216], the effect of intermittent hemodialysis on OATP function has not been assessed previously. Although the originally published data that we employed in the present work showed an increase in 20-minute $^{14}CO_2$ flux post-HD, the effect of hemodialysis on OATP activity was not interpreted and unclear as erythromycin was as-

[14]The adjustment factor for CYP3A4 activity in Figure 20(A) is treated as an independent parameter, so its clinical role in multiple functionally dependent adjustment factors need to be evaluated in a well-designed prospective clinical study.

sumed to be a phenotypic probe for CYP3A4 [128]. Tan et al. reported that OATP activity decreases with declining kidney function [92, 93]. However, OATP activity between patients with ESRD during off-dialysis periods versus patients on-dialysis periods was inconclusive. Even if a small improvement in OATP activity is elicited by hemodialysis it is likely to be difficult to detect due to the high interindividual variability in uptake transport observed in the patients with ESRD across hemodialysis. This estimated variability may also explain visually observed heterogeneity in the $^{14}CO_2$ production rate-time curve among 12 patients pre- and post-HD (Figure 23). The 20-minute $^{14}CO_2$ flux of the observed data showed CV values of 34% and 35% pre- and post-HD, respectively [127], which is viewed as a result of projection of a trajectory in a high dimensional space (as a solution of a system of nonlinear ODEs) to one plane in iPBPK-R as detailed in Chapter 2. iPBPK-R allowed us to differentiate the multiple functionally dependent adjustment factors and to estimate them, including the adjustment factor for OATP activity that showed a large variability. This estimated large variability aligns with the meta-analysis literature [68] as discussed in Section 3.5, and thus it presents the soundness of the iPBPK-R method. Our findings regarding the effect of hemodialysis on OATP activity are exploratory and they should be confirmed in future well-planned, independent clinical studies.

We observed sex-differences in CYP3A4 activity pre- and post-HD (Figure 28). Higher CYP3A4 activity in females was also observed in the EBT study of healthy subjects in Chapter 3 [105]. This is also supported by a study of human liver bank samples where expression levels of CYP3A4 were higher in females than in males [173]. On the other hand, a correlation between CYP3A4 activity and age was observed in all patients pre- and post-HD. An age-dependent change in CYP3A4 activity cannot be excluded as a confounder even though it was excluded in our previous study [105].

The co-optimized adjustment factor for hepatocyte volume was largely variable across patients and it was higher in females than males on average (Table 20). This result is intuitively contrary from what we expected relative to sex. A possible explanation for this sex-difference is that iPBPK-R uses a reduced order model and thus simulates for total hepatocyte volume. Accordingly, instead of modeling the detailed sex-difference in total hepatocyte volume, the adjustment factor for hepatocyte volume may have reflected the

sex-difference in the composition of hepatocyte such as proteasomes and lipids [217, 218]. However, the exact reason is unclear.

Generally, if patients experience an improved uremic state and an increased activity of OATPs or CYP3A4, a negative correlation will be observed between uremic solutes and clearance activities. BUN was not statistically correlated with any of the nonrenal elimination pathways in our patient cohort. This result differed from the study in healthy subjects in Chapter 3 [105] where BUN was inversely correlated with nonrenal elimination parameters. Since BUN was well dialyzed in *all* patients (Figure 30(D)), it may not have an ability to differentiate changes in nonrenal elimination pathways that were highly inter-variable in the patient cohort. Thus, BUN may not serve as a candidate biomarker for evaluating the nonrenal drug disposition in the patient population of ESRD. The observed relationships between TNF-α and total passive diffusion of ^{14}C-erythromycin between the extracellular space and hepatocyte varied pre-HD, post-HD, and from pre- to post-HD, showing inverse correlation, no correlation, and positive correlation, respectively (Table 21). Whether TNF-α has an impact on ^{14}C-erythromycin passive diffusion has not been reported previously.

The exploratory HCA identified two patients who showed improved CYP3A4 activity. The observed decrease of iPTH in two patients was well separated from the other patients (with no statistical power). PTH is known to decrease CYP3A activity in rats [219, 220]. While a direct relationship between PTH and CYP3A4 has not been evaluated clinically, Michaud et al. showed that uremic pre-HD serum obtained from patients with ESRD decreased CYP3A4 activity compared to serum obtained from healthy subjects in a rat liver microsome stability assay [205]. Post-HD serum of the same patients improved the CYP3A4 activity compared to the pre-HD serum (but not to the level of CYP3A4 activity shown with the serum from the healthy subjects) . Separately, it is known that elevated PTH can occur as hyperparathyroidism in patients with renal insufficiency [221], and it has also been shown that dialysis removes serum iPTH in patients with ESRD [207, 208]. These together might indicate that it is important to explore the patient population in ESRD in greater depth, which may solicit unique biomarker-based responders within the heterogeneous population. The purpose of this HCA analysis is to just suggest a new approach and its feasibility, i.e., using iPBPK-R-based parameter estimates in a subsequent exploratory analysis of uremic

toxins (as an example) in the context of hypothesis-generating research. When combined with HCA analysis, iPBPK-R may have the potential to become a tool that can inform which uremic toxin(s) to explore as well as which patients may respond to an intervention. Our approach can be viewed as an illustration of a first step of biomarker reserach and this could eventually support biomarker-based precision medicine approaches in patients with kidney disease in a well-designed large clinical study.

This study has several limitations: (1) Due to the nature of the reduced order model, multiple uptake OATP transporters were modeled as a meta-transporter. (2) ^{14}C-erythromycin and erythromycin were not differentiated in IVIVE calculations. The two compounds are often used indistinguishably in clinical research. (3) Genetic variant data of OATPs was not available, which did not allow us to investigate the cause of the observed variability in the OATPs activity. (4) We used population IVIVE values calculated for a 70 kg male. The variability in body size may be partly reflected in the adjustment factor for the total hepatic volume. (5) The fitted iPBPK-R models cannot be validated against the measurements other than the $^{14}CO_2$ production rate data. We showed the excellent model fit via visual inspection and goodness-of-fit plots across all individual patients. Our analysis establishes that the model was not overfit.

4.6 Conclusions

In this chapter, nested co-optimized iPBPK-R models allowed us to simultaneously estimate the effect of hemodialysis on the multiple non-renal elimination pathways of ^{14}C-erythromycin in individual patients with ESRD. iPBPK-R results indicate that CYP3A4 activity increased by 2.2% post-HD. Although OATP activity did not increase post-HD, it exhibited high interindividuality, which likely contributes to the heterogeneity in the$^{14}CO_2$ production rate-time curves among patients. To our knowledge, this is the first study to apply iPBPK-R to quantify and simultaneously characterize the effect of hemodialysis on nonrenal elimination pathways in patients with ESRD while accounting for system- and drug-specific parameters and their dependency using a single phenotypic probe. Although it

is exploratory, other findings included that females had higher CYP3A activity than males pre- and post-HD. Hierarchical cluster analysis with iPBPK-R may provide mechanistic insights as two patients were identified to show a greater decrease in iPTH and a greater increase in CYP3A4 activity compared to the other patients after hemodialysis. iPBPK-R can be applied to multiple sets of rate data from repeated administrations of a single probe in order to evaluate alteration in drug disposition in individual patients.

5.0 Simultaneous Assessment of the Effect of Rifampin on Hepatic Transport and Metabolism Pathways using iPBPK-R Modeling of Temsirolimus and its Metabolite Sirolimus

5.1 Abstract

Temsirolimus, used to treat renal cell carcinoma by intravenous dosing, is a nonrenally cleared drug with overlapping substrate specificity for enzymes and transporter. We evaluated the ability of our iPBPK-R to distinguish and simultaneously estimate the contributions of nonrenal elimination pathways mediated by CYP3A4 and P-gp to the disposition of temsirolimus and its metabolite sirolimus within healthy individuals. We also estimated the effect of co-administered rifampin on the elimination pathways. A reduced order PBPK model was built for temsirolimus and sirolimus. Linear CYP3A4 clearance and nonlinear P-gp clearance with a Michaelis-Menten term were included in hepatocyte-related equations. Thirteen PBPK parameters were selected for nested co-optimization on the Bridges supercomputer based on sensitivity analysis using four time series of blood concentrations of a DDI study with rifampin. Scaling factors (induction/inhibition coefficients) for CYP3A4 and P-gp activity were estimated to evaluate the effect of rifampin. iPBPK-R simultaneously captured the time-dependent behavior of concentrations of temsirolimus and sirolimus in 15 healthy subjects. The estimated scaling factors[1] indicated that rifampin did not affect the CYP3A4-mediated pathway of temsirolimus but increased CYP3A4 clearance of sirolimus by 73%[2]. P-gp transport of temsirolimus and sirolimus was not altered by rifampin. The application of iPBPK-R to the four sets of drug concentration data enables us to differentially quantify the extent and changes of P-gp versus CYP3A4-mediated elimination pathways of temsirolimus and sirolimus in a DDI study with rifampin in healthy individuals.

[1]These iPBPK-R's scaling factors were included to measure the effect of rifampin on CYP3A4 and P-gp clearances in the system of nonlinear ODEs for temsirolimus and sirolimus. In our model, esterase activity was assumed to be constant during the study (see Section 5.3.5).

[2]The scaling factors were designed to indicate a decrease if its estimated value is less than 1; an increase if the estimated value is greater than 1. See Section 5.3.6.

5.2 Introduction

Temsirolimus formulated for intravenous infusion was approved by the FDA in 2007, and it is a first-in-class mammalian target of rapamycin (mTOR) inhibitor for treating advanced renal cell carcinoma [222, 223]. Inhibiting mTOR, a kinase enzyme which plays a central role to control cell growth, proliferation, metabolism and angiogenesis, confers an anti-cancer effect [224, 225]. Temsirolimus undergoes hepatic elimination via multiple pathways [226], mainly CYP3A4 and efflux drug transporter P-gp [227]. Its major metabolite sirolimus (known as rapamycin) is also pharmacological active [227,228]. The conversion from temsirolimus to sirolimus is mediated by esterase, which is a different metabolism pathway from CYP-dependent pathways [229–232]. Sirolimus itself is used as an immunosuppressant and it is suggested to be a dual substrate of CYP3A4 and P-gp *in vitro*[3] [228,233]. However, the extent of their contributions or interplay in the non-renal clearance of each compound is unclear [234–237]. Both temsirolimus and sirolimus in the class of mTOR inhibitors have shown large interindividual variability in drug concentration profiles, which is essential to be accounted for in drug dosing [236,238,239]. The concern of interindividual variability and the overlapping dual substrate specificity of the parent drug and its metabolite provide a unique opportunity to evaluate the contributions of nonrenal elimination pathways in individuals. We apply iPBPK-R to the drug concentration data of temsirolimus and sirolimus to extract physiological parameter information and specifically evaluate hepatic enzyme and transporter activities.

Estimating multiple contributions of drug elimination pathways in the liver is challenging as we cannot directly access information to measure *in vivo* activities. We previously developed and applied iPBPK-R to two cohort datasets of EBT to simultaneously estimate parameters of non-renal elimination activities, including uptake drug transporter OATPs and CYP3A4 enzyme [105, 106]. The iPBPK-R method utilizes *production rate* or the first derivative measurement of drug concentration data since such data are more sensitive to underlying physiological parameters than drug concentration data [105, 134, 152]. In this study

[3]Temsirolimus is intravenously administered due to poor bioavailability [227], and data on bioavailability and intestinal uptake of temsirolimus are not publicly available.

we extend the application of iPBPK-R to *multiple coupled drug concentration datasets* per individual instead of production rate data. The dataset of intravenously administered temsirolimus and its metabolite sirolimus concentration measurements together provide the rate information in the model fit with the system of nonlinear ODEs so that multiple parameters for non-renal elimination activities can be simultaneously estimated. In the application of iPBPK-R, the overlapping substrate specificity is currently a necessary property.

Classical population PK modeling of temsirolimus and sirolimus was shown by Boni et al. using the original PK DDI study of temsirolimus with the concomitant drug rifampin in healthy subjects [240]. Based on the PK analysis of IV temsirolimus and its metabolite sirolimus, rifampin did not change the mean AUC, C_{max}, or $t_{1/2}$ of IV temsirolimus but decreased the mean AUC by 56%, C_{max} by 65%, and $t_{1/2}$ by 20% of sirolimus. In addition, they also analyzed PK profiles of PO temsirolimus which differed with and without rifampin. Rifampin is as well-known *in vivo* inducer of CYP3A4 and typically used in clinical DDI studies [241]. For example, rifampin dramatically decrease PK profile of the sensitive CYP3A4 index substrate midazolam in a healthy cohort [241–243]. Rifampin also serves as an inducer for CYP2C19, CYP1A2, CYP2B6, CYP2C8, and CYP2C9. Furthermore, P-gp activity is also reported to be affected by rifampin [244]. As rifampin generally increases the hepatic and intestinal CYP3A4 activity, Boni et al. concluded that rifampin induces the hepatic metabolism of sirolimus but not the hepatic metabolism of IV temsirolimus. In their population PK modeling, only CYP3A4 activity was evaluated without accounting for other nonrenal elimination pathways. In fact, it is not possible to specifically estimate *in vivo* CYP3A4 activity and account for multiple nonrenal elimination pathways by using population PK modeling applied to just one type of DDI data (i.e., PK study data of IV temsirolimus alone and IV temsirolimus plus rifampin).

In this chapter, our goal is to simultaneously estimate multiple parameters of the nonrenal elimination activities and demonstrate its feasibility to facilitate the use of iPBPK-R. By introducing induction and inhibition coefficients as part of scaling factors in iPBPK-R we evaluated the effect of co-administered rifampin on the nonrenal elimination pathway activities in healthy individuals. Here, we emphasize that our aim is to conduct multiple parameter estimation given observed data but not prediction of drug concentration-time

profiles. The aims of this work were (1) to differentially estimate contributions of nonrenal clearance pathways to temsirolimus and sirolimus in healthy subjects, and (2) to investigate the effect of rifampin on these pathways.

5.3 Method

5.3.1 Clinical Data Sources

The whole-blood concentration data of temsirolimus and its metabolite sirolimus were obtained from clinical literature [240]. Briefly, the study of the observed data was an open-label sequential study where the effect of multiple oral doses of the potent CYP3A4 inducer rifampin on the PK profile of a single 25-mg IV dose was evaluated in healthy adults. The study included two dosing periods; temsirolimus alone (Period 1), followed by temsirolimus with concomitant rifampin (Period 2). Temsirolimus 25mg was administered as a single 30-minute IV infusion in both periods. Whole blood concentrations of temsirolimus and sirolimus were serially measured at 13 timepoints (at 0 (as predose), and 0.5, 1, 2, 3, 8, 24, 48, 72, 96, 120, 144, and 168 hours) over 7 days in period 1 and repeated in period 2. All subjects were to receive daily oral doses (2×300mg capsules) of rifampin from Days 15 to 27. Period 2 began on Day 21 with repeat dosing of temsirolimus 25mg IV. All of the 16 enrolled subjects were male, and 14 subjects were Caucasian. In iPBPK-R modeling, 15 individual data were used since one withdrew and did not provide the data in the second period[4]. In addition, in order to present the actual observed data and to illustrate the goodness-of-fit of the iPBPK-R method in Figure 33, mean concentration data of temsirolimus and sirolimus were digitized from the literature [240] using GetData Digitizer (version 2, www.getdata-graph-digitizer.com) and they were plotted. Thus, these mean datasets were treated as individual observed data solely for presenting visual performance of iPBPK-R to supplement the limitation of the data confidentiality of the original individual data and not for evaluating

[4]We do not describe the individual data further as this work was conducted during the FDA ORISE fellowship which is subject to the FDA data confidentiality under the Code of Federal Regulations Title 21 Part 20 [245].

the parameter estimates in iPBPK-R.

5.3.2 PBPK Model Structure

A PBPK model consisting of seven organ/tissue compartments and sub-compartments (①-⑦ in Figure 31) was built with a set of physiological and kinetic parameters (i.e., PBPK parameters) for temsirolimus and sirolimus, respectively. The compartments included were artery (Art), vein, lung (LG), liver (LV), kidney (KD), and combined other organs (OT). The liver compartment consisted of extracellular space (ES) and liver cell (LC) sub-compartments. For each compound, *total passive diffusion* was included to model the drug transfer between ES and LC. Furthermore, linear CYP3A4 clearance and esterase (EST) clearance, and non-linear efflux transporter (P-gp) with maximum velocity and Michaelis-Menten constante were modeled in LC. In LC, temsirolimus gets converted to sirolimus by EST [229–232] and thus the two sets of models, one for temsirolimus and one for sirolimus, are linked through the esterification of temsirolimus. Lastly, we also included a non-CYP3A4-dependent metabolism pathway for the sirolimus model based on the literature [246] where the metabolites formed by CYP3A4/3A5 approximately represented 10% of the total intrinsic clearance observed in *in vitro* experiments using human liver microsomes. Assuming that abundance of CYP3A5 is very small and negligible in the liver [246, 247], this non-CYP3A4-dependent intrinsic clearance was denoted as $CL_{NONCYP3A4(m)}$. $CL_{NONCYP3A4(m)}$ was assumed to be independent of esterase since temsirolimus is an ester analog of sirolimus [248].

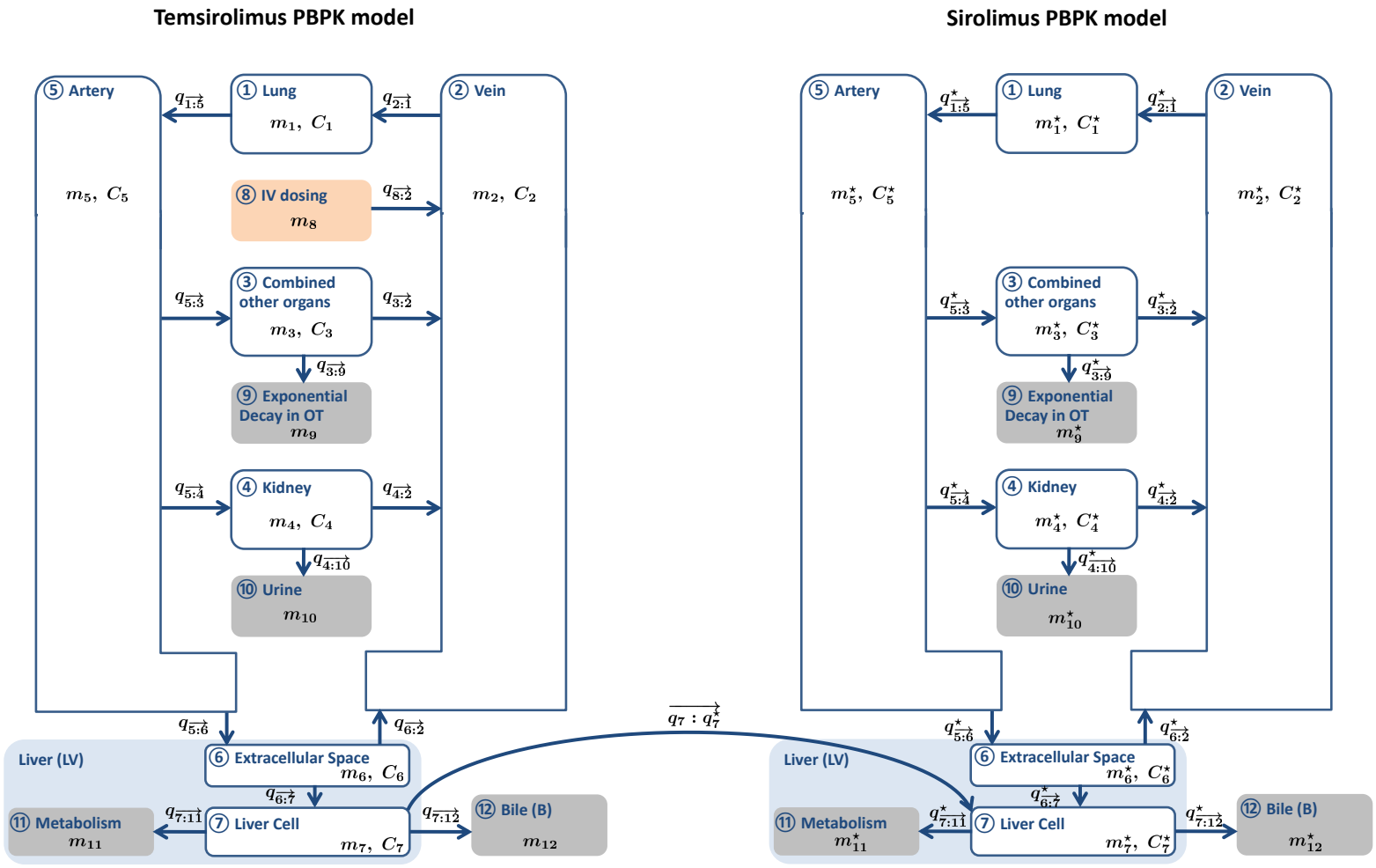

Figure 31: PBPK model structures of temsirolimus and sirolimus in iPBPK-R.

$q_{\overrightarrow{W:Z}}$ denotes a mass flow from W compartment to Z compartment and it is represented by an arrow. Similar to the mass balance in the iPBPK-R application to EBT data (Appendix B.2), the mass balance is retained in the whole system.

5.3.3 Ordinary Differential Equations, Kinetic Parameters, and Data Input

A set of ODEs describes drug concentration dynamics of all compartments for temsirolimus and sirolimus, respectively. In iPBPK-R, vein and artery compartments were separately modeled as our previous publication [105]. Permeability-limited liver models were used in the ODEs associated with ES and LC [101]. Based on the drug mass flows shown in Figure 31 and following the similar procedure discussed in Chapter 3 (see Appendix B), the set of ODEs was constructed as in Appendix C. Tables 26 and 27 provide PBPK parameters for temsirolimus and sirolimus, respectively, some of which were calculated using IVIVE equations. Note that the calculated IVIVE values of nonrenal elimination pathways for temsirolimus are not shown in Table 26 due to the FDA data confidentiality under the Code of Federal Regulations Title 21 Part 20 [245] similar to Section 5.3.1. Accordingly, initial % contributions of these nonrenal elimination pathways cannot be shown. Derivation of IVIVE equations for P-gp clearance and passive diffusion for sirolimus are described as an example in Appendix D. These parameters were used as input values in the estimation of scaling factors, which is described later.

5.3.4 Coupled Concentration Data and Reduced Order Model

The first derivative of concentration data or production rate data are mathematically higher *information content* (i.e., it enables higher accuracy of estimated model parameters) compared to equivalently sampled concentration data [105, 134, 152]. iPBPK-R was developed based on this concept and previously applied to breath sample data [105]. In this chapter, we extend iPBPK-R application to multiple coupled drug concentration datasets (i.e., temsirolimus and sirolimus blood concentration data) per individual since such coupled multiple datasets are mathematically high information content via the system of ODEs. The iPBPK-R model was simultaneously fit to the temsirolimus and sirolimus concentration-time data of Period 1 and Period 2 (in the absence and presence of rifampin in the system, respectively) via a nested co-optimization procedure. Multiple nonrenal elimination pathways, i.e., enzymatic metabolism, efflux transport, and total passive diffusion parameters were estimated via scaling factors relative to IVIVE using the single IV dose of temsirolimus. The

types of scaling factors used were: (1) co-optimized adjustment factors, (2) independent adjustment factors, and (3) scaling coefficients (induction or inhibition coefficients). To achieve high precision in the iPBPK-R model fit, we used a reduced order model [198]. Reduced order models are complex enough to capture the behavior of interest but manageable to be well-posed, providing estimable parameters. For this mathematical reason, the total number of compartments and sub-compartments was limited to seven in the same fashion of our previous application [105].

5.3.5 Model Assumptions

Adopting the concept of reduced order model enabled us to present a goodness-of-fit in iPBPK-R modeling of temsirolimus and sirolimus and to implement high-dimensional co-parameter estimation. We performed the iPBPK-R modeling under the assumption listed in Table 22.

5.3.6 Simulations and Optimizations

Concentration-time curves of temsirolilmus and sirolimus were simulated for individual patients using the system of ODEs. The ODEs are shown in Appendix D (See Subsection 5.3.3 for the construction of ODEs).

Prior to conducting the high-dimensional parameter optimization for healthy subjects, the impactful and/or biologically relevant parameters to shape the concentration-time curves were identified using manual sensitivity analysis. The identified parameters we detail in outer and inner loops below were found to be essential for fitting the model to the four series of blood concentration data simultaneously.

iPBPK-R uses a nested co-optimization procedure, which consists of the inner loop and outer loop to optimize PBPK parameters (Figure 32). In the *outer loop*, thirteen scaling factors for the following PBPK parameters were optimized[5]: for the temsirolimus

[5]The number of observed samples per individual in this simultaneous PBPK model fit is 13 time points $\times$ 4 datasets (for parent and metabolite drugs in Period 1 and 2) = 52 data points. Therefore, the number of functionally dependent parameters to optimize here (i.e., 13 outer loop parameters) is sound since the same argument in the analysis of iPBPK-R estimation using regularization in Section 2.4.7 applies.

Table 22: List of assumptions used in iPBPK-R of temsirolimus and sirolimus for healthy subjects

Number	Assumption
1	The duration of intravenous dosing of temsirolimus was 30 minutes.
2	The iPBPK-R model is well-stirred [183, 199]. All compartments except for the liver compartment are perfusion-limited.
3	Pathways from the extracellular space to the liver cells (ES $\rightarrow$ LC sub-compartment)) for temsirolimus and sirolimus are total passive diffusion.
4	In the LC sub-compartment, there are CYP3A4 and esterase-mediated metabolism pathways for temsirolimus. Esterification (hydrolysis) of temsirolimus by esterase (EST) produces sirolimus. We assumed linearity for the intrinsic clearance of CYP3A4 and esterase.
5	Sirolimus is metabolized by CYP3A4 [246] In addition, other metabolites of sirolimus are reported in literature [229, 232, 249, 250]. These enzyme-mediated pathway(s) were modeled as a meta linear non-CYP3A4 metabolism (i.e., non-CYP3A4 clearance for sirolimus in the LC sub-compartment).
6	Both temsirolilmus and sirolimus are substrates of efflux drug transporter P-gp. In the apical side of LC sub-compartment, these drug transport processes are modeled to be non-linear elimination processes. We assumed that relative activity factor (RAF) in the IVIVE-based intrinsic clearance of P-gp is commonly shared between temsirolimus and sirolimus at the beginning of study.
7	Rifampin does not affect EST activity on temsirolimus.
8	As described in 3 to 6, the liver consisting of ES and LC sub-compartments is an elimination organ. In addition, parameters μ and $\mu_{(\mathrm{m})}$ were incorporated in the OT compartment to explain the exponential decay of temsirolimus and sirolimus, respectively. We expected that μ and $\mu_{(\mathrm{m})}$ would improve the co-model fitting of four series of datasets per individual. The exponential decay was assumed to account for any loss or decomposition of the drug before the drug reaches the liver within the system.
9	The unbound drug was subject to efflux transport, enzymatic metabolism, and elimination in the liver.

model, CYP3A4 clearance (CL_{CYP3A4}), esterase clearance (CL_{EST}), and partition coefficient of the combined other organs to plasma ($P_{OT:P}$); for the sirolimus model, CYP3A4 clearance ($CL_{CYP3A4(m)}$), non-CYP3A4-dependent clearance ($CL_{NONCYP3A4(m)}$), partition coefficient of the combined other organs to plasma ($P_{OT:P(m)}$), and total passive diffusion between extracellular space and hepatocyte ($Q_{ES-LC(m)}$); for both temsirolimus and sirolimus models, maximum velocity of P-gp (assuming proportional $J_{max,OUT1}$ and $J_{max,OUT1(m)}$), volume of total hepatocyte (V_{LC}), arterial blood flow into the combined other organs ($Q_{Art,OT}$), venous blood flow from the combined other organs ($Q_{Vein,OT}$), volume of vein (V_{Vein}), and volume of the combined other organs (V_{OT}). These parameters were assumed to take a common value between Period 1and Period 2, and thus they were co-optimized across periods within individuals. These scaling factors are called as *co-optimized adjustment factors*. In model fitting, a co-optimized adjustment factor measures the extent of the patient-specific baseline adjustment from the population IVIVE (or an initial input value) through the entire study.

In the *inner loop*, one and seven scaling factors were *independently* optimized in the respective study period: In Period 1, a scaling parameter for relative activity factor for P-gp (RAF), which is a linear component of the IVIVE input [68][6], was optimized, and in Period 2 scaling parameters for maximum velocity of P-gp for temsirolimus and sirolimus ($J_{max,OUT1}$ and $J_{max,OUT1(m)}$) , CL_{CYP3A4}, $CL_{CYP3A4(m)}$, $CL_{NONCYP3A4(m)}$, $P_{OT:P}$, and $P_{OT:P(m)}$ were optimized. The scaling parameter in Period 1 was included to adjust the IVIVE-based intrinsic clearance for P-gp under an assumption that the RAF is commonly shared between temsirolimus and sirolimus. The scaling parameters for P-gp in Period 2 are interpreted as *non-competitive induction or inhibition coefficients* in the presence of rifampin. The scaling coefficients for metabolic enzymes in Period 2 are used to evaluate induction and inhibition of the enzyme activity in the presence of rifampin. If the coefficient value is estimated to be within 0 to 1, then the biological activity is considered to be inhibited. If the coefficient value is estimated to be greater than 1, the activity is considered to be induced. Scaling factors were estimated via nested co-optimization that minimizes the errors of the fitted model of temsirolimus and sirolimus.

[6]RAF is the expression ratio between *in vivo* and *in vitro* hepatocytes, which is one of the commonly used factors appearing in IVIVE equations [68].

The model fit was evaluated using average normalized residuals between predicted and observed rates, visual inspection, and plausibility of the parameter estimates. Among the PBPK parameters in Tables 26 and 27, outer loop and inner loop parameters described above were selected for optimization.

Simulations and parameter co-optimization were implemented with R 3.4.4. The R package *deSolve* was used for solving the set of ODEs, and large-scale simulations were performed via the Bridges supercomputer at the PSC [126]. Methodological details of iPBPK-R are described in Chapter 2.

5.3.7 Statistical Analysis

Mean± SD and/or median (range) were used as descriptive statistics. Box plots were created for visualization of estimation results. No statistical test was powered in advance since the study explored feasibility and estimability. For comparing parameters between Period 1 and Period 2, two-sided paired t-tests were conducted in case of normally distributed measurements. Otherwise, two-sided Wilcoxon signed-rank tests were conducted. In all comparisons a P-value < 0.05 was considered statistically significant. All statistical analyses were conducted using SAS 9.4 (SAS Institute Inc., Cary, NC).

5.4 Results

The iPBPK-R model was simultaneously fit to the four series of observed blood concentration - time data, i.e., concentration data of temsirolimus and sirolimus in the absence of rifampin (Period 1) and in the presence of rifampin (Period 2) in the 15 healthy subjects (Figure 33). Due to the FDA data confidentiality under the Code of Federal Regulations Title 21 Part 20 [245], the individual observed data are not shown (see Section 5.3.1). To assess the goodness-of-fit of iPBPK-R, we calculated means (SDs) of the average normalized residual of all model fits: 36.2% (9.2%) in Period 1 and 31.4% (10.5%) in Period 2 for temsirolimus and 0.9% (0.3%) in Period 1 and 1.1% (0.2%) in Period 2 for sirolimus, all

of which indicated a good model fit. Furthermore, the observed *mean* concentration-time curves of temsirolimus and sirolimus were treated as data for one hypothetical individual, and the observed mean plots and iPBPK-R-based simulated curves are shown in Figure 33. The PK parameters of the observed and simulated curves in the hypothetical individual are compared in Table 23. C_{max}, $t_{1/2}$, and AUC indicated that the simulated curves had an early higher peak than the observed curve for temsirolimus while they indicated that simulated and observed concentration-time curves are well comparable for sirolimus in both study periods.

The nested co-optimization procedure yielded parameter estimates for all patients except for the scaling parameter of RAF for P-gp in two subjects. In these two subjects, the scaling parameter for RAF was resulted in 0 at baseline, suggesting that P-gp activity did not mathematically have an essential role in the model. Accordingly, these subjects were excluded from the analysis on P-gp. Figure 34 provides an example of 3D concentration-time curve simulations in one healthy subject where the nested co-optimization leads to the final model fit to temsirolimus and sirolimus in Period 1 and Period 2, *simultaneously*.

Table 24 shows 13 co-optimized adjustment factors for CL_{CYP3A4}, CL_{EST}, $P_{OT:P}$, $CL_{CYP3A4(m)}$, $CL_{NONCYP3A4(m)}$, $P_{OT:P(m)}$, $Q_{ES-LC(m)}$, $J_{max,OUT1}$, V_{LC}, $Q_{Art,OT}$, $Q_{Vein,OT}$, V_{Vein}, and V_{OT} in the outer loop (Figure 32). The mean co-optimized adjustment factors for P-gp activity on temsirolimus and sirolimus, CYP3A4 activity on temsirolimus, and the hepatocyte volume ($J_{max,OUT1}$, CL_{CYP3A4}, and V_{LC}) were close to 1, respectively, indicating that little adjustment of IVIVE or population input value was needed. The mean co-optimized adjustment factors for the volume of blood and the volume of the combined other organs (V_{Vein}, and V_{OT}) were also closed to 1. The co-optimized adjustment factor for esterase activity on temsirolimus (CL_{EST}) was much higher than 1 (mean ± SD, 13.99 ± 0.05). The co-optimized adjustment factors for CYP3A4 and non-CYP3A4-dependent enzyme activities on sirolimus were estimated to be lower than 1 (0.15 ± 0.05 for $CL_{CYP3A4(m)}$ and 0.03 ± 0.05 for $CL_{NONCYP3A4(m)}$, respectively) while the co-optimized adjustment factor for the passive diffusion of sirolimus between extracellular space and hepatocyte was quite large and inter-individually variable (200.09 ± 0.32 for $Q_{ES-LC(m)}$). In the OT compartment, all co-optimized adjustment factors differed from 1 (0.23 ± 0.05 for $P_{OT:P(m)}$, 0.30 ± 0.06 for

$P_{OT:P(m)}$, 0.19 ± 0.04 for $Q_{Art,OT}$, and 0.23 ± 0.04 for $Q_{Vein,OT}$) (Table 24). These adjustment factors in the OT compartment do not provide biological implication, but they were optimized for the purpose of model fitting similarly to our other iPBPK-R studies [105,106].

In the inner loop, a scaling factor for RAF of P-gp in Period 1 and other scaling coefficients in Period 2 were estimated independently (Table 25 and Figure 32). In Figure 35(A) and Table 25, P-gp activity on both temsirolimus and sirolimus did not alter by rifampin since the scaling factors (induction or inhibition coefficients) were not significantly different from 1 (0.98 ± 0.07, p=0.95 for temsirolimus; 1.05 ± 0.10, p=0.10 for sirolimus). In Figure 35(B) and Table 25, the scaling factor for RAF of P-gp was estimated to be lower than 1 and interindividually variable at Period 1 (0.36 ± 0.31, p<0.0001). In Figure 36 and Table 25, the estimated scaling factors (induction/inhibition coefficients) indicated that rifampin did not change CYP3A4-mediated clearance of temsirolimus (scaling coefficient 0.95 ± 0.17, p=0.72) but significantly increased the CYP3A4 and non-CYP3A4-dependent metabolic activities on sirolimus by 73% and 153%, respectively (1.73 ± 0.52, p<0.0001 for $CL_{CYP3A4(m)}$; 2.53 ± 0.52, p<0.0001 for $CL_{NONCYP3A4(m)}$). The interindividual variability of the induction/inhibition coefficient of CYP3A4 activity was also large for sirolimus. Rifampin altered scaling factors for partition coefficient on temsirolimus and sirolimus in OT (Table 25). These parameters in the combined other organs (i.e., a lumped-up compartment) were selected for independent optimization between study periods to achieve a good model fit. The resulted scaling factors indicate that rifampin altered mass flows of temsirolimus and sirolimus among the non-hepatic compartments.

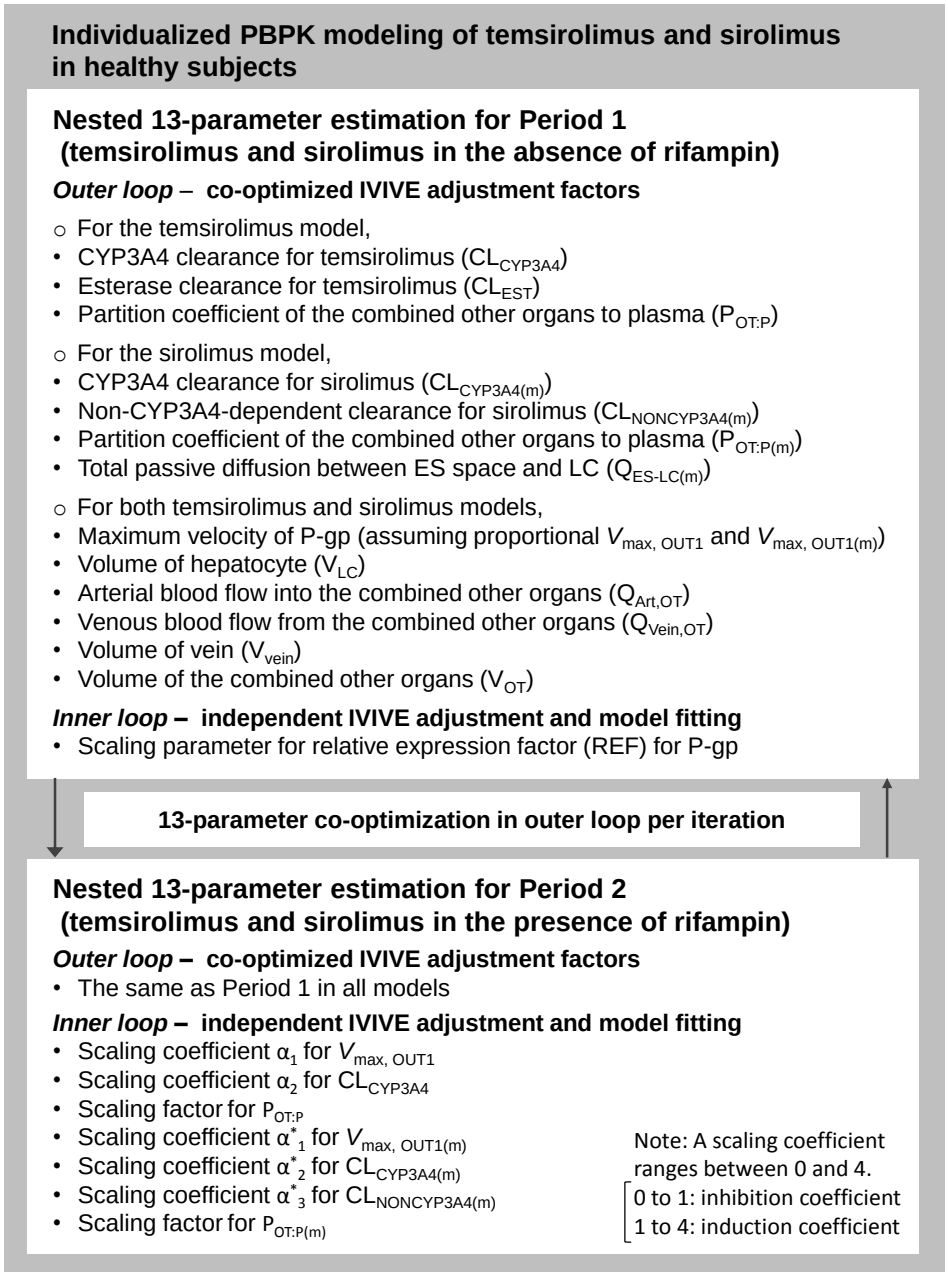

Figure 32: Framework of the application of iPBPK-R to the four time series of blood concentration data of a drug-drug interaction study of temsirolimus with rifampin in 15 healthy individuals.

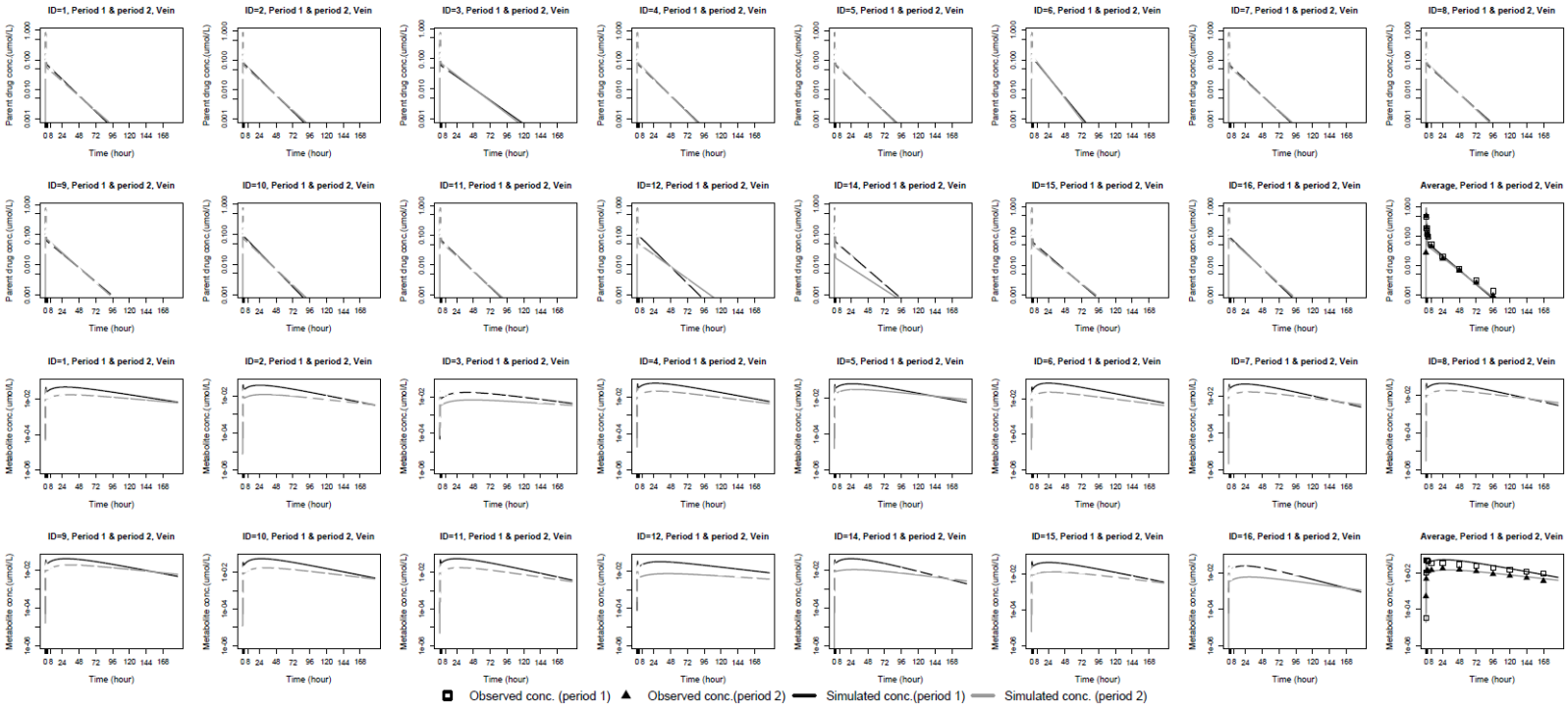

Individual observed plots are not shown due to data confidentiality under the Code of Federal Regulations Title 21 Part 20. Mean observed & simulated plots demonstrate the goodness-of-fit performance of iPBPK-R.

Average normalized residual mean (SD) between simulated and observed data for parent drug (N=15), Study period 1 (no rifampin): 0.362 (0.092); Study period 2 (with rifampin): 0.314 (0.105)
Average normalized residual mean (SD) between simulated and observed data for metabolite (N=15), Study period 1 (no rifampin): 0.009 (0.003); Study period 2 (with rifampin): 0.011 (0.002)

Figure 33: iPBPK-R simultaneous model fitting to the individual concentration data of temsirolimus and sirolimus in the absence and presence of rifampin from the 15 healthy subjects.

The black lines and dashed gray lines are modeled curves in Period 1 (without rifampin) and in Period 2 (with rifampin), respectively. We also showed the simulated curves and observed plots of the mean concentration data treated as a hypothetical

individual to show the goodness-of-fit of iPBPK-R. Mean observed data are shown with open squares for Period 1 and black triangles for Period 2. Individual observed plots are not shown due to data confidentiality under the Code of Federal Regulation Title 21 Part 20 [245].

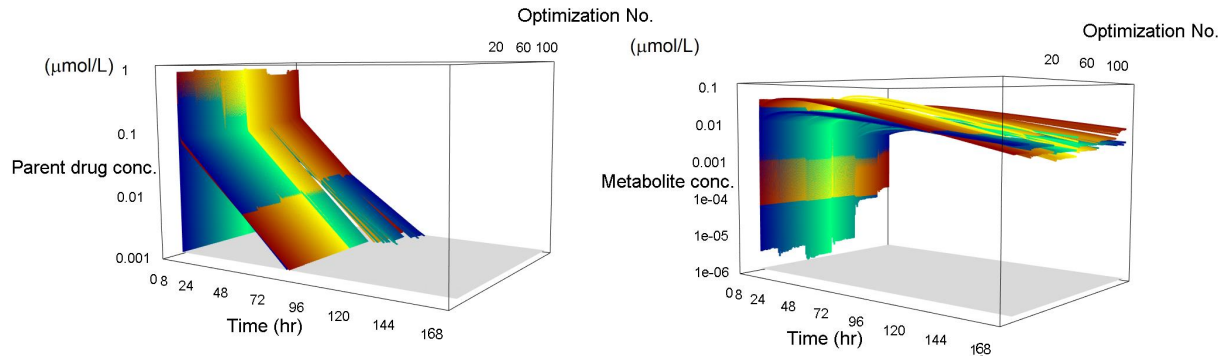

Figure 34: An example of 3D blood concentration-time curve simulations for temsirolimus and sirolimus in one healthy individual.

The nested co-optimization simultaneously leads to the final model fit in Period 1 and Period 2. The 3D curves for temsirolimus are shown in the left panel and 3D curves for sirolimus are shown in the right panel. The curves in the red–yellow–red color transition are the simulated curves in the absence of rifampin (Period 1) and the curves in the blue–green–blue color transition are the simulated curves in the presence of rifampin (Period 2) during the nested parameter co-optimization (high-dimensional parameter estimation). Both curves were simultaneously fit to the subject's observed data at the end of the optimization process.

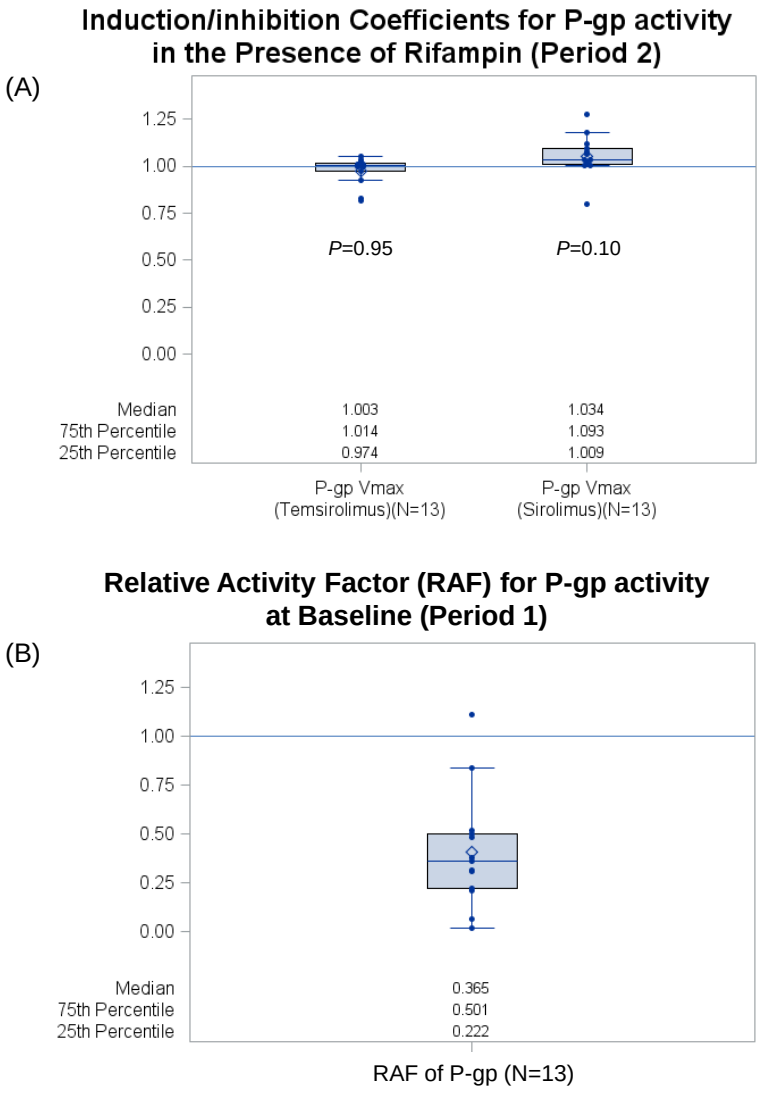

Figure 35: Box plots of estimated scaling factors.

(A) Estimated scaling factors (induction/inhibition coefficients) for P-gp activity on temsirolimus and sirolimus in the presence of rifampin (Period 2) compared to the baseline without rifampin (Period 1) in the liver. (B) Estimated scaling factor for relative activity factor (RAF)[7] of P-gp at baseline. The limitation regarding P-gp polymorphism is discussed in Section 5.5.

[7]See Section 5.3.6.

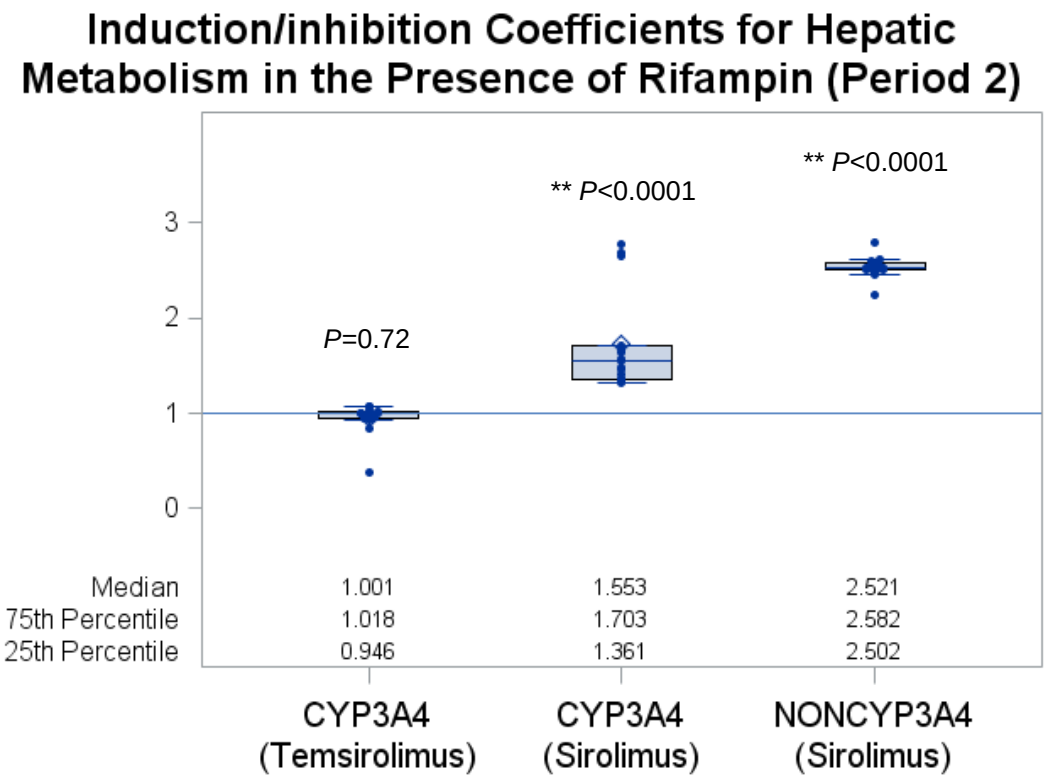

Figure 36: Box plots of estimated induction/inhibition coefficients for CYP3A4 activity on temsirolimus, CYP3A4 activity on sirolimus, and non-CYP3A4 activity on sirolimus in the presence of rifampin (Period 2) compared to the baseline without rifampin (Period 1) in the liver.

** indicates a statistically significant difference from 1 at a significance level of 0.01. N = 15 in all box plots.

Table 23: Pharmacokinetic parameters of the observed and iPBPK-R-based simulated data of the hypothetical healthy individual

PK parameters	Temsirolimus Observed data[a]	Simulated data[b]	Ratio[d]	Sirolimus Observed data[a]	Simulated data[b]	Ratio[d]
Without rifampin						
C_{max}(ng/mL)	512	954	1.86	50.6	52.8	1.04
t_{max}(hr)	0.53	0.5		NA[c]		
$t_{1/2}$(hr)	23.0	13.1		69.4	38.3	
AUC (ng·h/mL)	2056	1907	0.93	4564	4911	1.08
With rifampin						
C_{max}(ng/mL)	532	951	1.79	17.7	26.7	1.51
t_{max}(hr)	0.47	0.5		NA[c]		
$t_{1/2}$(hr)	22.6	14.3		55.1	63.4	
AUC (ng·h/mL)	1879	1715	0.91	2004	1940	0.97

[a]The PK parameter values were obtained from literature [240]. [b]The PK parameters of simulated iPBPK-R data were calculated using a standard noncompartmental method in Phoenix WinNonlin 8.2. [c]Not available in the literature. [d]Ratio (relative difference) of *simulated* to *observed* PK parameters.

Table 24: Co-optimized parameter estimates via the nested co-optimization in the iPBPK-R modeling of temsirolimus and sirolimus in 15 healthy subjects across two study periods

Co-optimized parameter	Drug modeled with the optimized parameter	Mean ± SD	Median (Range)
IVIVE or input adjustment for:			
CYP3A4 clearance[a]	Temsirolimus	1.01 ± 0.02	1.01 (0.97, 1.04)
Esterase clearance[a]	Temsirolimus	13.99 ± 0.05	13.99 (13.90,14.15)
Partition coefficient in the combined other organs	Temsirolimus	0.23 ± 0.05	0.25 (0.12, 0.31)
CYP3A4 clearance[a]	Sirolimus	0.15 ± 0.05	0.14 (0.08, 0.31)
Non-CYP3A4-dependent clearance[a]	Sirolimus	0.03 ± 0.04	0.02 (0.00, 0.15)
Partition coefficient in the combined other organs	Sirolimus	0.30 ± 0.06	0.28 (0.24, 0.42)
Total passive diffusion between ES and LC	Sirolimus	200.09 ± 0.32	200.00 (199.87, 201.23)
P-gp maximum velocity[ab]	Temsirolimus and sirolimus	1.02 ± 0.09	1.00 (0.95, 1.32)
Hepatocyte volume	Temsirolimus and sirolimus	0.98 ± 0.05	1.00 (0.86, 1.02)
Arterial blood flow in the combined other organs	Temsirolimus and sirolimus	0.19 ± 0.04	0.19 (0.09, 0.28)
Venous blood flow from the combined other organs	Temsirolimus and sirolimus	0.23 ± 0.04	0.22 (0.18, 0.30)
Volume of blood compartment	Temsirolimus and sirolimus	1.04 ± 0.04	1.03 (0.95, 1.16)
Volume of the combined other organs	Temsirolimus and sirolimus	1.05 ± 0.15	1.00 (0.93, 1.46)

IVIVE, in-vitro in-vivo extrapolation; CYP3A4, cytochrome P450 3A4; P-gp, P-glycoprotein;

[a]The adjustment factor measures the baseline deviation from IVIVE. [b]The sample size was 13 since P-gp clearance did not mathematically have an essential role as a result of iPBPK-R model fit in two healthy subjects.

Table 25: Independent parameter estimates via the nested co-optimization in the iPBPK-R modeling of temsirolimus and sirolimus in 15 healthy subjects in Period 1 (without rifampin) and Period 2 (without rifampin), respectively

Independently optimized parameter	Drug modeled with the optimized parameter	Mean ± SD	Median (Range)	P-value[c]
Induction/inhibition coefficient[a] in Period 2 for:				
Maximum velocity of nonlinear P-gp clearance[b]	Temsirolimus	0.98 ± 0.07	1.00 (0.82, 1.05)	0.95
CYP3A4 clearance	Temsirolimus	0.95 ± 0.17	1.00 (0.38, 1.08)	0.72
Maximum velocity of nonlinear P-gp clearance[b]	Sirolimus	1.05 ± 0.10	1.03 (0.80, 1.28)	0.10[d]
CYP3A4 clearance	Sirolimus	1.73 ± 0.52	1.55 (1.32, 2.77)	$< 0.0001^{\star\star}$
Non-CYP3A4-dependent clearance	Sirolimus	2.53 ± 0.11	2.52 (2.24, 2.79)	$< 0.0001^{\star\star}$
Scaling factor for:				
Partition coefficient in OT in Period 2	Temsirolimus	1.29 ± 0.70	1.15 (0.84, 3.59)	$0.04^{\star}$
Partition coefficient in OT in Period 2	Sirolimus	2.32 ± 0.05	2.34 (2.20, 2.38)	$< 0.0001^{\star\star}$
RAF for P-gp in Period 1[b]	Temsirolimus and sirolimus	0.36 ± 0.31	0.32 (0.00, 1.11)	$< 0.0001^{d\star\star}$

CYP3A4, cytochrome P450 3A4; P-gp, P-glycoprotein; RAF, relative activity ratio; OT, the combined other organs compartment

[a]An induction/inhibition coefficient value < 1.0 means that the biological activity is inhibited. If the value is > 1.0, the activity is considered to be induced. The value 1.0 was used as a null hypothesis for all statistical testing. [b]The sample size was 13 since P-gp clearance did not mathematically have an essential role as a result of iPBPK-R model fit in two healthy subjects. [c]Wilcoxon signed rank tests were conducted. ; [d]One-sampled t-tests were conducted. * and ** indicate a statistically difference from 1.0 in the presence of rifampin at a significance level of 0.05 and 0.01, respectively.

Table 26: Parameters used for iPBPK-R simulations of temsirolimus for healthy subjects

Description (units)	Notation	Value	Reference/Comments
Intravenous dose of temsirolimus (mg)		25	[240]
Volume of kidney (L)	V_{KD} (= V_4)	0.270	[184]
Volume of lung (L)	V_{LG} (= V_1)	0.775	[184]
Volume of vein (L)	V_{vein} (= V_2)	2.700	[184]
Volume of the combined other organs (L)	V_{OT} (= V_3)	372.67	Calculated [184, 251–254]
Volume of artery (L)	V_{art} (= V_5)	2.700	[184]
Volume of extracellular space in the liver (L)	V_{ES} (= V_6)	0.340	Calculated [101, 184, 185]
Effective volume of Extracellular space in the liver (L)	$V_{ES,eff}$ (= V'_6)	0.4313	Calculated with approximation [101, 255]
Volume of hepatocyte (L)	V_{LC} (= V_7)	1.139	Calculated [101, 184, 185]
Blood flow of kidney (L/hr)	Q_{KD} (= Q_4)	66	[5]
Renal clearance of sirolimus (L/hr)	CL_R	(Period 1) 0.58 (Period 2) 0.65	Calculated based on total clearance [240] and % renally excreted [256]
Total body blood flow (L/hr)	Q_{Total} (= Q_1)	300	[5]
Blood flow of the combined other organs (L/hr)	Q_{OT} (= Q_3)	136	Calculated [5]
Blood flow of hepatic artery (L/hr)	$Q_{LV,Art}$ (= Q_5)	98	Calculated [186]; Portal blood hepatic artery blood flow were combined to simplify the model
Blood flow of hepatic vein (L/hr)	$Q_{LV,Vein}$ (= Q_2)	98	[186]
Total passive diffusion between extracellular space and hepatocyte (L/hr)	Q_{ES-LC} (= Q_{67})	NA	Approximated with a calculated value [5, 67, 68, 227, 257–259]
Clearance via Pgp (L/hr)	CL_{OUT1}	NA	Calculated [5, 67, 68, 227, 257–260]
Clearance via CYP3A4 (L/hr)	CL_{CYP3A4} (= Q_{cyp})	NA	Calculated [5, 67, 159, 227, 259]
Clearance via esterase (L/hr)	CL_{EST}	CL_{CYP3A4}	Assumed to be the same as CL_{CYP3A4} as an initial input
Fraction unbound in blood	$f_{u,BL}$ (= f_b)	0.15	[261]
Fraction unbound in extracellular space	$f_{u,ES}$ (= f_6)	0.261	Calculated Khor et al. [189][8]

[8] $f_{u,ES}$ was calculated applying the assumption proposed for general physiological PK modeling by Khor

Table 26: Parameters used for iPBPK-R simulations of temsirolimus for healthy subjects

Description (units)	Notation	Value	Reference/Comments
Fraction unbound in hepatocyte	$f_{u,LC}$ (= f_7)	0.167	Calculated [262–264]
Volume of distribution at steady state (L/kg)	V_{SS}	NA	[259]
Partition coefficient of lung to plasma	$P_{LG:P}$	26.28	Calculated [184, 195, 196]
Partition coefficient of the combined other organs to plasma	$P_{OT:P}$	7.58	Calculated [184, 195, 196]
Partition coefficient of blood to plasma	$P_{BL:P}$ (= P_b)	NA	[259]
Partition coefficient of kidney to plasma	$P_{KD:P}$	9.565	Calculated [184, 195, 196]
Partition coefficient of hepatocyte to plasma	$P_{LC:P}$ (= P_{7p})	6.87	Calculated [184, 195, 196]
Partition coefficient of extracellular space to plasma	$P_{ES:P}$ (= P_{6p})	6.87	Calculated [184, 195, 196]
Michaelis constant of P-gp (mmol/hr)	$K_{m,OUT1}$ (= K_b)	NA	Calculated [227, 259]
Exponential decay in the combined other organs (L/hr)	μ	12.5	Assumed based on sensitivity analysis

NA, not available due to the FDA data confidentiality under the Code of Federal Regulations Title 21 Part 20 [245], the individual observed data are not shown.

et al. to our modeling. This assumption was 'the blood protein to which the drug binds is also present in interstitial fluid and that the association binding constant is the same in both blood and interstitial fluid' [189]. It is not clear which particular protein binds to temsirolimus (or sirolimus). However, extracellular space matrix (ECM) is known to have many proteins such as fibrillar collagens, proteoglycans, growth factors, cytokines, chemokines, enzymes, among others [193]. We treat these proteins in ECM in the liver as a general protein that can bind to temsirolimus in the modeling.

Table 27: Parameters used for iPBPK-R simulations of sirolimus for healthy subjects

Description (units)	Notation	Value	Reference/Comments
Volume of kidney (L)	V_{KD} (= V_4)	0.270	[184]
Volume of lung (L)	V_{LG} (= V_1)	0.775	[184]
Volume of vein (L)	V_{vein} (= V_2)	2.700	[184]
Volume of the combined other organs (L)	$V_{OT(m)}$ (= V_3)	271.92	Calculated [184, 251–254]
Volume of artery (L)	V_{art} (= V_5)	2.700	[184]
Volume of extracellular space in the liver (L)	V_{ES} (= V_6)	0.340	Calculated [101, 184, 185]
Effective volume of Extracellular space in the liver (L)	$V_{ES,eff(m)}$ (= V'_6)	0.967	Calculated with approximation [101, 255]
Volume of hepatocyte (L)	V_{LC} (= V_7)	1.139	Calculated [101, 184, 185]
Blood flow of kidney (L/hr)	Q_{KD} (= Q_4)	66	[5]
Renal clearance of sirolimus (L/hr)	$CL_{R(m)}$	0.0	Assumed [249, 265]
Total body blood flow (L/hr)	Q_{Total} (= Q_1)	300	[5]
Blood flow of the combined other organs (L/hr)	Q_{OT} (= Q_3)	136	Calculated [5]
Blood flow of hepatic artery (L/hr)	$Q_{LV,Art}$ (= Q_5)	98	Calculated based on [186]; Portal blood hepatic artery blood flow were combined to simplify the model
Blood flow of hepatic vein (L/hr)	$Q_{LV,Vein}$ (= Q_2)	98	[186]
Total passive diffusion between extracellular space and hepatocyte (L/hr)	$Q_{ES-LC(m)}$ (= Q_{67})	0.921	Calculated [5, 67, 68, 233, 258, 266]; Also see Appendix D
Clearance via Pgp (L/hr)	$CL_{OUT1(m)}$	74.07	Calculated [5, 67, 68, 233, 258, 266]; Also see Appendix D
Clearance via CYP3A4 (L/hr)	$CL_{CYP3A4(m)}$ (= Q_{cyp})	844.7	Calculated [5, 246, 247]
Clearance via non-CYP3A4 dependent metabolism (L/hr)	$CL_{NONCYP3A4(m)}$	3065.67	Calculated assuming that abundance of CYP3A5 was very small and negligible [246, 247]
Fraction unbound in blood	$f_{u,BL(m)}$ (= f_b)	NA	[259]
Fraction unbound in extracellular space	$f_{u,ES(m)}$ (= f_6)	NA	[189, 259][9]
Fraction unbound in hepatocyte	$f_{u,LC(m)}$ (= f_7)	0.416	Calculated [249, 263]

[9] $f_{u,ES(m)}$ was calculated applying the assumption proposed for general physiological PK modeling by Khor et al. to our modeling. See the comments on $f_{u,ES}$ in Table 26. The same argument applies to protein binding regarding $f_{u,ES(m)}$.

Table 27: Parameters used for iPBPK-R simulations of sirolimus for healthy subjects

Description (units)	Notation	Value	Reference/Comments
Volume of distribution at steady state (L/kg)	$V_{SS(m)}$	NA	[259]
Partition coefficient of lung to plasma	$P_{LG:P(m)}$	21.8	Calculated [184, 195, 196]
Partition coefficient of the combined other organs to plasma	$P_{OT:P(m)}$	6.31	Calculated [184, 195, 196]
Partition coefficient of blood to plasma	$P_{BL:P(m)}$ (= P_b)	NA	[259]
Partition coefficient of kidney to plasma	$P_{KD:P(m)}$	7.99	Calculated [184, 195, 196]
Partition coefficient of hepatocyte to plasma	$P_{LC:P(m)}$ (= P_{7p})	6.52	Calculated [184, 195, 196]
Partition coefficient of extracellular space to plasma	$P_{ES:P(m)}$ (= P_{6p})	6.52	Calculated [184, 195, 196]
Maximum velocity of P-gp (μmol/hr)	$J_{max,OUT1(m)}$ (= J_b)	0.89	Calculated [233]
Exponential decay in the combined other organs (L/hr)	$\mu_{(m)}$	0.0001	Assumed based on sensitivity analysis

NA, not available due to the FDA data confidentiality under the Code of Federal Regulations Title 21 Part 20 [245], the individual observed data are not shown.
(m) denotes metabolite sirolimus.

5.5 Discussion

Both temsirolimus and sirolimus are mTOR inhibitors [223, 267]. However, water solubility and chemical stability of sirolimus is poorer than those of temsirolimus [201, 224, 265, 267, 268]. Because of the difference in these properties, Ballou et al. discussed that temsirolimus can be administered intravenously and rapidly converted to sirolimus which seems to be responsible for the difference in pharmacological effects from sirolimus [267]. Although the exact mechanism of inhibition of mTORC1 complex (a complex formed by mTOR when it binds to regulatory subunits of lipid kinases of the phosphatidylinositol 3-kinase [PI3K]

family) by these drugs is unclear [267], temsirolimus clinically exhibits an anti-cancer effect with a less immunosuppressive effect than the immunosuppressant, sirolimus [223].

Temsirolimus is an ester analog of sirolimus and it gets converted to sirolimus by esterase. Both temsirolimus and sirolimus undergo CYP3A4- and P-gp-mediated elimination pathways in the liver [227,229]. There are some metabolism pathways other than CYP3A4 for the two entities including CYP3A5 and CYP2C8 [246,248–250]. However, CYP3A4 is a predominant pathway among CYP enzymes [229, 246, 249]. Furthermore, the abundance of CYP3A5 was found to be very small and negligible in human hepatocytes [247][10]. Accordingly, our focus was to model CYP3A4 and P-gp activities for which both temsirolimus and sirolimus are substrates. We also modeled a non-CYP3A4-dependent clearance to describe relatively large undetermined metabolic pathway(s)[11] of sirolimus reported in preclinical literature [246] as described in Section 5.3.2.

The extent of each contribution of elimination pathways and the effect of rifampin on the pathways are hard to evaluate when we have the overlapping metabolism of temsirolimus and sirolimus. It is also essential to consider a potential interplay between CYP3A4 and P-gp activities with interindividual variabilities. CYP3A4 and P-gp are shown to interplay in several rifampin-inducing drug-drug interactions (DDIs) [110,270]. A marked interindividual variation has been also seen in rifampin-induced CYP3A4 expression [271]. On the other hand, the role of P-gp has been inconsistent in the context of interplay between CYP3A4 and P-gp. P-gp is less expressed in the human liver compared to the intestine [244, 247, 272, 273].

Rifampin is known to be a strong inducer of CYP3A4 for P450-mediated metabolisms for concomitant use in clinical DDI studies [241]. For example, rifampin has been shown to reduce AUC of concentration-time data of the sensitive CYP3A4 index substrate midazolam

[10]Note that temsirolimus is a relatively recently approved drug and clinical pathway contributions (%) of esterase and CYP enzymes have not been published. Determining all metabolites of temsirolimus is analytically difficult and they are not fully determined [232]. As in Section 5.3.3, the initial input parameters related to these pathways are either not shown due to the FDA data confidentiality or assumed. See Table 26.

[11]Undetermined metabolic pathway(s) means the metabolic pathway(s) other than CYP3A4, CYP3A5, and CYP2C8-mediated pathway(s) [250]. The specification regarding these metabolic pathways was not available for the *in vitro* data we used for IVIVE calculation. Accordingly, the model structure could not be specified if we did not limit the hepatic metabolic pathways to evaluate. In addition, multiple metabolic pathways in iPBPK-R are likely to be indistinguishable mathematically as discussed in the limitations later in this section. The bioavailability of sirolimus has been reported to be 14% using a two-stage population analysis of meta-data consisting of single IV, single PO, or multiple PO doses [269], which is not relevant information in the context of this hepatic model building for sirolimus as a metabolite of temsirolimus.

(PO, 15mg) by 96% in healthy subjects [241–243]. Strong inducers are defined to decrease the AUC of sensitive index substrates of a given metabolic pathway by greater than or equal to 80%. Rifampin serves as a strong inducer for CYP2C19 and as a moderate inducer for CYP1A2, CYP2B6, CYP2C8, and CYP2C9 for concomitant use in DDI studies as well. Furthermore, P-gp activity is also reported to be affected by rifampin [244]. In this study, we applied iPBPK-R to the four series of blood concentration datasets of temsirolimus and sirolimus. To the best of our knowledge, this is the first study to simultaneously estimate each contribution of CYP3A4 and P-gp to the nonrenal elimination pathways of temsirolimus and sirolimus and the effect of rifampin in healthy individuals in an integral fashion via iPBPK-R modeling.

Compared to our previous applications of iPBPK-R to production rate data [105, 106], fitting the iPBPK-R model to multiple concentration datasets was a harder problem and required more computation resources. Model fit took on average 160 times as long as in our previous work. Accordingly, the model fit was a little compromised. However, we could observe a good model fit across the four datasets where the average normalized residual means in Period 1 and Period 2 were 36% and 31% for temsirolimus and 0.9% and 1.1% for sirolimus (Figure 33) since the general acceptable criterion for PBPK model prediction of *mean* C_{max} and AUC (thus, not even for *individual* C_{max} or AUC) is 2-fold or 200% of observed C_{max} or AUC (see Section 1.4.5). In our iPBPK-R the relative difference in AUC for the hypothetical individual ranged from 0.91 to 1.08 (Table 23). Note that fitting C_{max} for temsirolimus was relatively hard in this one hypothetical individual (relative difference: 1.86 without rifampin and 1.79 with rifampin in Table 23) given the complex model structures for two compounds being used in the simultaneous high-dimensional parameter optimization. This may be improved if the parameter dependency relationships are fully established. However, this requires enormous evaluation time and is out of scope. In addition, these relative differences are still within the general criterion 2-fold, confirming the overall good performance of the PBPK model fit.

In this study, 13 co-adjustment factors were selected for nested co-optimization as they were impactful enough to change the shape of simulated curves and/or biologically relevant. Most of the adjustment factors were closed to 1 including the ones for volumes of

compartment and for CYP3A4 and P-gp activities on temsirolimus. Adjustment factors related to CYP3A4 and non-CYP3A4-dependent pathways of sirolimus were lower than 1. These are within a reasonable range provided that only a little metabolism information was available in the literature for calculating IVIVEs due to the complexity and instability of metabolites [229]. The adjustment factors for esterase activity on temsirolimus and for passive diffusion of sirolimus resulted in high values. These are not surprising results since the IVIVE values were not available but assumed value or calculated based on surrogate experimental data (Table 26). Despite the limited input data available, all estimated standard deviations of adjustment factors were tight, indicating that the performance of iPBPK-R was consistent across all subjects. Methodologically, iPBPK-R uses a pre-determined model structure and it does not require a validation step unlike predictive modeling. For this reason, successful high-dimensional parameter optimization across all individuals serves model validation.

In the inner loop optimization, a total of eight scaling parameters were independently optimized. The scaling factor for RAF of P-gp at baseline was estimated to be 0 for two subjects and 0.36 on average for the other subjects, suggesting that P-gp does not have an essential role on nonrenal clearance of temsirolimus and sirolimus in the model. At the same time, the scaling factor for RAF of P-gp showed large interindividual variability. There is no data regarding RAF of P-gp in literature while relative expression factor (REF; relative expression factor *in vivo* compared with *in vitro*) of P-gp has been shown to be variable with a CV value of 50% in meta-analysis of healthy Caucasian adult database [68]. Under the assumption that the abundance of the transporter is correlated with its activity, our estimated result of REF was consistent with the literature. In case that this assumption does not hold, the value of RAF can be only obtained by fitting clinical PK data [68]. In this case, to our knowledge this is the first study to have estimated RAF of P-gp using model fitting. Rifampin did not affect P-gp activities on temsirolimus and sirolimus according to the estimated scaling coefficients in Period 2. Rifampin did not significantly affect CYP3A4 activity on temsirolimus either. However, rifampin significantly increased CYP3A4 activity on sirolimus by 73% in the estimated coefficient on average with a great interindividual variability. The asymmetric effect of rifampin on CYP3A4 activities for temsirolimus and for sirolimus may

be explained by the difference in chemical structure. Temsirolimus is synthesized by introducing the 2,2-bis-(hydroxymethyl)-propionate side chain at the C40 position (the same C40 position of sirolimus)[12] [232]. It is suggested that this structural difference result in significant steric hindrance and block CYP3A4 activity on the 39-O-methyl group of temsirolimus. Cai et al. discussed that sirolimus (or temsirolimus) may alter its structure conformation after binding to target proteins *in vivo* and thus changes CYP3A4 action and results in a different biotransformation profile than that found *in vitro* [229]. Our iPBPK-R application quantified the asymmetric role of CYP3A4 on temsirolimus and sirolimus and its alteration by rifampin, which was consistent with the preclinical literature [229]. The estimated scaling factor (induction/inhibition coefficient) indicated that rifampin increased not only CYP3A4 activity but also non-CYP3A4 dependent metabolism of sirolimus in the liver. Based on the abundance of hepatic CYP3A5 which is the shared pathway of temsirolimus and sirolimus, CYP3A5 activity for sirolimus was assumed to be negligible in Section 5.3.2. Accordingly, the part of enzymes responsible for the non-CYP3A4-dependent metabolism of sirolimus may be CYP2C8 as discussed above. The increase of non-CYP3A4-dependent metabolic activity on sirolimus may be partly explained by that rifampin is a CYP2C8 inducer as well [241]. However, the literature used for calculating the IVIVE input of non-CYP3A4-dependent clearance did not provide the full specifications of these non-CYP3A4 enzymes *in vitro* [246]. Jacobsen et al. discussed that other than CYP2C8 (and CYP3A4/3A5) there are likely to be undetermined CYP enzymes responsible for the metabolism of sirolimus *in vivo* [250], and thus non-CYP3A4 enzymes other than CYP2C8 cannot be determined as discussed below.

This study has several limitations. First, among potential CYP-mediated pathways CYP3A4 alone was modeled for temsirolimus assuming that CYP3A4 clearance is a dominant metabolism pathway. However, the recently published literature suggested that CYP3A5 and CYP2C8 are also responsible for metabolizing temsirolimus to a lesser extent [232]. Due to the nature of the reduced order model structure, multiple CYPs cannot be mathematical distinguishable in terms of parameter optimization of iPBPK-R. How to add multiple CYPs in

[12]This numbering in the chemical structure follows the IUPAC nomenclature as Shokati et al. adapted [232] and it may appear to be different from some literatures which did not follow IUPAC like Cai et al. [229].

the complex model structure of temsirolimus and sirolimus and how to differentiate parameters in estimation will be investigated in our future studies. Second, population IVIVE values were calculated for a 70 kg male. The variability in body size may be partly reflected in the adjustment factors for the volumes of compartments such as hepatocyte compartment and combined other organs compartment. Third, the fitted iPBPK-R models cannot be validated against the measurements other than the blood concentration data. We confirmed a good model fit via visual inspection (observed data not shown due to the data confidentiality) and average normalized residuals across all individuals. Multiple coupled blood concentrations were measurements in this study, which added a unique challenge compared to our former applications where the dynamic first derivative of concentrations was a measurement. However, the PK parameters (i.e., AUC, C_{max}, and $t_{1/2}$) of the original population PK analysis of temsirolimus and sirolimus conducted by Boni et al. [240] were overall comparable with the PK parameters calculated based on the iPBPK-R result of the hypothetical individual data as discussed above. Thus, our finding on the asymmetric effect of rifampin on CYP3A4 activities aligned with the published result by Boni et al. that rifampin did not change the hepatic metabolism of temsirolimus but increased the hepatic metabolism of sirolimus. Fourth, P-gp is known to have single nucleotide polymorphisms associated with altered drug disposition of P-gp substrates [274]. For the healthy subjects of which we modeled the PK profiles of temsirolimus and sirolimus, genetic variant data of P-gp was not available. Therefore, for instance we could not evaluate whether the large variability in the estimated RAF of P-gp was caused by the P-gp variants or not. Fifth, we did not model esterase activity of non-hepatic organs since no *in vitro* literature information of non-hepatic esterase was available for temsirolimus as well as estimating parameters in iPBPK-R requires a reduced order model (see Chapter 2). The purpose of this chapter is to present the feasibility of extending the iPBPK-R method to multiple coupled drug concentrations rather than rate data and to evaluate the effect of rifampin on hepatic elimination pathways. While esterase which converts temsirolimus to sirolimus is distributed outside of the liver in humans [275] and was not explicitly modeled in iPBPK-R, exponential parameters included in combined other organs compartment may explain the esterase activity outside of the liver. In addition, rifampin was assumed not to affect esterase activity in Table 22. Therefore, using the

reduced order model does not critically affect our achieving the objectives.

Regarding goodness-of-fit, the faster transient and higher peak of the simulated curves for temsirolimus may be improved. One possible approach may be to model the esterase clearance instead of general exponential decay in the other organs compartment. Another approach could be to model sub-level compartments for the vein compartment. However, these approaches require further input values from the literature and extensive evaluation on the Bridges supercomputer, and it is not immediately implementable. Our future studies include evaluation of the effect of rifampin on the interplay between CYP3A4 and P-gp in patients with chronic kidney disease via iPBPK-R since Vitamin D receptor is reported to affect the CYP3A4 induction [244]. We are also interested in exploring relationships between nonrenal pathway parameters and uremic toxins as potential biomarkers using iPBPK-R analysis when uremic toxin data become available.

5.6 Conclusions

In conclusion, parameters related to multiple non-renal elimination pathways of temsirolimus and sirolimus and the effect of rifampin on these pathways were simultaneously estimated using iPBPK-R in healthy individuals. The iPBPK-R framework was applied to multiple blood concentration datasets and the potential interplay between CYP3A4 and P-gp was evaluated for both temsirolimus and sirolimus. iPBPK-R showed a good model fit to both temsirolimus and sirolimus concentration-time data individually across two study periods. We found that rifampin did not affect CYP3A4 activity on temsirolimus but increased it for sirolimus by 73% in the estimated coefficient. These results of CYP3A4 activity aligned with the published results of population PK modeling of the same data by Boni et al [240] where rifampin did not change the hepatic metabolism of temsirolimus but increased the hepatic metabolism of sirolimus. However, iPBPK-R allowed us to make further inferences on nonrenal elimination pathways. Thus, the increase of CYP3A4 by rifampin was also interindividually variable. Rifampin did not affect P-gp activity on temsirolimus or sirolimus. iPBPK-R enabled estimation of all scaling parameters to measure the effect of

rifampin on the different nonrenal elimination pathways, which cannot be implemented via classical population PK modeling of the same datasets. In the future, iPBPK-R will be applied to a similar type of multiple coupled concentration datasets in patients. This will facilitate exploring relationships of the mechanistic alteration with pathphysiological states and identifying the cause and extent of interindividuality in a patient cohort. We anticipate that iPBPK-R will be a pragmatic tool towards future precision medicine.

6.0 Conclusions and Future Directions

6.1 Summary and Key Findings

The purpose of this dissertation research was to develop a novel PBPK model and measurement procedure, *iPBPK-R*, to simultaneously estimate parameters for hepatic drug elimination pathways in individuals and evaluate the effect of kidney impairment on these pathways. Furthermore, the potential to extend application of iPBPK-R to drug concentration data was explored through estimation of nonrenal elimination pathways of parent drug and its metabolite in healthy subjects.

In Chapter 2 we have mathematically described the iPBPK-R framework. It allows us to estimate multiple physiological parameters in individuals using a single probe drug. iPBPK-R is an indirect signal processing-based measurement method for biological quantities in humans that cannot be directly measured. As guiding example we showed a procedure to estimate hepatic enzyme and drug transporter activities through breath samples clinically obtained via EBT: a small dose of radio-labeled erythromycin is intravenously administered and the subsequent content of radio-labeled CO_2 is measured repeatedly in exhaled breath; the resulting time series was analyzed. We developed a 14-variable non-linear reduced order dynamical model that describes the behavior of the drug and its metabolites in the human body well enough to capture all biological phenomena of interest. Based on this system of coupled non-linear ODEs we treated the measurement problem as inverse problem: we estimated the ODE parameters in individual subjects from the measured EBT time series. These estimates then provided a measurement of the hepatic activity of interest. The parameters are hard to estimate as the ODEs are stiff[1] and the problem needs to be regularized to ensure stable convergence. In iPBPK-R, regularization was achieved via penalty terms (e.g, bias, lower bound, drift, and X-shift) in objective functions that are used in nested optimization or co-optimization. We developed a formal framework based on operators represented

[1] "Stiff equation" is a standard numerical analysis term commonly used in pharmacometrics modeling and simulation and in software/programs including NONMEM, Madonna, and R [276–278]. Certain numerical methods for solving stiff equations are numerically unstable if the step size is not set to be very small [279].

as matrices of scalar function to capture and treat the specific non-linearities present, and perform perturbation analysis to establish properties of the estimation procedure and its solution. Development of the method required 150,000 CPU hours at a supercomputing center. Figure 37 depicts the iPBPK-R approach contrasting with general PBPK modeling.

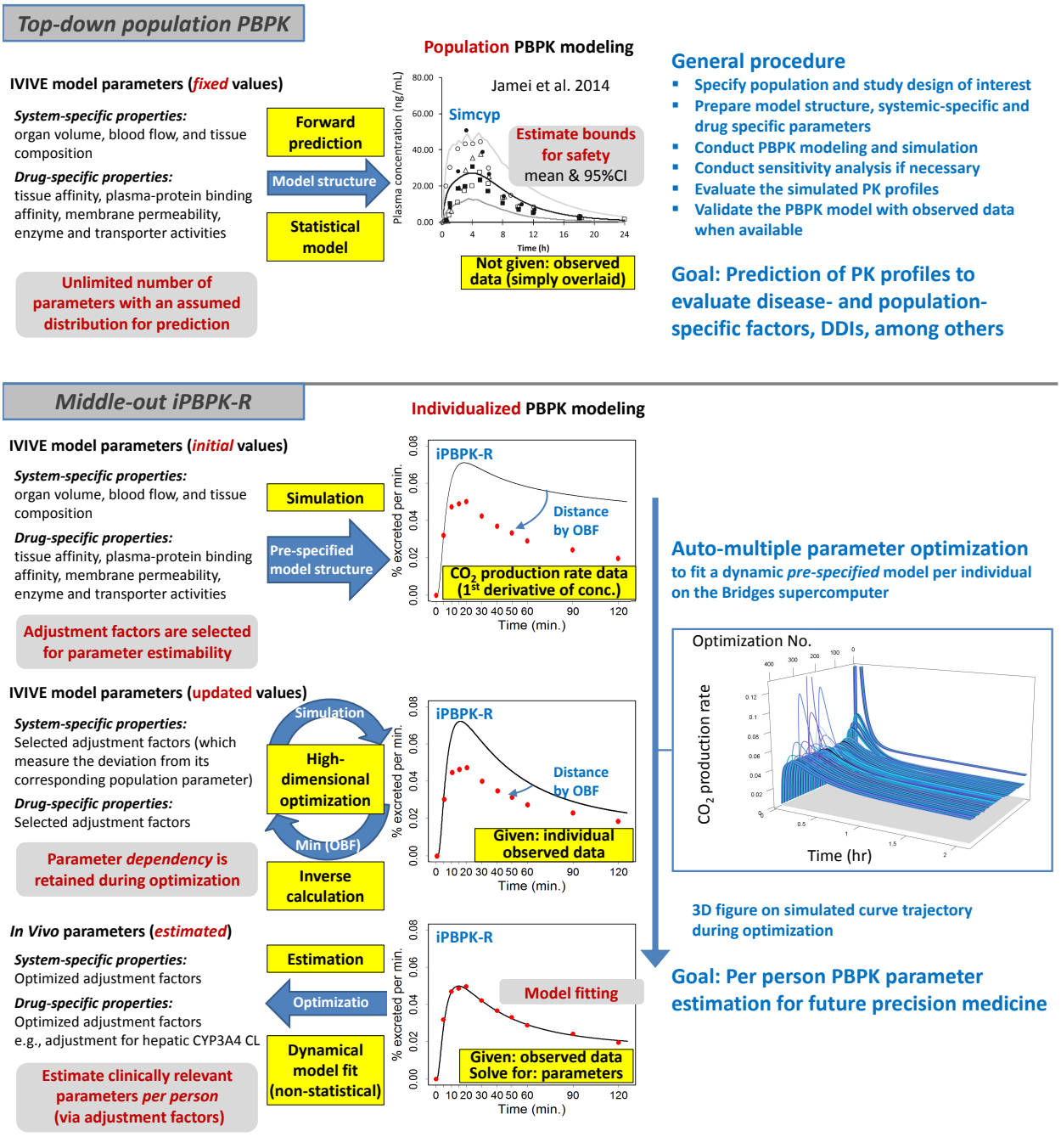

Figure 37: Comparison between general bottom-up PBPK approaches and the middle-out iPBPK-R approach.

Scheme and features are highlighted for general bottom-up PBPK approaches (top panel) and the middle-out iPBPK-R (bottom panel) [280]. The concentration-time plot in the top panel is reprinted from Jamei et al [101].

In Chapter 3, a 7-compartment model (a system of nonlinear ODEs) including linear CYP3A4 clearance and nonlinear transporter clearances were fit to $^{14}CO_2$ production rate –time curves obtained from an EBT study in healthy individuals [127]. ^{14}C-erythromycin in EBT is a substrate of hepatic CYP3A4, OATPs, P-gp, and MRP2. Using a nested parameter estimation method developed in iPBPK-R, scaling factors called adjustment factors for IVIVE inputs on maximum velocity (J_{max}) of transporters, CYP3A4 clearance, among others, were simultaneously estimated. Multiple parameter estimation, in particular, estimation on nonlinear transporter clearance in the system of ODEs, is mathematically difficult [59] [73] [97] [99]. Rate data for $^{14}CO_2$ production, as the approximate first derivative of $^{14}CO_2$ concentration data, turned out to be more dynamic and sensitive data than concentration data, allowing iPBPK-R to successfully extract parameter information related to nonrenal elimination pathways regardless of rate-limiting steps. Sensitivity analysis was used to show that multiple PK parameters including CYP3A4 and OATPs activities control the shape of $^{14}CO_2$ production rate–time curve. Estimated multiple parameters indicated that CYP3A4 activity is much lower than the baseline IVIVE input (median: 12.2% of the IVIVE) in 12 healthy subjects[2]. Females had a higher CYP3A4 activity than males by 11.3%. In addition, the low molecular weight uremic toxin BUN and the adjustment factor for J_{max} of OATPs transporter had a negative correlation in an exploratory analysis.

CKD is known to differentially affect nonrenal clearance (CL_{NR}) pathways [17]. Though highly variable, generally OATP activity decreases as kidney function declines [30, 92, 93, 209, 210, 216] while CYP3A4 remains relatively unaffected [210]. In contrast to the accumulate evidence regarding the effect of CKD on transporter- and enzyme-mediated activities in CL_{NR}, the effect of hemodialysis on individual CL_{NR} pathways has not been elucidated. iPBPK-R and erythromycin breath test data can be leveraged to assess CL_{NR} pathways. In Chapter 4, iPBPK-R was applied to two sets of $^{14}CO_2$ production rate data (EBT data) in 12 ESRD patients receiving standard hemodialysis [128]. The iPBPK-R model was fit to the observed production rate-time curves pre- and post-HD in all patients, showing an excellent

[2]Note that the IVIVE inputs here are reference values and get optimized. As long as parameter optimization in iPBPK-R is sound which is shown in Chapter 2, the initial value of IVIVE × adjustment factor always captures and estimates the true parameter value for the pre-specified model structure. In this sense, the validity of the input value is not essential while the consistency in parameter estimates within a reasonable distributional range self-validates the iPBPK-R method as discussed in Chapter 2.

model fit. The iPBPK-R parameter estimates indicated that CYP3A4 activity increased only marginally post-hemodialysis. OATP activity was not increased post-hemodialysis but showed high interindividual variability. Females had 22.2% and 29.8% higher median CYP3A4 activity than males pre- and post-hemodialysis, respectively. Thus, the higher CYP3A4 activity in females than males was consistent with the PBPK analysis in healthy subjects. No relationship between BUN and activity of CL_{NR} pathways was observed. Exploratory hierarchical cluster analysis identified two patients with highly improved CYP3A4 activity with decreased iPTH, which was not statistically tested. Considering that *in vitro* metabolic clearance tends to have a high interindividual variability [66], estimation of individual adjustment factors in iPBPK-R can account for a deviation from a reference IVIVE. This work provides a proof of principle that iPBPK-R may be used to evaluate the effect of hemodialysis on CL_{NR} pathways.

In Chapter 5, iPBPK-R application was extended to multiple coupled concentration datasets rather than production rate data. Our objective was to evaluate the ability of iPBPK-R to distinguish and simultaneously estimate the contributions of nonrenal elimination pathways mediated by CYP3A4 and P-gp to the disposition of temsirolimus and its metabolite sirolimus within healthy individuals. Intravenously administered temsirolimus gets converted to its metabolite sirolimus by esterase while both temsirolimus and sirolimus are substrates of hepatic CYP3A4 and P-gp. In a classical PK analysis of a DDI study of temsirolimus, rifampin did not affect PK profiles of temsirolimus but decreased Cmax and AUC of sirolimus in a healthy cohort [240]. iPBPK-R was applied to four concentration datasets and each contribution and potential interplay of CYP3A4 and P-gp was simultaneously evaluated for temsirolimus and sirolimus. iPBPK-R analysis indicated that rifampin increased CYP3A4 activity on sirolimus by 73% but not temsirolimus or P-gp activity in healthy individuals. The estimated induction was also interindividually variable. The iPBPK-R application in this chapter allowed us to quantify the asymmetric role of CYP3A4 on temsirolimus and sirolimus and its alteration by rifampin. This asymmetric result was consistent with the preclinical literature [229].

6.2 Clinical Implications and Limitations

6.2.1 Clinical implications

In clinical pharmacology research, EBT was once used as a CYP3A4 probe based on the premise that the radio-labeled drug ^{14}C-erythromycin undergoes enzymatic metabolism by CYP3A4 in the liver and a final by-product $^{14}CO_2$ in this elimination pathway gets released into the breath. However, erythromycin has overlapping substrate specificity for not only CYP3A4 but also for uptake and efflux transporters (OATPs, MRP2, and P-gp) so that the simple interpretation on CYP3A4 activity will be misleading.

In Chapters 3 and 4, iPBPK-R enabled us to distinguish and simultaneously estimate the activity of multiple non-renal elimination pathways of erythromycin in healthy subjects and patients with kidney disease receiving hemodialysis. Using iPBPK-R a new interpretation of EBT data was obtained. We found that production rate data has rich information allowing estimation of per-person PBPK parameters. These application studies serve as proof of principle that the iPBPK-R framework is a novel tool for delineating rate-limiting and non-rate-limiting elimination pathways using a single probe. We anticipate that iPBPK-R will enable us to evaluate the mechanistic impact of disease or intervention on drug disposition with individualized multiple parameter estimation.

iPBPK-R can be applied to other rate-derived data like volatile organic compounds collected and measured from breath samples (called *breath biopsy samples*) [124] beyond EBT, which was shown theoretically in Chapter 2. Breath biopsy analysis is an emerging area since breath tests can be used non-invasively for biomarker research and conducted efficiently with advanced technology [125, 131]. Breath tests are also potentially cost-effective. As the latest topic, some volatile organic compounds (VOCs) that can be measured in breath samples are studied to see if they can be biomarkers for detecting individuals infected with Coronavirus Disease 2019 (COVID-19) [125]. Including this current pandemic example, potential areas to apply iPBPK-R in breath biopsy research are drug-drug interaction, pathophysiological effects on drug disposition, among others. In kidney disease, the role of biomarkers on hemodialysis efficiency can be evaluated by exploring correlations between iPBPK-R-based

parameter estimates and uremic toxin concentrations.

iPBPK-R has a potential to be a tool to evaluate candidate biomarkers. Although it is an exploratory analysis, BUN was negatively correlated with hepatic OATP activity in healthy subjects but not in ESRD patients. This may suggest that BUN is well dialyzable and not a good candidate biomarker to evaluate nonrenal drug disposition in patients on hemodialysis. When a panel of uremic toxin data is available, iPBPK-R analysis enables us to identify uremic toxins that have altered relationships with nonrenal elimination pathways in patients with kidney disease compared to healthy subjects. Such uremic toxins may be found to be good biomarker candidates to identify kidney disease at an early stage.

In Chapter 5, the asymmetric effect of rifampin on CYP3A4 activity, which was estimated using two scaling parameters to specifically measure the changes of CYP3A4 clearance for temsirolimus and for sirolimus in iPBPK-R, may be explained by the difference in chemical structure. In an article published this year Shokati et al. discussed that temsirolimus having the 2,2-bis-(hydroxymethyl)-propionate side chain at the C40 position (the same C40 position of sirolimus)[3] may block CYP3A4 activity on the 39-O-methyl group of temsirolimus due to a steric hindrance [232]. As a result, a different biotransformation profile between temsirolimus and sirolimus may have been found *in vivo*. This is the first PBPK model-based estimation work that quantified the asymmetric effect of temsirolimus and sirolimus *in vivo*. This presents an ability of iPBPK-R to allow us to evaluate physiologically dependent data of clinical pharmacology studies and gain mechanistical insights *in vivo*.

Throughout the dissertation research, iPBPK-R provided a solution with high accuracy in model fit and biological plausibility. This may enable iPBPK-R to facilitate drug dosing based on measured personalized parameter value after extensive clinical research to identify appropriate substrate probe(s) and validate them using the method. The estimated personalized parameters cannot be measured without the mechanistic model fitting. Thus, personalized parameter estimation could be seen as one candidate approach, *individualized modeling*, suggested to use for precision dosing [281] [282].

[3]This numbering in the chemical structure follows the IUPAC nomenclature as Shokati et al. adapted [232] and it may appear to be different from some literatures which did not follow IUPAC like Cai et al. [229].

6.2.2 Limitations

There are also limitations in the method and applications of iPBPK-R. First, iPBPK-R uses pre-specified reduced order models. Determining the model structure and the parameters to be optimized require sufficient prior knowledge about system- and drug-properties and various sensitivity tests to make it work. When two transporters have the same role in the system of nonlinear ODEs, they need to be treated as one global transporter so that its combined parameters can be optimized. Accordingly, it is important to initially evaluate whether a substrate is a good candidate to apply iPBPK-R based on the detailed mechanism of drug disposition (i.e., the the enzymes and transporters) involved.

Second, when PBPK modeling is conducted, it may not be possible to obtain all necessary *in vitro* experimental data in the literature to calculate IVIVE values, especially for newer drugs. For example, we could not obtain *in vitro* clearance value of esterase for temsirolimus, and its IVIVE value was a best assumed value. However, this would be a more critical problem for population PBPK modeling to predict PK profiles but not so much for iPBPK-R to estimate parameters since the parameters are to be optimized in iPBPK-R while the assumed IVIVE value is treated as a reference value. When an experimental *in vitro* data becomes available, the assumed reference can be replaced with a newly calculated IVIVE using the *in vitro* data. Then, the original estimated parameters (e.g., adjustment factors estimated in iPBPK-R) can be simply recalculated and updated by multiplying the original parameter estimates with the ratio of the original and new references if needed.

Third, the sample sizes of the clinical studies in Chapters 3 and 4 were small. Although the sample sizes are typical for clinical pharmacology studies, all correlation analyses with uremic toxins had an exploratory nature due to a lack of statistical power. Our conclusions on uremic toxin require validation with large-scaled clinical trials. Note that the actual minimum number of required sample size can be calculated based on a pre-determined effect size of a particular uremic toxin between females and males, for example, as well as based on the statistical power one wants to achieve. The sample size calculation is not derived by iPBPK-R modeling itself. Therefore, the minimum sample size cannot be generalized and it needs to determined at a stage of designing a clinical study according to its specific study

objectives.

Fourth, no genetic variant data of OATPs was available for the application studies of iPBPK-R in Chapters 3 and 4. Therefore for instance, we cannot conclude whether CYP3A4 activity solely had a sex difference or this finding was biased by the interplay with OATP variants. However, the sex difference in CYP3A4 activity was consistent between healthy subjects and patients with kidney disease and further investigation on the sex difference is warranted.

Fifth, CYP3A4 and transporter activity estimates derived from iPBPK-R modeling were not compared to or validated using substrate specific probes as controls. The fitted model cannot be validated against the measurements beyond the breath data although visual inspection and normalized residuals calculated from predicted and observed curves indicated excellent model fit across all individuals. When clinical studies will be designed to apply iPBPK-R, it is also essential to plan to collect different samples (e.g., plasma or urine samples) in order to validate the simulation results with observed PK parameters and build confidence on the applications of iPBPK-R. Similarly, in Chapter 5 the fitted iPBPK-R models were not validated against the measurements other than the blood concentration data. We confirmed a good model fit via average normalized residuals across all individuals. In addition, simulated PK parameters were within 2-fold of observed ones for the mean data (which was used as a hypothetical individual). However, the overall goodness-of-fit of the EBT studies seemed to be better than that in the application of iPBPK-R to the coupled concentration datasets of temsirolimus and sirolimus. Improving the model fit for the drug concentration data under mathematical constraints may be further investigated. Potential avenues of exploration include speeding up optimization procedures that will enable understanding functional dependency in the system of nonlinear ODEs for temsirolimus and sirolimus. Another avenue may be to account for the minor enzyme-mediated pathways (e.g., CYP3A5, CYP2C8, etc.) in the model for which pharmacometrics research on how to distinguished the same type of clearance terms of ODEs is required and for which the IVIVE values for temsirolimus are not available in literature.

In terms of the iPBPK-R method development, simulations and parameter optimization demanded high computational resources (the *Bridges* supercomputer) because it was imple-

mented in R. To make it a useful tool for clinical practice, an efficient programming language like C++ would need to be used to shorten the simulation time enormously and improve the efficiency of iPBPK-R. This would require substantial development effort and cost.

6.3 Future Directions

We anticipate that iPBPK-R can become a step towards precision drug dosing and personalized medicine. iPBPK-R is a mechanistic and indirect measurement approach so that for instance *in vivo* CYP3A4 activity can be estimated for a particular individual using a single probe given the individual's high resolution measurement data. In such estimation, other physiological activities are simultaneously accounted for via iPBPK-R. CYP3A4 activity can be repeatedly estimated before and after intervention or disease progression, so not only inter-individual comparisons but also longitudinal individual monitoring can be implemented. This indicates that sources of inter-individual variability can be mechanistically identified and that iPBPK-R may also provide a means of personalized dosing of narrow therapeutic drugs based on the particular individual's physiological activity. For example, if the source of inter-individual variability is identified to be a particular uremic toxin and if the corresponding individuals who exhibit a great increase in estimated activity of nonrenal elimination pathway (e.g., CYP3A4) are identified post-hemodialysis (as an intervention), a higher dosage of CYP3A4 substrate drug could be considered to optimize the drug dosing for these patients (after iPBPK-R is validated with necessary clinical studies). Alternatively, the uremic toxin may be used as a biomarker for evaluating the activity of the associated nonrenal elimination pathway in the individuals and thus used for dose optimization based on the evaluated pathway activity. Potential fields of application of iPBPK-R includes nephrology, oncology, pediatrics, and other health conditions where exact knowledge of patient would be of high value.

In Chapters 3 and 4, we could show exploratory results of correlations between uremic toxins and nonrenal elimination-related parameters in healthy individuals and CKD patients. Our next step is to design exploratory and confirmatory clinical trials in a sequential fashion

where many subjects with different CKD severity are evaluated for their nonrenal elimination pathways and the effect of kidney disease on these pathways. Furthermore, uremic solutes as candidate biomarkers will be investigated using iPBPK-R analysis and one or some of them will be identified as early diagnostic biomarker(s) for kidney disease.

To establish iPBPK-R as a feasible method with clinical utility, we need to validate the method with applications in appropriate large-scale clinical trials using breath test samples. In the past decade, development of breath sampler tool kits has been advanced [125] and breath biopsy/biomarker research is emerging as well [124, 131]. Given this environment, we anticipate that there will be opportunities to apply iPBPK-R. To facilitate use of iPBPK-R, substrate probes with preferable properties would need to be explored. The substrate probes will be or converted to VOCs to be measured in breath samples. VOCs should originate from exogenous compounds since they can be directly used as probes [124]. VOC probes can have multiple substrate specificity but they should be distinguishable in high-dimensional parameter estimation. For example, ^{13}C-methacetin breath test has been under development as a VOC breath test for assessment of maximal liver function as $^{13}CO_2$ is its by-product in the CYP1A2-mediated metabolism pathway that is altered in liver dysfunction [283]. Some VOC probes could be partially converted to generate radio-labeled CO_2 by oxidation if CYP3A4 is responsible for the biotransformation [284].

Another future direction for the iPBPK-R methodology is to explore its utility for drug concentration data since concentration data is a common measurement in Clinical Pharmacology research. In Chapter 5, we presented the application of iPBPK-R to multiple coupled drug concentration data series of temsirolimus and its metabolite sirolimus in healthy subjects. In this application, intravenously administered temsirolimus can be viewed as a single probe. One of the findings was the asymmetric effect of rifampin on the activity of CYP3A4 for the two compounds as estimated using the scaling parameters in iPBPK-R. Our future studies include evaluation of the effect of rifampin on the interplay between CYP3A4 and P-gp in patients with CKD via iPBPK-R since Vitamin D receptor is reported to affect the CYP3A4 induction [244]. iPBPK-R will allow us to quantify such induction or inhibition and show mechanistic relationships of disease or intervention, potential biomarkers (e.g., uremic toxins or Vitamin D), and *in vivo* activities related to nonrenal clearance. Similarly, iPBPK-

R may be broadly applied to the same type of multiple coupled concentration datasets in patients to establish its utility. Ideal drugs that provide such concentration data may have following properties: (1) multiple disposition pathways are known, (2) two different types of concentration data are available and they can be coupled through a system of nonlinear ODEs, (3) elimination half-life is relatively long to differentiate parameter estimates, (4) concentrations are frequently measured in samples collected in the early phase of PK profile, (5) In vitro data is sufficiently available to calculate IVIVE values, (6) IV dosing is preferable to use reduced order models (PO dosing is theoretically possible but actual application of iPBPK-R requires extensive research starting with specification of model structure), and (7) individual concentration data are available in both healthy subjects and patients. Defining specific criteria for these properties will require further methodological research. Success in establishing use of iPBPK-R for drug concentration data will also lead to exploring relationships of mechanistic alterations in nonrenal clearance with disease severity and eventually identifying diagnostic biomarkers as well as the cause and extent of interindividuality in a patient cohort. We anticipate that iPBPK-R will be a pragmatic tool towards future precision medicine or personalized dosing as described above.

In all iPBPK-R applications, simulations and parameter optimization demanded high computational resources (the Bridges supercomputer) because it was implemented in R. The execution time depends on the difficulty of the optimization problem. By switching to a more efficient programming language like C++ and targeting modern computer platforms with multicore CPUs and GPUs, it would be possible to shorten the simulation time enormously and improve the efficiency of iPBPK-R. This would come at substantial development effort and cost but such development is also essential to make the method more widely applicable. It may be possible to make a user-friendly (cloud based) phone application of iPBPK-R when simulations can be implemented much faster with a more efficient programming language.

Lastly, regardless of the data type used in iPBPK-R (i.e., rate or coupled concentration data series), conducting optimal clinical studies to obtain clinical data will be enormously costly and it may not be realistic to conduct them in the immediate future. To overcome this issue, machine-learning and deep learning (ML/DL) or artificial intelligence (AI) can help to generate approximate clinical data based on literature so that iPBPK-R can be applied

to the generated datasets and be evaluated for its utility. In Appendix E we outline a procedure to generate a clinical dataset using neural ODEs [285], which is one of the latest ML methods that can capture and extrapolate a data series. For example, the limitation of presenting observed clinical data due to confidentiality (e.g., Figure 33) can be supplemented along with this type of ML/DL and AI research, and the application of iPBPK-R can be further facilitated.

In summary, we anticipate that iPBPK-R will serve as a tool to estimate parameters on both rate-limiting step and non-rate-limiting steps in nonrenal clearance of a single probe with multiple substrate specificity utilizing clinical rate measurement. It allows us to study the correlation of nonrenal elimination pathways and uremic solutes and to differentiate patients with difference in uremic solutes. It may eventually provide clinical utility to evaluate alterations of drug disposition caused by disease or intervention as well as inter-individuality. It may identify unique subgroups based on potential uremic solute biomarkers in a patient population with CKD. It may facilitate drug dosing based on personalized parameter estimation. This can lead to an innovative approach of precision medicine.

Appendix A

Mass Balance Theorem and Quality Analysis

A.1 Proof of Theorem 1

Here we provide the proof of theorem 1.

PROOF We use

$$m_i(t) = M_i + \int_{s=0}^{t} \dot{m}_i(s)ds$$

where $M_i = m_i(0)$ is the initial drug mass in compartment V_i. By (2.10) at time $t = 0$ we have

$$\sum_{i=1}^{n} m_i(0) = \sum_{i=1}^{n} M_i = M_0.$$

Therefore,

$$\begin{aligned}
\sum_{i=1}^{n} m_i(t) &= \sum_{i=1}^{n} \Big(M_i + \int_{s=0}^{t} \dot{m}_i(s)ds \Big) \\
&= M_0 + \sum_{i=1}^{n} \int_{s=0}^{t} \sum_{j=1}^{n} q_{ji}(s)ds \\
&= M_0 + \int_{s=0}^{t} \sum_{i=1}^{n} \sum_{j=1}^{n} q_{ji}(s)ds \\
&= M_0 + \int_{s=0}^{t} \sum_{i=1}^{n} \Big(\underbrace{q_{ii}(s)}_{=0} + \sum_{j=i+1}^{n} \underbrace{\big(q_{ji}(s) + q_{ij}(s) \big)}_{=0} \Big) ds \\
&= M_0.
\end{aligned}$$

To establish correctness of mass balance for the model eq. (2.45)–eq. (2.51) used in iPBPK-R we have to show that eq. (2.45)–eq. (2.51) is an instance of eq. (2.9) and that indeed eq. (2.11) holds for all edges $e_{ij} \in \mathrm{V} \times \mathrm{V}$, and that eq. (2.12) holds for all compartments $V_i,\ 1 \leq i \leq n$. Careful inspection of eq. (2.45)–eq. (2.51) establishes this, which proves that the invariant eq. (2.10) holds for eq. (2.45)–eq. (2.51). Note that in eq. (2.45)–eq. (2.51) as

instances of eq. (2.9), q_{ij} and $-q_{ji}$ may be used interchangeably. The choice between q_{ij} and $-q_{ji}$ is determined by the arrow in a graph.

A.2 EBT Analysis

In this section we analyze the operator (2.25) to derive its eigendecomposition and thus be able to make statements about estimable parameters. We pick one (healthy) individual from the first example from section 2.6.4 and pick concentration $\vec{C} = \vec{0}$, i.e., no drug in the system as operating point. At this point all Michaelis Menten non-linearities are fully linear. Thus we are computing $\mathbf{A}^+ = (\mathbf{X} + \mathbf{Y}^+)$. The same analysis can be done for the fully saturated case $\mathbf{A}^-$. The resulting matrix is given by

$$\mathbf{A} = \begin{bmatrix}
-2003.519 & 387.097 & 0 & 0 & 387.097 & 0 & 0 & 0 & 0 & 0 & 0 & 0 & 0 & 0 \\
287.542 & -185.926 & 2.860 & 93.612 & 0 & 28.179 & 0 & 0 & 0 & 0 & 0 & 0 & 0 & 0 \\
0 & 2.599 & -0.404 & 0 & 3.177 & 0 & 0 & 0 & 0 & 0 & 0 & 0 & 0 & 0 \\
0 & 244.444 & 0 & -189.179 & 244.444 & 0 & 0 & 0 & 0 & 0 & 0 & 0 & 0 & 0 \\
287.542 & 0 & 3.497 & 9.361 & -197.144 & -36.296 & 0 & 0 & 0 & 0 & 0 & 0 & 0 & 0 \\
0 & 0 & 0 & 0 & 180.479 & -430.361 & 57.137 & 0 & 0 & 0 & 0 & 0 & 0 & 0 \\
0 & 0 & 0 & 0 & 0 & 223.407 & -3.957 & 0 & 0 & 0 & 0 & 0 & 0 & 0 \\
0 & 0 & 0 & 0 & 0 & 0 & 0 & 0 & 0 & 0 & 0 & 0 & 0 & 0 \\
0 & 0 & 0.076 & 0 & 0 & 0 & 0 & 0 & 0 & 0 & 0 & 0 & 0 & 0 \\
0 & 0 & 0 & 1.954 & 0 & 0 & 0 & 0 & 0 & 0 & 0 & 0 & 0 & 0 \\
0 & 0 & 0 & 0 & 0 & 0 & 0.423 & 0 & 0 & 0 & 0 & 0 & 0 & 0 \\
0 & 0 & 0 & 0 & 0 & 0 & 0.003 & 0 & 0 & 0 & 0 & 0 & 0 & 0 \\
0 & 0 & 0 & 0 & 0 & 0 & 0.423 & 0 & 0 & 0 & 0 & 0 & -12.72 & 0 \\
0 & 0 & 0 & 0 & 0 & 0 & 0 & 0 & 0 & 0 & 0 & 0 & 12.72 & 0
\end{bmatrix} \tag{A.1}$$

The matrix $\mathbf{A}$ has eigenvalues

$$\theta_i = 0.0,\ 0.0,\ 0.0,\ 0.0,\ 0.0,\ -12.7,\ -2119.7,\ -434.0,\ -290.5,\ -221.4,\ 23.7,\ 32.1,\ -0.7,\ 0.0 \tag{A.2}$$

The spectrum contains two positive eigenvalues 32.1 and 23.7 responsible for the initial spike in the concentration-time curve. The dominant negative eignevalue is -2119.7 which captures the initial decay. The terminal slope is driven by the three negative eigenvalues of similar magnitude, -434.0, -290.5, and -221.4. The dimension of the null space of the matrix $\mathbf{A}$ is 6, capturing the source and sink compartments.

The eigenbasis of A in ordered according to the eigenvalues is given by

$$\mathbf{C} = \begin{bmatrix}
0 & 0 & 0 & 0 & 0 & 0 & 0.977 & 0.007 & 0.071 & 0.003 & -0.009 & -0.070 & -0.019 & 0 \\
0 & 0 & 0 & 0 & 0 & 0 & -0.147 & -0.097 & 0.542 & 0.590 & -0.054 & -0.284 & -0.082 & 0 \\
0 & 0 & 0 & 0 & 0 & 0 & 0.000 & 0.000 & -0.002 & 0.001 & -0.005 & -0.031 & 0.909 & 0 \\
0 & 0 & 0 & 0 & 0 & 0 & 0.037 & -0.030 & -0.754 & -0.117 & -0.056 & -0.405 & -0.130 & 0 \\
0 & 0 & 0 & 0 & 0 & 0 & -0.146 & 0.127 & -0.229 & -0.574 & 0.006 & -0.083 & -0.019 & 0 \\
0 & 0 & 0 & 0 & 0 & 0 & 0.016 & 0.876 & -0.224 & -0.387 & -0.122 & -0.137 & 0.001 & 0 \\
0 & 0 & 0 & 0 & 0 & 0 & -0.002 & -0.455 & 0.175 & 0.398 & -0.989 & -0.850 & 0.066 & 0 \\
0 & 0 & 0 & 0 & 0 & 0 & 0 & 0 & 0 & 0 & 0 & 0 & 0 & 1 \\
0 & 1 & 0 & 0 & 0 & 0 & 0 & 0 & 0 & 0 & 0 & 0.000 & -0.099 & 0 \\
0 & 0 & 1 & 0 & 0 & 0 & 0 & 0.000 & 0.005 & 0.001 & -0.005 & -0.025 & 0.362 & 0 \\
0 & 0 & 0 & 1 & 0 & 0 & 0 & 0.000 & 0.000 & -0.001 & -0.018 & -0.011 & -0.040 & 0 \\
0 & 0 & 0 & 0 & 1 & 0 & 0 & 0 & 0 & 0 & 0.000 & 0.000 & 0.000 & 0 \\
0 & 0 & 0 & 0 & 0 & 0.707 & 0 & 0.001 & 0.000 & -0.001 & -0.012 & -0.008 & 0.002 & 0 \\
1 & 0 & 0 & 0 & 0 & -0.707 & 0 & 0 & 0 & 0 & -0.006 & -0.003 & -0.042 & 0
\end{bmatrix} \tag{A.3}$$

This shows that $\mathbf{A}$ indeed is a simple matrix and has eigendecomposition (2.42).

Further, factorizing out the null space of $\mathbf{A}$ shows that the basis vectors have sufficiently large angles between them so that the problem does not degenerate. The (i, j) entry of the matrix below shows the scalar product of projected normalized eigenvector i with projected normalized eigenvector j of the column space:

$$\begin{pmatrix}
1 & 0.016 & -0.009 & -0.011 & -0.004 & -0.030 & -0.010 \\
0.016 & 1 & -0.334 & -0.646 & 0.351 & 0.295 & -0.022 \\
-0.009 & -0.334 & 1 & 0.696 & -0.135 & 0.048 & 0.072 \\
-0.011 & -0.646 & 0.696 & 1 & -0.375 & -0.358 & 0.005 \\
-0.004 & 0.351 & -0.135 & -0.375 & 1 & 0.897 & -0.063 \\
-0.030 & 0.295 & 0.048 & -0.358 & 0.897 & 1 & -0.006 \\
-0.010 & -0.022 & 0.072 & 0.005 & -0.063 & -0.006 & 1
\end{pmatrix} \tag{A.4}$$

The scalar product of two normalized eigenvectors is between 0.004 and 0.897, which indicates that all vectors are sufficiently pairwise non-parallel. This together provides evidence that the EBT problem indeed follows the assumptions of section 2.4.7. To fully establish a proof of soundness one would have to analyze $\mathbf{A}^+$ and $\mathbf{A}^-$ for all twelve individuals. The results shown in section 2.6.3 provide further experimental evidence that the analysis holds, as the modes computed in this section are visible in the results shown in Figure 15 of chapter 3. This overall adds to the soundness of our approach.

Appendix B

Detailed ODEs and Proof of Mass Balance for Healthy Subjects

We detail the set of ordinary differential equations (ODEs) used in Chapter 3, our PBPK model of EBT for healthy subjects. These are actual examples of ODEs in Tables 7 and table:6 in Chapter 2 using the notation in Table 12. Furthermore, C, $C^{\star}$, and $C^{\star\star}$ stand for the blood concentrations of ^{14}C-erythromycin, $\mathrm{H}^{14}\mathrm{CO}_3^-$, and $^{14}\mathrm{CO}_2$, respectively.

B.1 ODEs for Concentration Change

- Lung (LG) compartment

$$\frac{dC_{\mathrm{LG}}}{dt} = \frac{1}{\mathrm{V_{LG}}}\left[\mathrm{Q_{Total}}\left(C_{\mathrm{Vein}} - \frac{C_{\mathrm{LG}}}{\mathrm{P_{LG:P}}/\mathrm{P_{BL:P}}}\right) - \mathrm{Q_{Total}}\left(\frac{C_{\mathrm{LG}}}{\mathrm{P_{LG:P}}/\mathrm{P_{BL:P}}} - C_{\mathrm{Art}}\right)\right] \tag{B.1}$$

- Venous blood (Vein) compartment

$$\begin{aligned}\frac{dC_{\mathrm{Vein}}}{dt} = \frac{1}{\mathrm{V_{Vein}}}\Bigg[&\mathrm{Q_{KD}}\left(\frac{C_{\mathrm{KD}}}{\mathrm{P_{KD:P}}/\mathrm{P_{BL:P}}} - C_{\mathrm{Vein}}\right) + \mathrm{Q_{LV}}C_{\mathrm{LV}} \\ &+ \mathrm{Q_{OT}}\left(\frac{C_{\mathrm{OT}}}{\mathrm{P_{OT:P}}/\mathrm{P_{BL:P}}} - C_{\mathrm{Vein}}\right) - \mathrm{Q_{Total}}\left(C_{\mathrm{Vein}} - \frac{C_{\mathrm{LG}}}{\mathrm{P_{LG:P}}/\mathrm{P_{BL:P}}}\right)\Bigg]\end{aligned} \tag{B.2}$$

- The combined other organs (OT) compartment

$$\frac{dC_{\mathrm{OT}}}{dt} = \frac{1}{\mathrm{V_{OT}}}\left[\mathrm{Q_{OT}}\left(C_{\mathrm{Art}} - \frac{C_{\mathrm{OT}}}{\mathrm{P_{OT:P}}/\mathrm{P_{BL:P}}}\right) - \mathrm{Q_{OT}}\left(\frac{C_{\mathrm{OT}}}{\mathrm{P_{OT:P}}/\mathrm{P_{BL:P}}} - C_{\mathrm{Vein}}\right) - \mu C_{\mathrm{OT}}\right] \tag{B.3}$$

where μ is a parameter of exponential decay that explains loss or decomposition of the parent drug.

- Kidney (KD) compartment

$$\frac{dC_{\mathrm{KD}}}{dt} = \frac{1}{\mathrm{V_{KD}}}\Bigg[\mathrm{Q_{KD}}\left(C_{\mathrm{Art}} - \frac{C_{\mathrm{KD}}}{\mathrm{P_{KD:P}/P_{BL:P}}}\right) - \mathrm{Q_{KD}}\left(\frac{C_{\mathrm{KD}}}{\mathrm{P_{KD:P}/P_{BL:P}}} - C_{\mathrm{Vein}}\right) - \left(\delta\mathrm{eGFR}\frac{\mathrm{f_{u,BL}}C_{\mathrm{KD}}}{\mathrm{P_{KD:P}/P_{BL:P}}} + \frac{\mathrm{J_{max,OUT1,KD}}\left(\frac{\mathrm{f_{u,BL}}}{\mathrm{P_{KD:P}/P_{BL:P}}}\right)C_{\mathrm{KD}}}{\mathrm{K_{m,OUT1,KD}} + \left(\frac{\mathrm{f_{u,BL}}}{\mathrm{P_{KD:P}/P_{BL:P}}}\right)C_{\mathrm{KD}}}\right)\Bigg] \tag{B.4}$$

where δ is the fraction of the drug filtered via the glomerulus.

- Arterial blood (Art) compartment

$$\frac{dC_{\mathrm{Art}}}{dt} = \frac{1}{\mathrm{V_{Art}}}\Bigg[\mathrm{Q_{Total}}\left(\frac{C_{\mathrm{LG}}}{\mathrm{P_{LG:P}/P_{BL:P}}} - C_{\mathrm{Art}}\right) - \mathrm{Q_{KD}}\left(C_{\mathrm{Art}} - \frac{C_{\mathrm{KD}}}{\mathrm{P_{KD:P}/P_{BL:P}}}\right) - \mathrm{Q_{LV}}C_{\mathrm{Art}} - \mathrm{Q_{OT}}\left(C_{\mathrm{Art}} - \frac{C_{\mathrm{OT}}}{\mathrm{P_{OT:P}/P_{BL:P}}}\right)\Bigg] \tag{B.5}$$

- Extracellular space (ES) sub-compartment

$$\frac{dC_{\mathrm{ES}}}{dt} = \frac{1}{\mathrm{V_{ES,eff}}}\Bigg[\mathrm{Q_{LV,Art}}C_{\mathrm{Art}} - \mathrm{Q_{LV,Vein}}\frac{C_{\mathrm{ES}}}{(\mathrm{P_{ES:P}/P_{BL:P}})} - \mathrm{Q_{ES-LC,LV}}\left(\mathrm{f_{u,ES}}\frac{C_{\mathrm{ES}}}{\mathrm{P_{ES:P}}} - \mathrm{f_{u,LC}}\frac{C_{\mathrm{LC}}}{\mathrm{P_{LC:P}}}\right) - \frac{\mathrm{J_{max,UP1,ES}}\left(\frac{\mathrm{f_{u,ES}}}{\mathrm{P_{ES:P}}}\right)C_{\mathrm{ES}}}{\mathrm{K_{m,UP1,ES}} + \left(\frac{\mathrm{f_{u,ES}}}{\mathrm{P_{ES:P}}}\right)C_{\mathrm{ES}}}\Bigg] \tag{B.6}$$

- Hepatocyte or liver cell (LC) sub-compartment

$$\frac{dC_{\mathrm{LC}}}{dt} = \frac{1}{\mathrm{V_{LC}}}\Bigg[\frac{\mathrm{J_{max,UP1,ES}}\left(\frac{\mathrm{f_{u,ES}}}{\mathrm{P_{ES:P}}}\right)C_{\mathrm{ES}}}{\mathrm{K_{m,UP1,ES}} + \left(\frac{\mathrm{f_{u,ES}}}{\mathrm{P_{ES:P}}}\right)C_{\mathrm{ES}}} + \mathrm{Q_{ES-LC,LV}}\left(\mathrm{f_{u,ES}}\frac{C_{\mathrm{ES}}}{\mathrm{P_{ES:P}}} - \mathrm{f_{u,LC}}\frac{C_{\mathrm{LC}}}{\mathrm{P_{LC:P}}}\right) - \frac{\mathrm{J_{max,OUT1,LC}}\left(\frac{\mathrm{f_{u,LC}}}{\mathrm{P_{LC:P}}}\right)C_{\mathrm{LC}}}{\mathrm{K_{m,OUT1,LC}} + \left(\frac{\mathrm{f_{u,LC}}}{\mathrm{P_{LC:P}}}\right)C_{\mathrm{LC}}} - \frac{\mathrm{J_{max,OUT2,LC}}\left(\frac{\mathrm{f_{u,LC}}}{\mathrm{P_{LC:P}}}\right)C_{\mathrm{LC}}}{\mathrm{K_{m,OUT2,LC}} + \left(\frac{\mathrm{f_{u,LC}}}{\mathrm{P_{LC:P}}}\right)C_{\mathrm{LC}}} - \mathrm{CL_{CYP}}\mathrm{f_{u,LC}}\frac{C_{\mathrm{LC}}}{\mathrm{P_{LC:P}}}\Bigg] \tag{B.7}$$

- Bicarbonate $\mathrm{H^{14}CO_3^-}$ in HC sub-compartment

$$\frac{dC^{\star}_{\mathrm{LC}}}{dt} = \frac{1}{\mathrm{V_{LC}}}\Bigg[\mathrm{CL_{CYP}}\mathrm{f_{u,LC}}\frac{C_{\mathrm{LC}}}{\mathrm{P_{LC:P}}}\Bigg] - (\mathrm{k_{pool1}} + \mathrm{k_{resp}})C^{\star}_{\mathrm{LC}} + \mathrm{k_{pool2}}C^{\star}_{\mathrm{pool,BL}} \tag{B.8}$$

where $C^{\star}_{\mathrm{pool,BL}}$ is the concentration of $\mathrm{H^{14}CO_3^-}$ in the pool compartment ($\mathrm{H^{14}CO_3^-}$ is dis-

solved in the blood) in the same fashion of equation (5) in Sugiyama et al. 2011. We referred to their in vivo rat PBPK study and set both parameters k_{pool1} and k_{pool2} to 0.

- Carbon Dioxide $^{14}CO_2$ in LG compartment

$$\frac{dA^{\star\star}_{LG}}{dt} = \phi V_{LC}\left[k_{resp} C^{\star}_{LC}\right] \tag{B.9}$$

where $A^{\star\star}_{LG}$ is the exhaled amount of $^{14}CO_2$ in breath, and ϕ is a conversion factor of $^{14}CO_2$ from its molecular weight to Ci (a unit of radioactivity) ($\phi = 1$ in our simulations since all the calculations of concentrations were done in molar base). $dA^{\star\star}_{LG}/dt$ is the radioactivity measured from $^{14}CO_2$ in the lung at time t. We assume that the respired amount of $H^{14}CO_3^-$ and exhaled$^{14}CO_2$ have a one-to-one molar relationship (no rate-limiting step) in Equation (B.9).

B.2 Mass Balance

Similarly to all other pharmacokinetics models, our model uses approximation of physiological behavior. Importantly, we do not intend that our model is a classical PBPK model that is usually used for *prediction*. iPBPK-R is rather different, mathematically correct, and useful for our research purpose of *estimating* the parameters related to non-renal elimination pathways after observed data is obtained (i.e., not for prediction). Here we provide a proof that the mass balance of ^{14}C-erythromycin is retained in our iPBPK-R. As presented in the application of Chapter 3 (and Chapter 4), the model served our goal well as an application of the novel approach.

Figure 38 depicts the masses and mass flows of the drug (^{14}C-erythromycin) in the system. The system is closed, i.e., no drug mass is created or lost. The system consists of 12 compartments. Among 12 compartments, there is one source compartment (IV dosing compartment colored with light orange in the figure) and three waste compartments (Exponential decay in OT, Urine, Metabolism, and Bile compartments colored with light gray in the figure). Note that seven-compartmental iPBPK-R in Chapter 3 is the result of not

showing the five input and waste compartments from 12 compartments. In each compartment, there is one state variable, m, which denotes drug mass. $q_{\overrightarrow{\mathrm{W:Z}}}$ denotes a mass flow from W compartment to Z compartment and it is represented by an arrow in Figure 38. In this closed system, at any time the total amount of the drug is constant m_0 which is a system invariant. This drug content m_0 is in the source compartment (IV dosing compartment) at time 0 and in the waste compartments at infinite time. Each flow is a directed and anti-symmetric quantity, which means what flows out of one compartment flows into the other compartment. The two compartments are connected with an arrow. We assume that the type of each flow is one or a combination of the following:

- with diffusion (proportional to difference in concentrations between two compartments)
- without diffusion (proportional to concentration of one compartment)
- proportional to non-linear Michaelis–Menten clearance
- proportional to linear clearance

B.3 Equations Depicting Mass Flow as Shown in Figure 38

Then, mass flows in the figure are defined as below where non-linear kinetics are described with a general function form of $\mathrm{MM}_{\alpha,\beta}(X) = \frac{\alpha X}{\beta + X}$.

- $q_{\overrightarrow{\mathrm{IV:VN}}} = \begin{cases} m_0/t_0 & \text{for} \quad 0 \le t \le t_0, \\ 0 & \text{else} \end{cases}$
- $q_{\overrightarrow{\mathrm{VN:LG}}} = \mathrm{Q}_{\mathrm{Total}} \left(C_{\mathrm{Vein}} - \frac{C_{\mathrm{LG}}}{\mathrm{P}_{\mathrm{LG:P}}/\mathrm{P}_{\mathrm{BL:P}}} \right),$
- $q_{\overrightarrow{\mathrm{LG:Art}}} = \mathrm{Q}_{\mathrm{Total}} \left(\frac{C_{\mathrm{LG}}}{\mathrm{P}_{\mathrm{LG:P}}/\mathrm{P}_{\mathrm{BL:P}}} - C_{\mathrm{Art}} \right),$
- $q_{\overrightarrow{\mathrm{KD:VN}}} = \mathrm{Q}_{\mathrm{KD}} \left(\frac{C_{\mathrm{KD}}}{\mathrm{P}_{\mathrm{KD:P}}/\mathrm{P}_{\mathrm{BL:P}}} - C_{\mathrm{Vein}} \right),$
- $q_{\overrightarrow{\mathrm{KD:U}}} = \delta \mathrm{eGFR} \frac{\mathrm{f}_{\mathrm{u,BL}} C_{\mathrm{KD}}}{\mathrm{P}_{\mathrm{KD:P}}/\mathrm{P}_{\mathrm{BL:P}}} + \mathrm{MM}_{\mathrm{J}_{\mathrm{max,OUT1,KD}},\mathrm{K}_{\mathrm{m,OUT1,KD}}} \left(\frac{\mathrm{f}_{\mathrm{u,BL}} C_{\mathrm{KD}}}{\mathrm{P}_{\mathrm{KD:P}}/\mathrm{P}_{\mathrm{BL:P}}} \right)$
  where OUT1 stands for efflux transporter P-gp,
- $q_{\overrightarrow{\mathrm{Art:KD}}} = \mathrm{Q}_{\mathrm{KD}} \left(C_{\mathrm{Art}} - \frac{C_{\mathrm{KD}}}{\mathrm{P}_{\mathrm{KD:P}}/\mathrm{P}_{\mathrm{BL:P}}} \right),$
- $q_{\overrightarrow{\mathrm{OT:VN}}} = \mathrm{Q}_{\mathrm{OT}} \left(\frac{C_{\mathrm{OT}}}{\mathrm{P}_{\mathrm{OT:P}}/\mathrm{P}_{\mathrm{BL:P}}} - C_{\mathrm{Vein}} \right),$
- $q_{\overrightarrow{\mathrm{Art:OT}}} = \mathrm{Q}_{\mathrm{OT}} \left(C_{\mathrm{Art}} - \frac{C_{\mathrm{OT}}}{\mathrm{P}_{\mathrm{OT:P}}/\mathrm{P}_{\mathrm{BL:P}}} \right),$
- $q_{\overrightarrow{\mathrm{OT:D}}} = \mu C_{\mathrm{OT}},$

- $q_{\overrightarrow{\mathrm{Art:ES}}} = \mathrm{Q_{LV}} C_{\mathrm{Art}}$,
- $q_{\overrightarrow{\mathrm{ES:VN}}} = \mathrm{Q_{LV}} C_{\mathrm{LV}}$,
- $q_{\overrightarrow{\mathrm{ES:LC}}} = \mathrm{Q_{ES-LC,LV}} \left(\mathrm{f_{u,ES}} \frac{C_{\mathrm{ES}}}{\mathrm{P_{ES:P}}} - \mathrm{f_{u,LC}} \frac{C_{\mathrm{LC}}}{\mathrm{P_{LC:P}}} \right) + \mathrm{MM}_{\mathrm{J_{max,UP1,ES}, K_{m,UP1,ES}}} \left(\frac{\mathrm{f_{u,ES}} C_{\mathrm{ES}}}{\mathrm{P_{ES:P}}} \right)$,
- $q_{\overrightarrow{\mathrm{LC:B}}} = \mathrm{MM}_{\mathrm{J_{max,OUT1,LC}, K_{m,OUT1,LC}}} \left(\frac{\mathrm{f_{u,LC}} C_{\mathrm{LC}}}{\mathrm{P_{LC:P}}} \right) + \mathrm{MM}_{\mathrm{J_{max,OUT2,LC}, K_{m,OUT2,LC}}} \left(\frac{\mathrm{f_{u,LC}} C_{\mathrm{LC}}}{\mathrm{P_{LC:P}}} \right)$
  where UP1 stands for OATPs and OUT2 stands for efflux transporter MRP-2,
- $q_{\overrightarrow{\mathrm{LC:M}}} = \mathrm{CL_{CYP}} \mathrm{f_{u,LC}} \frac{C_{\mathrm{LC}}}{\mathrm{P_{LC:P}}}$.

Generally, state equation per compartment can be defined as:

$$\text{change in mass} = \text{sum of all inflows of mass} - \text{sum of all outflows of mass.}$$

Accordingly, using the above defined mass flows $q_{\overrightarrow{\mathrm{W:Z}}}$, the state equation (mass balance equation) for each compartment in the closed system (Figure 38) can be written as Equations (10) to (21) below. Using Equations (10) to (21), the mass balance in the system can be confirmed by:

$$\frac{dm_{\mathrm{IV}}}{dt} + \frac{dm_{\mathrm{LG}}}{dt} + \frac{dm_{\mathrm{Vein}}}{dt} + \frac{dm_{\mathrm{OT}}}{dt} + \frac{dm_{\mathrm{KD}}}{dt} + \frac{dm_{\mathrm{Art}}}{dt} + \frac{dm_{\mathrm{ES}}}{dt} + \frac{dm_{\mathrm{LC}}}{dt} + \frac{dm_{\mathrm{B}}}{dt} + \frac{dm_{\mathrm{U}}}{dt} + \frac{dm_{\mathrm{M}}}{dt} + \frac{dm_{\mathrm{D}}}{dt} = 0.$$

Thus, when summed up, all terms on the right hand sides of these equations cancel out, which indicates that the mass balance is held.

B.4 ODEs for Mass Change

- IV dosing compartment

$$\frac{dm_{\mathrm{IV}}}{dt} = -q_{\overrightarrow{\mathrm{IV:VN}}} \tag{B.10}$$

- Lung (LG) compartment

$$\frac{dm_{\mathrm{LG}}}{dt} = q_{\overrightarrow{\mathrm{VN:LG}}} - q_{\overrightarrow{\mathrm{LG:Art}}} \tag{B.11}$$

- Venous blood (Vein) compartment

$$\frac{dm_{\text{Vein}}}{dt} = q_{\overrightarrow{\text{KD:VN}}} + q_{\overrightarrow{\text{ES:VN}}} + q_{\overrightarrow{\text{OT:VN}}} - q_{\overrightarrow{\text{VN:LG}}} + q_{\overrightarrow{\text{IV:VN}}} \tag{B.12}$$

- The combined other organs (OT) compartment

$$\frac{dm_{\text{OT}}}{dt} = q_{\overrightarrow{\text{Art:OT}}} - q_{\overrightarrow{\text{OT:VN}}} - q_{\overrightarrow{\text{OT:D}}} \tag{B.13}$$

- Kidney (KD) compartment

$$\frac{dm_{\text{KD}}}{dt} = q_{\overrightarrow{\text{Art:KD}}} - q_{\overrightarrow{\text{KD:VN}}} - q_{\overrightarrow{\text{KD:U}}} \tag{B.14}$$

- Arterial blood (Art) compartment

$$\frac{dm_{\text{Art}}}{dt} = q_{\overrightarrow{\text{LG:Art}}} - q_{\overrightarrow{\text{Art:KD}}} - q_{\overrightarrow{\text{Art:ES}}} - q_{\overrightarrow{\text{Art:OT}}} \tag{B.15}$$

- Extracellular space (ES) sub-compartment

$$\frac{dm_{\text{ES}}}{dt} = q_{\overrightarrow{\text{Art:ES}}} - q_{\overrightarrow{\text{ES:VN}}} - q_{\overrightarrow{\text{ES:LC}}} \tag{B.16}$$

- Hepatocyte or liver cell (LC) sub-compartment

$$\frac{dm_{\text{LC}}}{dt} = q_{\overrightarrow{\text{ES:LC}}} - q_{\overrightarrow{\text{LC:B}}} - q_{\overrightarrow{\text{LC:M}}} \tag{B.17}$$

- Bile compartment

$$\frac{dm_{\text{B}}}{dt} = q_{\overrightarrow{\text{LC:B}}} \tag{B.18}$$

- Urine compartment

$$\frac{dm_{\text{U}}}{dt} = q_{\overrightarrow{\text{KD:U}}} \tag{B.19}$$

- Compartment for Metabolism in LC

$$\frac{dm_{\text{M}}}{dt} = q_{\overrightarrow{\text{LC:M}}} \tag{B.20}$$

- Exponential Decay Compartment out of OT

$$\frac{dm_{\text{D}}}{dt} = q_{\overrightarrow{\text{OT:D}}} \tag{B.21}$$

The ODE equations for *change in drug concentrations*, Equations (1) to (7), can be derived by dividing both sides of each equation of Equations (11) to (17) by the volume of the corresponding compartment, V_{LG}, V_{Vein}, V_{OT}, V_{KD}, V_{Art}, $V_{ES,eff}$, and V_{LC}, respectively. Note that $q_{\overrightarrow{IV:VN}}$ is omitted from the ODE equation of Vein compartment, i.e., Equation (2). In addition, we assume that the mass flow $q_{\overrightarrow{Art:ES}}$ from Artery to ES compartment is fast and thus modeled instantaneous as

$$C_{Art} = C_{ES}. \tag{B.22}$$

For the mass flow $q_{\overrightarrow{ES:VN}}$ between ES and Vein compartments, we assume an algebraic relationship

$$C_{LV} = \frac{C_{ES}}{(P_{ES:P}/P_{BL:P})} \tag{B.23}$$

provided by the well-stirred model assumption in our 2-blood compartment model for the blood tissue (i.e., Vein and Artery compartments are modeled separately in iPBPK-R). In other words, Equations (22) and (23) are necessary assumptions in iPBPK-R to approximate the drug flows between the blood tissue and liver organ when the blood is modeled with two separate compartments, Artery and Vein, while retaining the well-stirred model assumption for the blood tissue. This 2-blood compartment model is described in Chapter 2 under preparation (Franchetti et al. In preparation) as well.

In summary, (i) no drug mass is created or lost in the system (the mass invariant holds) since all terms of the right hand sides of Equations (10) - (21) cancel out, (ii) all arrows in Figure 38 align with the signs of the respective flows in the state equations, (iii) all flows are anti-symmetric since an in-flow on one compartment is the same as the out-flow on the other compartment, and (iv) all drug flows and compartments correspond to Figure 38. Our purpose is to estimate the parameters related to non-renal elimination pathways with observed clinical data. While its set-up may differ from a conventional PBPK model, the iPBPK-R model served this goal well. Our model is mathematically consistent and correct given the mathematical principle of mass balance in a closed system established by (i)-(iv).

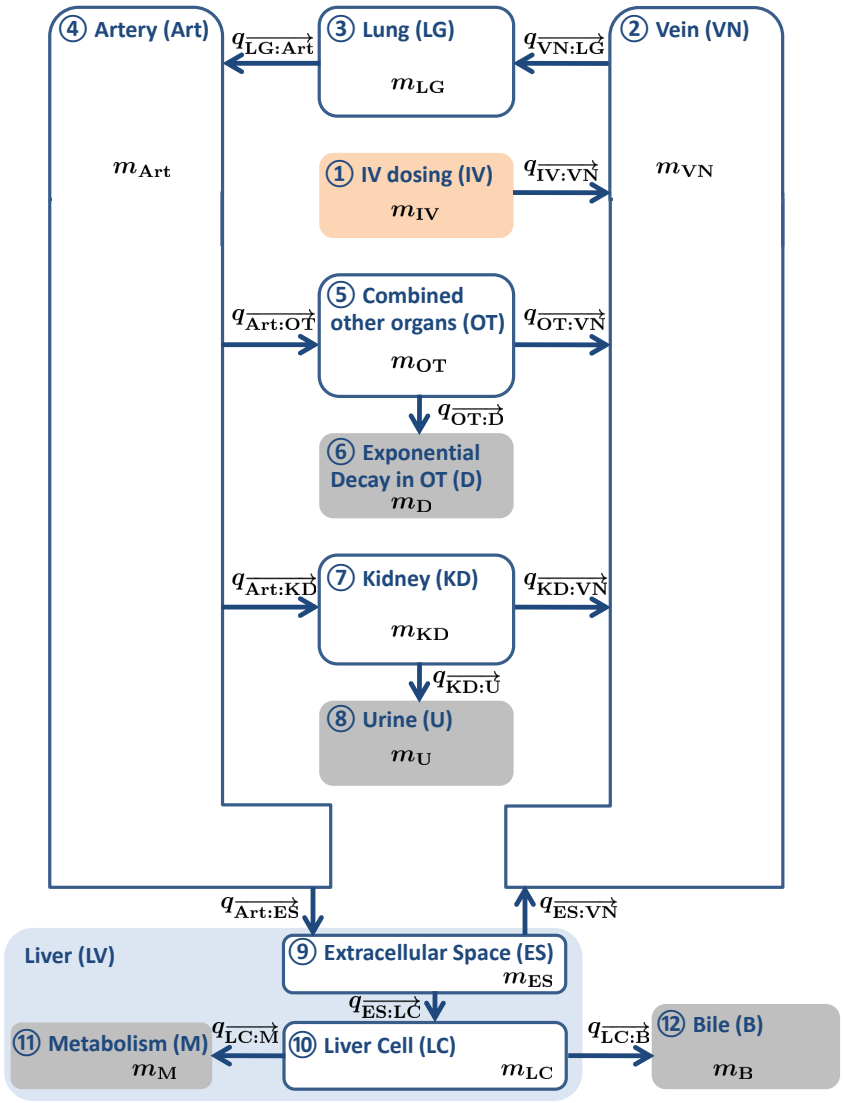

Figure 38: Mass balance in iPBPK-R

Appendix C

Nonlinear Systems of ODEs for Temsirolimus and Sirolimus in Healthy Subjects

We detail the set of ODEs used in Chapter 5, i.e., the PBPK models of temsirolimus and sirolimus for healthy subjects. These were built following the procedure to set up the PBPK model of ^{14}C-erythromycin as shown in Tables 7 and 9 in Chapter 2.

C.1 ODEs for Concentration Change

C.1.1 Parent drug: Temsirolimus

A set of ODEs to model the rate of change in parent drug concentrations for healthy subjects in Period 1 (IV dosing of temsirolimus alone) or Period 2 (IV dosing of temsirolimus with orally administered rifampin) are listed below. C stands for the blood concentrations of temsirolimus. Note that initial concentrations (at time 0) in all compartments are 0 except Vein compartment. Other related notation are shown in Table 24.

- Lung (LG) compartment

$$\frac{dC_{\mathrm{LG}}}{dt} = \frac{1}{\mathrm{V_{LG}}}\left[\mathrm{Q_{Total}}\left(C_{\mathrm{Vein}} - \frac{C_{\mathrm{LG}}}{\mathrm{P_{LG:P}/P_{BL:P}}}\right) - \mathrm{Q_{Total}}\left(\frac{C_{\mathrm{LG}}}{\mathrm{P_{LG:P}/P_{BL:P}}} - C_{\mathrm{Art}}\right)\right] \quad \text{(C.1)}$$

- Venous blood (Vein) compartment

$$\frac{dC_{\text{Vein}}}{dt} = \frac{1}{\text{V}_{\text{Vein}}}\Bigg[\text{Q}_{\text{KD}}\left(\frac{C_{\text{KD}}}{\text{P}_{\text{KD:P}}/\text{P}_{\text{BL:P}}} - C_{\text{Vein}}\right) + \text{Q}_{\text{LV}}\frac{C_{\text{LV}}}{\text{P}_{\text{ES:P}}/\text{P}_{\text{BL:P}}} + \text{Q}_{\text{OT}}\left(\frac{C_{\text{OT}}}{\text{P}_{\text{OT:P}}/\text{P}_{\text{BL:P}}} - C_{\text{Vein}}\right) - \text{Q}_{\text{Total}}\left(C_{\text{Vein}} - \frac{C_{\text{LG}}}{\text{P}_{\text{LG:P}}/\text{P}_{\text{BL:P}}}\right)\Bigg] + \text{infusion rate } (\mu\text{mol/L/time}) \tag{C.2}$$

- The combined other organs (OT) compartment

$$\frac{dC_{\text{OT}}}{dt} = \frac{1}{\text{V}_{\text{OT}}}\left[\text{Q}_{\text{OT}}\left(C_{\text{Art}} - \frac{C_{\text{OT}}}{\text{P}_{\text{OT:P}}/\text{P}_{\text{BL:P}}}\right) - \text{Q}_{\text{OT}}\left(\frac{C_{\text{OT}}}{\text{P}_{\text{OT:P}}/\text{P}_{\text{BL:P}}} - C_{\text{Vein}}\right) - \mu C_{\text{OT}}\right] \tag{C.3}$$

where μ is a parameter of exponential decay that explains loss or decomposition of the parent drug (temsirolimus).

- Kidney (KD) compartment

$$\frac{dC_{\text{KD}}}{dt} = \frac{1}{\text{V}_{\text{KD}}}\left[\text{Q}_{\text{KD}}\left(C_{\text{Art}} - \frac{C_{\text{KD}}}{\text{P}_{\text{KD:P}}/\text{P}_{\text{BL:P}}}\right) - \text{Q}_{\text{KD}}\left(\frac{C_{\text{KD}}}{\text{P}_{\text{KD:P}}/\text{P}_{\text{BL:P}}} - C_{\text{Vein}}\right) - \text{CL}_{\text{R}}\frac{C_{\text{KD}}}{\text{P}_{\text{KD:P}}/\text{P}_{\text{BL:P}}}\right] \tag{C.4}$$

where CL_{R} is overall renal clearance so fraction unbound in the kidney compartment is not accounted for.

- Arterial blood (Art) compartment

$$\frac{dC_{\text{Art}}}{dt} = \frac{1}{\text{V}_{\text{Art}}}\Bigg[\text{Q}_{\text{Total}}\left(\frac{C_{\text{LG}}}{\text{P}_{\text{LG:P}}/\text{P}_{\text{BL:P}}} - C_{\text{Art}}\right) - \text{Q}_{\text{KD}}\left(C_{\text{Art}} - \frac{C_{\text{KD}}}{\text{P}_{\text{KD:P}}/\text{P}_{\text{BL:P}}}\right) - \text{Q}_{\text{LV}}C_{\text{Art}} - \text{Q}_{\text{OT}}\left(C_{\text{Art}} - \frac{C_{\text{OT}}}{\text{P}_{\text{OT:P}}/\text{P}_{\text{BL:P}}}\right)\Bigg] \tag{C.5}$$

- Extracellular space (ES) sub-compartment

$$\frac{dC_{\text{ES}}}{dt} = \frac{1}{\text{V}_{\text{ES,eff}}}\Bigg[\text{Q}_{\text{LV,Art}}C_{\text{Art}} - \text{Q}_{\text{LV,Vein}}\frac{C_{\text{ES}}}{(\text{P}_{\text{ES:P}}/\text{P}_{\text{BL:P}})} - \text{Q}_{\text{ES-LC,LV}}\left(\text{f}_{\text{u,ES}}\frac{C_{\text{ES}}}{\text{P}_{\text{ES:P}}} - \text{f}_{\text{u,LC}}\frac{C_{\text{LC}}}{\text{P}_{\text{LC:P}}}\right)\Bigg] \tag{C.6}$$

where $\text{Q}_{\text{ES-LC,LV}}$ is the clearance by passive diffusion and $\text{V}_{\text{ES,eff}}$ is the effective volume of extracellular space defined as $\text{V}_{\text{ES,eff}} = \text{V}_{\text{ES}} + \frac{\text{V}_{\text{VS}}}{\text{K}_{\text{EW:B}}}$. VS and EW stand for vascular space

and extracellular water, respectively.

- Hepatocyte or liver cell (LC) sub-compartment

$$\frac{dC_{\mathrm{LC}}}{dt} = \frac{1}{\mathrm{V_{LC}}}\Bigg[\mathrm{Q_{ES-LC,LV}}\Big(\mathrm{f_{u,ES}}\frac{C_{\mathrm{ES}}}{\mathrm{P_{ES:P}}} - \mathrm{f_{u,LC}}\frac{C_{\mathrm{LC}}}{\mathrm{P_{LC:P}}}\Big) - \frac{\alpha_1 \mathrm{J_{Max,OUT1,LC}}(\frac{\mathrm{f_{u,LC}}}{\mathrm{P_{LC:P}}})C_{\mathrm{LC}}}{\mathrm{K_{m,OUT1,LC}} + (\frac{\mathrm{f_{u,LC}}}{\mathrm{P_{LC:P}}})C_{\mathrm{LC}}} - \alpha_2 \mathrm{CL_{CYP3A4}}\mathrm{f_{u,LC}}\frac{C_{\mathrm{LC}}}{\mathrm{P_{LC:P}}} - \mathrm{CL_{EST}}\mathrm{f_{u,LC}}\frac{C_{\mathrm{LC}}}{\mathrm{P_{LC:P}}}\Bigg] \tag{C.7}$$

where OUT1 stands for P-gp efflux transporter while CYP3A4 and EST stand for metabolism by CYP3A4 and esterase, respectively. α_1 and α_2 are scaling factors (inhibition and/or induction coefficients) when rifampin is co-administered in period 2.

C.1.2 Active metabolite: Sirolimus

A set of ODEs to model the rate of change in active metabolite concentrations for healthy subjects in Period 1 (IV dosing of temsirolimus alone) or Period 2 (IV dosing of temsirolimus with orally administered rifampin) are listed below. $C^\star$ stands for the blood concentrations of sirolimus and $\star$ denotes sirolimus. Note that initial concentrations (at time 0) in all compartments are 0. Other related notation are shown in Table 24.

- Lung (LG) compartment

$$\frac{dC^\star_{\mathrm{LG}}}{dt} = \frac{1}{\mathrm{V_{LG}}}\left[\mathrm{Q_{Total}}\left(C^\star_{\mathrm{Vein}} - \frac{C^\star_{\mathrm{LG}}}{\mathrm{P^\star_{LG:P}}/\mathrm{P^\star_{BL:P}}}\right) - \mathrm{Q_{Total}}\left(\frac{C^\star_{\mathrm{LG}}}{\mathrm{P^\star_{LG:P}}/\mathrm{P^\star_{BL:P}}} - C^\star_{\mathrm{Art}}\right)\right] \tag{C.8}$$

- Venous blood (Vein) compartment

$$\frac{dC^\star_{\mathrm{Vein}}}{dt} = \frac{1}{\mathrm{V_{Vein}}}\Bigg[\mathrm{Q_{KD}}\left(\frac{C^\star_{\mathrm{KD}}}{\mathrm{P^\star_{KD:P}}/\mathrm{P^\star_{BL:P}}} - C^\star_{\mathrm{Vein}}\right) + \mathrm{Q_{LV}}\frac{C^\star_{\mathrm{LV}}}{\mathrm{P^\star_{ES:P}}/\mathrm{P^\star_{BL:P}}} + \mathrm{Q_{OT}}\left(\frac{C^\star_{\mathrm{OT}}}{\mathrm{P^\star_{OT:P}}/\mathrm{P^\star_{BL:P}}} - C^\star_{\mathrm{Vein}}\right) - \mathrm{Q_{Total}}\left(C^\star_{\mathrm{Vein}} - \frac{C^\star_{\mathrm{LG}}}{\mathrm{P^\star_{LG:P}}/\mathrm{P^\star_{BL:P}}}\right)\Bigg] \tag{C.9}$$

- The combined other organs (OT) compartment

$$\frac{dC^\star_{\mathrm{OT}}}{dt} = \frac{1}{\mathrm{V_{OT}}}\left[\mathrm{Q_{OT}}\left(C^\star_{\mathrm{Art}} - \frac{C^\star_{\mathrm{OT}}}{\mathrm{P^\star_{OT:P}}/\mathrm{P^\star_{BL:P}}}\right) - \mathrm{Q_{OT}}\left(\frac{C^\star_{\mathrm{OT}}}{\mathrm{P^\star_{OT:P}}/\mathrm{P^\star_{BL:P}}} - C^\star_{\mathrm{Vein}}\right) - \mu^\star C^\star_{\mathrm{OT}}\right] \tag{C.10}$$

where $\mu^\star$ is a parameter of exponential decay that explains loss or decomposition of the active metabolite drug (sirolimus).

- Kidney (KD) compartment

$$\frac{dC^\star_{\mathrm{KD}}}{dt} = \frac{1}{\mathrm{V_{KD}}}\Bigg[\mathrm{Q_{KD}}\left(C^\star_{\mathrm{Art}} - \frac{C^\star_{\mathrm{KD}}}{\mathrm{P^\star_{KD:P}}/\mathrm{P^\star_{BL:P}}}\right) - \mathrm{Q_{KD}}\left(\frac{C^\star_{\mathrm{KD}}}{\mathrm{P^\star_{KD:P}}/\mathrm{P^\star_{BL:P}}} - C^\star_{\mathrm{Vein}}\right) - \mathrm{CL^\star_R}\frac{C^\star_{\mathrm{KD}}}{\mathrm{P^\star_{KD:P}}/\mathrm{P^\star_{BL:P}}}\Bigg] \tag{C.11}$$

where $\mathrm{CL^\star_R}$ is overall renal clearance so fraction unbound in the kidney compartment is not accounted for.

- Arterial blood (Art) compartment

$$\frac{dC^\star_{\mathrm{Art}}}{dt} = \frac{1}{\mathrm{V_{Art}}}\Bigg[\mathrm{Q_{Total}}\left(\frac{C^\star_{\mathrm{LG}}}{\mathrm{P^\star_{LG:P}}/\mathrm{P^\star_{BL:P}}} - C^\star_{\mathrm{Art}}\right) - \mathrm{Q_{KD}}\left(C^\star_{\mathrm{Art}} - \frac{C^\star_{\mathrm{KD}}}{\mathrm{P^\star_{KD:P}}/\mathrm{P^\star_{BL:P}}}\right) - \mathrm{Q_{LV}}C^\star_{\mathrm{Art}} - \mathrm{Q_{OT}}\left(C^\star_{\mathrm{Art}} - \frac{C^\star_{\mathrm{OT}}}{\mathrm{P^\star_{OT:P}}/\mathrm{P^\star_{BL:P}}}\right)\Bigg] \tag{C.12}$$

- Extracellular space (ES) sub-compartment

$$\frac{dC^\star_{\mathrm{ES}}}{dt} = \frac{1}{\mathrm{V^\star_{ES,eff}}}\Bigg[\mathrm{Q_{LV,Art}}C^\star_{\mathrm{Art}} - \mathrm{Q_{LV,Vein}}\frac{C^\star_{\mathrm{ES}}}{(\mathrm{P^\star_{ES:P}}/\mathrm{P^\star_{BL:P}})} - \mathrm{Q^\star_{ES-LC,LV}}\left(\mathrm{f^\star_{u,ES}}\frac{C^\star_{\mathrm{ES}}}{\mathrm{P^\star_{ES:P}}} - \mathrm{f^\star_{u,LC}}\frac{C^\star_{\mathrm{LC}}}{\star\mathrm{P_{LC:P}}}\right)\Bigg] \tag{C.13}$$

where $\mathrm{Q^\star_{ES-LC,LV}}$ is the clearance by passive diffusion and $\mathrm{V_{ES,eff}}$ is the effective volume of extracellular space defined as $\mathrm{V^\star_{ES,eff}} = \mathrm{V_{ES}} + \frac{\mathrm{V_{VS}}}{\mathrm{K^\star_{EW:B}}}$. VS and EW stand for vascular space and extracellular water, respectively.

- Hepatocyte or liver cell (LC) sub-compartment

$$\frac{dC_{\mathrm{LC}}}{dt} = \frac{1}{\mathrm{V_{LC}}}\Bigg[\mathrm{Q^\star_{ES-LC,LV}}\left(\mathrm{f^\star_{u,ES}}\frac{C^\star_{\mathrm{ES}}}{\mathrm{P^\star_{ES:P}}} - \mathrm{f^\star_{u,LC}}\frac{C^\star_{\mathrm{LC}}}{\mathrm{P^\star_{LC:P}}}\right) - \frac{\alpha^\star_1\mathrm{J^\star_{Max,OUT1,LC}}(\frac{\mathrm{f^\star_{u,LC}}}{\mathrm{P^\star_{LC:P}}})C^\star_{\mathrm{LC}}}{\mathrm{K^\star_{m,OUT1,LC}} + (\frac{\mathrm{f^\star_{u,LC}}}{\mathrm{P^\star_{LC:P}}})C^\star_{\mathrm{LC}}} - \alpha^\star_2\mathrm{CL^\star_{CYP3A4}}\mathrm{f^\star_{u,LC}}\frac{C^\star_{\mathrm{LC}}}{\mathrm{P^\star_{LC:P}}} - \alpha^\star_3\mathrm{CL^\star_{NONCYP3A4}}\mathrm{f^\star_{u,LC}}\frac{C^\star_{\mathrm{LC}}}{\mathrm{P^\star_{LC:P}}} + \mathrm{CL_{EST}}\mathrm{f_{u,LC}}\frac{C_{\mathrm{LC}}}{\mathrm{P_{LC:P}}}\Bigg] \tag{C.14}$$

where OUT1 stands for P-gp efflux transporter while CYP3A4 and NONCYP3A4 stand

for metabolism by CYP3A4 and non-CYP3A4 dependent enzyme, respectively. $\alpha_1^\star$, $\alpha_2^\star$, and $\alpha_3^\star$ are scaling factors (inhibition and/or induction coefficients) when rifampin is co-administered in period 2.

We assume that the metabolized amount of temsirolimus by esterase and generation of sirolimus in hepatocyte have a one-to-one molar relationship (no rate-limiting step) in Equation (C.14).

Appendix D

Derivation of IVIVE Values based on MDR1-MDCK Data for sirolimus

In this appendix, derivations of surrogate IVIVE values for intrinsic clearance of P-gp and total passive diffusion between extracellular space and hepatocyte are shown. These surrogate IVIVEs were used as initial inputs in the iPBPK-R modeling for sirolimus (Table 27). The surrogate IVIVE values for temsirolimus (Table 26) were calculated in a similar fashion.

D.1 In vivo intrinsic clearance of P-gp for sirolimus $\mathrm{CL_{OUT1(m)}}$

The *in vitro* P-gp clearance data for sirolimus from literature [233] was used to calculate the surrogate *in vivo* intrinsic clearance of P-gp for sirolimus ($\mathrm{CL_{OUT1(m)}}$ in Table 27). The cell culture system of this *in vitro* experiment was based on MDR1-transfected MDCK cells but not hepatocytes. Therefore, the IVIVE calculation was adjusted by multiplying an IVIVE equation in literature with the ratio of cell volumes between MDCK and hepatocyte. First, adopting Burt et al. [68], an IVIVE equation to calculate *in vivo* intrinsic clearance of P-gp transpoter in the liver for sirolimus can be expressed as

$$\mathrm{CL_{OUT1(m)[L/hr]}} = \mathrm{CL_{int(m)}} \times \mathrm{RAF} \times \mathrm{F} \times \mathrm{HPGL} \times \mathrm{Liver\,Weight} \times 60^{-6}, \tag{D.1}$$

where $\mathrm{CL_{int(m)}}$ is the *in vitro* intrinsic clearance for P-gp [μL/(min$\cdot$ million hepatocytes)], RAF is the activity ratio of P-gp between *in vivo* and *in vitro* hepatocytes, F is the relative abundance for the phenotype of P-gp, HPGL is the number of hepatocytes per gram of the human liver, and Liver Weight is the human liver weight in gram.

For convenience, we convert the units in the above equation as follows.

$$\mathrm{CL_{OUT1(m)[L/hr]}} = \mathrm{CL_{int,cell(m)}} \times \mathrm{RAF} \times \mathrm{F} \times \mathrm{HPGL} \times \mathrm{Liver\,Weight}, \tag{D.2}$$

where $\mathrm{CL_{int,cell(m)}}$ is the *in vitro* intrinsic clearance for P-gp [μL/(hr· hepatocytes)]. Next, we approximate $\mathrm{CL_{int,cell(m)}}$ using the ratio of typical cell volumes between MDCK and hepatocyte as

$$\mathrm{CL_{int,cell(m)[\mu L/(hr\cdot hepatocytes)]}} = \frac{\beta \cdot \frac{2.08\times10^{-9}[\mathrm{cm^3}]}{3.4\times10^{-9}[\mathrm{cm^3}]}}{\mathrm{N_{cells}}},$$

where β is the *in vitro* intrinsic transporter clearance per cell for P-gp in MDR1-MDCK, $2.08 \times 10^{-9}[\mathrm{cm^3}]$ is the typical cell volume of MDCK [266], $3.4 \times 10^{-9}[\mathrm{cm^3}]$ is the typical cell volume of hepatocyte [258], and $\mathrm{N_{cells}}$ is the number of cells per insert in the *in vitro* experiment. Note that the typical cell volumes of MDCK and MDR1-MDCK cells are assumed to be the same in the above equation.

Let us assume that RAF = 1 and F = 1 in eq. (D.2) since RAF for P-gp activity was designed to be estimated as part of the iPBPK-R modeling (see section 5.3.6, Figure 32, and Table 22). Furthermore, $\mathrm{HPGL} = 99 \times 10^6_{\mathrm{[cells/gLiver]}}$ [67] and Liver Weight for a 70-kg male is 2.3% of the body weight [5]. Therefore, by replacing $\mathrm{CL_{int,cell(m)}}$ with the above equation into eq. (D.2),

$$\mathrm{CL_{OUT1(m)[L/hr]}} = \frac{\beta \cdot \frac{2.08\times10^{-9}[\mathrm{cm^3}]}{3.4\times10^{-9}[\mathrm{cm^3}]}}{\mathrm{N_{cells}}} \times 1 \times 1 \times (99 \times 10^6)_{\mathrm{[cells/gLiver]}} \times (70_{\mathrm{[kg]}} \times 0.023 \times 10^3)_{\mathrm{[gLiver]}}, \tag{D.3}$$

D.2 In vivo total passive diffusion between extracellular space and hepatocyte for sirolimus $\mathrm{Q_{ES-LC(m)}}$

In the calculation of the surrogate IVIVE of total passive diffusion for sirolimus ($\mathrm{Q_{ES-LC(m)}}$ in Table 27), the same MDR1-MDCK experimental data above was used [233]. Therefore, the derived form of our IVIVE equation below is similar to the one for P-gp eq. (D.3).

$$\mathrm{Q_{ES-LC(m)[L/hr]}} = \frac{\alpha \cdot \frac{2.08\times10^{-9}[\mathrm{cm^3}]}{3.4\times10^{-9}[\mathrm{cm^3}]}}{\mathrm{N_{cells}}} \times 1 \times 1 \times (99 \times 10^6)_{\mathrm{[cells/gLiver]}} \times (70_{\mathrm{[kg]}} \times 0.023 \times 10^3)_{\mathrm{[gLiver]}}, \tag{D.4}$$

where α is the *in vitro* intrinsic passive diffusion in MDR1-MDCK and N_{cells} is the number of cells per insert in the *in vitro* experiment. Similar to the RAF for P-gp, this surrogate IVIVE of passive diffusion for sirolilmus was optimized based on the sensitivity analysis of the iPBPK-R modeling (see section 5.3.6 and Figure 32).

D.3 Calculation of in vitro values for sirolimus from literature

In this subsection, we derive the *in vitro* intrinsic transporter clearance for P-gp in MDR1-MDCK (β in eq. (D.3)) and the *in vitro* intrinsic passive diffusion in MDR1-MDCK (α in eq. (D.4)) from the experimental data in literature [233]. N_{cells} that is commonly used in these equations will be also calculated.

Let us suppose that the transwell cell culture system used in the literature can be illustrated with parameters as in Figure 39. A and B denote the apical side and basolateral side of the MDR1-MDCK cell monolayer, respectively. The left panel of the figure shows the cell monolayer model with parameters used when we consider the permeability from A to B (i.e., $P_{APP(A\to B)}$), while the right panel shows the same cell monolayer model with parameters when we consider the permeability from B to A (i.e., $P_{APP(B\to A)}$).

In the left panel of Figure 39, C_1, C_2, and C_3 denote concentrations of sirolimus in A, in the cell monolayer, and in B, respectively. In the right panel of Figure 39, C_1', C_2', and C_3' denote concentrations of sirolimus in B, in the cell monolayer, and in A, respectively. In both panels, γ_1, γ_2, and γ_3 denote the observed fluxes (i.e., velocities or observed amounts transferred per time) of sirolimus via P-gp, passive diffusion at A, and passive diffusion at B, respectively. Both panels show the direction of each γ with a red arrow for setting up equations of flux shortly.

Using the literature data [233], let $C_1 = C_1' = 1[\mu\text{M}]$, and $C_3 = C_3' = 0[\mu\text{M}]$ at time 0 [sec]. C_2 and C_2' are unknown and assumed to be consistent at steady-state. Note that all fluxes are assumed to be linear in time in this calculation. Then, to each of the net fluxes with permeability $P_{APP(A\to B)}$ and $P_{APP(B\to A)}$ in Figure 39, we apply a general net flux

equation of an *in vitro* transwell experiment,

$$\mathrm{J} = \mathrm{V}\frac{dC}{dt} = \mathrm{P_{APP}} \cdot \mathrm{A} \cdot (C_{\mathrm{out}} - C_{\mathrm{in}}), \tag{D.5}$$

where J is a net flux, V is volume of flux, A is surface area of the membrane, C_{out} is the drug concentration at the side where the drug is applied in the transwell experiment, and C_{in} is the drug concentration at the other side of the transwell (based on fluid dynamics). Accordingly, based on the left and right panels of Figure 39, the net fluxes of A to B and B to A (denoting $\mathrm{K_1}$ and $\mathrm{K_2}$, respectively) are calculated as

$$\begin{aligned}
\mathrm{K_1} &= \mathrm{P_{APP(A\to B)}} \cdot \mathrm{A} \cdot (C_1 - C_3) \\
&= (0.043 \times 10^{-7}_{[\mathrm{dm/s}]}) \cdot (4.2 \times 10^{-2}_{[\mathrm{dm^2}]}) \cdot 1_{[\mu\mathrm{mol/L}]}, \qquad \text{(D.6)} \\
&= 1.806 \times 10^{-10}_{[\mu\mathrm{mol/s}]}, \text{ and} \\
\mathrm{K_2} &= \mathrm{P_{APP(B\to A)}} \cdot \mathrm{A} \cdot (C_1' - C_3') \\
&= (0.35 \times 10^{-6}_{[\mathrm{dm/s}]}) \cdot (4.2 \times 10^{-2}_{[\mathrm{dm^2}]}) \cdot 1_{[\mu\mathrm{mol/L}]}, \qquad \text{(D.7)} \\
&= 1.47 \times 10^{-8}_{[\mu\mathrm{mol/s}]}.
\end{aligned}$$

Then, each observed flux γ can be expressed with α, β and C, and from the constructed equations α and β can be eventually calculated. First, based on the left panel of Figure 39, the net flux $\mathrm{K_1}$ in eq. (D.6) is expressed with γ as

$$\mathrm{K_1} = \gamma_1 = \gamma_2 - \gamma_3. \tag{D.8}$$

Since each observed flux γ is

$$\gamma_1 = \alpha(C_2 - C_3) = \alpha C_2, \tag{D.9}$$

$$\gamma_2 = \alpha(C_1 - C_2) = \alpha(1_{[\mu\mathrm{M}]} - C_2), \text{ and} \tag{D.10}$$

$$\gamma_3 = \beta C_2, \tag{D.11}$$

plugging eq. (D.9)–eq. (D.11) into eq. (D.8) gives

$$\mathrm{K_1} = \frac{\alpha^2}{2\alpha + \beta}. \tag{D.12}$$

Similarly, based on the right panel of Figure 39, we set up

$$\mathrm{K}_2 = \gamma_1 = \gamma_2 + \gamma_3, \text{ where} \tag{D.13}$$

$$\gamma_1 = \alpha(C_1' - C_2') = \alpha(1_{[\mu\mathrm{M}]} - C_2'), \tag{D.14}$$

$$\gamma_2 = \alpha(C_2' - C_3') = \alpha C_2', \text{ and} \tag{D.15}$$

$$\gamma_3 = \beta C_2'. \tag{D.16}$$

Plugging eq. (D.14)–eq. (D.16) into eq. (D.13) gives

$$\mathrm{K}_2 = \frac{\alpha + \beta}{2\alpha + \beta}. \tag{D.17}$$

Solving the eq. (D.12) and eq. (D.17) for α and β,

$$\alpha = \mathrm{K}_1 + \mathrm{K}_2, \text{ and} \tag{D.18}$$

$$\beta = \frac{{\mathrm{K}_2}^2 - {\mathrm{K}_1}^2}{\mathrm{K}_1}. \tag{D.19}$$

Plugging the values of K_1 and K_2 in eq. (D.6)–eq. (D.7) into eq. (D.18) and eq. (D.19), the *in vitro* P-gp clearance (β) and total passive diffusion (α) are calculated as

$$\alpha = 1.48806 \times 10^{-8}_{[\mathrm{L/s}]} = 5.357 \times 10^{-5}_{[\mathrm{L/hr}]} \quad \text{and}$$
$$\beta = 1.196331 \times 10^{-6}_{[\mathrm{L/s}]} = 4.3068 \times 10^{-3}_{[\mathrm{L/hr}]}.$$

Lastly, in this *in vitro* MDR1-MDCK transwell experiment [233], 250,000 [cells/insert] were seeded into inserts of diameter 4.2 [cm^2], and experiments were conducted after maintaining the culture for 4 to 5 days. Assuming that the cell cycle was 24 [hrs] on average, $\mathrm{N}_{\mathrm{cells}}$ is approximated as

$$\mathrm{N}_{\mathrm{cells}} = 250,000 \times 2^{4.5[\mathrm{days}]} = 5.67 \times 10^{6}_{[\mathrm{cells/insert}]}.$$

Thus, the surrogate IVIVE values of intrinsic P-gp and total passive diffusion in the liver can be calculated by plugging the above β, α and $\mathrm{N}_{\mathrm{cells}}$ into eq. (D.3) and eq. (D.4), respectively.

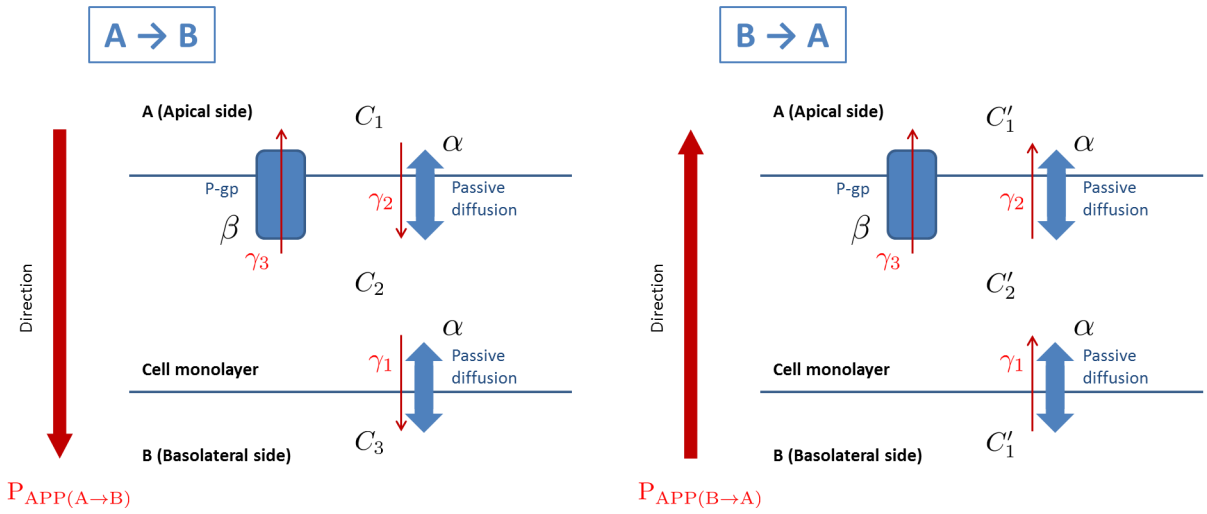

Figure 39: MDR1-MDCK monolayer models for calculating *in vitro* values for sirolimus.

Appendix E

A Procedure to Conduct Deep Learning Simulations for Evaluating iPBPK-R

Presenting individual observed data may not be always possible due to data confidentiality, for instance. To address this issue and demonstrate the performance of iPBPK-R model fit, we outline a procedure to simulate individual clinical datasets using the neural ordinary differential equation approach [285], which is one of the latest machine learning techniques. For instance, individual datasets of temsirolimus and sirolimus can be simulated based on the mean and standard deviation of the same published data [240] used in Chapter 5. The procedure to simulate the individual datasets is as follows.

1. Conduct iPBPK-R model fit to the mean value of the healthy cohort as a virtual person.
2. Obtain 16 optimized parameter values from the iPBPK-R model fit.
3. Randomly sample 10,000 parameter sets from the ± 10% of the parameter values.
4. Use the PBPK models of temsirolimus and sirolimus to simulate 10,000 curves using the 10,000 parameter sets.
5. Train the neural ODE model with the 10,000 curves.
6. Pick independent values randomly at 3 to 5 of 13 sampling time points within the distributional range of the published data (defined with the observed mean ± SD). Then, let the system predict the curve based on the picked values. Take values at the 13 time points from the predicted curve as a simulated data series.
7. Repeat 6. so that a data series can be simulated for N individuals. All simulated datasets will be within the distributional range of the published data.

Using the simulated datasets for N subjects, iPBPK-R model fit can be conducted similar to the study in Chapter 5. Simulating clinical datasets via ML/DL or AI research will facilitate not only the evaluation of iPBPK-R but also overall clinical pharmacology research.

Bibliography

[1] Centers for Disease Control and Prevention. Chronic kidney disease in the united states, 2019. 2019. URL: https://www.cdc.gov/kidneydisease/publications-resources/2019-national-facts.html.

[2] US Department of Health, Human Services Food, Drug Administration Center for Drug Evaluation, and Research (NIDDK). Kidney disease statistics for the united states. Report, December 2016. URL: https://www.niddk.nih.gov/health-information/health-statistics/kidney-disease.

[3] Matthew R Weir and Jeffrey C Fink. Safety of medical therapy in patients with chronic kidney disease and end-stage renal disease. *Current opinion in nephrology and hypertension*, 23(3):306–313, 2014.

[4] M. Pfister, T. D. Nolin, and V. Arya. Optimizing drug development and use in patients with kidney disease: opportunities, innovations, and challenges. *J Clin Pharmacol*, 52(1 Suppl):4S–6S, 2012. URL: https://www.ncbi.nlm.nih.gov/pubmed/22232753, doi:10.1177/0091270011415414.

[5] Malcolm Rowland and Thomas N Tozer. *Clinical pharmacokinetics and pharmacodynamics: Concepts and Applications*. Lippincott Williams and Wilkins Philadelphia, 4 edition, 2011.

[6] M. Neely, D. Bayard, A. Desai, L. Kovanda, and A. Edginton. Pharmacometric modeling and simulation is essential to pediatric clinical pharmacology. *J Clin Pharmacol*, 58 Suppl 10:S73–S85, 2018. URL: https://www.ncbi.nlm.nih.gov/pubmed/30248199, doi:10.1002/jcph.1316.

[7] TD Nolin, J Naud, FA Leblond, and V Pichette. Emerging evidence of the impact of kidney disease on drug metabolism and transport. *Clinical Pharmacology & Therapeutics*, 83(6):898–903, 2008.

[8] US Food and Drug Administration. Physiologically based pharmacokinetic analyses — format and content guidance for industry. Report, US Food and Drug Administration, 2018. URL: https://www.fda.gov/media/101469/download.

[9] M. M. Reidenberg. Early research on renal function and drug action. *J Clin Pharmacol*, 52(1 Suppl):7S–9S, 2012. URL: https://www.ncbi.nlm.nih.gov/pubmed/22232758, doi:10.1177/0091270011413587.

[10] L. Dettli, P. Spring, and R. Habersang. Drug dosage in patients with impaired renal function. *Postgrad Med J*, pages Suppl:32–5, 1970. URL: https://www.ncbi.nlm.nih.gov/pubmed/5488205.

[11] D. W. Cockcroft and M. H. Gault. Prediction of creatinine clearance from serum creatinine. *Nephron*, 16(1):31–41, 1976. URL: https://www.ncbi.nlm.nih.gov/pubmed/1244564, doi:10.1159/000180580.

[12] A. S. Levey, J. P. Bosch, J. B. Lewis, T. Greene, N. Rogers, and D. Roth. A more accurate method to estimate glomerular filtration rate from serum creatinine: a new prediction equation. modification of diet in renal disease study group. *Ann Intern Med*, 130(6):461–70, 1999. URL: https://www.ncbi.nlm.nih.gov/pubmed/10075613.

[13] A. S. Levey, L. A. Stevens, C. H. Schmid, Y. L. Zhang, 3rd Castro, A. F., H. I. Feldman, J. W. Kusek, P. Eggers, F. Van Lente, T. Greene, J. Coresh, and E. P. I. Ckd. A new equation to estimate glomerular filtration rate. *Ann Intern Med*, 150(9):604–12, 2009. URL: https://www.ncbi.nlm.nih.gov/pubmed/19414839, doi:10.7326/0003-4819-150-9-200905050-00006.

[14] J. L. Steffl, W. Bennett, and A. J. Olyaei. The old and new methods of assessing kidney function. *J Clin Pharmacol*, 52(1 Suppl):63S–71S, 2012. URL: https://www.ncbi.nlm.nih.gov/pubmed/22232755, doi:10.1177/0091270011420260.

[15] F. Rodieux, M. Wilbaux, J. N. van den Anker, and M. Pfister. Effect of kidney function on drug kinetics and dosing in neonates, infants, and children. *Clin Pharmacokinet*, 54(12):1183–204, 2015. URL: https://www.ncbi.nlm.nih.gov/pubmed/26138291, doi:10.1007/s40262-015-0298-7.

[16] Y Zhang, L Zhang, S Abraham, S Apparaju, T-C Wu, JM Strong, S Xiao, AJ Atkinson, Kenneth E Thummel, and JS Leeder. Assessment of the impact of renal impairment on systemic exposure of new molecular entities: evaluation of recent new drug applications. *Clinical Pharmacology & Therapeutics*, 85(3):305–311, 2009.

[17] T. N. Lea-Henry, J. E. Carland, S. L. Stocker, J. Sevastos, and D. M. Roberts. Clinical pharmacokinetics in kidney disease: Fundamental principles. *Clin J Am Soc Nephrol*, 13(7):1085–1095, 2018. URL: https://www.ncbi.nlm.nih.gov/pubmed/29934432, doi:10.2215/CJN.00340118.

[18] M. M. Reidenberg, H. Kostenbauder, and W. P. Adams. Rate of drug metabolism in obese volunteers before and during starvation and in azotemic patients. *Metabolism*, 18(3):209–13, 1969. URL: https://www.ncbi.nlm.nih.gov/pubmed/4887616, doi:10.1016/0026-0495(69)90040-7.

[19] M. M. Reidenberg. Kidney disease and drug metabolism. *Med Clin North Am*, 58(5):1059–62, 1974. URL: https://www.ncbi.nlm.nih.gov/pubmed/4608133, doi:10.1016/s0025-7125(16)32101-0.

[20] J. K. Aronson and D. G. Grahame-Smith. Altered distribution of digoxin in renal failure–a cause of digoxin toxicity? *Br J Clin Pharmacol*, 3(6):1045–51, 1976. URL: https://www.ncbi.nlm.nih.gov/pubmed/22216528, doi:10.1111/j.1365-2125.1976.tb00356.x.

[21] A. L. Rubin, K. H. Stenzel, and M. M. Reidenberg. Symposium on drug action and metabolism in renal failure: foreword. *Am J Med*, 62(4):459–60, 1977. URL: https://www.ncbi.nlm.nih.gov/pubmed/851112, doi:10.1016/0002-9343(77)90396-5.

[22] M. M. Reidenberg. The binding of drugs to plasma proteins and the interpretation of measurements of plasma concentrations of drugs in patients with poor renal function. *Am J Med*, 62(4):466–70, 1977. URL: https://www.ncbi.nlm.nih.gov/pubmed/851114, doi:10.1016/0002-9343(77)90398-9.

[23] D. T. Lowenthal and M. M. Reidenberg. The heart rate response to atropine in uremic patients, obese subjects before and during fasting, and patients with other chronic illnesses. *Proc Soc Exp Biol Med*, 139(2):390–3, 1972. URL: https://www.ncbi.nlm.nih.gov/pubmed/4550935, doi:10.3181/00379727-139-36150.

[24] Astrid M Suchy-Dicey, Thomas Laha, Andrew Hoofnagle, Rick Newitt, Tammy L Sirich, Timothy W Meyer, Ken E Thummel, N David Yanez, Jonathan Himmelfarb, and Noel S Weiss. Tubular secretion in ckd. *J Am Soc Nephrol*, 27(7):2148–55, 2016.

[25] J. Q. Hudson and T. D. Nolin. Pragmatic use of kidney function estimates for drug dosing: The tide is turning. *Adv Chronic Kidney Dis*, 25(1):14–20, 2018. URL: https://www.ncbi.nlm.nih.gov/pubmed/29499882, doi:10.1053/j.ackd.2017.10.003.

[26] S. Hirata. [appropriate pharmacotherapy in patients with chronic kidney disease - new approach -]. *Yakugaku Zasshi*, 132(4):461–70, 2012. URL: https://www.ncbi.nlm.nih.gov/pubmed/22465923, doi:10.1248/yakushi.132.461.

[27] L. A. Stevens, J. Coresh, T. Greene, and A. S. Levey. Assessing kidney function–measured and estimated glomerular filtration rate. *N Engl J Med*, 354(23):2473–83, 2006. URL: https://www.ncbi.nlm.nih.gov/pubmed/16760447, doi:10.1056/NEJMra054415.

[28] A. S. Levey, J. Coresh, T. Greene, L. A. Stevens, Y. L. Zhang, S. Hendriksen, J. W. Kusek, F. Van Lente, and Collaboration Chronic Kidney Disease Epidemiology. Using standardized serum creatinine values in the modification of diet in renal disease study equation for estimating glomerular filtration rate. *Ann Intern Med*, 145(4):247–54, 2006. URL: https://www.ncbi.nlm.nih.gov/pubmed/16908915, doi:10.7326/0003-4819-145-4-200608150-00004.

[29] J. O. Miners, X. Yang, K. M. Knights, and L. Zhang. The role of the kidney in drug elimination: Transport, metabolism, and the impact of kidney disease on drug clearance. *Clin Pharmacol Ther*, 102(3):436–449, 2017. URL: https://www.ncbi.nlm.nih.gov/pubmed/28599065, doi:10.1002/cpt.757.

[30] Melanie S Joy, Reginald F Frye, Thomas D Nolin, Brittney V Roberts, Mary K La, Jinzhao Wang, Kim LR Brouwer, Mary Anne Dooley, and Ronald J Falk. In vivo alterations in drug metabolism and transport pathways in patients with chronic kidney diseases. *Pharmacotherapy*, 34(2):114–122, 2014.

[31] M. S. Joy. Impact of glomerular kidney diseases on the clearance of drugs. *J Clin Pharmacol*, 52(1 Suppl):23S–34S, 2012. URL: https://www.ncbi.nlm.nih.gov/pubmed/22232750, doi:10.1177/0091270011413895.

[32] R. Vanholder, R. De Smet, G. Glorieux, A. Argiles, U. Baurmeister, P. Brunet, W. Clark, G. Cohen, P. P. De Deyn, R. Deppisch, B. Descamps-Latscha, T. Henle, A. Jorres, H. D. Lemke, Z. A. Massy, J. Passlick-Deetjen, M. Rodriguez, B. Stegmayr, P. Stenvinkel, C. Tetta, C. Wanner, W. Zidek, and Group European Uremic Toxin Work. Review on uremic toxins: classification, concentration, and interindividual variability. *Kidney Int*, 63(5):1934–43, 2003. URL: https://www.ncbi.nlm.nih.gov/pubmed/12675874, doi:10.1046/j.1523-1755.2003.00924.x.

[33] N. Meert, E. Schepers, R. De Smet, A. Argiles, G. Cohen, R. Deppisch, T. Drueke, Z. Massy, G. Spasovski, B. Stegmayr, W. Zidek, J. Jankowski, and R. Vanholder. Inconsistency of reported uremic toxin concentrations. *Artif Organs*, 31(8):600–11, 2007. URL: https://www.ncbi.nlm.nih.gov/pubmed/17651115, doi:10.1111/j.1525-1594.2007.00434.x.

[34] Flore Duranton, Gerald Cohen, Rita De Smet, Mariano Rodriguez, Joachim Jankowski, Raymond Vanholder, and Angel Argiles. Normal and pathologic concentrations of uremic toxins. *Journal of the American Society of Nephrology*, page ASN. 2011121175, 2012.

[35] D. A. Volpe, G. A. Tobin, F. Tavakkoli, T. C. Dowling, P. D. Light, and R. J. Parker. Effect of uremic serum and uremic toxins on drug metabolism in human microsomes. *Regul Toxicol Pharmacol*, 68(2):297–303, 2014. URL: https://www.ncbi.nlm.nih.gov/pubmed/24184159, doi:10.1016/j.yrtph.2013.10.006.

[36] Chia-Hsiang Hsueh, Kenta Yoshida, Ping Zhao, Timothy W Meyer, Lei Zhang, Shiew-Mei Huang, and Kathleen M Giacomini. Identification and quantitative assessment of uremic solutes as inhibitors of renal organic anion transporters, oat1 and oat3. *Molecular Pharmaceutics*, 13(9):3130–3140, 2016.

[37] M. A. Tortorici, D. L. Cutler, A. Hazra, T. D. Nolin, K. Rowland-Yeo, and K. Venkatakrishnan. Emerging areas of research in the assessment of pharmacokinetics in patients with chronic kidney disease. *J Clin Pharmacol*, 55(3):241–50, 2015. URL: https://www.ncbi.nlm.nih.gov/pubmed/25501531, doi:10.1002/jcph.444.

[38] J. H. Beumer, F. Ding, H. Tawbi, Y. Lin, D. Viluh, I. Chatterjee, M. Rinker, S. L. Chow, and S. P. Ivy. Effect of renal dysfunction on toxicity in three decades of cancer therapy evaluation program-sponsored single-agent phase i studies. *J Clin Oncol*, 34(2):110–6, 2016. URL: https://www.ncbi.nlm.nih.gov/pubmed/26392101, doi:10.1200/JCO.2014.59.7302.

[39] M. A. Casal, T. D. Nolin, and J. H. Beumer. Estimation of kidney function in oncology: Implications for anticancer drug selection and dosing. *Clin J Am Soc Nephrol*, 14(4):587–595, 2019. URL: https://www.ncbi.nlm.nih.gov/pubmed/30890575, doi:10.2215/CJN.11721018.

[40] B. Smyth, C. Jones, and J. Saunders. Prescribing for patients on dialysis. *Aust Prescr*, 39(1):21–4, 2016. URL: https://www.ncbi.nlm.nih.gov/pubmed/27041803, doi:10.18773/austprescr.2016.008.

[41] A. Secora, G. C. Alexander, S. H. Ballew, J. Coresh, and M. E. Grams. Kidney function, polypharmacy, and potentially inappropriate medication use in a community-based cohort of older adults. *Drugs Aging*, 35(8):735–750, 2018. URL: https://www.ncbi.nlm.nih.gov/pubmed/30039344, doi:10.1007/s40266-018-0563-1.

[42] S. D. Krens, G. Lassche, F. G. A. Jansman, I. M. E. Desar, N. A. G. Lankheet, D. M. Burger, C. M. L. van Herpen, and N. P. van Erp. Dose recommendations for anticancer drugs in patients with renal or hepatic impairment. *Lancet Oncol*, 20(4):e200–e207, 2019. URL: https://www.ncbi.nlm.nih.gov/pubmed/30942181, doi:10.1016/S1470-2045(19)30145-7.

[43] Y. Zhang, N. Mehta, E. Muhari-Stark, G. J. Burckart, J. van den Anker, and J. Wang. Pediatric renal ontogeny and applications in drug development. *J Clin Pharmacol*, 59 Suppl 1:S9–S20, 2019. URL: https://www.ncbi.nlm.nih.gov/pubmed/31502684, doi:10.1002/jcph.1490.

[44] A. K. Lew, R. L. Crass, and G. Eschenauer. Evolution of equations for estimating renal function and their application to the dosing of new antimicrobials. *Ann Pharmacother*, page 1060028019890346, 2019. URL: https://www.ncbi.nlm.nih.gov/pubmed/31762287, doi:10.1177/1060028019890346.

[45] B. Meibohm and H. Zhou. Characterizing the impact of renal impairment on the clinical pharmacology of biologics. *J Clin Pharmacol*, 52(1 Suppl):54S–62S, 2012. URL: https://www.ncbi.nlm.nih.gov/pubmed/22232754, doi:10.1177/0091270011413894.

[46] D. Raj, B. Tomar, A. Lahiri, and S. R. Mulay. The gut-liver-kidney axis: Novel regulator of fatty liver associated chronic kidney disease. *Pharmacol Res*, 152:104617, 2020. URL: https://www.ncbi.nlm.nih.gov/pubmed/31881272, doi:10.1016/j.phrs.2019.104617.

[47] C. J. Lin, T. C. Liou, C. F. Pan, P. C. Wu, F. J. Sun, H. L. Liu, H. H. Chen, and C. J. Wu. The role of liver in determining serum colon-derived uremic solutes. *PLoS One*, 10(8):e0134590, 2015. URL: https://www.ncbi.nlm.nih.gov/pubmed/26258409, doi:10.1371/journal.pone.0134590.

[48] M. Neely. Scalpels not hammers: The way forward for precision drug prescription. *Clin Pharmacol Ther*, 101(3):368–372, 2017. URL: https://www.ncbi.nlm.nih.gov/pubmed/27984653, doi:10.1002/cpt.593.

[49] D. K. Kim, J. W. Lee, K. H. Shin, S. Kim, K. H. Oh, M. Kim, K. S. Yu, J. P. Lee, C. S. Lim, Y. S. Kim, and K. W. Joo. Dose selection method for pharmacokinetic study in hemodialysis patients using a subpharmacological dose: oseltamivir as a model drug. *BMC Nephrol*, 15:46, 2014. URL: https://www.ncbi.nlm.nih.gov/pubmed/24636040, doi:10.1186/1471-2369-15-46.

[50] M. A. Tortorici, D. Cutler, L. Zhang, and M. Pfister. Design, conduct, analysis, and interpretation of clinical studies in patients with impaired kidney function. *J Clin Pharmacol*, 52(1 Suppl):109S–18S, 2012. URL: https://www.ncbi.nlm.nih.gov/pubmed/22232746, doi:10.1177/0091270011416364.

[51] Lei Zhang, Nancy Xu, Shen Xiao, Vikram Arya, Ping Zhao, Lawrence J Lesko, and Shiew-Mei Huang. Regulatory perspectives on designing pharmacokinetic studies and optimizing labeling recommendations for patients with chronic kidney disease. *The Journal of Clinical Pharmacology*, 52(S1):79S–90S, 2012.

[52] J. J. Gagne, N. F. Khan, T. S. Raj, L. R. Patel, and N. K. Choudhry. Strength of evidence for labeled dosing recommendations in renal impairment. *Clin Trials*, 14(2):219–221, 2017. URL: https://www.ncbi.nlm.nih.gov/pubmed/27780884, doi:10.1177/1740774516673818.

[53] G. R. Matzke, T. C. Dowling, S. A. Marks, and J. E. Murphy. Influence of kidney disease on drug disposition: An assessment of industry studies submitted to the fda for new chemical entities 1999-2010. *J Clin Pharmacol*, 56(4):390–8, 2016. URL: https://www.ncbi.nlm.nih.gov/pubmed/26238947, doi:10.1002/jcph.604.

[54] J. J. Xiao, J. S. Chen, B. L. Lum, and R. A. Graham. A survey of renal impairment pharmacokinetic studies for new oncology drug approvals in the usa from 2010 to early 2015: a focus on development strategies and future directions. *Anticancer Drugs*, 28(7):677–701, 2017. URL: https://www.ncbi.nlm.nih.gov/pubmed/28542036, doi:10.1097/CAD.0000000000000513.

[55] S. M. Huang, R. Temple, S. Xiao, L. Zhang, and L. J. Lesko. When to conduct a renal impairment study during drug development: Us food and drug administration perspective. *Clin Pharmacol Ther*, 86(5):475–9, 2009. URL: https://www.ncbi.nlm.nih.gov/pubmed/19844224, doi:10.1038/clpt.2009.190.

[56] S. Willmann, L. Zhang, M. Frede, D. Kubitza, W. Mueck, S. Schmidt, A. Solms, X. Yan, and D. Garmann. Integrated population pharmacokinetic analysis of rivaroxaban across multiple patient populations. *CPT Pharmacometrics Syst Pharmacol*, 7(5):309–320, 2018. URL: https://www.ncbi.nlm.nih.gov/pubmed/29660785, doi:10.1002/psp4.12288.

[57] E. Borella, I. Poggesi, and P. Magni. Prediction of the effect of renal impairment on the pharmacokinetics of new drugs. *Clin Pharmacokinet*, 57(4):505–514, 2018. URL: https://www.ncbi.nlm.nih.gov/pubmed/28667460, doi:10.1007/s40262-017-0574-9.

[58] M. Jamei, G. L. Dickinson, and A. Rostami-Hodjegan. A framework for assessing inter-individual variability in pharmacokinetics using virtual human populations and integrating general knowledge of physical chemistry, biology, anatomy, physiology and genetics: A tale of 'bottom-up' vs 'top-down' recognition of covariates. *Drug Metab Pharmacokinet*, 24(1):53–75, 2009. URL: https://www.ncbi.nlm.nih.gov/pubmed/19252336, doi:10.2133/dmpk.24.53.

[59] Malcolm Rowland, Carl Peck, and Geoffrey Tucker. Physiologically-based pharmacokinetics in drug development and regulatory science. *Annual review of pharmacology and toxicology*, 51:45–73, 2011.

[60] Karen Rowland Yeo, Mohsen Aarabi, Masoud Jamei, and Amin Rostami-Hodjegan. Modeling and predicting drug pharmacokinetics in patients with renal impairment. *Expert review of clinical pharmacology*, 4(2):261–274, 2011.

[61] Y. Wang, H. Zhu, R. Madabushi, Q. Liu, S. M. Huang, and I. Zineh. Model-informed drug development: Current us regulatory practice and future considerations. *Clin Pharmacol Ther*, 105(4):899–911, 2019. URL: https://www.ncbi.nlm.nih.gov/pubmed/30653670, doi:10.1002/cpt.1363.

[62] Pravin R Jadhav, Jack Cook, Vikram Sinha, Ping Zhao, Amin Rostami-Hodjegan, Vaishali Sahasrabudhe, Norman Stockbridge, and J Robert Powell. A proposal for scientific framework enabling specific population drug dosing recommendations. *The Journal of Clinical Pharmacology*, 55(10):1073–1078, 2015.

[63] A. Rostami-Hodjegan. Physiologically based pharmacokinetics joined with in vitro-in vivo extrapolation of adme: a marriage under the arch of systems pharmacology. *Clin Pharmacol Ther*, 92(1):50–61, 2012. URL: https://www.ncbi.nlm.nih.gov/pubmed/22644330, doi:10.1038/clpt.2012.65.

[64] A. Rostami-Hodjegan and G. T. Tucker. Simulation and prediction of in vivo drug metabolism in human populations from in vitro data. *Nat Rev Drug Discov*, 6(2):140–8, 2007. URL: https://www.ncbi.nlm.nih.gov/pubmed/17268485, doi:10.1038/nrd2173.

[65] H. Tang and M. Mayersohn. A global examination of allometric scaling for predicting human drug clearance and the prediction of large vertical allometry. *J Pharm Sci*, 95(8):1783–99, 2006. URL: https://www.ncbi.nlm.nih.gov/pubmed/16795013, doi:10.1002/jps.20481.

[66] M. Chiba, Y. Ishii, and Y. Sugiyama. Prediction of hepatic clearance in human from in vitro data for successful drug development. *AAPS J*, 11(2):262–76, 2009. URL: https://www.ncbi.nlm.nih.gov/pubmed/19408130, doi:10.1208/s12248-009-9103-6.

[67] Z. E. Barter, M. K. Bayliss, P. H. Beaune, A. R. Boobis, D. J. Carlile, R. J. Edwards, J. B. Houston, B. G. Lake, J. C. Lipscomb, O. R. Pelkonen, G. T. Tucker, and A. Rostami-Hodjegan. Scaling factors for the extrapolation of in vivo metabolic drug clearance from in vitro data: reaching a consensus on values of human microsomal protein and hepatocellularity per gram of liver. *Curr Drug Metab*, 8(1):33–45, 2007. URL: https://www.ncbi.nlm.nih.gov/pubmed/17266522.

[68] H. J. Burt, A. E. Riedmaier, M. D. Harwood, H. K. Crewe, K. L. Gill, and S. Neuhoff. Abundance of hepatic transporters in caucasians: A meta-analysis. *Drug Metab Dispos*, 44(10):1550–61, 2016. URL: https://www.ncbi.nlm.nih.gov/pubmed/27493152, doi:10.1124/dmd.116.071183.

[69] Y. Chen, L. Liu, K. Nguyen, and A. J. Fretland. Utility of intersystem extrapolation factors in early reaction phenotyping and the quantitative extrapolation of human liver microsomal intrinsic clearance using recombinant cytochromes p450. *Drug Metab Dispos*, 39(3):373–82, 2011. URL: https://www.ncbi.nlm.nih.gov/pubmed/21148079, doi:10.1124/dmd.110.035147.

[70] J. E. Sager, J. Yu, I. Ragueneau-Majlessi, and N. Isoherranen. Physiologically based pharmacokinetic (pbpk) modeling and simulation approaches: A systematic review of published models, applications, and model verification. *Drug Metab Dispos*, 43(11):1823–37, 2015. URL: https://www.ncbi.nlm.nih.gov/pubmed/26296709, doi:10.1124/dmd.115.065920.

[71] K. S. Pang, H. J. Maeng, and J. Fan. Interplay of transporters and enzymes in drug and metabolite processing. *Mol Pharm*, 6(6):1734–55, 2009. URL: https://www.ncbi.nlm.nih.gov/pubmed/19891494, doi:10.1021/mp900258z.

[72] C. Hartmanshenn, M. Scherholz, and I. P. Androulakis. Physiologically-based pharmacokinetic models: approaches for enabling personalized medicine. *J Pharmacokinet Pharmacodyn*, 43(5):481–504, 2016. URL: https://www.ncbi.nlm.nih.gov/pubmed/27647273, doi:10.1007/s10928-016-9492-y.

[73] N. Marsousi, J. A. Desmeules, S. Rudaz, and Y. Daali. Usefulness of pbpk modeling in incorporation of clinical conditions in personalized medicine. *J Pharm Sci*, 106(9):2380–2391, 2017. URL: https://www.ncbi.nlm.nih.gov/pubmed/28456730, doi:10.1016/j.xphs.2017.04.035.

[74] P. Zhao, M. Rowland, and S. M. Huang. Best practice in the use of physiologically based pharmacokinetic modeling and simulation to address clinical pharmacology regulatory questions. *Clin Pharmacol Ther*, 92(1):17–20, 2012. URL: https://www.ncbi.nlm.nih.gov/pubmed/22713733, doi:10.1038/clpt.2012.68.

[75] US Food and Drug Administration. Guidance for industry pharmacokinetics in patients with impaired renal function — study design, data analysis, and impact on dosing and labeling. Report, March 2010. URL: http://www.fda.gov/downloads/Drugs/GuidanceComplianceRegulatoryInformation/Guidances/UCM204959.pdf.

[76] W. Huang and N. Isoherranen. Development of a dynamic physiologically based mechanistic kidney model to predict renal clearance. *CPT Pharmacometrics Syst Pharmacol*, 7(9):593–602, 2018. URL: https://www.ncbi.nlm.nih.gov/pubmed/30043446, doi:10.1002/psp4.12321.

[77] Vicky Hsu, Manuela de LT Vieira, Ping Zhao, Lei Zhang, Jenny Huimin Zheng, Anna Nordmark, Eva Gil Berglund, Kathleen M Giacomini, and Shiew-Mei Huang. Towards quantitation of the effects of renal impairment and probenecid inhibition on kidney uptake and efflux transporters, using physiologically based pharmacokinetic modelling and simulations. *Clinical pharmacokinetics*, 53(3):283–293, 2014.

[78] A. Selen, G. L. Amidon, and P. G. Welling. Pharmacokinetics of probenecid following oral doses to human volunteers. *J Pharm Sci*, 71(11):1238–42, 1982. URL: https://www.ncbi.nlm.nih.gov/pubmed/7175716, doi:10.1002/jps.2600711114.

[79] M. M. Posada, E. A. Cannady, C. D. Payne, X. Zhang, J. A. Bacon, Y. A. Pak, J. W. Higgins, N. Shahri, S. D. Hall, and K. M. Hillgren. Prediction of transporter-mediated drug-drug interactions for baricitinib. *Clin Transl Sci*, 10(6):509–519, 2017. URL: https://www.ncbi.nlm.nih.gov/pubmed/28749581, doi:10.1111/cts.12486.

[80] B. Feng, S. Hurst, Y. Lu, M. V. Varma, C. J. Rotter, A. El-Kattan, P. Lockwood, and B. Corrigan. Quantitative prediction of renal transporter-mediated clinical drug-drug interactions. *Mol Pharm*, 10(11):4207–15, 2013. URL: https://www.ncbi.nlm.nih.gov/pubmed/24066726, doi:10.1021/mp400295c.

[81] B. Feng and M. V. Varma. Evaluation and quantitative prediction of renal transporter-mediated drug-drug interactions. *J Clin Pharmacol*, 56 Suppl 7:S110–21, 2016. URL: https://www.ncbi.nlm.nih.gov/pubmed/27385169, doi:10.1002/jcph.702.

[82] Manthena V Varma, K Sandy Pang, Nina Isoherranen, and Ping Zhao. Dealing with the complex drug–drug interactions: towards mechanistic models. *Biopharmaceutics & drug disposition*, 36(2):71–92, 2015.

[83] Daniel Scotcher, Christopher Jones, Maria Posada, Amin Rostami-Hodjegan, and Aleksandra Galetin. Key to opening kidney for in vitro–in vivo extrapolation entrance in health and disease: Part i: In vitro systems and physiological data. *The AAPS Journal*, 18(5):1067–1081, 2016.

[84] D Scotcher, CR Jones, A Galetin, and A Rostami-Hodjegan. Delineating the role of various factors in renal disposition of digoxin through application of physiologically-based kidney model to renal impairment populations. *The Journal of pharmacology and experimental therapeutics*, 2017.

[85] Chuang Lu, Ajit Suri, Wen Chyi Shyu, and Shimoga Prakash. Assessment of cytochrome p450-mediated drug–drug interaction potential of orteronel and exposure changes in patients with renal impairment using physiologically based pharmacokinetic modeling and simulation. *Biopharmaceutics & drug disposition*, 35(9):543–552, 2014.

[86] US Food and Drug Administration. Guidance for industry drug interaction studies — study design, data analysis, implications for dosing, and labeling recommendations. draft guidance. 2012.

[87] Thomas D Nolin. Altered nonrenal drug clearance in esrd. *Curr Opin Nephrol Hypertens*, 17(6):555–559, 2008.

[88] F. P. Guengerich. Cytochrome p450 and chemical toxicology. *Chem Res Toxicol*, 21(1):70–83, 2008. URL: https://www.ncbi.nlm.nih.gov/pubmed/18052394, doi:10.1021/tx700079z.

[89] J. A. Williams, R. Hyland, B. C. Jones, D. A. Smith, S. Hurst, T. C. Goosen, V. Peterkin, J. R. Koup, and S. E. Ball. Drug-drug interactions for udp-glucuronosyltransferase substrates: a pharmacokinetic explanation for typically observed low exposure (auci/auc) ratios. *Drug Metab Dispos*, 32(11):1201–8, 2004. URL: https://www.ncbi.nlm.nih.gov/pubmed/15304429, doi:10.1124/dmd.104.000794.

[90] P. Zhao, L. Vieira Mde, J. A. Grillo, P. Song, T. C. Wu, J. H. Zheng, V. Arya, E. G. Berglund, Jr. Atkinson, A. J., Y. Sugiyama, K. S. Pang, K. S. Reynolds, D. R. Abernethy, L. Zhang, L. J. Lesko, and S. M. Huang. Evaluation of exposure change of nonrenally eliminated drugs in patients with chronic kidney disease

using physiologically based pharmacokinetic modeling and simulation. *J Clin Pharmacol*, 52(1 Suppl):91S–108S, 2012. URL: https://www.ncbi.nlm.nih.gov/pubmed/22232759https://accp1.onlinelibrary.wiley.com/doi/abs/10.1177/0091270011415528, doi:10.1177/0091270011415528.

[91] Kenta Yoshida, Bo Sun, Lei Zhang, Ping Zhao, Darrell R Abernethy, Thomas D Nolin, Amin Rostami-Hodjegan, Issam Zineh, and S-M Huang. Systematic and quantitative assessment of the effect of chronic kidney disease on cyp2d6 and cyp3a4/5. *Clinical Pharmacology & Therapeutics*, 2016.

[92] M. L. Tan, K. Yoshida, P. Zhao, L. Zhang, T. D. Nolin, M. Piquette-Miller, A. Galetin, and S. M. Huang. Effect of chronic kidney disease on nonrenal elimination pathways: A systematic assessment of cyp1a2, cyp2c8, cyp2c9, cyp2c19, and oatp. *Clin Pharmacol Ther*, 103(5):854–867, 2018. URL: https://www.ncbi.nlm.nih.gov/pubmed/28990182, doi:10.1002/cpt.807.

[93] M. L. Tan, P. Zhao, L. Zhang, Y. F. Ho, M. V. S. Varma, S. Neuhoff, T. D. Nolin, A. Galetin, and S. M. Huang. Use of physiologically based pharmacokinetic modeling to evaluate the effect of chronic kidney disease on the disposition of hepatic cyp2c8 and oatp1b drug substrates. *Clin Pharmacol Ther*, 105(3):719–729, 2019. URL: https://www.ncbi.nlm.nih.gov/pubmed/30074626, doi:10.1002/cpt.1205.

[94] Albert W Dreisbach and Juan JL Lertora. The effect of chronic renal failure on drug metabolism and transport. *Expert opinion on drug metabolism & toxicology*, 4(8):1065–1074, 2008.

[95] AW Dreisbach. The influence of chronic renal failure on drug metabolism and transport. *Clinical Pharmacology & Therapeutics*, 86(5):553–556, 2009.

[96] T. C. Marbury, J. L. Ruckle, V. Hatorp, M. P. Andersen, K. K. Nielsen, W. C. Huang, and P. Strange. Pharmacokinetics of repaglinide in subjects with renal impairment. *Clin Pharmacol Ther*, 67(1):7–15, 2000. URL: https://www.ncbi.nlm.nih.gov/pubmed/10668848, doi:10.1067/mcp.2000.103973.

[97] May Almukainzi, Ranih Gabr, Ghada Abdelhamid, and Raimar Löbenberg. Mechanistic understanding of the effect of renal impairment on metformin oral absorption using computer simulations. *Journal of Pharmaceutical Investigation*, 47(2):151–161, 2017.

[98] H. J. Burt, S. Neuhoff, L. Almond, L. Gaohua, M. D. Harwood, M. Jamei, A. Rostami-Hodjegan, G. T. Tucker, and K. Rowland-Yeo. Metformin and cimetidine: Physiologi-

cally based pharmacokinetic modelling to investigate transporter mediated drug-drug interactions. *Eur J Pharm Sci*, 88:70–82, 2016. URL: https://www.ncbi.nlm.nih.gov/pubmed/27019345, doi:10.1016/j.ejps.2016.03.020.

[99] Yoko Franchetti, Thomas D Nolin, and Franz Franchetti. Indirect measurement of hepatic drug clearance by fitting dynamical models (in preparation). 2020.

[100] H. Sayama, H. Takubo, H. Komura, M. Kogayu, and M. Iwaki. Application of a physiologically based pharmacokinetic model informed by a top-down approach for the prediction of pharmacokinetics in chronic kidney disease patients. *AAPS J*, 16(5):1018–28, 2014. URL: https://www.ncbi.nlm.nih.gov/pubmed/24912798, doi:10.1208/s12248-014-9626-3.

[101] M. Jamei, F. Bajot, S. Neuhoff, Z. Barter, J. Yang, A. Rostami-Hodjegan, and K. Rowland-Yeo. A mechanistic framework for in vitro-in vivo extrapolation of liver membrane transporters: prediction of drug-drug interaction between rosuvastatin and cyclosporine. *Clin Pharmacokinet*, 53(1):73–87, 2014. URL: https://www.ncbi.nlm.nih.gov/pubmed/23881596https://www.ncbi.nlm.nih.gov/pmc/articles/PMC3889821/pdf/40262_2013_Article_97.pdf, doi:10.1007/s40262-013-0097-y.

[102] T. M. Polasek, G. T. Tucker, M. J. Sorich, M. D. Wiese, T. Mohan, A. Rostami-Hodjegan, P. Korprasertthaworn, V. Perera, and A. Rowland. Prediction of olanzapine exposure in individual patients using physiologically based pharmacokinetic modelling and simulation. *Br J Clin Pharmacol*, 84(3):462–476, 2018. URL: https://www.ncbi.nlm.nih.gov/pubmed/29194718, doi:10.1111/bcp.13480.

[103] J. Jornil, K. G. Jensen, F. Larsen, and K. Linnet. Identification of cytochrome p450 isoforms involved in the metabolism of paroxetine and estimation of their importance for human paroxetine metabolism using a population-based simulator. *Drug Metab Dispos*, 38(3):376–85, 2010. URL: https://www.ncbi.nlm.nih.gov/pubmed/20007670, doi:10.1124/dmd.109.030551.

[104] K. Rowland Yeo, M. Jamei, J. Yang, G. T. Tucker, and A. Rostami-Hodjegan. Physiologically based mechanistic modelling to predict complex drug-drug interactions involving simultaneous competitive and time-dependent enzyme inhibition by parent compound and its metabolite in both liver and gut - the effect of diltiazem on the time-course of exposure to triazolam. *Eur J Pharm Sci*, 39(5):298–309, 2010. URL: https://www.ncbi.nlm.nih.gov/pubmed/20025966, doi:10.1016/j.ejps.2009.12.002.

[105] Y. Franchetti and T. D. Nolin. Simultaneous assessment of hepatic transport and metabolism pathways with a single probe using individualized pbpk modeling of

(14)co2 production rate data. *J Pharmacol Exp Ther*, 371(1):151–161, 2019. URL: https://www.ncbi.nlm.nih.gov/pubmed/31399494, doi:10.1124/jpet.119.257212.

[106] Yoko Franchetti and Thomas D Nolin. Application of individualized physiologically-based pharmacokinetic modeling of rate data (ipbpk-r) to estimate the effect of hemodialysis on nonrenal clearance pathways. American Society of Nephrology. URL: https://www.asn-online.org/education/kidneyweek/archives/.

[107] Cyrielle Dumont, France Mentré, Clare Gaynor, Karl Brendel, Charlotte Gesson, and Marylore Chenel. Optimal sampling times for a drug and its metabolite using simcyp® simulations as prior information. *Clinical pharmacokinetics*, 52(1):43–57, 2013.

[108] Daniel Scotcher, Christopher Jones, Amin Rostami-Hodjegan, and Aleksandra Galetin. Novel minimal physiologically-based model for the prediction of passive tubular reabsorption and renal excretion clearance. *European Journal of Pharmaceutical Sciences*, 94:59–71, 2016.

[109] Daniel Scotcher, Christopher Jones, Maria Posada, Aleksandra Galetin, and Amin Rostami-Hodjegan. Key to opening kidney for in vitro-in vivo extrapolation entrance in health and disease: Part ii: Mechanistic models and in vitro-in vivo extrapolation. *The AAPS Journal*, 18(5):1082–1094, 2016.

[110] Leslie Z Benet. The drug transporter- metabolism alliance: uncovering and defining the interplay. *Molecular pharmaceutics*, 6(6):1631–1643, 2009.

[111] FDA US. Guidance for industry clinical drug interaction studies — study design, data analysis, and clinical implications. draft guidance. Report, US Food and Drug Administration, 2017.

[112] Islam R Younis, J Robert Powell, Amin Rostami-Hodjegan, Brian Corrigan, Norman Stockbridge, Vikram Sinha, Ping Zhao, Pravin Jadhav, Bruno Flamion, and Jack Cook. Utility of model-based approaches for informing dosing recommendations in specific populations: Report from the public aaps workshop. *The Journal of Clinical Pharmacology*, 57(1):105–109, 2017.

[113] Binfeng Xia, Tycho Heimbach, Rakesh Gollen, Charvi Nanavati, and Handan He. A simplified pbpk modeling approach for prediction of pharmacokinetics of four primarily renally excreted and cyp3a metabolized compounds during pregnancy. *The AAPS journal*, 15(4):1012–1024, 2013.

[114] N. Sharma, A. Sircar, H. J. Anders, and A. B. Gaikwad. Crosstalk between kidney and liver in non-alcoholic fatty liver disease: mechanisms and therapeutic approaches. *Arch Physiol Biochem*, pages 1–15, 2020. URL: https://www.ncbi.nlm.nih.gov/pubmed/32223569, doi:10.1080/13813455.2020.1745851.

[115] K. W. K. Cheung, B. D. van Groen, E. Spaans, M. D. van Borselen, Acjm de Bruijn, Y. Simons-Oosterhuis, D. Tibboel, J. N. Samsom, R. M. Verdijk, B. Smeets, L. Zhang, S. M. Huang, K. M. Giacomini, and S. N. de Wildt. A comprehensive analysis of ontogeny of renal drug transporters: mrna analyses, quantitative proteomics, and localization. *Clin Pharmacol Ther*, 106(5):1083–1092, 2019. URL: https://www.ncbi.nlm.nih.gov/pubmed/31127606, doi:10.1002/cpt.1516.

[116] T. N. Lam and C. A. Hunt. Mechanistic insight from in silico pharmacokinetic experiments: roles of p-glycoprotein, cyp3a4 enzymes, and microenvironments. *J Pharmacol Exp Ther*, 332(2):398–412, 2010. URL: https://www.ncbi.nlm.nih.gov/pubmed/19864617, doi:10.1124/jpet.109.160739.

[117] W. Huang and N. Isoherranen. Sampling site has a critical impact on physiologically based pharmacokinetic modeling. *J Pharmacol Exp Ther*, 372(1):30–45, 2020. URL: https://www.ncbi.nlm.nih.gov/pubmed/31604807, doi:10.1124/jpet.119.262154.

[118] B. Grabowska-Polanowska, P. Miarka, M. Skowron, G. Chmiel, A. Pietrzycka, and I. Sliwka. Breath analysis as promising indicator of hemodialysis efficiency. *Clin Exp Nephrol*, 23(2):251–257, 2019. URL: https://www.ncbi.nlm.nih.gov/pubmed/30121801, doi:10.1007/s10157-018-1625-8.

[119] Raymond Vanholder, Ulrich Baurmeister, Philippe Brunet, Gerald Cohen, Griet Glorieux, and Joachim Jankowski. A bench to bedside view of uremic toxins. *Journal of the American Society of Nephrology*, 19(5):863–870, 2008.

[120] R. J. Keizer, R. Ter Heine, A. Frymoyer, L. J. Lesko, R. Mangat, and S. Goswami. Model-informed precision dosing at the bedside: Scientific challenges and opportunities. *CPT Pharmacometrics Syst Pharmacol*, 7(12):785–787, 2018. URL: https://www.ncbi.nlm.nih.gov/pubmed/30255663, doi:10.1002/psp4.12353.

[121] C. Dartois, K. Brendel, E. Comets, C. M. Laffont, C. Laveille, B. Tranchand, F. Mentre, A. Lemenuel-Diot, and P. Girard. Overview of model-building strategies in population pk/pd analyses: 2002-2004 literature survey. *Br J Clin Pharmacol*, 64(5):603–12, 2007. URL: https://www.ncbi.nlm.nih.gov/pubmed/17711538, doi:10.1111/j.1365-2125.2007.02975.x.

[122] N. F. Smith, F. I. Raynaud, and P. Workman. The application of cassette dosing for pharmacokinetic screening in small-molecule cancer drug discovery. *Mol Cancer Ther*, 6(2):428–40, 2007. URL: https://www.ncbi.nlm.nih.gov/pubmed/17308044, doi:10.1158/1535-7163.MCT-06-0324.

[123] H. Zhou, Z. Tong, and J. F. McLeod. "cocktail" approaches and strategies in drug development: valuable tool or flawed science? *J Clin Pharmacol*, 44(2):120–34, 2004. URL: https://www.ncbi.nlm.nih.gov/pubmed/14747420, doi:10.1177/0091270003261333.

[124] E. Gaude, M. K. Nakhleh, S. Patassini, J. Boschmans, M. Allsworth, B. Boyle, and M. P. van der Schee. Targeted breath analysis: exogenous volatile organic compounds (evoc) as metabolic pathway-specific probes. *J Breath Res*, 13(3):032001, 2019. URL: https://www.ncbi.nlm.nih.gov/pubmed/30965287, doi:10.1088/1752-7163/ab1789.

[125] L. Mertz. The great exhale: Using breath analysis to detect disease. *IEEE Pulse*, 11(3):7–11, 2020. URL: https://www.ncbi.nlm.nih.gov/pubmed/32584769, doi:10.1109/MPULS.2020.2993684.

[126] John Towns, Timothy Cockerill, Maytal Dahan, Ian Foster, Kelly Gaither, Andrew Grimshaw, Victor Hazlewood, Scott Lathrop, Dave Lifka, and Gregory D. Peterson. Xsede: accelerating scientific discovery. *Comput Sci Eng*, 16(5):62–74, 2014.

[127] Thomas D Nolin, Kofi Appiah, Scott A Kendrick, Ellen Phuong Le McMonagle, and Jonathan Himmelfarb. Effect of hemodialysis on hepatic cyp3a4 activity. *Clin Pharmacol Ther*, 79(2):23, PI–60, 2006.

[128] Thomas D Nolin, Kofi Appiah, Scott A Kendrick, Phuong Le, Ellen McMonagle, and Jonathan Himmelfarb. Hemodialysis acutely improves hepatic cyp3a4 metabolic activity. *J Am Soc Nephrol*, 17(9):2363–2367, 2006.

[129] M. E. Krecic-Shepard, C. R. Barnas, J. Slimko, J. C. Gorski, I. W. Wainer, and J. B. Schwartz. In vivo comparison of putative probes of cyp3a4/5 activity: erythromycin, dextromethorphan, and verapamil. *Clin Pharmacol Ther*, 66(1):40–50, 1999. URL: https://www.ncbi.nlm.nih.gov/pubmed/10430108, doi:10.1016/S0009-9236(99)70052-4.

[130] Y. Krivoruk, M. T. Kinirons, A. J. Wood, and M. Wood. Metabolism of cytochrome p4503a substrates in vivo administered by the same route: lack of correlation between

alfentanil clearance and erythromycin breath test. *Clin Pharmacol Ther*, 56(6 Pt 1):608–14, 1994. URL: https://www.ncbi.nlm.nih.gov/pubmed/7995002.

[131] Sagnik Das and Mrinal Pal. Non-invasive monitoring of human health by exhaled breath analysis: A comprehensive review. *Journal of The Electrochemical Society*, 167(3):037562, 2020.

[132] Laurent P Rivory, Kellie A Slaviero, Janelle M Hoskins, and Stephen J Clarke. The erythromycin breath test for the prediction of drug clearance. *Clinical pharmacokinetics*, 40(3):151–158, 2001.

[133] L. P. Rivory and P. B. Watkins. Erythromycin breath test. *Clin Pharmacol Ther*, 70(4):395–9, 2001. URL: https://www.ncbi.nlm.nih.gov/pubmed/11673756.

[134] Alan V. Oppenheim and Ronald W. Schafer. *Discrete-Time Signal Processing*. Prentice Hall Press, 2009.

[135] Reinhard Diestel. Graph theory. 2005. *Grad. Texts in Math*, 101, 2005.

[136] Dominic Jordan, Peter Smith, and Peter Smith. *Nonlinear ordinary differential equations: an introduction for scientists and engineers*, volume 10. Oxford University Press on Demand, 2007.

[137] Vivian Hutson, J Pym, and M Cloud. *Introduction to nonlinear operators*, volume 200, book section 4, pages 115–146. Elsevier, 2005.

[138] Franz Franchetti, de Frédéric Mesmay, Daniel McFarlin, and Markus Püschel. *Operator language: A program generation framework for fast kernels, in IFIP Working Conference on Domain Specic Languages (DSL WC)*, volume 5658, pages 385–410. Springer, 2009.

[139] Franz Franchetti, Tze Meng Low, Doru Thom Popovici, Richard M Veras, Daniele G Spampinato, Jeremy R Johnson, Markus Püschel, James C Hoe, and José MF Moura. Spiral: Extreme performance portability, special issue on "from high level specication to high performance code". *Proceedings of the IEEE*, 106(11):1935–1968, 2018.

[140] Vivian Hutson, J Pym, and M Cloud. *Applications of functional analysis and operator theory*. Elsevier, 2 edition, 2005.

[141] E Kreyszig, H Kreyszig, and EJ Norminton. *H. and Norminton, EJ (2011) Advanced Engineering Mathematics*. Wiley, NY, Hoboken, NJ, 10 edition, 2011.

[142] Tosio Kato. *Perturbation theory for linear operators*, volume 132. Springer Science & Business Media, 2013.

[143] M Peifer and J Timmer. Parameter estimation in ordinary differential equations for biochemical processes using the method of multiple shooting. *IET Systems Biology*, 1(2):78–88, 2007.

[144] Thorsten G Müller and Jens Timmer. Fitting parameters in partial differential equations from partially observed noisy data. *Physica D: Nonlinear Phenomena*, 171(1-2):1–7, 2002.

[145] O Richter, P Nörtersheuser, and W Pestemer. Non-linear parameter estimation in pesticide degradation. *Science of the total environment*, 123:435–450, 1992.

[146] K Schittkowski. Parameter estimation in systems of nonlinear equations. *Numerische Mathematik*, 68(1):129–142, 1994.

[147] Klaus Schittkowski. *Numerical data fitting in dynamical systems: a practical introduction with applications and software*, volume 77. Springer Science & Business Media, Boston, MA, 2002.

[148] Hans Georg Bock. *Numerical treatment of inverse problems in chemical reaction kinetics*, pages 102–125. Springer, 1981.

[149] Kenneth Levenberg. A method for the solution of certain non-linear problems in least squares. *Quarterly of applied mathematics*, 2(2):164–168, 1944.

[150] Donald W Marquardt. An algorithm for least-squares estimation of nonlinear parameters. *Journal of the society for Industrial and Applied Mathematics*, 11(2):431–441, 1963.

[151] Navid Azizan and Babak Hassibi. Stochastic gradient/mirror descent: Minimax optimality and implicit regularization. *arXiv preprint arXiv:1806.00952*, 2018.

[152] J Stoer and R Bulirsch. Introduction to numerical analysis, 2. aufl., ser. *Texts in Applied Mathematics*, 12, 2013.

[153] Ya-Xiang Yuan. Recent advances in numerical methods for nonlinear equations and nonlinear least squares. *Numerical algebra, control and optimization*, 1(1):15–34, 2011.

[154] Paulo Cortez. *Modern optimization with R*. Springer, 2014.

[155] Mendel Fygenson. Modeling and predicting extrapolated probabilities with outlooks. *Statistica Sinica*, pages 9–40, 2008.

[156] N. J. Proctor, G. T. Tucker, and A. Rostami-Hodjegan. Predicting drug clearance from recombinantly expressed cyps: intersystem extrapolation factors. *Xenobiotica*, 34(2):151–78, 2004. URL: https://www.ncbi.nlm.nih.gov/pubmed/14985145, doi:10.1080/00498250310001646353.

[157] G. T. Tucker, J. B. Houston, and S. M. Huang. Optimizing drug development: strategies to assess drug metabolism/transporter interaction potential-toward a consensus. *Clin Pharmacol Ther*, 70(2):103–14, 2001. URL: https://www.ncbi.nlm.nih.gov/pubmed/11503003, doi:10.1067/mcp.2001.116891.

[158] Torsten Teorell. Kinetics of distribution of substances administered to the body, i: the extravascular modes of administration. *Archives internationales de pharmacodynamie et de therapie*, 57:205–225, 1937.

[159] M. R. Shiran, N. J. Proctor, E. M. Howgate, K. Rowland-Yeo, G. T. Tucker, and A. Rostami-Hodjegan. Prediction of metabolic drug clearance in humans: in vitro-in vivo extrapolation vs allometric scaling. *Xenobiotica*, 36(7):567–80, 2006. URL: https://www.ncbi.nlm.nih.gov/pubmed/16864504, doi:10.1080/00498250600761662.

[160] Certara USA Inc. Simcyp simulator: The standard for population-based pharmacokinetic modeling and simulation. 2019. URL: https://www.certara.com/software/physiologically-based-pharmacokinetic-modeling-and-simulation / simcyp-simulator / ?ap%5B0%5D=PKPD&ap%5B1%5D=PBPK.

[161] ICON plc. Nonmem®: The gold standard software in population pharmacokinetic and pharmacokinetic-pharmacodynamic modelling. 2019. URL: https://www.iconplc.com/innovation/nonmem/.

[162] Universtiy of Sourthern California Biomedical Simulation Resourse (USC BMSR). Adapt. 2019. URL: https://bmsr.usc.edu/software/adapt/.

[163] USC BMSR. Adapt 5 user's guide. 2019. URL: https://bmsr.usc.edu/files/2013/02/ADAPT5-User-Guide.pdf.

[164] The R foundation. What is r? introduction to r. 2019. URL: https://www.r-project.org/about.html.

[165] The R foundation. Package 'desolve'. 2019. URL: https://cran.r-project.org/web/packages/deSolve/deSolve.pdf.

[166] Karline Soetaert, Thomas Petzoldt, and R. Woodrow Setzer. Package desolve: Solving initial value differential equations in r. Report, 2010. URL: https://cran.r-project.org/web/packages/deSolve/vignettes/deSolve.pdf.

[167] The R foundation. optim. 2019. URL: https://www.rdocumentation.org/packages/stats/versions/3.6.1/topics/optim.

[168] P. B. Watkins. Noninvasive tests of cyp3a enzymes. *Pharmacogenetics*, 4(4):171–84, 1994. URL: https://www.ncbi.nlm.nih.gov/pubmed/7987401.

[169] LA Frassetto, S Poon, C Tsourounis, C Valera, and LZ Benet. Effects of uptake and efflux transporter inhibition on erythromycin breath test results. *Clin Pharmacol Ther*, 81(6):828–832, 2007.

[170] D. Kurnik, A. J. Wood, and G. R. Wilkinson. The erythromycin breath test reflects p-glycoprotein function independently of cytochrome p450 3a activity. *Clin Pharmacol Ther*, 80(3):228–34, 2006. URL: https://www.ncbi.nlm.nih.gov/pubmed/16952489, doi:10.1016/j.clpt.2006.06.002.

[171] RM Franke, CS Lancaster, CJ Peer, AA Gibson, AM Kosloske, SJ Orwick, RH Mathijssen, WD Figg, SD Baker, and Alex Sparreboom. Effect of abcc2 (mrp2) transport function on erythromycin metabolism. *Clin Pharmacol Ther*, 89(5):693–701, 2011.

[172] E. Sugiyama, A. Kikuchi, M. Inada, and H. Sato. The use of 13c-erythromycin as an in vivo probe to evaluate cyp3a-mediated drug interactions in rats. *J Pharm Sci*, 100(9):3995–4005, 2011. URL: https://www.ncbi.nlm.nih.gov/pubmed/21618542, doi:10.1002/jps.22616.

[173] R. Wolbold, K. Klein, O. Burk, A. K. Nussler, P. Neuhaus, M. Eichelbaum, M. Schwab, and U. M. Zanger. Sex is a major determinant of cyp3a4 expression

in human liver. *Hepatology*, 38(4):978–88, 2003. URL: https://www.ncbi.nlm.nih.gov/pubmed/14512885, doi:10.1053/jhep.2003.50393.

[174] Xiaoyan Chu, Ken Korzekwa, Robert Elsby, Katherine Fenner, Aleksandra Galetin, Yurong Lai, Pär Matsson, Aaron Moss, Swati Nagar, and Gus R Rosania. Intracellular drug concentrations and transporters: measurement, modeling, and implications for the liver. *Clinical Pharmacology & Therapeutics*, 94(1):126–141, 2013.

[175] Justine L Lam, Hideaki Okochi, Yong Huang, and Leslie Z Benet. In vitro and in vivo correlation of hepatic transporter effects on erythromycin metabolism: characterizing the importance of transporter-enzyme interplay. *Drug metabolism and disposition*, 34(8):1336–1344, 2006.

[176] S. N. de Wildt, M. J. Berns, and J. N. van den Anker. 13c-erythromycin breath test as a noninvasive measure of cyp3a activity in newborn infants: a pilot study. *Ther Drug Monit*, 29(2):225–30, 2007. URL: https://www.ncbi.nlm.nih.gov/pubmed/17417078, doi:10.1097/FTD.0b013e31803d156d.

[177] J. Hirth, P. B. Watkins, M. Strawderman, A. Schott, R. Bruno, and L. H. Baker. The effect of an individual's cytochrome cyp3a4 activity on docetaxel clearance. *Clin Cancer Res*, 6(4):1255–8, 2000. URL: https://www.ncbi.nlm.nih.gov/pubmed/10778948.

[178] D. K. Turgeon, A. B. Leichtman, D. S. Blake, R. L. Schmouder, K. S. Lown, T. M. Annesley, and P. B. Watkins. Prediction of interpatient and intrapatient variation in og 37-325 dosing requirements by the erythromycin breath test. a prospective study in renal transplant recipients. *Transplantation*, 57(12):1736–41, 1994. URL: https://www.ncbi.nlm.nih.gov/pubmed/8016878.

[179] L. B. Lan, J. T. Dalton, and E. G. Schuetz. Mdr1 limits cyp3a metabolism in vivo. *Mol Pharmacol*, 58(4):863–9, 2000. URL: https://www.ncbi.nlm.nih.gov/pubmed/10999959.

[180] Hong Sun, Yong Huang, Lynda Frassetto, and Leslie Z Benet. Effects of uremic toxins on hepatic uptake and metabolism of erythromycin. *Drug metabolism and disposition*, 32(11):1239–1246, 2004.

[181] Angela Spivey. Safer doses are a breath away. *Endeavors*, Fall, September 1 2000. URL: http://endeavors.unc.edu/fall2000/dosing.htm.

[182] M. E. O'Hara, T. H. Clutton-Brock, S. Green, and C. A. Mayhew. Endogenous volatile organic compounds in breath and blood of healthy volunteers: examining breath analysis as a surrogate for blood measurements. *J Breath Res*, 3(2):027005, 2009. URL: https://www.ncbi.nlm.nih.gov/pubmed/21383460, doi:10.1088/1752-7155/3/2/027005.

[183] Shinichi Kanamitsu, Kiyomi Ito, Carol E Green, Charles A Tyson, Noriaki Shimada, and Yuichi Sugiyama. Prediction of in vivo interaction between triazolam and erythromycin based on in vitro studies using human liver microsomes and recombinant human cyp3a4. *Pharm Res*, 17(4):419–426, 2000.

[184] Robert A Freitas. *Nanomedicine, volume I: basic capabilities*, volume 1. Landes Bioscience Georgetown, TX, 1999.

[185] D. G. Levitt. The pharmacokinetics of the interstitial space in humans. *BMC Clin Pharmacol*, 3:3, 2003. URL: https://www.ncbi.nlm.nih.gov/pubmed/12890292, doi:10.1186/1472-6904-3-3.

[186] J. A. Grillo, P. Zhao, J. Bullock, B. P. Booth, M. Lu, K. Robie-Suh, E. G. Berglund, K. S. Pang, A. Rahman, L. Zhang, L. J. Lesko, and S. M. Huang. Utility of a physiologically-based pharmacokinetic (pbpk) modeling approach to quantitatively predict a complex drug-drug-disease interaction scenario for rivaroxaban during the drug review process: implications for clinical practice. *Biopharm Drug Dispos*, 33(2):99–110, 2012. URL: https://www.ncbi.nlm.nih.gov/pubmed/22270945, doi:10.1002/bdd.1771.

[187] Yoshiyuki Yabe, Aleksandra Galetin, and J Brian Houston. Kinetic characterization of rat hepatic uptake of 16 actively transported drugs. *Drug Metab Dispos*, 39(10):1808–1814, 2011.

[188] H Sun, LA Frassetto, Y Huang, and LZ Benet. Hepatic clearance, but not gut availability, of erythromycin is altered in patients with end-stage renal disease. *Clin Pharmacol Ther*, 87(4):465–472, 2010.

[189] SP Khor and Michael Mayersohn. Potential error in the measurement of tissue to blood distribution coefficients in physiological pharmacokinetic modeling. residual tissue blood. i. theoretical considerations. *Drug Metab Dispos*, 19(2):478–485, 1991.

[190] Oliver Langer, Rudolf Karch, Ulrich Müller, Georg Dobrozemsky, Aiman Abrahim, Markus Zeitlinger, Edith Lackner, Christian Joukhadar, Robert Dudczak, and Kurt

Kletter. Combined pet and microdialysis for in vivo assessment of intracellular drug pharmacokinetics in humans. *J Nucl Med*, 46(11):1835–1841, 2005.

[191] H. Araki, N. Ogake, R. Tsuneda, S. Minami, Y. Watanabe, I. Tamai, and A. Tsuji. Muscle distribution of antimicrobial agents after a single intravenous administration to rats. *Drug Metab Pharmacokinet*, 17(3):237–44, 2002. URL: https://www.ncbi.nlm.nih.gov/pubmed/15618675.

[192] Stuart W Paine, Alison J Parker, Philip Gardiner, Peter JH Webborn, and Robert J Riley. Prediction of the pharmacokinetics of atorvastatin, cerivastatin, and indomethacin using kinetic models applied to isolated rat hepatocytes. *Drug Metab Dispos*, 36(7):1365–1374, 2008.

[193] M. A. Karsdal, T. Manon-Jensen, F. Genovese, J. H. Kristensen, M. J. Nielsen, J. M. Sand, N. U. Hansen, A. C. Bay-Jensen, C. L. Bager, A. Krag, A. Blanchard, H. Krarup, D. J. Leeming, and D. Schuppan. Novel insights into the function and dynamics of extracellular matrix in liver fibrosis. *Am J Physiol Gastrointest Liver Physiol*, 308(10):G807–30, 2015. URL: https://www.ncbi.nlm.nih.gov/pubmed/25767261, doi:10.1152/ajpgi.00447.2014.

[194] L Gaohua, J Wedagedera, BG Small, L Almond, K Romero, D Hermann, D Hanna, M Jamei, and I Gardner. Development of a multicompartment permeability-limited lung pbpk model and its application in predicting pulmonary pharmacokinetics of antituberculosis drugs. *CPT Pharmacometrics Syst Pharmacol*, 4(10):605–613, 2015.

[195] S. Bjorkman. Prediction of the volume of distribution of a drug: which tissue-plasma partition coefficients are needed? *J Pharm Pharmacol*, 54(9):1237–45, 2002. URL: https://www.ncbi.nlm.nih.gov/pubmed/12356278, doi:10.1211/0022357023204020 80.

[196] R. Jansson, U. Bredberg, and M. Ashton. Prediction of drug tissue to plasma concentration ratios using a measured volume of distribution in combination with lipophilicity. *J Pharm Sci*, 97(6):2324–39, 2008. URL: https://www.ncbi.nlm.nih.gov/pubmed/17724666, doi:10.1002/jps.21130.

[197] Aki T. Heikkinen, Neil Parrott, Tom Dunkley, and Paul Cutler. *Targeted Proteomics to Support Transporter IVIVE and PBPK*, volume 2, pages 44–72. Royal Society of Chemistry, Cambridge, UK, 2016.

[198] Wilhelmus HA Schilders, Henk A Van der Vorst, and Joost Rommes. *Model order reduction: theory, research aspects and applications*, volume 13. Springer, 2008.

[199] Kazuya Maeda and Yuichi Sugiyama. *Prediction of Hepatic Transporter-Mediated Drug–Drug Interaction from In Vitro Data*, pages 121–153. Springer New York, New York, NY, 2013. doi:10.1007/978-1-4614-8229-1_6.

[200] James D Evans. *Straightforward statistics for the behavioral sciences*. Brooks/Cole, 1996.

[201] Leslie Z Benet, Fabio Broccatelli, and Tudor I Oprea. Bddcs applied to over 900 drugs. *The AAPS journal*, 13(4):519–547, 2011.

[202] M. F. Paine, D. A. Wagner, K. A. Hoffmaster, and P. B. Watkins. Cytochrome p450 3a4 and p-glycoprotein mediate the interaction between an oral erythromycin breath test and rifampin. *Clin Pharmacol Ther*, 72(5):524–35, 2002. URL: https://www.ncbi.nlm.nih.gov/pubmed/12426516, doi:10.1067/mcp.2002.128387.

[203] Ellen F Carney. The impact of chronic kidney disease on global health. *Nat Rev Nephrol*, 16(5):251–251, 2020.

[204] GBD Chronic Kidney Disease Collaboration. Global, regional, and national burden of chronic kidney disease, 1990-2017: a systematic analysis for the global burden of disease study 2017. *Lancet*, 395(10225):709–733, 2020. URL: https://www.ncbi.nlm.nih.gov/pubmed/32061315, doi:10.1016/S0140-6736(20)30045-3.

[205] J. Michaud, T. D. Nolin, J. Naud, M. Dani, J. P. Lafrance, F. A. Leblond, J. Himmelfarb, and V. Pichette. Effect of hemodialysis on hepatic cytochrome p450 functional expression. *J Pharmacol Sci*, 108(2):157–63, 2008. URL: https://www.ncbi.nlm.nih.gov/pubmed/18845914, doi:10.1254/jphs.08042fp.

[206] D. M. Roberts, J. Sevastos, J. E. Carland, S. L. Stocker, and T. N. Lea-Henry. Clinical pharmacokinetics in kidney disease: Application to rational design of dosing regimens. *Clin J Am Soc Nephrol*, 13(8):1254–1263, 2018. URL: https://www.ncbi.nlm.nih.gov/pubmed/30042221, doi:10.2215/CJN.05150418.

[207] A. L. De Francisco, J. A. Amado, M. Prieto, G. Alcalde, S. Sanz de Castro, J. C. Ruiz, P. Morales, and M. Arias. Dialysis membranes and pth changes during hemodialysis in patients with secondary hyperparathyroidism. *Nephron*, 66(4):442–6, 1994. URL: https://www.ncbi.nlm.nih.gov/pubmed/8015649, doi:10.1159/000187861.

[208] S. H. Makar, H. K. Sawires, T. M. Farid, W. M. Ali, and M. Schaalan. Effect of high-flux versus low-flux dialysis membranes on parathyroid hormone. *Iran J Kidney Dis*, 4(4):327–32, 2010. URL: https://www.ncbi.nlm.nih.gov/pubmed/20852376.

[209] B. K. Thomson, T. D. Nolin, T. J. Velenosi, D. A. Feere, M. J. Knauer, L. J. Asher, A. A. House, and B. L. Urquhart. Effect of ckd and dialysis modality on exposure to drugs cleared by nonrenal mechanisms. *Am J Kidney Dis*, 65(4):574–82, 2015. URL: https://www.ncbi.nlm.nih.gov/pubmed/25453994, doi:10.1053/j.ajkd.2014.09.015.

[210] Thomas D Nolin, Reginald F Frye, Phuong Le, Hooman Sadr, Judith Naud, Francois A Leblond, Vincent Pichette, and Jonathan Himmelfarb. Esrd impairs nonrenal clearance of fexofenadine but not midazolam. *J Am Soc Nephrol*, 20(10):2269–2276, 2009.

[211] T. L. Sirich, B. A. Funk, N. S. Plummer, T. H. Hostetter, and T. W. Meyer. Prominent accumulation in hemodialysis patients of solutes normally cleared by tubular secretion. *J Am Soc Nephrol*, 25(3):615–22, 2014. URL: https://www.ncbi.nlm.nih.gov/pubmed/24231664, doi:10.1681/ASN.2013060597.

[212] H. Jones and K. Rowland-Yeo. Basic concepts in physiologically based pharmacokinetic modeling in drug discovery and development. *CPT Pharmacometrics Syst Pharmacol*, 2:e63, 2013. URL: https://www.ncbi.nlm.nih.gov/pubmed/23945604, doi:10.1038/psp.2013.41.

[213] Polly Kwok, Marianna Leung, and Fong Huynh. Dialyzeihd: Dialyzability of medications during intermittent hemodialysis. 2013. URL: http://www.bcrenalagency.ca/resource-gallery/Documents/Dialyze%20IHD%20Nursing%20Poster%20BCKD%202013_0.pdf.

[214] George R. Bailie and Nancy A. Mason. *Dialysis of Drugs*. Renal Pharmacy Consultants, LLC., Saline, Michigan, 2013.

[215] Department of Statistics University of California Berkeley. Cluster analysis. 2019. URL: https://www.stat.berkeley.edu/~s133/Cluster2a.html.

[216] Y. Suzuki, H. Ono, R. Tanaka, F. Sato, Y. Sato, K. Ohno, H. Mimata, and H. Itoh. Recovery of oatp1b activity after living kidney transplantation in patients with end-stage renal disease. *Pharm Res*, 36(4):59, 2019. URL: https://www.ncbi.nlm.nih.gov/pubmed/30809779, doi:10.1007/s11095-019-2593-8.

[217] E. Bellavista, M. Martucci, F. Vasuri, A. Santoro, M. Mishto, A. Kloss, E. Capizzi, A. Degiovanni, C. Lanzarini, D. Remondini, A. Dazzi, S. Pellegrini, M. Cescon, M. Capri, S. Salvioli, A. D'Errico-Grigioni, B. Dahlmann, G. L. Grazi, and C. Franceschi. Lifelong maintenance of composition, function and cellular/subcellular distribution of proteasomes in human liver. *Mech Ageing Dev*, 141-142:26–34, 2014. URL: https://www.ncbi.nlm.nih.gov/pubmed/25265087, doi:10.1016/j.mad.2014.09.003.

[218] Kelly Ethun. *Sex and gender differences in body composition, lipid metabolism, and glucose regulation*, pages 145–165. Elsevier, 2016.

[219] J. Michaud, J. Naud, J. Chouinard, F. Desy, F. A. Leblond, K. Desbiens, A. Bonnardeaux, and V. Pichette. Role of parathyroid hormone in the downregulation of liver cytochrome p450 in chronic renal failure. *J Am Soc Nephrol*, 17(11):3041–8, 2006. URL: https://www.ncbi.nlm.nih.gov/pubmed/17021269, doi:10.1681/ASN.2006010035.

[220] H. Watanabe, R. Sugimoto, K. Ikegami, Y. Enoki, T. Imafuku, R. Fujimura, J. Bi, K. Nishida, Y. Sakaguchi, M. Murata, H. Maeda, K. Hirata, S. Jingami, Y. Ishima, M. Tanaka, K. Matsushita, H. Komaba, M. Fukagawa, M. Otagiri, and T. Maruyama. Parathyroid hormone contributes to the down-regulation of cytochrome p450 3a through the camp/pi3k/pkc/pka/nf-kappab signaling pathway in secondary hyperparathyroidism. *Biochem Pharmacol*, 145:192–201, 2017. URL: https://www.ncbi.nlm.nih.gov/pubmed/28843775, doi:10.1016/j.bcp.2017.08.016.

[221] A. L. de Francisco, M. A. Cobo, M. A. Setien, E. Rodrigo, G. F. Fresnedo, M. T. Unzueta, J. A. Amado, J. C. Ruiz, M. Arias, and M. Rodriguez. Effect of serum phosphate on parathyroid hormone secretion during hemodialysis. *Kidney Int*, 54(6):2140–5, 1998. URL: https://www.ncbi.nlm.nih.gov/pubmed/9853280, doi:10.1046/j.1523-1755.1998.00221.x.

[222] S. Faivre, G. Kroemer, and E. Raymond. Current development of mtor inhibitors as anticancer agents. *Nat Rev Drug Discov*, 5(8):671–88, 2006. URL: https://www.ncbi.nlm.nih.gov/pubmed/16883305, doi:10.1038/nrd2062.

[223] H. Y. Zhou and S. L. Huang. Current development of the second generation of mtor inhibitors as anticancer agents. *Chin J Cancer*, 31(1):8–18, 2012. URL: https://www.ncbi.nlm.nih.gov/pubmed/22059905, doi:10.5732/cjc.011.10281.

[224] S. Huang and P. J. Houghton. Targeting mtor signaling for cancer therapy. *Curr Opin Pharmacol*, 3(4):371–7, 2003. URL: https://www.ncbi.nlm.nih.gov/pubmed/12901945, doi:10.1016/s1471-4892(03)00071-7.

[225] H. Zhou, Y. Luo, and S. Huang. Updates of mtor inhibitors. *Anticancer Agents Med Chem*, 10(7):571–81, 2010. URL: https://www.ncbi.nlm.nih.gov/pubmed/20812900, doi:10.2174/187152010793498663.

[226] E. Raymond, J. Alexandre, S. Faivre, K. Vera, E. Materman, J. Boni, C. Leister, J. Korth-Bradley, A. Hanauske, and J. P. Armand. Safety and pharmacokinetics of escalated doses of weekly intravenous infusion of cci-779, a novel mtor inhibitor, in patients with cancer. *J Clin Oncol*, 22(12):2336–47, 2004. URL: https://www.ncbi.nlm.nih.gov/pubmed/15136596, doi:10.1200/JCO.2004.08.116.

[227] US Food and Drug Administration. Drug approval package: Torisel (temsirolimus) intravenous clinical pharmacology and biopharmaceutics review(s); solution company: Wyeth pharmaceuticals inc. application no.: 022088 approval date: 05/30/2007. Report, US Food and Drug Administration,, 2012. URL: https://www.accessdata.fda.gov/drugsatfda_docs/nda/2007/022088s000_ClinPharmR.pdf.

[228] US Food and Drug Administration. Drug approval package: Rapamune (sirolimus) oral solution; company: Wyeth-ayerst research application no.: 021083 approval date: 19/15/1999. Report, US Food and Drug Administration,, 2001. URL: https://www.accessdata.fda.gov/drugsatfda_docs/nda/99/21083A_Rapamune_clinphrmr.pdf.

[229] P. Cai, R. Tsao, and M. E. Ruppen. In vitro metabolic study of temsirolimus: preparation, isolation, and identification of the metabolites. *Drug Metab Dispos*, 35(9):1554–63, 2007. URL: https://www.ncbi.nlm.nih.gov/pubmed/17540708, doi:10.1124/dmd.107.014746.

[230] Janice P Dutcher. mtor pathway-directed agents in renal cell carcinoma. *Renal cancer, emerging cancer therapeutics*, pages 137–44, 2011.

[231] Pfizer Canada Inc. Product monograph torisel temsirolimus concentration for injection 25mg/ml mtor kinase inhibitor - antineoplastic agent (submission control number 199380). Report, 2016. URL: https://www.pfizer.ca/sites/default/files/201710/TORISEL_PM_199380_21Dec2016_E.pdf.

[232] T. Shokati, M. Hartmann, B. Davari, J. Klawitter, J. Klawitter, and U. Christians. Temsirolimus metabolic pathways revisited. *Xenobiotica*, 50(6):640–653, 2020. URL:

https://www.ncbi.nlm.nih.gov/pubmed/31596164, doi:10.1080/00498254.2019.1678793.

[233] C. L. Cummins, W. Jacobsen, U. Christians, and L. Z. Benet. Cyp3a4-transfected caco-2 cells as a tool for understanding biochemical absorption barriers: studies with sirolimus and midazolam. *J Pharmacol Exp Ther*, 308(1):143–55, 2004. URL: https://www.ncbi.nlm.nih.gov/pubmed/14569063, doi:10.1124/jpet.103.058065.

[234] A. Crowe, A. Bruelisauer, L. Duerr, P. Guntz, and M. Lemaire. Absorption and intestinal metabolism of sdz-rad and rapamycin in rats. *Drug Metab Dispos*, 27(5):627–32, 1999. URL: https://www.ncbi.nlm.nih.gov/pubmed/10220493.

[235] V. C. Dias and R. W. Yatscoff. Investigation of rapamycin transport and uptake across absorptive human intestinal cell monolayers. *Clin Biochem*, 27(1):31–6, 1994. URL: https://www.ncbi.nlm.nih.gov/pubmed/8200112, doi:10.1016/0009-9120(94)90008-6.

[236] L. C. Mbatchi, M. Gassiot, P. Pourquier, A. Goberna, H. Mahammedi, L. Mourey, F. Joly, S. Lumbroso, A. Evrard, and N. Houede. Association of nr1i2, cyp3a5 and abcb1 genetic polymorphisms with variability of temsirolimus pharmacokinetics and toxicity in patients with metastatic bladder cancer. *Cancer Chemother Pharmacol*, 80(3):653–659, 2017. URL: https://www.ncbi.nlm.nih.gov/pubmed/28676933, doi:10.1007/s00280-017-3379-5.

[237] V. J. Wacher, J. A. Silverman, S. Wong, P. Tran-Tau, A. O. Chan, A. Chai, X. Q. Yu, D. O'Mahony, and Z. Ramtoola. Sirolimus oral absorption in rats is increased by ketoconazole but is not affected by d-alpha-tocopheryl poly(ethylene glycol 1000) succinate. *J Pharmacol Exp Ther*, 303(1):308–13, 2002. URL: https://www.ncbi.nlm.nih.gov/pubmed/12235265, doi:10.1124/jpet.102.036541.

[238] A. MacDonald, J. Scarola, J. T. Burke, and J. J. Zimmerman. Clinical pharmacokinetics and therapeutic drug monitoring of sirolimus. *Clin Ther*, 22 Suppl B:B101–121, 2000. URL: https://www.ncbi.nlm.nih.gov/pubmed/10823378, doi:10.1016/s0149-2918(00)89027-x.

[239] M. I. Saez, C. Quero, J. M. Trigo, B. Muros, and E. Alba. Practical guidelines for dose individualization of anticancer targeted drugs. *Clin Transl Oncol*, 14(11):812–9, 2012. URL: https://www.ncbi.nlm.nih.gov/pubmed/23065600, doi:10.1007/s12094-012-0932-x.

[240] J. Boni, C. Leister, J. Burns, M. Cincotta, B. Hug, and L. Moore. Pharmacokinetic profile of temsirolimus with concomitant administration of cytochrome p450-inducing medications. *J Clin Pharmacol*, 47(11):1430–9, 2007. URL: https://www.ncbi.nlm.nih.gov/pubmed/17913896, doi:10.1177/0091270007306957.

[241] FDA US. Drug development and drug interactions: Table of substrates, inhibitors and inducers. Report, US Food and Drug Administration, 2020. URL: https://www.fda.gov/drugs/drug-interactions-labeling/drug-development-and-drug-interactions-table-substrates-inhibitors-and-inducers.

[242] M. Niemi, J. T. Backman, M. F. Fromm, P. J. Neuvonen, and K. T. Kivisto. Pharmacokinetic interactions with rifampicin : clinical relevance. *Clin Pharmacokinet*, 42(9):819–50, 2003. URL: https://www.ncbi.nlm.nih.gov/pubmed/12882588, doi:10.2165/00003088-200342090-00003.

[243] J. T. Backman, K. T. Olkkola, and P. J. Neuvonen. Rifampin drastically reduces plasma concentrations and effects of oral midazolam. *Clin Pharmacol Ther*, 59(1):7–13, 1996. URL: https://www.ncbi.nlm.nih.gov/pubmed/8549036, doi:10.1016/S0009-9236(96)90018-1.

[244] J. Chen and K. Raymond. Roles of rifampicin in drug-drug interactions: underlying molecular mechanisms involving the nuclear pregnane x receptor. *Ann Clin Microbiol Antimicrob*, 5:3, 2006. URL: https://www.ncbi.nlm.nih.gov/pubmed/16480505, doi:10.1186/1476-0711-5-3.

[245] U.S. Food Administration and Drug. Cfr - code of federal regulations title 21–food and drugs chapter i – food and drug administration department of health and human services subchapter a – general, part 20 public information subpart d eexemptions. Report, U.S. Department of Health and Human Services, April 1, 2019 1994. URL: https://www.accessdata.fda.gov/scripts/cdrh/cfdocs/cfcfr/CFRSearch.cfm?fr=20.61.

[246] N. Picard, N. Djebli, F. L. Sauvage, and P. Marquet. Metabolism of sirolimus in the presence or absence of cyclosporine by genotyped human liver microsomes and recombinant cytochromes p450 3a4 and 3a5. *Drug Metab Dispos*, 35(3):350–5, 2007. URL: https://www.ncbi.nlm.nih.gov/pubmed/17151193, doi:10.1124/dmd.106.012161.

[247] O. von Richter, O. Burk, M. F. Fromm, K. P. Thon, M. Eichelbaum, and K. T. Kivisto. Cytochrome p450 3a4 and p-glycoprotein expression in human small intestinal enterocytes and hepatocytes: a comparative analysis in paired tissue specimens. *Clin Pharmacol Ther*, 75(3):172–83, 2004. URL: https://www.ncbi.nlm.nih.gov/pubmed/15001968, doi:10.1016/j.clpt.2003.10.008.

[248] E. Galanis, J. C. Buckner, M. J. Maurer, J. I. Kreisberg, K. Ballman, J. Boni, J. M. Peralba, R. B. Jenkins, S. R. Dakhil, R. F. Morton, K. A. Jaeckle, B. W. Scheithauer, J. Dancey, M. Hidalgo, D. J. Walsh, and Group North Central Cancer Treatment. Phase ii trial of temsirolimus (cci-779) in recurrent glioblastoma multiforme: a north central cancer treatment group study. *J Clin Oncol*, 23(23):5294–304, 2005. URL: https://www.ncbi.nlm.nih.gov/pubmed/15998902, doi:10.1200/JCO.2005.23.622.

[249] C. Emoto, T. Fukuda, R. Venkatasubramanian, and A. A. Vinks. The impact of cyp3a5*3 polymorphism on sirolimus pharmacokinetics: insights from predictions with a physiologically-based pharmacokinetic model. *Br J Clin Pharmacol*, 80(6):1438–46, 2015. URL: https://www.ncbi.nlm.nih.gov/pubmed/26256674, doi:10.1111/bcp.12743.

[250] W. Jacobsen, N. Serkova, B. Hausen, R. E. Morris, L. Z. Benet, and U. Christians. Comparison of the in vitro metabolism of the macrolide immunosuppressants sirolimus and rad. *Transplant Proc*, 33(1-2):514–5, 2001. URL: https://www.ncbi.nlm.nih.gov/pubmed/11266932, doi:10.1016/s0041-1345(00)02116-3.

[251] L. M. Berezhkovskiy. Determination of drug binding to plasma proteins using competitive equilibrium binding to dextran-coated charcoal. *J Pharmacokinet Pharmacodyn*, 33(5):595–608, 2006. URL: https://www.ncbi.nlm.nih.gov/pubmed/16841186, doi:10.1007/s10928-006-9024-2.

[252] Certara. *Prediction of concentration-time profiles: Static versus dynamic approaches*, pages 75–92. Certara, 2017.

[253] R Dominguez. Studies of renal excretion of creatinine. ii. volume of distribution. *Proceedings of the Society for Experimental Biology and Medicine*, 31(9):1146–1149, 1934.

[254] P. Poulin and F. P. Theil. A priori prediction of tissue:plasma partition coefficients of drugs to facilitate the use of physiologically-based pharmacokinetic models in drug discovery. *J Pharm Sci*, 89(1):16–35, 2000. URL: https://www.ncbi.nlm.nih.gov/pubmed/10664535, doi:10.1002/(SICI)1520-6017(200001)89:1<16::AID-JPS3>3.0.CO;2-E.

[255] Leonid M Berezhkovskiy. A valid equation for the well-stirred perfusion limited physiologically based pharmacokinetic model that consistently accounts for the blood–tissue drug distribution in the organ and the corresponding valid equation for the steady state volume of distribution. *Journal of pharmaceutical sciences*, 99(1):475–485, 2010.

[256] Torisel kit (temsirolimus) injection, for intravenous use, pfizer wyeth pharmaceuticals inc, philadelphia pa; initial u.s. approval: 2007. Report, 2018. URL: https://www.accessdata.fda.gov/drugsatfda_docs/label/2018/022088s021s023lbl.pdf.

[257] K. Bittermann and K. U. Goss. Predicting apparent passive permeability of caco-2 and mdck cell-monolayers: A mechanistic model. *PLoS One*, 12(12):e0190319, 2017. URL: https://www.ncbi.nlm.nih.gov/pubmed/29281711, doi:10.1371/journal.pone.0190319.

[258] Harvey Lodish, Arnold Berk, S Lawrence Zipursky, Paul Matsudaira, David Baltimore, and James Darnell. Molecular cell biology 4th edition. *National Center for Biotechnology Information, Bookshelf*, 9, 2000.

[259] US Food and Drug Administration. Nda application no.: 022088 drug approval package and history: Torisel (temsirolimus) intravenous company: Wyeth pharmaceuticals inc. approval date: 05/30/2007. Report, US Food and Drug Administration,, February 8, 2019 - July 8, 2020 2019.

[260] Nico Scheer, Xiaoyan Chu, Laurent Salphati, and M. J. Zamek-Gliszczynski. *Drug Transporters Volume 1: Knockout and humanised animal models to study membrane transporters in drug development.*, book section 8, pages 298–332. The Royal Society of Chemistry, Chmbridge, UK, 2016.

[261] US Food and Drug Administration. Drug approval package: Torisel (temsirolimus) intravenous pharmacology review(s); solution company: Wyeth pharmaceuticals inc. application no.: 022088 approval date: 05/30/2007. Report, US Food and Drug Administration,, 2012. URL: https://www.accessdata.fda.gov/drugsatfda_docs/nda/2007/022088s000_PharmR.pdf.

[262] The Canadian Institutes of Health Research; Canada Foundation for Innovation; The Metabolomics Innovation Centre (TMIC). The human metabolome database (hmdb): Metabocard for temsirolimus (hmdb0015632). 2018. URL: https://hmdb.ca/metabolites/HMDB0015632.

[263] R. P. Austin, P. Barton, S. Mohmed, and R. J. Riley. The binding of drugs to hepatocytes and its relationship to physicochemical properties. *Drug Metab Dispos*, 33(3):419–25, 2005. URL: https://www.ncbi.nlm.nih.gov/pubmed/15616151, doi:10.1124/dmd.104.002436.

[264] D. S. Wishart, Y. D. Feunang, A. Marcu, A. C. Guo, K. Liang, R. Vazquez-Fresno, T. Sajed, D. Johnson, C. Li, N. Karu, Z. Sayeeda, E. Lo, N. Assempour, M. Ber-

janskii, S. Singhal, D. Arndt, Y. Liang, H. Badran, J. Grant, A. Serra-Cayuela, Y. Liu, R. Mandal, V. Neveu, A. Pon, C. Knox, M. Wilson, C. Manach, and A. Scalbert. Hmdb 4.0: the human metabolome database for 2018. *Nucleic Acids Res*, 46(D1):D608–D617, 2018. URL: https://www.ncbi.nlm.nih.gov/pubmed/29140435, doi:10.1093/nar/gkx1089.

[265] Rapamune (sirolimus) oral solution, tablets, for oral use, pfizer wyeth pharmaceuticals inc, philadelphia pa; july 2011. Report, 1999. URL: https://www.accessdata.fda.gov/drugsatfda_docs/label/2017/021083s059,021110s076lbl.pdf.

[266] C. W. Tan, B. S. Gardiner, Y. Hirokawa, M. J. Layton, D. W. Smith, and A. W. Burgess. Wnt signalling pathway parameters for mammalian cells. *PLoS One*, 7(2):e31882, 2012. URL: https://www.ncbi.nlm.nih.gov/pubmed/22363759, doi:10.1371/journal.pone.0031882.

[267] L. M. Ballou and R. Z. Lin. Rapamycin and mtor kinase inhibitors. *J Chem Biol*, 1(1-4):27–36, 2008. URL: https://www.ncbi.nlm.nih.gov/pubmed/19568796, doi:10.1007/s12154-008-0003-5.

[268] L. Dudkin, M. B. Dilling, P. J. Cheshire, F. C. Harwood, M. Hollingshead, S. G. Arbuck, R. Travis, E. A. Sausville, and P. J. Houghton. Biochemical correlates of mtor inhibition by the rapamycin ester cci-779 and tumor growth inhibition. *Clin Cancer Res*, 7(6):1758–64, 2001. URL: https://www.ncbi.nlm.nih.gov/pubmed/11410517.

[269] US Food and Drug Administration. Drug approval package: Sirolimus (rapamycin), 1 mg/ml oral solution clinical pharmacology and biopharmaceutics review(s); company: Wyeth-ayerst research. application no.: 021083 approval date: 19/15/1999. Report, US Food and Drug Administration,, 2012. URL: https://www.accessdata.fda.gov/drugsatfda_docs/nda/99/21083A_Rapamune_clinphrmr.pdf.

[270] C. L. Cummins, L. Salphati, M. J. Reid, and L. Z. Benet. In vivo modulation of intestinal cyp3a metabolism by p-glycoprotein: studies using the rat single-pass intestinal perfusion model. *J Pharmacol Exp Ther*, 305(1):306–14, 2003. URL: https://www.ncbi.nlm.nih.gov/pubmed/12649383, doi:10.1124/jpet.102.044719.

[271] P. B. Watkins, S. A. Murray, L. G. Winkelman, D. M. Heuman, S. A. Wrighton, and P. S. Guzelian. Erythromycin breath test as an assay of glucocorticoid-inducible liver cytochromes p-450. studies in rats and patients. *J Clin Invest*, 83(2):688–97, 1989. URL: https://www.ncbi.nlm.nih.gov/pubmed/2913056, doi:10.1172/JCI113933.

[272] Y. Tanigawara. Role of p-glycoprotein in drug disposition. *Ther Drug Monit*, 22(1):137–40, 2000. URL: https://www.ncbi.nlm.nih.gov/pubmed/10688277, doi:10.1097/00007691-200002000-00029.

[273] F. Thiebaut, T. Tsuruo, H. Hamada, M. M. Gottesman, I. Pastan, and M. C. Willingham. Cellular localization of the multidrug-resistance gene product p-glycoprotein in normal human tissues. *Proc Natl Acad Sci U S A*, 84(21):7735–8, 1987. URL: https://www.ncbi.nlm.nih.gov/pubmed/2444983, doi:10.1073/pnas.84.21.7735.

[274] S. F. Zhou. Structure, function and regulation of p-glycoprotein and its clinical relevance in drug disposition. *Xenobiotica*, 38(7-8):802–32, 2008. URL: https://www.ncbi.nlm.nih.gov/pubmed/18668431, doi:10.1080/00498250701867889.

[275] L. M. Berry, L. Wollenberg, and Z. Zhao. Esterase activities in the blood, liver and intestine of several preclinical species and humans. *Drug Metab Lett*, 3(2):70–7, 2009. URL: https://www.ncbi.nlm.nih.gov/pubmed/19601867.

[276] W. Wang, K. M. Hallow, and D. A. James. A tutorial on rxode: Simulating differential equation pharmacometric models in r. *CPT Pharmacometrics Syst Pharmacol*, 5(1):3–10, 2016. URL: https://www.ncbi.nlm.nih.gov/pubmed/26844010, doi:10.1002/psp4.12052.

[277] W. S. Park. Pharmacometric models simulation using nonmem, berkeley madonna and r. *Transl Clin Pharmacol*, 25(3):125–133, 2017. URL: https://www.ncbi.nlm.nih.gov/pubmed/32095462, doi:10.12793/tcp.2017.25.3.125.

[278] R. J. Bauer. Nonmem tutorial part i: Description of commands and options, with simple examples of population analysis. *CPT Pharmacometrics Syst Pharmacol*, 2019. URL: https://www.ncbi.nlm.nih.gov/pubmed/31056834, doi:10.1002/psp4.12404.

[279] Ernst Hairer and Gerhard Wanner. *Chapter IV. Stiff Problems - One-Step Methods.* Solving ordinary differential equations II: Stiff and differential-algebraic problems. Springer Berlin Heidelberg, Berlin, 2 edition, 1996.

[280] Y. Franchetti and T. D. Nolin. Dose optimization in kidney disease: Opportunities for pbpk modeling and simulation. *J of Clin Pharmacol*, 60(S1):S36–S51, 2020. URL: https://accp1.onlinelibrary.wiley.com/doi/abs/10.1002/jcph.1741, doi:https://doi.org/10.1002/jcph.1741.

[281] Roger W. Jelliffe. Individualized, maximally precise drug therapy: A physician's bedside viewpoint. 2019. URL: https://www.fda.gov/media/130402/download.

[282] Sander Vinks. Clinical implementation of pk/pd model-informed decision support tools for precision dosing. 2019. URL: https://www.fda.gov/media/130411/download.

[283] G. S. Timmins. Stable isotope biomarker breath tests for human metabolic and infectious diseases: a review of recent patent literature. *Expert Opin Ther Pat*, 26(12):1393–1398, 2016. URL: https://www.ncbi.nlm.nih.gov/pubmed/27467014, doi:10.1080/13543776.2016.1217995.

[284] F. P. Guengerich and T. Shimada. Oxidation of toxic and carcinogenic chemicals by human cytochrome p-450 enzymes. *Chem Res Toxicol*, 4(4):391–407, 1991. URL: https://www.ncbi.nlm.nih.gov/pubmed/1912325, doi:10.1021/tx00022a001.

[285] Tian Qi Chen, Yulia Rubanova, Jesse Bettencourt, and David K Duvenaud. Neural ordinary differential equations. In *Advances in neural information processing systems*, pages 6571–6583.